NASA-CP-2419 19860016351

NASA Conference Publication 2419

Fourteenth NASTRAN® Users' Colloquium

Proceedings of a colloquium held in
San Diego, California
May 5-9, 1986

NASA

NASA Conference Publication 2419

Fourteenth NASTRAN® Users' Colloquium

Proceedings of a colloquium held in
San Diego, California
May 5–9, 1986

NASA
National Aeronautics
and Space Administration

**Scientific and Technical
Information Branch**

1986

FOREWORD

NASTRAN® (NASA STRUCTURAL ANALYSIS) is a large, comprehensive, nonproprietary, general purpose finite element computer code for structural analysis which was developed under NASA sponsorship and became available to the public in late 1970. It can be obtained through COSMIC® (Computer Software Management and Information Center), Athens, Georgia, and is widely used by NASA, other government agencies, and industry.

NASA currently provides continuing maintenance of NASTRAN through COSMIC. Because of the widespread interest in NASTRAN, and finite element methods in general, the Fourteenth NASTRAN Users' Colloquium was organized and held at the Sea Point Hotel, San Diego, California on May 5-9, 1986. (Papers from previous colloquia held in 1971, 1972, 1973, 1975, 1977, 1978, 1979, 1980, 1982 and 1983, are published in NASA Technical Memorandums X-2378, X-2637, X-2893, X-3278, X-3428, and NASA Conference Publications 2018, 2062, 2131, 2151, 2249, 2284, 2328 and 2373.) The Fourteenth Colloquium provides some comprehensive general papers on the application of finite element methods in engineering, comparisons with other approaches, unique applications, pre- and post-processing or auxiliary programs, and new methods of analysis with NASTRAN.

Individuals actively engaged in the use of finite elements or NASTRAN were invited to prepare papers for presentation at the Colloquium. These papers are included in this volume. No editorial review was provided by NASA or COSMIC; however, detailed instructions were provided each author to achieve reasonably consistent paper format and content. The opinions and data presented are the sole responsibility of the authors and their respective organizations.

NASTRAN® and COSMIC® are registered trademarks of the National Aeronautics and Space Administration.

CONTENTS

Page

FOREWORD iii

1. ENHANCEMENTS TO SPERRY/NASTRAN 1
by Tadashi Koga
(Nippon Univac Kaisha, Ltd.)

2. IMPROVED ISOPARAMETRIC SOLID AND MEMBRANE ELEMENTS . . . 28
by William R. Case and Richard E. Vandegrift
(NASA/Goddard Space Flight Center)

3. DYNAMIC AND AEROELASTIC ANALYSES OF TURBOSYSTEMS IN NASTRAN 56
by V. Elchuri
(Aerostructures)
and P. R. Pamidi
(RPK Corporation)

4. NASTRAN DATA DECK GENERATION ON THE PC 61
by Robert J. Guyan
(Rockwell International, Inc.)

5. PRE- AND POST-PROCESSING FOR COSMIC/NASTRAN ON PERSONAL COMPUTERS AND MAINFRAMES 73
by H. A. Kamel, Anton V. Mobley, Ben Nagaraj and K. W. Watkins
(CASA/GIFTS, Inc.)

6. NASTRAN INTERFACING MODULES WITHIN THE INTEGRATED ANALYSIS CAPABILITY (IAC) PROGRAM 103
by Harold P. Frisch
(NASA/Goddard Space Flight Center)

7. A SYSTEM APPROACH TO DESIGN - ANALYSIS 130
by Gil White
(Intergraph Corporation)

8. EXPERIENCES WITH NASTRAN IN A MULTIDISCIPLINARY OPTIMIZATION ENVIRONMENT 145
by Myles M. Hurwitz
(David W. Taylor Naval Ship Research and Development Center)

9. STRESS CONCENTRATION INVESTIGATIONS USING NASTRAN . . . 154
by M. C. Gillcrist and L. A. Parnell
(Naval Ocean Systems Center)

10. DIFFERENTIAL STIFFNESS EFFECTS 166
by Ben H. Ujihara and Edward T. Tong
(Rockwell International, Inc.)

11. TEST VS ANALYSIS - A DISCUSSION OF METHODS 173
by Thomas G. Butler
(Butler Analyses)

12. A COMPARISON OF NASTRAN (COSMIC) AND EXPERIMENTAL RESULTS FOR THE VIBRATION OF THICK OPEN CYLINDRICAL CANTILEVERED SHELLS 187
by Wayne L. Mindle
(Martin Marietta Orlando Aerospace)
and Peter J. Torvik
(Air Force Institute of Technology)

13. NASTRAN STRUCTURAL MODEL FOR THE LARGE GROUND ANTENNA PEDESTAL WITH APPLICATIONS TO HYDROSTATIC BEARING OIL FILM 205
by Chian T. Chian
(Jet Propulsion Laboratory)

14. SOLVING LARGE-SCALE DYNAMIC SYSTEMS USING BAND LANCZOS METHOD IN ROCKWELL NASTRAN ON CRAY X-MP 236
by Viney K. Gupta, Scott D. Zillmer and
Robert E. Allison
(Rockwell International, Inc.)

15. FLUTTER ANALYSIS OF LOW ASPECT RATIO WINGS 247
by L. A. Parnell
(Naval Ocean Systems Center)

16. FINITE ELEMENT MODELLING OF NON-LINEAR MAGNETIC CIRCUITS USING COSMIC NASTRAN 264
by T. J. Sheerer
(Texas Instruments)

17. CALCULATING FAR-FIELD RADIATED SOUND PRESSURE LEVELS FROM NASTRAN OUTPUT 282
by Robert R. Lipman
(David W. Taylor Naval Ship Research and
Development Center)

18. A GENERAL LOW FREQUENCY ACOUSTIC RADIATION CAPABILITY FOR NASTRAN 293
by G. C. Everstine, F. M. Henderson, E. A. Schroeder
and R. R. Lipman
(David W. Taylor Naval Ship Research and
Development Center)

19. A FINITE ELEMENT SURFACE IMPEDANCE REPRESENTATION FOR STEADY-STATE PROBLEM 311
by A. J. Kalinowski
(Naval Underwater Systems Center)

ENHANCEMENTS TO SPERRY/NASTRAN

Tadashi Koga
Nippon Univac Kaisha, Ltd.

SUMMARY

This paper reviews the enhancement to NASTRAN program performed by NUK (Nippon Univac Kaisha, Ltd.) added to Level 15.5. Features discussed include intermediate checkpoint-restart in triangular decomposition, I/O improvement, multibanked memory and new plate element. The first three improvements provides the capability to solve significantly large size problem, while the new elements release the analyst from the cumbersome work to constrain the singularities caused by the lack of stiffness of inplane rotation of old plate elements.

INTRODUCTION

Since 1974, NUK has been maintaining and developing a NASTRAN based on COSMIC level 15.5 and distributing it to the UNIVAC customer in Japan and Europe as SPERRY/NASTRAN in co-operation with Sperry Support Services. In Japan, more than 35 customer are using our version of NASTRAN.

Since the leasing policy and export restrictions of source code were placed on post level 15.5, our motivation to offer SPERRY/NASTRAN is to provide state-of-the-art analytical capabilities incorporated in level 16.0 or later and error corrections in a timely manner to the UNIVAC customers outside U. S. A. In addition to maintaining a SPERRY/NASTRAN, we are also publishing a Newsletter each time the new version in released, providing user training seminar 8 times a year and developing and maintaining pre and post processors.

These improved features are listed in Table 1 and some of them are discussed in this paper.

DCOMP2

In static analysis, the computing time associated with triangular decomposition forms 70-80% of total time if the number of grid points exceeds 3000. Since a checkpoint can be taken only after the completion of the module, if the decomposition is interrapted by unexpected error such as max time, dish fault, system hung up, the computation up to this point of error is completly lost. In this case, restart run can save only 10-15% of total run time. The use of new module DCOMP2 provides a method by which any number of intermediate checkpoints can by taken during symmetric matrix decomposition. The module supervises the existing symmetric decomposition routine (SDCOMP) by interrupting the factoring process at intervals specified by the user.

The new module, DCOMP2, must be applied to an analysis through a rigid format DMAP alter. (Fig 1)

DMAP Calling Sequence

DCOMP2 KLL / LLL, ULL, SCR / V, N, NPARA / V, N, MPARA $

Input Data Block

KLL - Partition of stiffness matrix - 1 set

Note : KLL is assumed to be symmetric and may not be purged.

Output Data Blocks

LLL - Lower triangular factor of KLL - 1 set.

ULL - Upper triangular factor of KLL - 1 set.

SCR - Scratch Data Block for checkpoint/restart, contains the front matrix currently held in open core.

Notes :
1. LLL and ULL may not be purged.
2. ULL is not a standard upper triangular matrix. Its format is compatible only for input to subroutine FBS.

Parameters

NPARA - Input/output - integer - no default
= -1 No operation is taken
= 0 Normal decomposition
= +N Number of intermediate checkpoints required.

MPARA - output - integer - no default, MPARA contains the number of checkpoints completed.

Notes :
1. The number of checkpoints required, NPARA, is decreased by 1 each time an intermediate checkpoint is made.
2. The number of checkpoints made, MPARA is increased by 1 each time an intermediate checkpoint is made.
3. Both parameters are saved in data block XVPS and used at the time of restart to determine current location in the decomposition procedure.

Method

The general procedure for utilizing the intermediate checkpoint feature, is to replace the existing symmetric decomposition instruction, e g. RBMG2 with the new module DCOMP2. This is accomplished by using a set of DMAP alters for rigid format.

The new module contains a parameter, MPARA, which is used to specify the number of intermediate checkpoints to be taken. The user must determine before the first execution, the value of NPARA. If a restart is required of a partially decomposed matrix, the value of NPARA supplied in the DMAP instruction is replaced by the value in the XVPS data block, which can be used to determine at which row in the KLL the last checkpoint occured.

It may be noted that the checkpoint dictionary provided after each intermediate checkpoint, specifies a re-entry into DMAP instruction 90, however, the use of DMAP alter forces re-execution of the inserted module. This action assured that the restart will re-enter the DMAP instruction 89. When the value of NPARA is reduced to 0 a normal exit from the SDCOMP routine will be made and NPARA set to -1. If a restart is made after the decomposition has been completed, NPARA = -1, the DCOMP2 module gives an immediate return, therefore, it is not necessary to remove the DMAP alter statements.

Fig. 1 describes the meaning of the parameter NPARA which determines how the matrix is broken into ΔN rows for decomposition. At the first entry to subroutine SDCOMP, ΔN is decided from NPARA and the matrix size N. When the decomposition is completed for every ΔN rows, SDCOMP copies the values in open core and scratch file (in case spill occures) to SCR, then gives an alternate return to DCOMP2. DCOMP2 calls XCHK to write LLL, ULL and SCR on NPTP and after returning from XCHK, calls SDCOMP again to continue the decomposition and increase the value of MPARA by 1.

In the restart run, SDCOMP recovers open core from SCR and resumes decomposition from MPARA *ΔN + 1 st row of matrix KLL.

IMPROVED I/O

SPERRY/NASTRAN has two improvements in I/O routine, asynchronous I/O and multiple I/O block read.

Asynchronous I/O

In conventional NASTRAN, one buffer area is assigned to each I/O unit and actual I/O request will be initiated when the buffer area is filled in case of write operation. The execution of NASTRAN is suspended until all data in buffer area is transfered to external storage.

In most of computer systems, asynchronous I/O capability is provided which makes it possible to process I/O operation and non-I/O operation simultaneously. To take full advantage of this capability, I/O routines of NASTRAN (GINO) were drastically rewritten.

The new GINO routine divides the I/O buffer into two parts. One of them is used for the data transfer for the higher level subprograms and the other is used to transfer the data from/to the external storage. (Fig 2-1)

This new capability has no effect to computer time, but the elapsed time (wall clock time) may be reduced to 2/3 of the old.

MREAD (Multiple Read Routine)

In real eigenvalue analysis, Invers Power Method is most papulary used due to its efficiency. Iterative procedure of this method is described as follows.

step		description
1	$\lambda_0 \rightarrow \lambda_1$	shift
2	$K-\lambda_1 M \rightarrow D$	form dynamic matrix
3	$D \rightarrow L \cdot U$	triangular decomposition
4	$M \cdot U_n \rightarrow V_{n+1}$	matrix multiplication
5	$(L \cdot U)^{-1} V_{n+1} \rightarrow W_{n+1}$	substitution
6	$W_{n+1}/c \rightarrow U_{n+1}$	normalization
7	convergence check	

where K : stiffness matrix
M : mass matrix
λ : estimated eigenvalue
u, v, w : iteration vector

Generally, for the extraction of one eigenvalue, step 4, 5 will be performed 8～10 times and step 3 will be done once. Regarding to computer time and memory size, step 3 and step 4, 5 have quite different characteristics described below.

step	CPU time	I/O time	memory size
3	$O(NB^2)$	O(NB)	B^2
4, 5	O(NB)	O(NB)	$14 \times N$

where N : size of matrix
B : semi-band width of matrix

As easily shown from this table, CPU time is dominant in step 3 while I/O time is dominant in step 4, 5, and the memory size in step 4, 5 is much less than that of step 3.

To reduce the I/O time in step 4, 5, we can remember the fact that I/O time depends on not only the number of words transfered but also the number of times I/O operations requested.

The new open routine (MOPEN) determines the number of I/O blocks held in open core. The lowest I/O routine (GINOIO) was changed so that the one I/O operation fills all of these I/O blocks and the I/O request of one block to GINOIO is considered to be a change of pointer to current I/O block untill all the I/O blocks held in open core were exhausted.

Since the size of I/O block was not changed, the size of actual I/O request can be determined according to the size of open core available.

This new capability is also applied to FBS (forward backward substitution), TRD (transient response displacement) and TRHT (transient response heat transfer). The numerical examples described in Fig 2.2 thru Fig 2.5 shows us that the I/O time will be reduced to 1/3 to 1/5 of the old.

MULTI BANKED MEMORY

At this time Univac system has no virtual storage capability, and the addressing limit of 262 KWD. Therefore, if the summation of B (semi-band width) and C (number of active columns) of stiffness matrix exceeds nealy 470, front matrix generated during the symmetric real decomposition (performed by SDCOMP) can not be held in the main memory. Some portion of this overflowed area (called 'spill') is processed in the area for active column, but remainder are stored in disk area. The processing of this spilled portion requires frequent I/O operation which results significant decrease of the execution efficiency.

On the other hand, the model size which is indicated by the number of grid point and number of elements has been increasing significantly due to the requirement of the engineers to obtain more precise simulation result. With the aid of powerful, easy to use preprocessors, the size of finite element model can easily exceeds the above limit.

To override this defect, SPERRY/NASTRAN provides automatic memory expansion capability to use banked memory as internal file up to 4MWD. The spilled portion of the front matrix is not stored in disk space but in this banked memory (called ADDITIONAL CORE). Since the data transfer to (or from) this banked memory is no longer an I/O operation but a simple store (or load) operation, the I/O time was significantly reduced. (Fig 3.1, 3.2)

For the implementation of this capability, following subroutines are developed.

OPENX - According to the number of words requested, reserve the banked memory via MCORE$ and external disk space if necessary.

READX/WRITEX - Transfer the data from/to the banked memory.

CLOSEX - Release the banked memory via LCORE$.

To examine the efficiency of this new capability, comparisons between the new and old NASTRAN are done. Because the comparison with large size problem which causes spill from 262 KWD requires much CPU time, middle size problems are examined restricting program size less than 200 KWD to cause spill processing.

From the results shown in Fig 3.3 and Fig 3.4, we can conclude that the significant reduction in I/O time is achieved while the CPU time reduction is a little. Since the number of words of spilled area is proportional to the square of B+C, the effect of this capability becomes more apparent as the problem size increases.

NEW PLATE ELEMENTS

NASTRAN assumes 6 degrees of freedom (d.o.f.) per grid point. However, all the original elements have 5 or less d.o.f.s at their grid point. Though the lack of stiffness of each grid point is checked and informed by NASTRAN automatically, the generation of appropriate constraint data for these singularities is a difficult work especially in the following case.

inclined flat plate model
curved shell which has a big radius of curvature

Some modules are developed to constrain these singularities by assuming that all the d.o.f. which remains singular should be constrained by SPC processing. Some other modules only made the card images to constrain such d.o.f.s by SPC or MPC processing. Considering the difficulties of such function due to the existence of MPC, we thought it better to incorporate the plate element which has 6 d.o.f.s at their grid points.

Two plate elements named TRIA3 and QUAD4 are incorporated. These elements are formulated from 'Pian's hybrid element'. Assuming the displacement function on each side of the element, the stress function within the element, the equilibrium equation on grid point is formulated based on the principle of complemental virtual work. Membrane element and bending element are produced independently and these are combined without coupling each other. Following are the outline of triangular element.

Membrane Element

The degrees of freedom on a grid point are u, v and θz. U and v are the components of displacements paralle to the axis of the local coordinate system. θz is the average value of the rotation of side, not the ratational angle of grid point itself. The displacement functions are defined on the side and shown as follows.

displacement tangential to side (Us) = linear function
displacement normal to side (Un) = cubic function
rotational angle ($\theta = \partial Un/\partial r$) = quadratic function

where
r is parameter on side
n is normal direction to side
s is tangential direction to side

The stress function is defined within element and as follows.

$$\{\sigma\} = \begin{Bmatrix} \sigma_x \\ \sigma_y \\ \tau_{xy} \end{Bmatrix} = \left[\begin{array}{ccc|ccc|ccc} \zeta_1 & & & \zeta_2 & & & \zeta_3 & & \\ & \zeta_1 & & & \zeta_2 & & & \zeta_3 & \\ & & \zeta_1 & & & \zeta_2 & & & \zeta_3 \end{array}\right] \begin{Bmatrix} \{\sigma\}_1 \\ \{\sigma\}_2 \\ \{\sigma\}_3 \end{Bmatrix}$$

$$\{\sigma\}i = \begin{Bmatrix} \sigma_x \\ \sigma_y \\ \sigma_{xy} \end{Bmatrix} \quad \text{at grid point i}$$

where ($\zeta_1, \zeta_2, \zeta_3$) are the area coordinates.

In order to satisfy the equilibrium equation within element, 2 components of 9 $\{\sigma\}_1, \{\sigma\}_2, \{\sigma\}_3$ are dependent.

Bending Element

The degrees of freedom on the grid point are W, Θx and Θy. W is the deflection normal to the x, y plane.
The displacement functions are defined on the side and shown as follows.

deflection W = cubic function
side direction slope $\partial W/\partial s$ = quadratic function
normal slope to side $\partial W/\partial n$ = linear function

The stress function is defined within element as follows.

$$\{\sigma\} = \begin{Bmatrix} m_x \\ m_y \\ m_{xy} \end{Bmatrix} = \left[\begin{array}{ccc|ccc|ccc} \zeta_1 & & & \zeta_2 & & & \zeta_3 & & \\ & \zeta_1 & & & \zeta_2 & & & \zeta_3 & \\ & & \zeta_1 & & & \zeta_2 & & & \zeta_3 \end{array}\right] \begin{Bmatrix} \{\sigma\}_1 \\ \{\sigma\}_2 \\ \{\sigma\}_3 \end{Bmatrix}$$

$$\{\sigma\}i = \begin{Bmatrix} m_x \\ m_y \\ m_{xy} \end{Bmatrix} \quad \text{at grid point i}$$

where $m_x = \int \sigma_x \cdot z \, dz$
the integration takes place over direction to plate thickness.

9 components of stress are independent.

Composite Shell Element

Shell element is composed of membrane element and bending element without coupling each other.

Quadrilateral Element

Quadrilateral element (QUAD4) is composed from the 4 overlapping TRIA3 elements. (Fig 4.1)

Numerical Evaluation

The model and loading condition are shown in Fig 4.2 and the results are shown in Fig 4.3 thru Fig 4.5. From these results, following conclusions are obtained.

(1) Inplane bending

Because the elements TRIA2 and QUAD2 absorbed the inplane bending as the form of shear, the deformed shape of such elements was not so good. In this viewpoint, TRIA3 and QUAD4 are recognized to be improved, and moreover the stress calculated falls in the safety side.

(2) Out of plane bending

Regarding the displacement, no visible difference between TRIA3 and TRIA2 is recognized. But the distribution of reaction forces reverses.

(3) Inplane tension

The TRIA2 and QUAD2 elements shows good results, on the other hand, the solution of new elements at the end side causes disorder.

(4) Summary

The accuracy of new elements TRIA3 and QUAD4 is better than TRIA2 and QUAD2 in many cases. Moreover, introduction of θz as additional d.o.f. makes lose the necessities of constraint by SPC or MPC card, troubles on modeling will be reduced.

CONCLUSIONS

Several improvements and enhancements performed by NUK (Nippon Univac Kaisha, Ltd.) are described in the paper. These modifications increase the usefulness and efficiency of the NASTRAN program.

Due to the leasing policy and export restrictions placed on post 15.5, and the requirement of Japanese customer such as, timely error corrections, response to technical questions which sometimes need the understanding of source code and Japanese manual, we will continue to develop our NASTRAN. But if NASA can consider alternatives to the current policies so that the Japanese company can respond above requirements, the number of users of COSMIC/NASTRAN will increase steadily.

The list of current development priorities for our NASTRAN are :

- FEER method
- HEXA element - 8 to 20 nodes (variable)
- PLOAD3, PLOAD4 - pressure load on solid surface
- BAR element including warping
- Improved solid element - incompatible mode
- Response spectrum
- Output of strain and strain energy

Table 1. Major Improvements Added to Level 15.5

Item		Description
1)	Isoparametric Elements	IS2D4, IS2D8, IS3D8, IS3D20
2)	RF14	Thermal transient-structural static
3)	RF13	Normal mode analysis with differential stiffness
4)	ELBOW	curved beam element
5)	PLOAD1	distributed load on BAR element
6)	TRIA3, QUAD4	Plate element with 6 d.o.f.s at each grid point
7)	RBAR, RBE2	Rigid elements
8)	AUTOSPC	Automatic constraint by SPC
9)	READ	Append capability
10)	RF4	Iterative procedure
11)	NOLIN	Iterative procedure
12)	GPSC	SPC, MPC generator
13)	DCOMP2	intermediate checkpoint-restart in SDCOMP
14)	GINO	asynchronous I/O, multiple block read
15)	SDCOMP	banked memory
16)	FBS, INVFBS	non-transmit type UNPACK
17)	TRIA6, QUAD8	higher order shell element
18)	PENTA	15 node wedge element
19)	SPRNG	Spring element

Remark) Items 1) thru 4) are performed by Sperry Support Services.

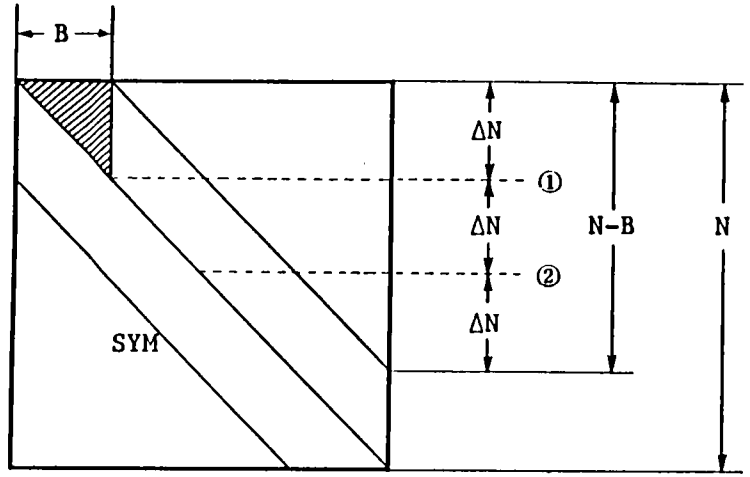

$$\Delta N = \frac{N - B}{NPARA + 1}$$

(Checkpoint will be taken NPARA times during decomposition)

Following DMAP ALTERs are required for Rigid Format 1.

```
ALTER   3
FILE    LLL=APPEND/ULL=APPEND/SCR=APPEND  $
ALTER   89,89
DCOMP2  KLL/LLL,ULL,SCR/V,N,NPARA=2/V,N,MPARA  $
ENDALTER
```

Fig. 1 Intermediate Checkpoint-restart in SDCOMP

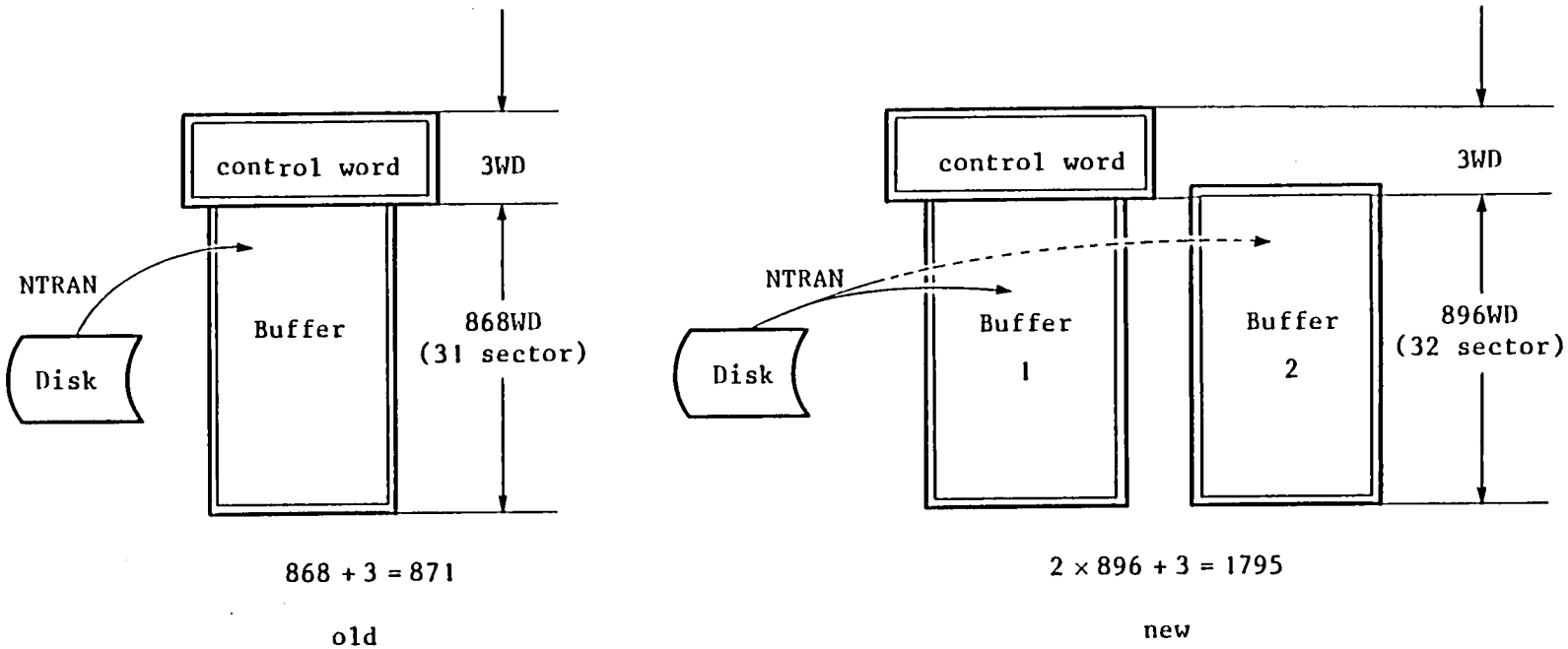

Fig. 2.1 Asynchronous I/O

		READ	No. of Decomp.	No. of Iteration	Memory size (WD)
old	CPU SUP	0.27 1.0	3	30	120K
new	CPU SUP	0.22 0.45	2	37	220K

SUP = CPU + I/O + overhead

No. of GRID points 688

No. of Elements 751

Total d.o.f. 3900

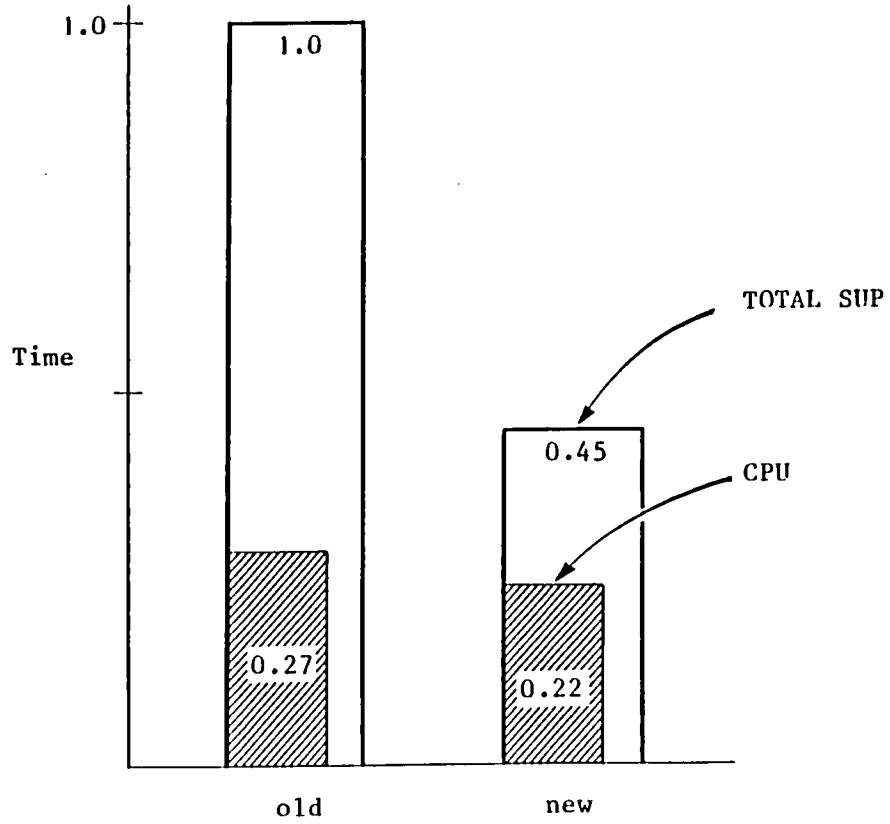

Fig. 2.2 MREAD in READ

		SDCOMP	TRD	Memory size (WD)
old	CPU SUP	0.03 0.05	0.26 1.0	100K
new	CPU SUP	0.03 0.05	0.25 0.42	257K

B + C : 193

Total d.o.f. : 2530

No. of time step : 30

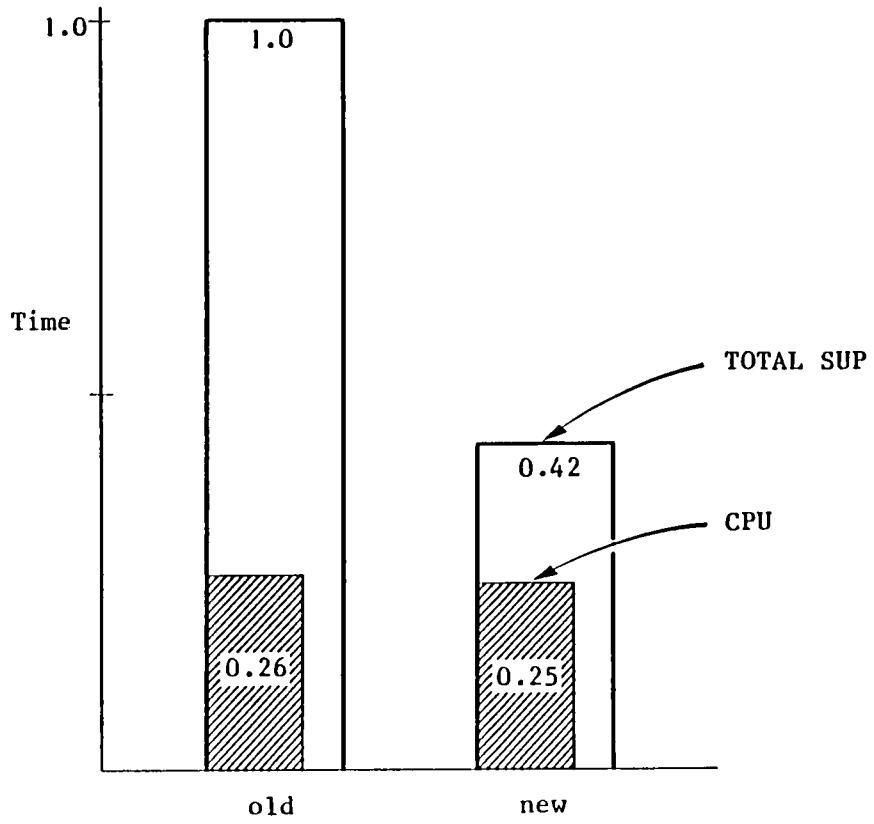

Fig. 2.3 MREAD in TRD

		SDCOMP	TRHT	Memory size (WD)
old	CPU SUP	0.01 0.03	0.24 1.0	70K
new	CPU SUP	0.01 0.03	0.24 0.45	217K

B + C : 22

Total d.o.f. : 1071

No. of time step : 31

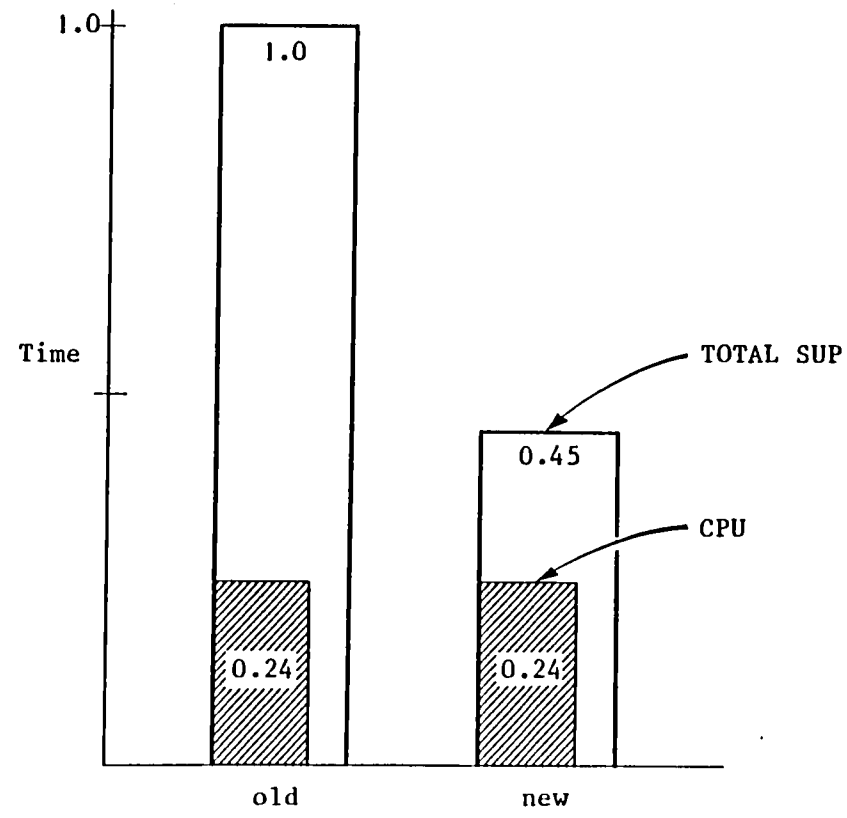

Fig. 2.4 MREAD in TRHT

		FBS	Memory size (WD)
old	CPU SUP	0.05 1.0	80K
new	CPU SUP	0.05 0.18	117K

B + C : 514

Total d.o.f.: 5072

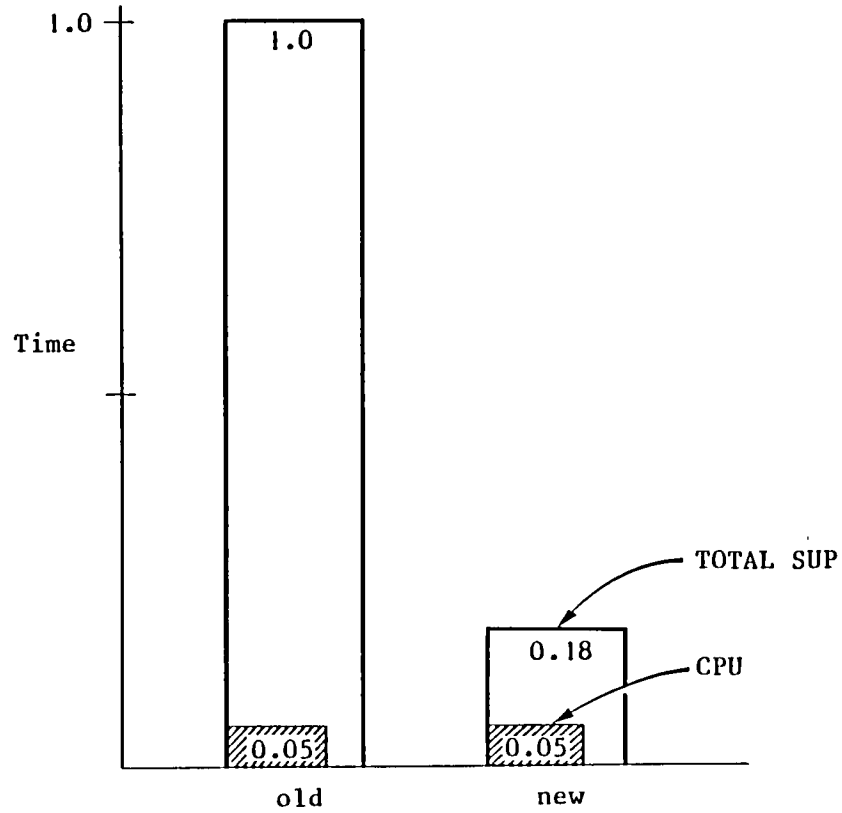

Fig. 2.5 MREAD in FBS

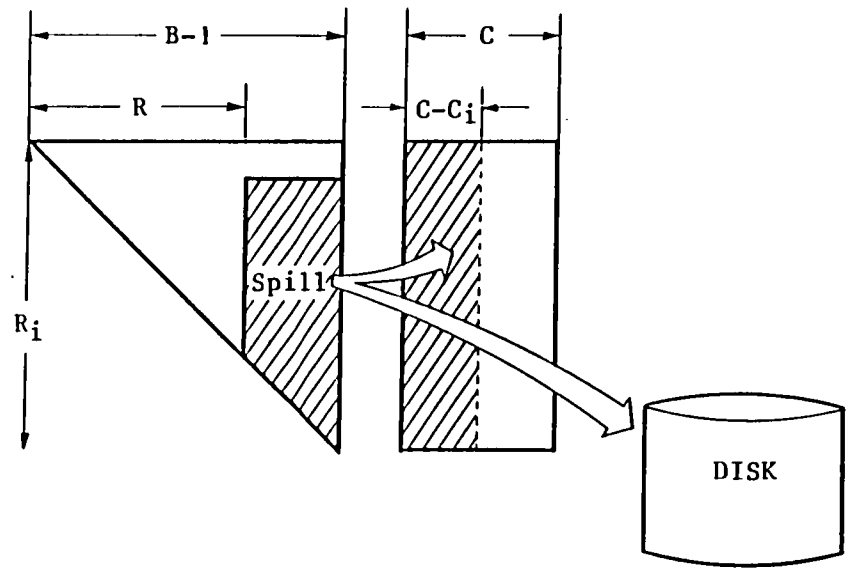

old

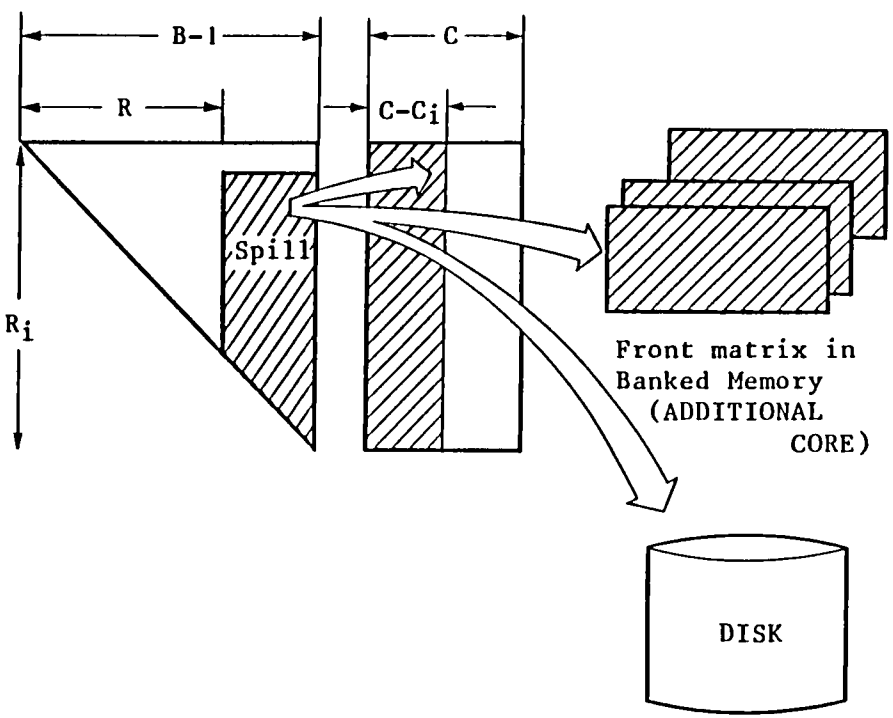

new

Fig. 3.1 Spill logic in SDCOMP

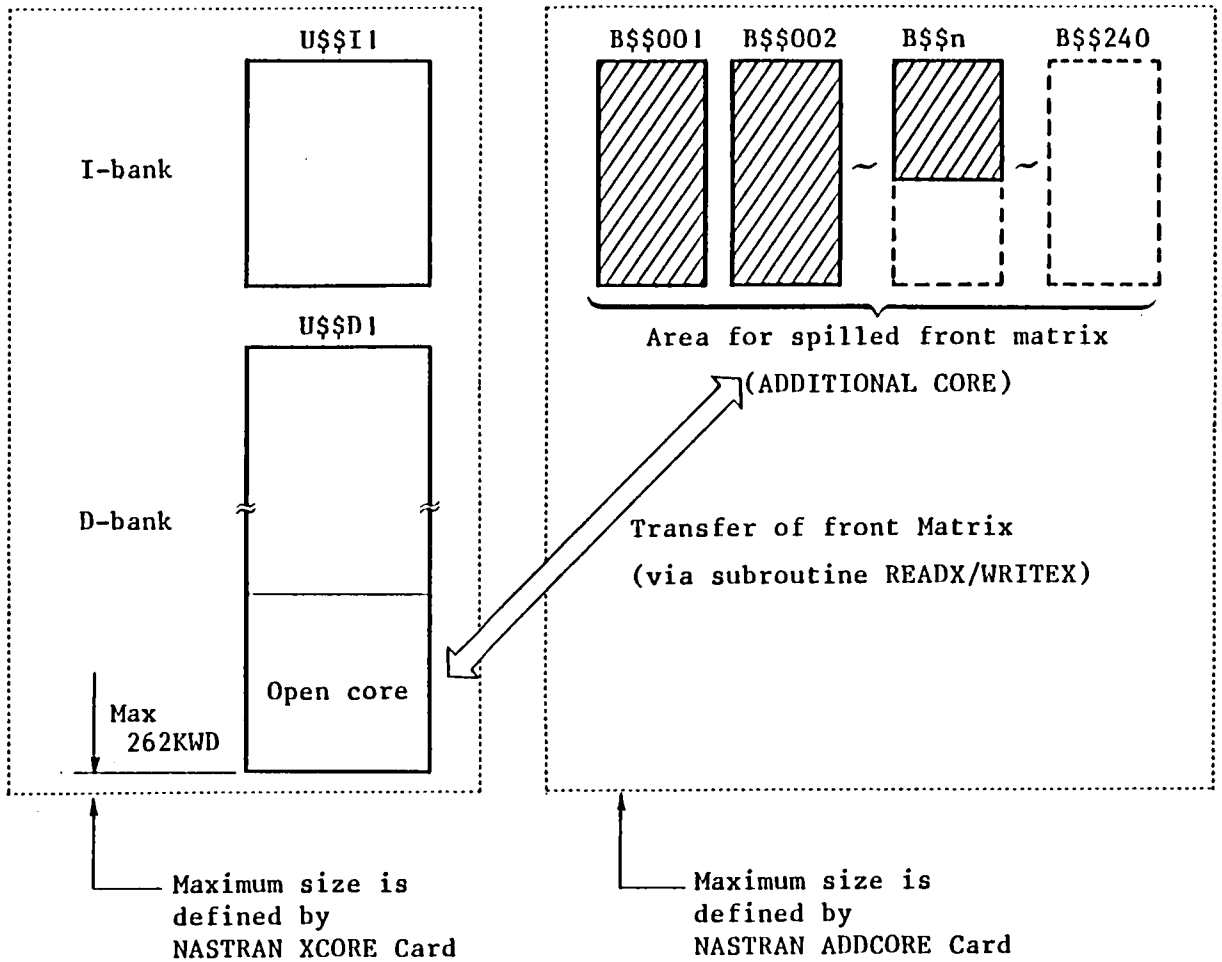

Bank name	Property	Contents
U$$I1	static	NASTRAN I-bank
U$$D1		NASTRAN D-bank
B$$001 ~ B$$240	dynamic	Area for spilled front matrix. Obtained by MCORE$ as much as required. Each bank size is the same as that of U$$I1.

Fig. 3.2 Bank structure

(a) Case A : old : 68KWD

new : 68KWD + ADDITIONAL CORE 24KWD

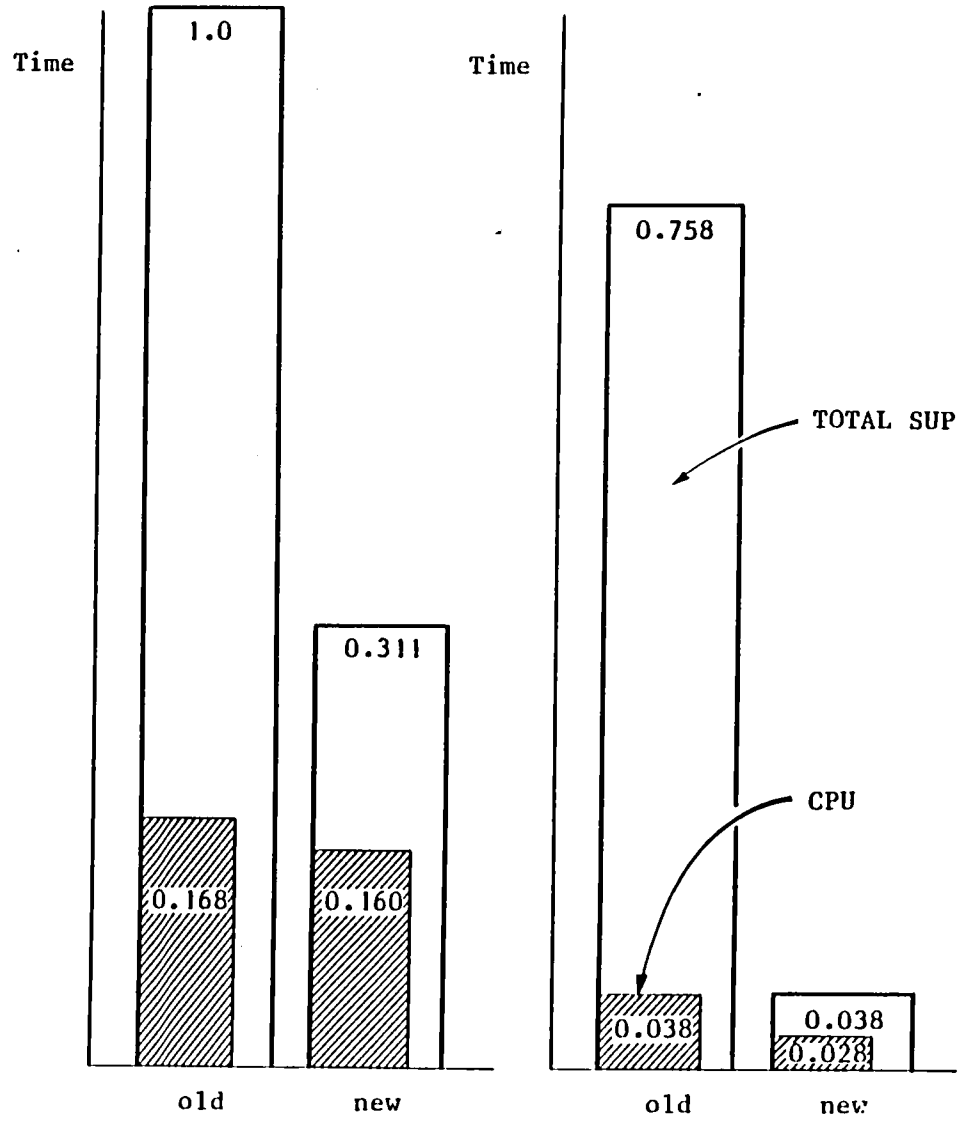

Case A

No. of Grid points	551
No. of Elements	992
B + C	230
N	2697

SUP in NASTRAN

	old	new
TOTAL SUP	1.0	0.311
CPU	0.168	0.160

SUP in SDCOMP

	old	new
TOTAL SUP	0.758	0.038
CPU	0.038	0.028

Fig. 3.3 Efficiency test - 1

(b) Case B : old : 200KWD

new : 200KWD + ADDITIONAL CORE 43KWD

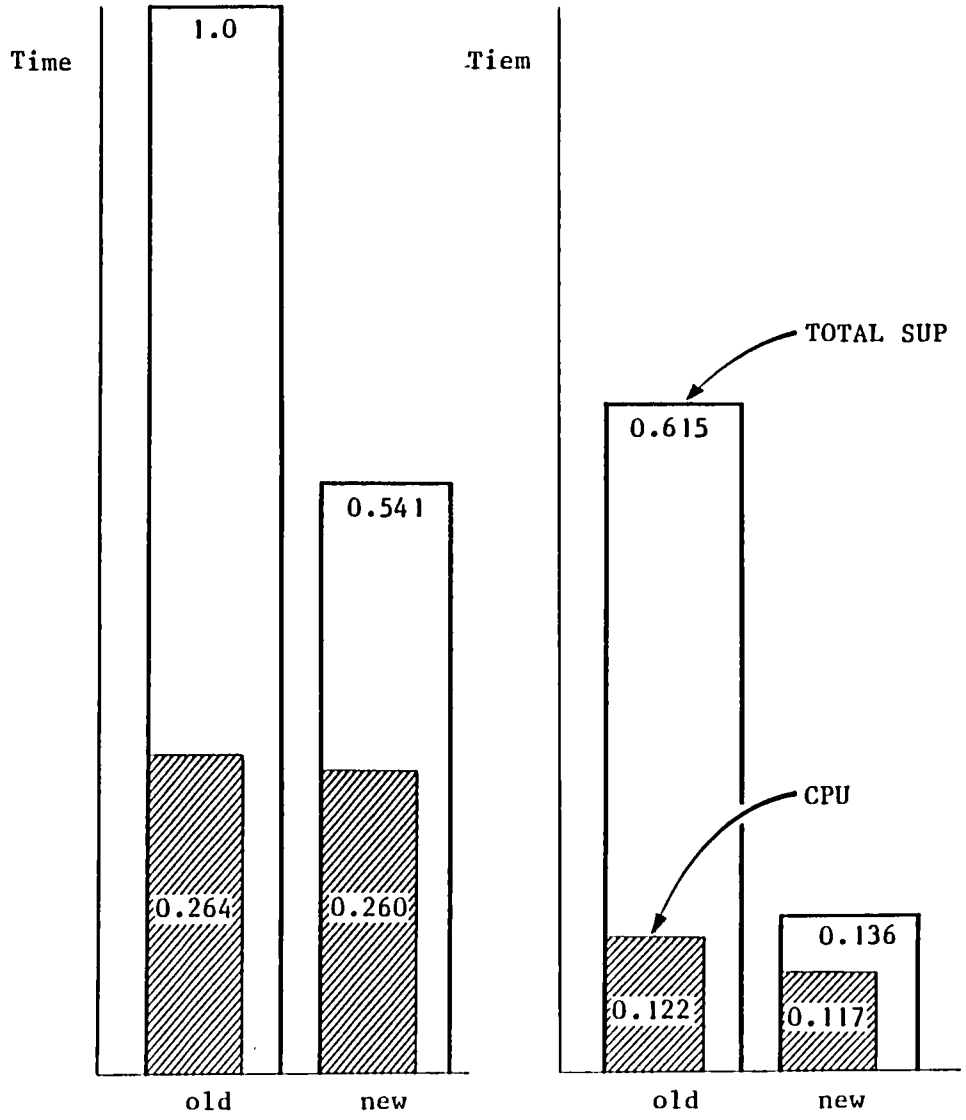

Case B

No. of GRID points	1061
No. of Elements	900
B + C	450
N	3966

SUP in NASTRAN

	old	new
TOTAL SUP	1.0	0.541
CPU	0.264	0.260

SUP in SDCOMP

	old	new
TOTAL SUP	0.615	0.136
CPU	0.122	0.117

Fig. 3.4 Efficiency test - 2

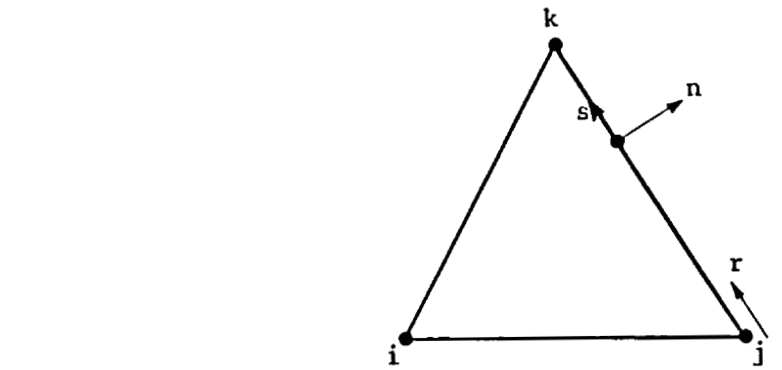

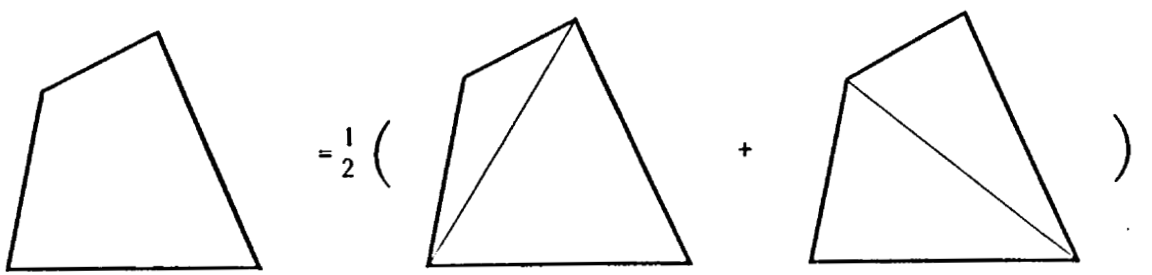

Fig. 4.1 TRIA3 and QUAD4

(3) Test Model

Triangular element

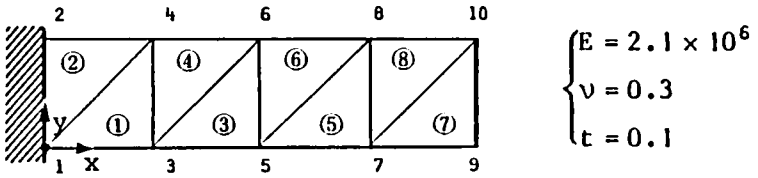

Quadrilateral element

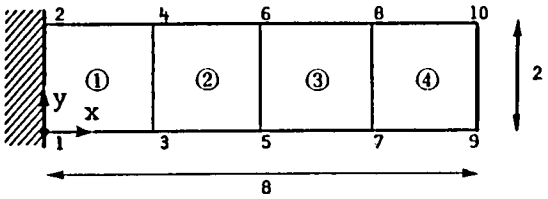

Loading Condition

① In plane Bending

-1.0 loading Y-direction on GRID 10.

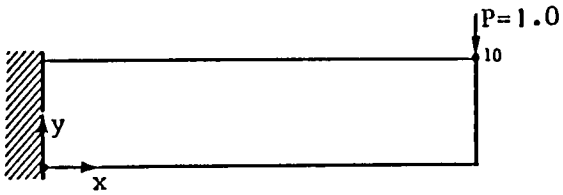

② Out of plane bending

-1.0 loading Z-direction on GRID 9 and 10.

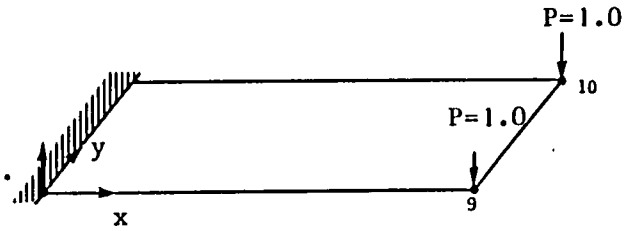

③ In plane tension

1.0 loaing X-direction on GRID 9 and 10.

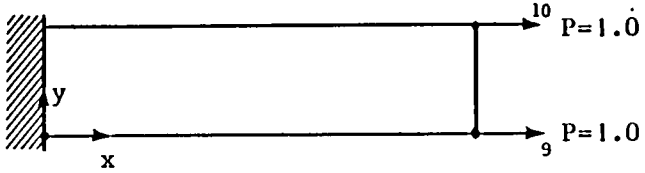

Fig. 4.2 Test Model for TRIA3 and QUAD4 element

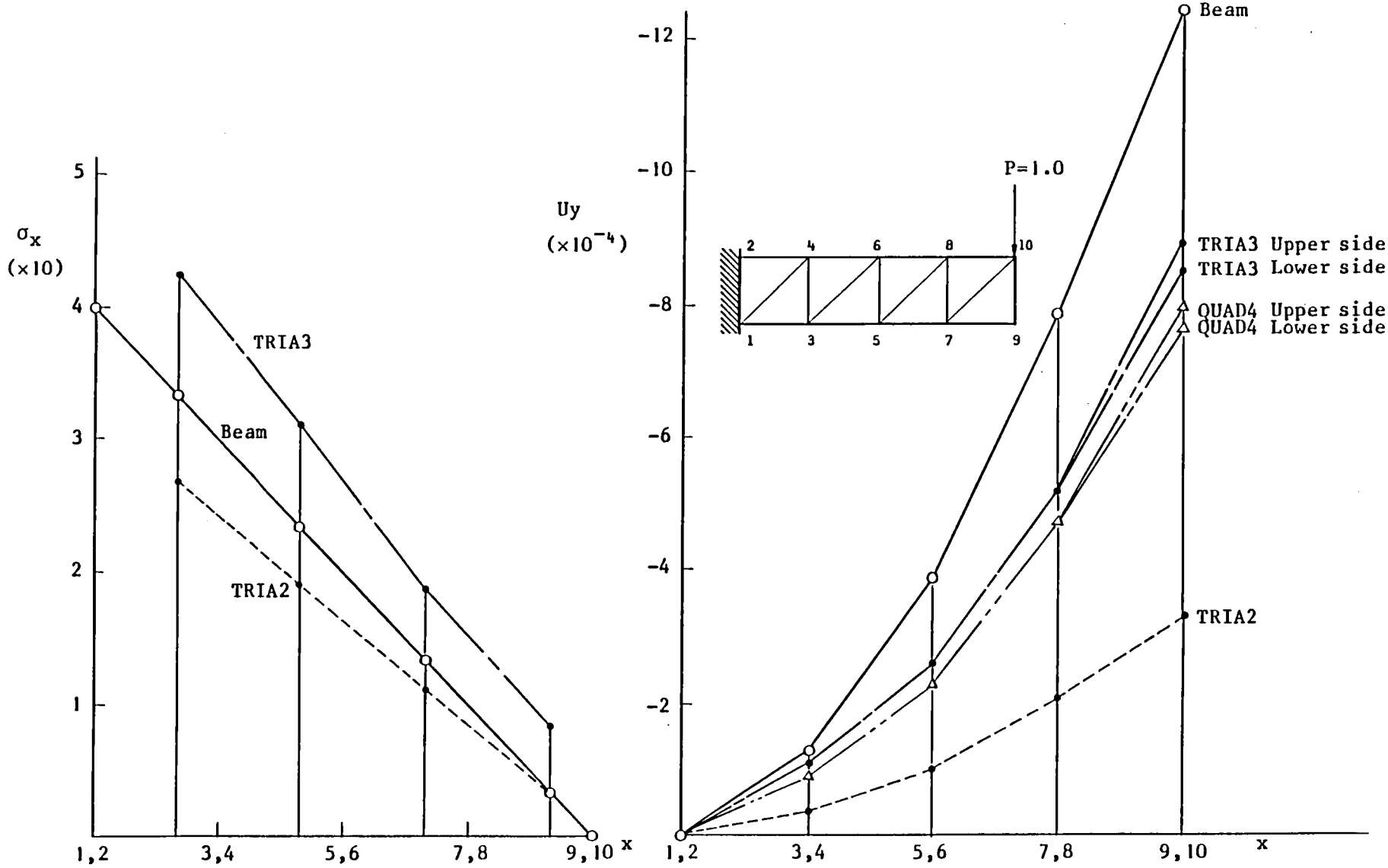

Fig. 4.3 Test Results of New Element - Inplane Bending

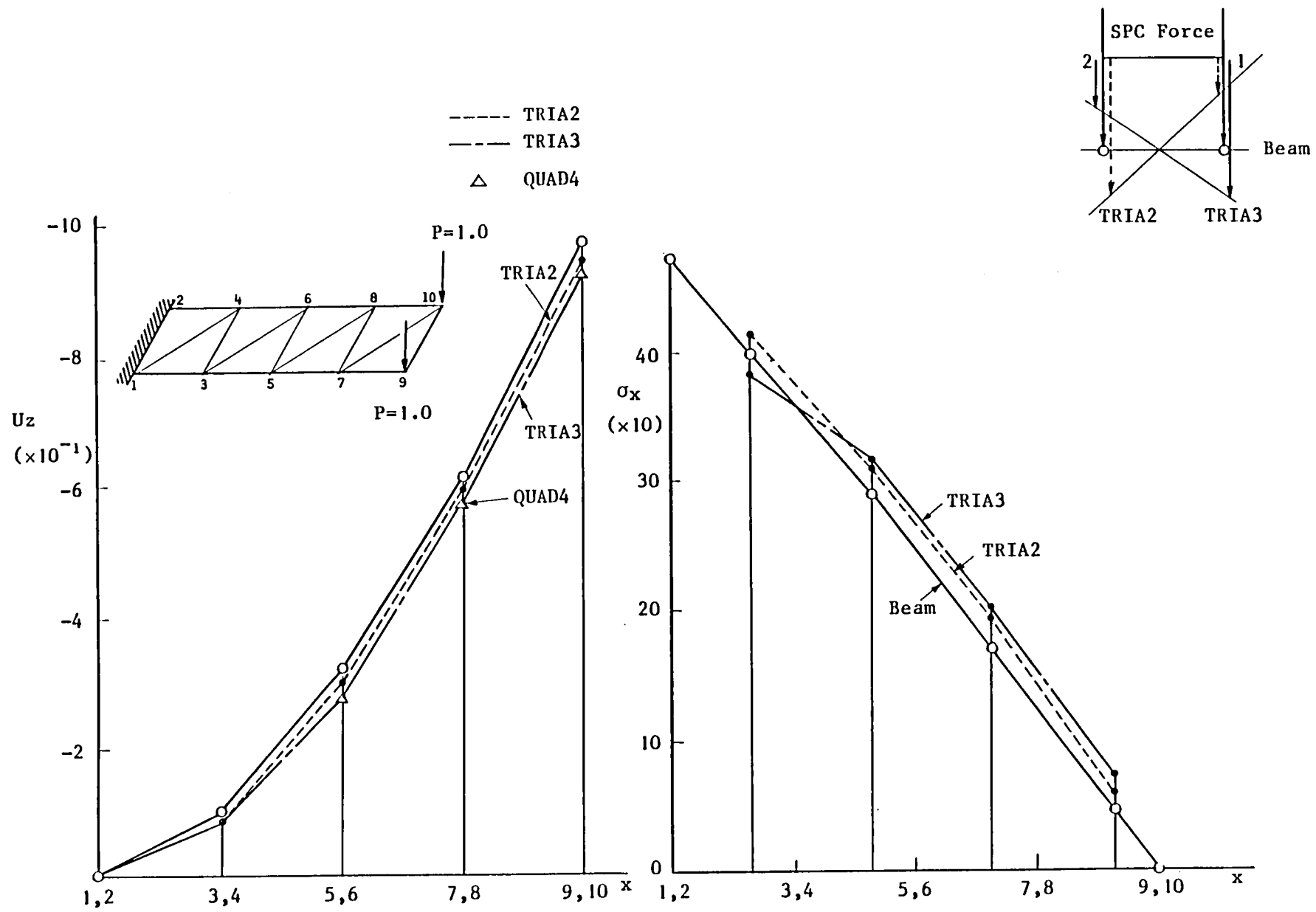

Fig. 4.4 Test Results of New Element - Out of Plane Bending

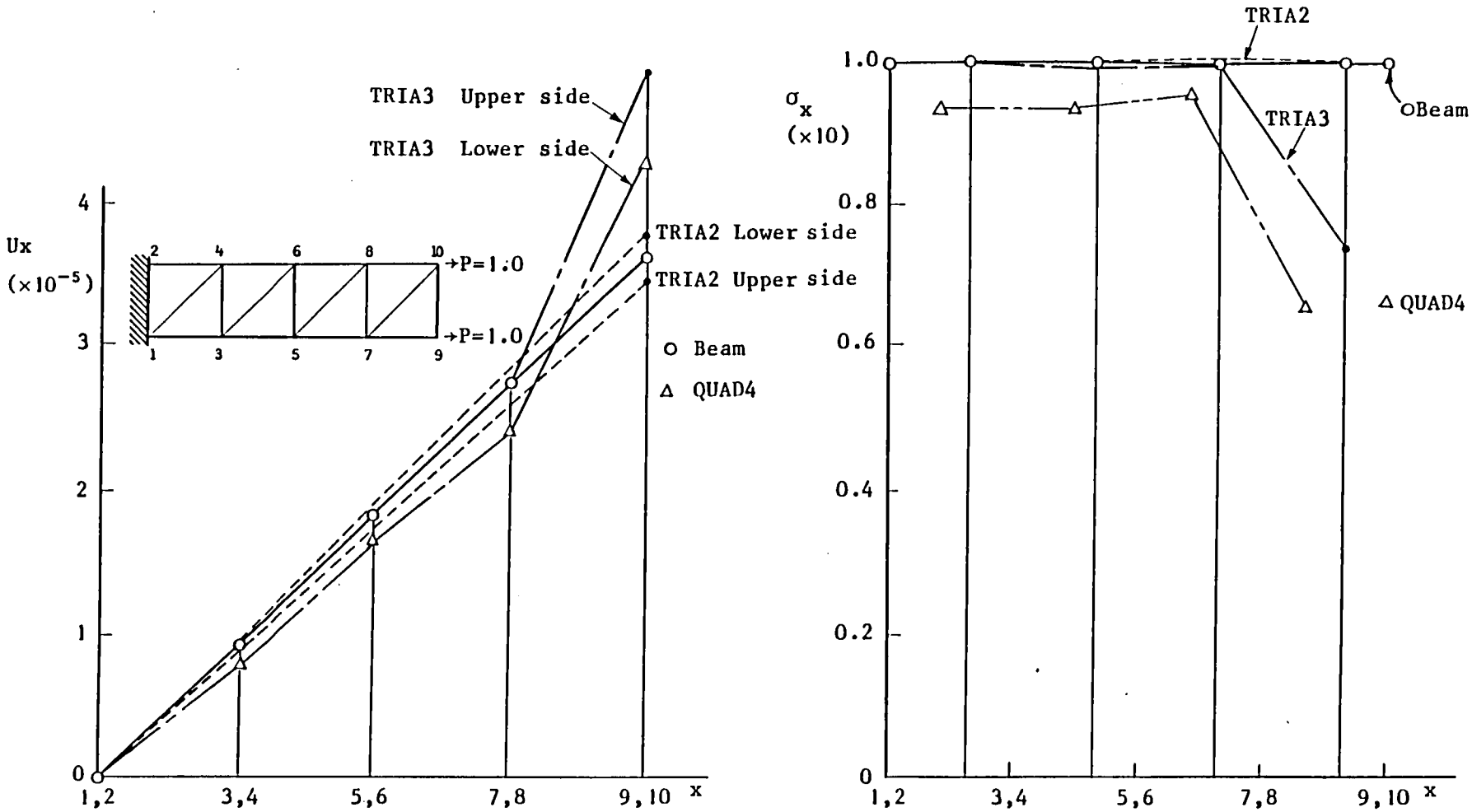

Fig. 4.5 Test Results of New Element - Inplane Tension

REFERENCES

1. Archie J. Jordan, Jr., William G. Ward : Modifications and Additions to NASTRAN at Marshall Space Flight Center.

   NASTRAN User's Experiences
   NASA TM X-2637, 1972

2. Caleb W. McCormick : Review of NASTRAN Development Relative to Efficiency of Execution.

   NASTRAN User's Experiences
   NASA TM X-2893, 1972

3. Ronald P. Schmitz : NASTRAN Maintenance and Enhancement Experiences.

   NASTRAN User's Experiences
   NASA TM X-3278, 1975

4. Edwin N. Hess : Dynamic Storage Expansion in NASTRAN.

   Seventh NASTRAN User's Colloquium
   NASA CP-2062, 1978

5. Shinichiro Harano : Improvements in Sparse Matrix Operations of NASTRAN.

   Ninth NASTRAN User's Colloquium
   NASA CP-2151, 1980

6. P. R. Pamidi : Recent Improvements and Enhancements to NASTRAN.

   Tenth NASTRAN User's Colloquium
   NASA CP-2249, 1982

7. "Sperry NASTRAN News letter" Vol.3 No.2 Sperry Support Services, Huntsville, Alabama, July 15, 1976

8. "Sperry NASTRAN Application Brief" 3.0 Sperry Support Services, Huntsville, Alabama, September 1, 1976

9. The NASTRAN User's Manual NASA SP-222 (01)

10. The NASTRAN Programmer's Manual NASA SP-223 (01)

11. Caleb W. McCormick : Sparse Matrix Operations in NASTRAN
    Proc. of 1973 Tokyo seminar on FEA, 1973 pp.611-631

12. T. H. H. Pian : Derivation of Element Stiffness Matrices by Assumed Stress Distribution. AIAA Journal Vol.2, 1964 pp.1333-1336

13. Yutaka Yoshida et al : A Flat Finite Element for Thin Shell Analysis Derived by Assumed Stress Approach. Proceedings of The Japan Society of Civil Engineers. No. 211, 1973

IMPROVED ISOPARAMETRIC SOLID AND MEMBRANE ELEMENTS

by

William R. Case and Richard E. Vandegrift
NASA/Goddard Space Flight Center
Greenbelt, Maryland 20771

Summary

Improvements that have been made to the COSMIC NASTRAN elements CIHEX1 and QDMEM1 are described. These elements are isoparametric representations of solid and membrane elastic behavior. Recent papers by the authors have shown the official COSMIC versions of these elements to be inferior to those available in the MacNeal-Schwendler Corporation (MSC) version of NASTRAN in that they are overly stiff for some loadings. Modifications have been made to these elements which reduce the order of integration for shear terms and, for the eight-mode solid element, add additional strain functions. The resulting element formulations give behavior similar to that of the MSC elements. The paper discusses the changes made in the element formulations and compares results of test problems with results from the official COSMIC elements and with the MSC elements.

Introduction

The isoparametric membrane quadrilateral element, QDMEM1, in COSMIC NASTRAN is a stand-alone element for use in modeling problems which exhibit plane stress behavior. It is a stand-alone element because there is no general plate element which currently uses the QDMEM1 for the membrane stiffness. In contrast, the MSC uses the QDMEM1 element for the membrane part of their QUAD4 general plate element.

The results of a finite element idealization study using all of the available membrane elements in NASTRAN was reported in [1]. Although the written version of the paper reported results only for elements available in MSC NASTRAN version 38, the version presented orally at the NASTRAN Colloquium showed results using both MSC-38 and COSMIC-15.5. As presented at the colloquium, there was a marked difference in results for the QDMEM1 elements from these two versions of NASTRAN. At the time, it was surmised that the discrepancy was due to a different manner in which the numerical integration was carried out in the two versions. In particular, it was shown that the COSMIC element exhibited overly stiff behavior for the problems investigated and that the MSC element was vastly superior.

A similar study was conducted by the authors for solid elements and reported in [2]. This study was aimed at finding the best of the available solid elements to model thermal and gravity deformation effects on optical mirrors. Of particular importance was investigation of problems that might be encountered with elements that have aspect ratios in the range of 5 to 10. Use of elements with this range of aspect ratio is necessary in modeling mirrors to avoid the need of extremely large models which would be required if element aspect ratios near unit were necessary. The results of

this study again clearly indicated the superiority of the MSC solid elements for modeling relatively thick plates for bending, as would occur for mirrors subjected to thermal gradients. For the eight-node solid isoparametric elements, it was again shown that there was a significant difference between the MSC element (HEXA-8) and the COSMIC element (CIHEX1). In addition, the COSMIC element showed extreme sensitivity to aspect ratio. Elements that had a thickness (in the plate thickness direction) smaller than its in-plane dimensions exhibited large errors. This was to be expected based on the above discussion of the membrane element deficiencies and the similarity of the formulation for the membrane and solid elements.

The purpose of the effort reported herein, then, was to investigate modifications that could be made to the COSMIC QDMEM1 and CIHEX1 elements which would improve their accuracy for modeling bending type behavior.

The next section discusses the cause of the overly stiff behavior of these elements. This has been investigated by others, [3] - [6], and is shown to be due to a parasitic shear that is introduced when these lower order isoparametric elements have bending modes of deformation.

The following section describes the modifications that are required for the CIHEX1 element in order for it to behave as the MSC HEXA-8 element. The authors gratefully acknowledge the MSC for providing the mathematical description [7] of their modifications to the eight-node solid element and the QUAD4 general shell element.

Following this is a brief description of the changes that are required for the QDMEM1 element, which consisted only of reducing the Gaussian integration order for the shear strain terms.

Finally, the results of several problems are presented showing the improvement of the modified COSMIC elements in comparison to the officially installed element.

Parasitic Shear in Bending in Lower Order Isoparametric Elements

The quadrilateral membrane element, QDMEM1, has four grid points with stiffness for the 2 in-plane degrees of freedom at each grid point yielding a total of 8 degrees of freedom for the element. As discussed in [3], the 8 degrees of freedom can be considered to be linear combinations of eight nodes of deformation, consisting of the three rigid body modes (two translation and one rotation in its plane) plus the following deformation modes:

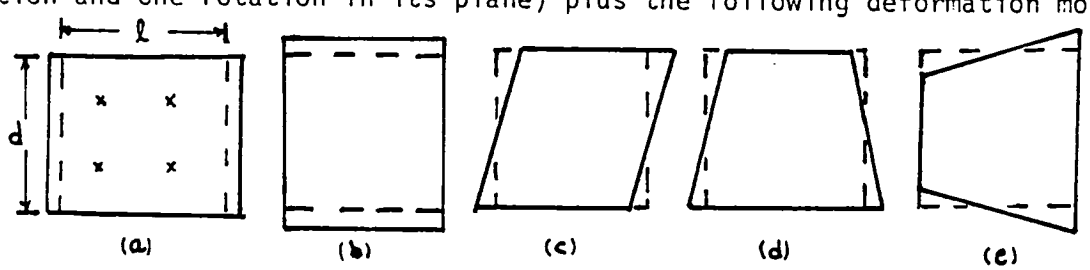

x: location of Gauss Points for 2x2 integration

Modes (a) — (c) are the three constant strain modes while (d) and (e) are similar to bending modes. Generally, Gaussian quadriture is used to evaluate the stiffness matrix for isoparametric elements in which case the 2x2 stiffness matrix for a pair of grid points is

$$\underset{\sim}{K}_{ij} = \sum_{q} w_q J_q \underset{\sim}{C}_{qi}^{T} \underset{\sim}{S}_q \underset{\sim}{C}_{qj}$$

The following section shows the details of this (for the 3-D element) with explanations of the terms.

For now, it is sufficient to point out that the summation in the above equation is over the Gauss points (four in this case) and that $\underset{\sim}{C}_{qi}$ is the matrix relating displacements at grid point i to strains at Gauss point q. At these Gauss points, the terms in the $\underset{\sim}{C}_{qi}$ matrix relating to shear strains are nonzero for the bending modes (d) and (e). Thus (d) and (e) modes will contribute shear strain energy in a situation where the element is used to model pure bending situations. In fact, as the element aspect ratio (ℓ/d) increases, this parasitic shear becomes a dominant part of the strain energy and the element becomes excessively stiff for modeling bending. If, instead of evaluating the terms in $\underset{\sim}{C}_{qi}$ which relate to shear strain at the Gauss points, terms were evaluated at the element center, it would be found that no shear strain energy would result in modes (d) and (e) since the shear strain is zero at the center. Then, since the shear is zero for modes (d) and (e) under this evaluation, modes (d) and (e) would indeed be pure bending; and the "effective" deformation in these modes would be:

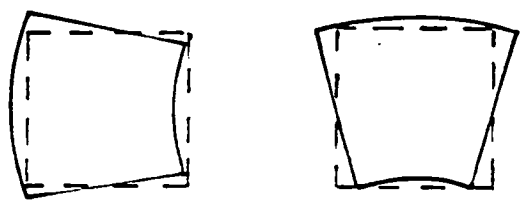

This is the motivation behind "reduced integration." One way to enforce the shear terms in $\underset{\sim}{C}_{qi}$ to be evaluated at the center is to use a 1x1 Gaussian integration (q=1) in evaluating the above stiffness matrix equation. However, another way (which preserves the element volume) is to use the required Gaussian integration order needed to exactly evaluate the volume integrals (2x2 in this case) and evaluate the appropriate $\underset{\sim}{C}_{qi}$ shear terms at the element center instead of at the Gauss point. It is this latter approach which is taken in modifying the COSMIC elements.

The solid isoparametric element CIHEX1 has the same difficulty but in three dimensions and is modified with a similar reduced order integration for shear.

Modified CIHEX1 Element

For a 3-D solid isoparametric element, the displacements at any point in the interior of the element are expressed as (see Figure 9)):

$$\underset{\sim}{\Delta} = \sum_i N_i \underset{\sim}{\Delta}_i \tag{1}$$

where

$$\underset{\sim}{\Delta} = \begin{Bmatrix} u(x,y,z) \\ v(x,y,z) \\ w(x,y,z) \end{Bmatrix}, \quad \underset{\sim}{\Delta}_i = \begin{Bmatrix} u_i \\ v_i \\ w_i \end{Bmatrix} \tag{2}$$

The summation on i is taken over all grid points of the element with $\underset{\sim}{\Delta}_i$ being the vector of grid point i displacements. The N_i are isoparametric interpolating functions in terms of the ξ, η, ζ coordinates which map the general hexahedron, in x,y,z coordinates into a rectangular parallelepiped in ξ, η, ζ coordinates. For an eight-node hex element:

$$N_i = \frac{1}{8}(1+\xi\xi_i)(1+\eta\eta_i)(1+\zeta\zeta_i) \tag{3}$$

with ξ_i, η_i, ζ_i the coordinates of grid point i

The element strains are related to displacements by

$$\underset{\sim}{\epsilon}_g = \sum_i \underset{\sim}{C}_{gi} \underset{\sim}{\Delta}_i \tag{4}$$

where

$$\underset{\sim}{\epsilon}_g^T = \begin{bmatrix} \epsilon_x & \epsilon_y & \epsilon_z & \gamma_{xy} & \gamma_{xz} & \gamma_{yz} \end{bmatrix}_g^T$$

is a vector of the element strains evaluated at the Gauss points

and

$$\underset{\sim}{C}_{gi} = \begin{bmatrix} N_{i,x} & 0 & 0 \\ 0 & N_{i,y} & 0 \\ 0 & 0 & N_{i,z} \\ N_{i,y} & N_{i,x} & 0 \\ 0 & N_{i,z} & N_{i,y} \\ N_{i,z} & 0 & N_{i,x} \end{bmatrix}_g \tag{5}$$

Note: $\sim$ under a quantity indicates it is a matrix.

where the comma denotes partial differentiation with respect to x,y, or z and the subscript g on the matrix indicates that the terms in the matrix are to be evaluated for ξ, η, ζ at a Gauss point. This is the form of the strain-displacement relationship for the classical eight-node hex element and is what is employed in the COSMIC CIHEX1 element. Element stresses at Gauss points are related to strains through

$$\underset{\sim}{\sigma}_g = \underset{\sim}{G}_g (\underset{\sim}{\epsilon}_g - \underset{\sim}{\alpha} T) \tag{6}$$

where $\underset{\sim}{G}_g$ is the 6x6 constitutive matrix of material constants at a Gauss point.

The element stiffness matrix is obtained using Gaussian quadriture from

$$\underset{\sim}{K}_{ij} = \sum_g w_g J_g \underset{\sim}{C}^T_{gi} \underset{\sim}{G}_g \underset{\sim}{C}_{gj} \tag{7}$$

where $\underset{\sim}{K}_{ij}$ is a 3x3 partition of the element stiffness matrix relating forces at grid point i to displacements at grid point j. For exact integration of the eight-node hex element, a 2x2x2 (g=8) Gaussian quadriture must be employed. Wg and Jg are Gauss integration weights and Jacobian.

It has been observed that the stiffness matrix thus derived can exhibit overly stiff behavior when modeling bending situations due to the presence of parasitic shear in the element. One technique of overcoming this difficulty is to employ a reduced integration (i.e., g less than 2x2x2). However, a general reduction of the integration order is not needed and can indeed lead to singular stiffness even when the element is restrained in a rigid body fashion. Instead, selective reduced integration is employed wherein only the terms in equation (7) which relate to shear strains have their integration order reduced.

The HEXA eight-mode element in MSC NASTRAN employs reduced integration for shear. As explained by R. Harder [7], the MSC element uses for $\underset{\sim}{C}_{gi}$ the modified form:

$$\underset{\sim}{C}^r_{gi} = \begin{bmatrix} N_{i,x} & 0 & 0 \\ 0 & N_{i,y} & 0 \\ 0 & 0 & N_{i,z} \\ \bar{N}_{i,y} & \bar{N}_{i,x} & 0 \\ 0 & \bar{N}_{i,z} & \bar{N}_{i,y} \\ \bar{N}_{i,z} & 0 & \bar{N}_{i,x} \end{bmatrix}_g \tag{8}$$

The terms in the upper half of equation (8) are identical to the form used in the classical isoparametric element. The terms in the lower portion of $\underset{\sim}{C}^{r}_{qi}$ are different from their classical counterparts due to employing a reduced integration scheme. Harder proposes to use a Gaussian weighted average of the $N_{i,x}$, etc., to obtain $\bar{N}_{i,x}$, etc.

$$\left(\bar{N}_{i,x}\right)_q = \frac{\sum_{\text{group}} J_g \left(N_{i,x}\right)_g}{\sum_{\text{group}} J_g} \tag{9}$$

with a similar definition for $\bar{N}_{i,y}$ and $\bar{N}_{i,z}$. The summations in equation (9) are taken over some of the Gauss points. In particular, when evaluating terms in the fourth row of equation (8), the group summation is over all Gauss points in the plane in which ζ is a constant. For terms in the fifth row, the group is all points in a plane of constant ξ and, for the sixth row, a plane of constant η. Harder shows that this Gaussian weighted averaging (thus reduced integration) scheme is necessary for the element to maintain its capability to pass a constant strain patch test.

In addition to employing this reduced integration for the shear terms, by averaging the related $\underset{\sim}{C}_{qi}$ coefficients, Harder also employs additional "strain functions" in the MSC element to allow higher order polynomial variation of the direct strain terms. Strain functions are somewhat like bubble modes (see, for example, [8]), which have been used in some elements to also overcome their relatively stiff behavior in bending problems. Conceptually, the additional strain terms are included by modifying the basic strain-displacement relation of equation (4). Following the development in [7]:

$$\underset{\sim}{\epsilon}_q = \sum_i \underset{\sim}{C}^{r}_{qi}\, \underset{\sim}{\Delta}_i + \underset{\sim}{C}_{q0}\, \underset{\sim}{\Delta}_0 \tag{10}$$

where $\underset{\sim}{C}^{r}_{qi}$ is the classical $\underset{\sim}{C}_{qi}$ modified to represent the reduced order integration for shear.

$\underset{\sim}{C}_{q0}$ is a 6xn matrix of strain coefficients and $\underset{\sim}{\Delta}_0$ a vector of the amplitudes of the n strain functions added. Recognizing that the strain energy for a linear material element is

$$U = \frac{1}{2} \sum_q w_q J_q \underset{\sim}{\epsilon}^{T}_q \underset{\sim}{\sigma}_q$$

and minimizing U with respect to the $\underset{\sim}{\Delta}_0$ amplitudes (keeping mind that $\underset{\sim}{\sigma}_q$ is a function of $\underset{\sim}{\Delta}_0$ through equations (6) and (10), it is found that

$$\frac{\partial U}{\partial \underset{\sim}{\Delta}_0} = 0 = \sum_q w_q J_q \underset{\sim}{C}^{T}_{q0}\, \underset{\sim}{\sigma}_q \tag{11}$$

Using (6) and (10) in (11), the $\underset{\sim}{\Delta}_0$ amplitudes are found as

$$\underset{\sim}{\Delta}_0 = \underset{\sim}{K}^{-1}_{00} \sum_i \underset{\sim}{K}^{r}_{0i}\, \underset{\sim}{\Delta}_i \tag{12}$$

where

$$\underset{\sim}{K}_{oo} = \sum_{g} w_g J_g \underset{\sim}{C}_{go}^{T} \underset{\sim}{G}_g \underset{\sim}{C}_{go} \tag{13}$$

$$\underset{\sim}{K}_{oi}^{r} = \sum_{g} w_g J_g \underset{\sim}{C}_{go}^{T} \underset{\sim}{G}_g \underset{\sim}{C}_{gi}^{r} \tag{14}$$

Finally, in combining (10) and (12), it is found that the strain displacement law in terms of only the physical degrees of freedom, $\underset{\sim}{\Delta}_i$, is

$$\underset{\sim}{\epsilon}_g = \sum_{i} \underset{\sim}{\bar{C}}_{gi} \underset{\sim}{\Delta}_i \tag{15}$$

where

$$\underset{\sim}{\bar{C}}_{gi} = \underset{\sim}{C}_{gi}^{r} - \underset{\sim}{C}_{go} \underset{\sim}{K}_{oo}^{-1} \underset{\sim}{K}_{oi}^{r} \tag{16}$$

With equation (15), the element stiffness matrix for the MSC eight-node hex element is generated as in equation (7) but with $\underset{\sim}{\bar{C}}_{gi}$ being used instead of $\underset{\sim}{C}_{gi}$. It remains to select the strain functions to be added--i.e., the terms in the $\underset{\sim}{C}_{go}$ matrix. In general, the $\underset{\sim}{C}_{go}$ terms are added to fill a need in terms of improvement in element accuracy for some particular application. Addition of these terms will almost certainly invalidate the interelement displacement continuity that exists with the classical element. However, this is not as significant as insuring that the modified element will still be capable of passing a constant strain patch test (see [9]) for a discussion of the patch test). Given the fact that the classical element does pass the constant strain patch test, Harder shows that the reduced integration technique will also pass the patch test and in order for the completely modified element to pass the patch test, it is required that:

$$\sum_{g} w_g J_g \underset{\sim}{C}_{go}^{T} \underset{\sim}{\sigma}_g = 0 \tag{17}$$

For a constant patch stress, and keeping in mind that $w_g = 1.0$ for the eight-node hex, equation (17) requires

$$\sum_{g} J_g \underset{\sim}{C}_{go}^{T} = 0 \tag{18}$$

As pointed out in [7], this can be accomplished if the terms in $\underset{\sim}{C}_{go}$ are of the form

$$\xi_g/J_g \;,\; \eta_g/J_g \;,\; \zeta_g/J_g \;,\; \xi_g\eta_g/J_g \;,\; \ldots.$$

Thus, the MSC element uses for $\underset{\sim}{C}_{go}$:

$$\underset{\sim}{C}_{go} = \frac{1}{J_g} \begin{bmatrix} \xi & 0 & 0 & \xi\eta & 0 & \xi\zeta \\ 0 & \eta & 0 & \xi\eta & \eta\zeta & 0 \\ 0 & 0 & \zeta & 0 & \eta\zeta & \xi\zeta \\ 0 & 0 & 0 & 0 & 0 & 0 \\ 0 & 0 & 0 & 0 & 0 & 0 \\ 0 & 0 & 0 & 0 & 0 & 0 \end{bmatrix}_g \tag{19}$$

Only terms are included in the first three rows as only the direct stresses are sought to be modified by the additional strain functions. It is not clear exactly why the particular form for $\underset{\sim}{C}_{q0}$ was chosen, aside from the considerations in equation (18); however, it is the form identified by Harder in [7].

Equation (16) is the form of the strain-displacement law that was used in the modified CIHEX1 element reported herein, with equations (8), (13), (14), and (19) defining the various terms in (16). This $\underset{\sim}{\bar{C}}_{qi}$ matrix must be used in the development of the stiffness matrix as well as the thermal load vector and in stress data recovery.

Modified QDMEM1 Element

For the 2-D isoparametric element, the stiffness matrix has the same general form as shown in the previous section:

$$\underset{\sim}{K}_{ij} = \sum_q w_q J_q \underset{\sim}{C}_{qi}^T \underset{\sim}{E}_q \underset{\sim}{C}_{qj} \quad , \quad \underset{\sim}{\Delta}_i = \begin{Bmatrix} u_i \\ v_i \end{Bmatrix} \tag{20}$$

However, for this element

$$\underset{\sim}{\epsilon}_q = \begin{Bmatrix} \epsilon_x \\ \epsilon_y \\ \gamma_{xy} \end{Bmatrix}_q \tag{21}$$

and

$$\underset{\sim}{C}_{qi} = \begin{bmatrix} N_{i,x} & 0 \\ 0 & N_{i,y} \\ N_{i,y} & N_{i,x} \end{bmatrix}_q \tag{22}$$

$$N_i = \tfrac{1}{4}(1+\xi\xi_i)(1+\eta\eta_i) \tag{23}$$

Following the procedure of the previous section, reduced integration for shear terms is employed by modifying (22) to

$$\underset{\sim}{C}^r_{qi} = \begin{bmatrix} N_{i,x} & 0 \\ 0 & N_{i,y} \\ \bar{N}_{i,y} & \bar{N}_{i,x} \end{bmatrix}_q \tag{24}$$

As in the previous section, the $\bar{N}$ terms could be defined as Jacobian weighted averages of the terms at the Gauss points. However, for this element, it is found that the same result is obtained if the terms are evaluated at the center of the element ($\xi=\eta=0$). Thus

$$\left(\bar{N}_{i,x}\right)_q = N_{i,x}(\xi=\eta=0) \quad , \quad \left(\bar{N}_{i,y}\right)_q = N_{i,y}(\xi=\eta=0)$$

MSC also uses strain functions for this element. From [7], for the membrane part of the QUAD4 general shell element

$$\underset{\sim}{C}_{q0} = \begin{bmatrix} \xi & 0 \\ 0 & \eta \\ 0 & 0 \end{bmatrix}_q$$

The complete formulation of $\bar{C}_{qi}$ then follows as in the previous section and $\bar{\underset{\sim}{C}}_{qi}$ would then be used in equation (20) instead of $\underset{\sim}{C}_{qi}$. For the modifications made to the COSMIC QDMEM1 element, however, the additional strain functions in $\underset{\sim}{C}_{q0}$ were not implemented. Only the reduced integration for shear was implemented; and, therefore, $\underset{\sim}{C}^{r}_{qi}$ is used in equation (20) instead of $\underset{\sim}{C}_{qi}$.

Code Changes to Implement Modified CIHEX1 Element

The purpose of the authors' work was to prove the worth and feasibility of the element formulations. Optimizing the implementation of the code changes was not examined. Therefore, a complete discussion of the modifications will not be provided; however, a mention of the extent of the changes and the subroutines where they appear is appropriate.

The alterations to the QDMEM1 were accomplished with a simple modification to the QDMM1D subroutine. At the point where partitions of the stiffness are numerically integrated, terms which include the shear modulus were separated. This allowed the order of Gaussian integration to be selected separately for in-plane stress and shear stress terms. As discussed earlier, the need was for a linear shear stress formulation. The current implementation does not implement aniosotropic materials.

The XIHEX subroutine, which calculates the mass and stiffness matrices for the CIHEX1, as well as the CIHEX2 and CIHEX3, received extensive modifications. Since the IHEX subroutine recalculates part of the element's stiffness in order to form temperature loads, it required some similar changes. The CIHEX2 and CIHEX3 formulations were not considered, and alterations to the CIHEX1 stress recovery subroutine have not been developed at this time.

The initial formulation of the CIHEX1 element matrices in COSMIC NASTRAN was made in the basic coordinate system. Due to the manner in which the reduced integration for shear was implemented in the modified element, it was necessary to develop the CIHEX1 matrices in a local element coordinate system nearly aligned with the ξ, η, ζ axes and then transform the matrices to the basic coordinate system. Additional subroutines needed to accomplish these tasks were written by the authors. Several options for selection of the "best" initial local system were looked at and are still being evaluated. For rectangular parallelepiped elements, the choice of a local system is trivial. For skewed elements, the ξ, η, ζ directions do not form an orthogonal set of vectors in x,y,z; so the choice of the initial local coordinate system is not obvious.

Test Problems

QDMEM1 Element

The test problems are the same as those utilized in the prior mesh study of the membrane elements reported in [1] and involved a deep cantilevered beam type structure with unit depth and beam aspect ratio (length/depth) of two. Figure 1 shows the geometry, coordinate system, boundary conditions, and beam physical properties used in the study. Membrane elements formed the beam model. The mesh subdivision technique as well as the method used to indicate mesh size and element aspect ratio are demonstrated in Figure 2.

The finite element model used work equivalent grid point forces for separate end moment and end shear loadings. This simulated the applied loads as well as the reactions at the cantilevered end (Figure 3). One should note, from Figure 1, that only kinematic constraints were imposed. Discussion of the theoretical solutions to these loading conditions can be found in [1].

In order to assess the effect of the reduced integration modification to the QDMEM1 element, the figures from [1] for the older membrane element mesh study were utilized. These curves, figure 4 through figure 8 herein, show the error in displacements and stresses at specific points on the beam as a function of mesh refinement or aspect ratio. The MSC element referred to in these figures is a CQUAD4 with only membrane properties specified on its PSHELL card; also, the 2,1 or 4,1 after COSMIC '84 refers to the number of Gaussian integration points for in-plane stress and shear stress terms, respectively. As indicated on the figures, the altered COSMIC element '84 w/4,1 reduced integration produces the same answers as the MSC element; and these answers are an improvement over the old COSMIC element.

CIHEX1 Element

The premise for selecting a test problem in [2] was the fact that solid elements are used to model large optical mirrors of spaceborne telescopes, and these mirrors often have thicknesses of as much as 10 percent of their diameter. The test problem involved a cubic slab of equal dimension in the x-y plane and whose thickness varies between one-twentieth and one half of the x-y plane dimensions. Figure 10 shows the geometry, coordinate system, boundary conditions, and basic material information used in the study. The constraints are kinematic and the problem is symmetric about the x=0 plane. That is, the x displacement is zero along the x=0 plane. Using this constraint, only half the slab needed to be included in the finite element model. The mesh subdivision technique and method used to indicate element aspect ratio is shown in Figure 11.

Originally, the test cases were chosen to measure the accuracy of various solid elements under temperature gradient and gravity loadings. Their value to this paper lies in that they provide separate bending and shear load cases. The linear temperature gradient produced a symmetric bending condition with a known theoretical answer. The gravity loading, however, was found to be non-converging and was used in this study only to show the

effect of the changes to CIHEX1 under a shear loading case. Further discussion of these load cases is provided in [2].

In order to assess effects of the changes to CIHEX1, three graphs were extracted from [2]. Data for the altered CIHEX1 was added to these graphs, which already included curves representing the original CIHEX1. Figures 13 and 14 present error in displacement, at a particular point, as a function of mesh size and aspect ratio, respectively. Actual displacements versus mesh size are shown in Figure 15 for the (non-convergent) gravity loading. Once again, the important factor to note in these graphs is that for each case the "improved" CIHEX1 provided the same answers as the comparable eight-node MSC element. For an aspect ratio of 10, not at all unreasonable when modeling large mirrors, the changes to the element totally eliminated a 48 percent error (in the temperature gradient case) when the old CIHEX1 element was used.

Conclusions

Modifications to the isoparametric membrane and solid elements, QDMEM1 and CIHEX1, have been implemented in the COSMIC NASTRAN code.

The modified CIHEX1 element performs identically to the MSC HEXA eight-mode element. With the modifications, especially the reduced shear integration, it is anticipated that the new element will perform better when modeling thick plates when only few elements are used through the thickness. In addition, for pure bending, the element gives exact answers when only one element is used through the thickness.

The modified QDMEM1 element has been shown to be superior to the original element when modeling bending situations. Neither element exhibits aspect ratio sensitivity in the modified form as it did in its original form.

References

1. Case, W. R., and Mason, J. B., NASTRAN Finite Element Idealization Study, Sixth NASTRAN Users Colloquium, NASA Conference Publication 2108, 1977, pp. 383-404.

2. Case, W. R., and Vandegrift, R.E., Accuracy of Three Dimensional Solid Finite Elements, Twelfth NASTRAN Users Colloquium, NASA Conference Publication 2328, 1984, pp. 26-46.

3. Pawsy, S. F., and Clough, R. W., Improved Numerical Integration of Thick Shell Finite Elements, International Journal for Numerical Methods in Engineering, Vol. 3, pp. 575-586 (1971).

4. Zienkiewicz, O. C., et al, Reduced Integration Technique in General Analysis of Plates and Shells, International Journal for Numerical methods in Engineering, Vol. 3, pp. 275-290 (1971).

5. MacNeal, R. H., A Simple Quadrilateral Shell Element, Computers and Structures, Vol. 8, pp. 175-183 (1978).

6. Irons, B. M. R., and Helen, R. K., On Reduced Integration in Solid isoparametric Elements When Used in Shells with Membrane Modes, International Journal for Numerical methods in Engineering (short communication), Vol. 7, pp. 1179-1182 (1975).

7. MacNeal-Schwendler Corporation Internal Memo No. RLH-35, Modified Isoparametric Finite Elements and Patch Tests, September 16. 1982.

8. Gallagher, R. H., Finite Element Analysis Fundamentals, 1975, Prentice Hall.

9. MacNeal-Schwendler Corporation, A Proposed Set of Problems to Test Finite Element Accuracy, MSC/NASTRAN Application Manual, Application Note, March 1984.

NOTATION

AR = PROBLEM ASPECT RATIO

AR_e = ELEMENT ASPECT RATIO

ND = NUMBER OF ELEMENTS THROUGH DEPTH

NL = NUMBER OF ELEMENTS ALONG LENGTH

FIG. 1

BEAM GEOMETRY AND PROPERTIES

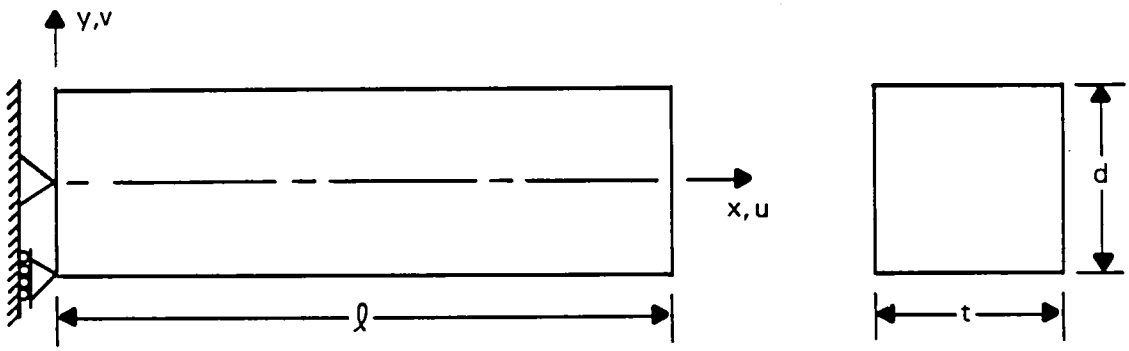

$$\ell = \begin{cases} .0508 \text{ M } (2.0 \text{ IN}) \text{ BASIC DEEP BEAM FOR MESH STUDY} \\ \text{VARIABLE FOR ASPECT RATION STUDY} \end{cases}$$

d = .0254 M (1.0 IN)

t = .0254 M (1.0 IN)

$E = 1.9305 \times 10^{10}$ N/m^2 (28×10^6 LB/IN^2)

$\nu = 0.3$

u = v = o AT x = y = o AND u = o AT x = o, y = −d/2

FIG. 2

FINITE ELEMENT MODEL MESH PATTERNS MEMBRANE ELEMENTS

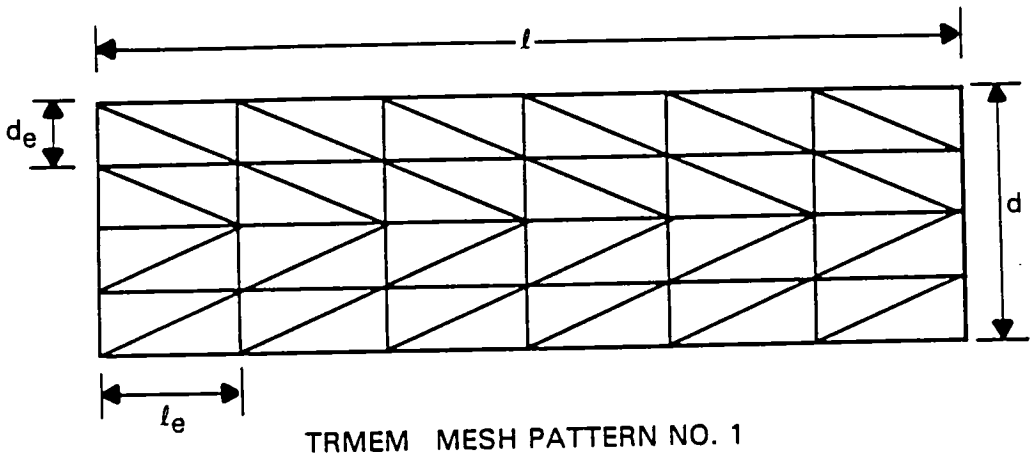

$AR_e = \ell_e/d_e$

$AR = \ell/d$

TRMEM MESH PATTERN NO. 1

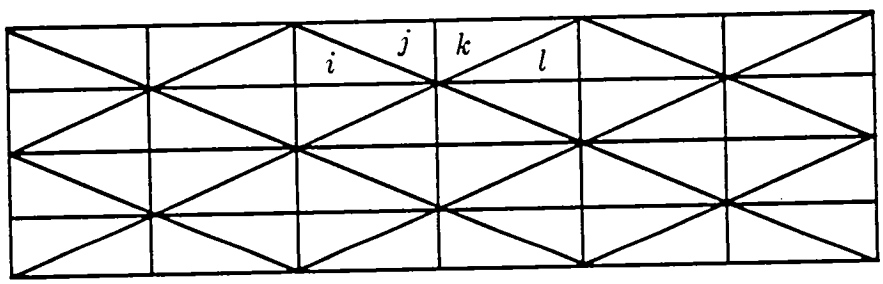

TRMEM MESH PATTERN NO. 2

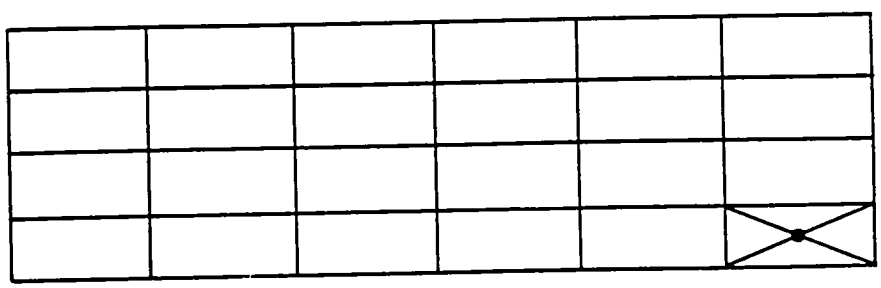

EXTRA NODE—QDMEM2 ELEMENT ONLY

QDMEM, QDMEM1, QDMEM2 MESH PATTERNS

FIG. 3

BEAM LOADS

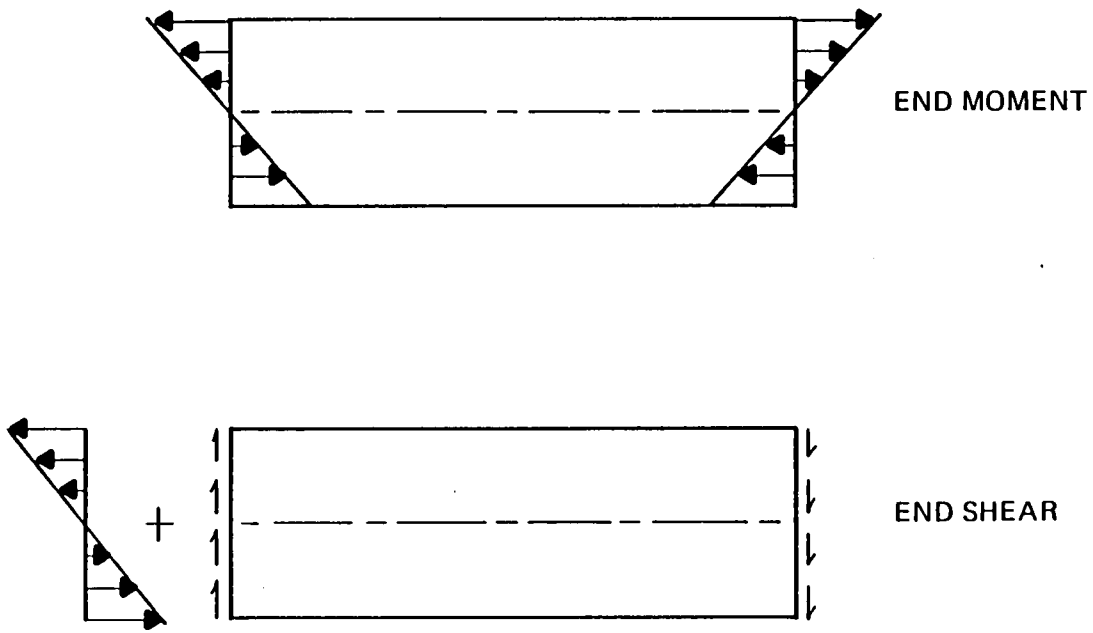

FIG. 4
TIP DEFLECTION ERROR
DEEP BEAM-END MOMENT LOADING
(MESH SIZE STUDY)

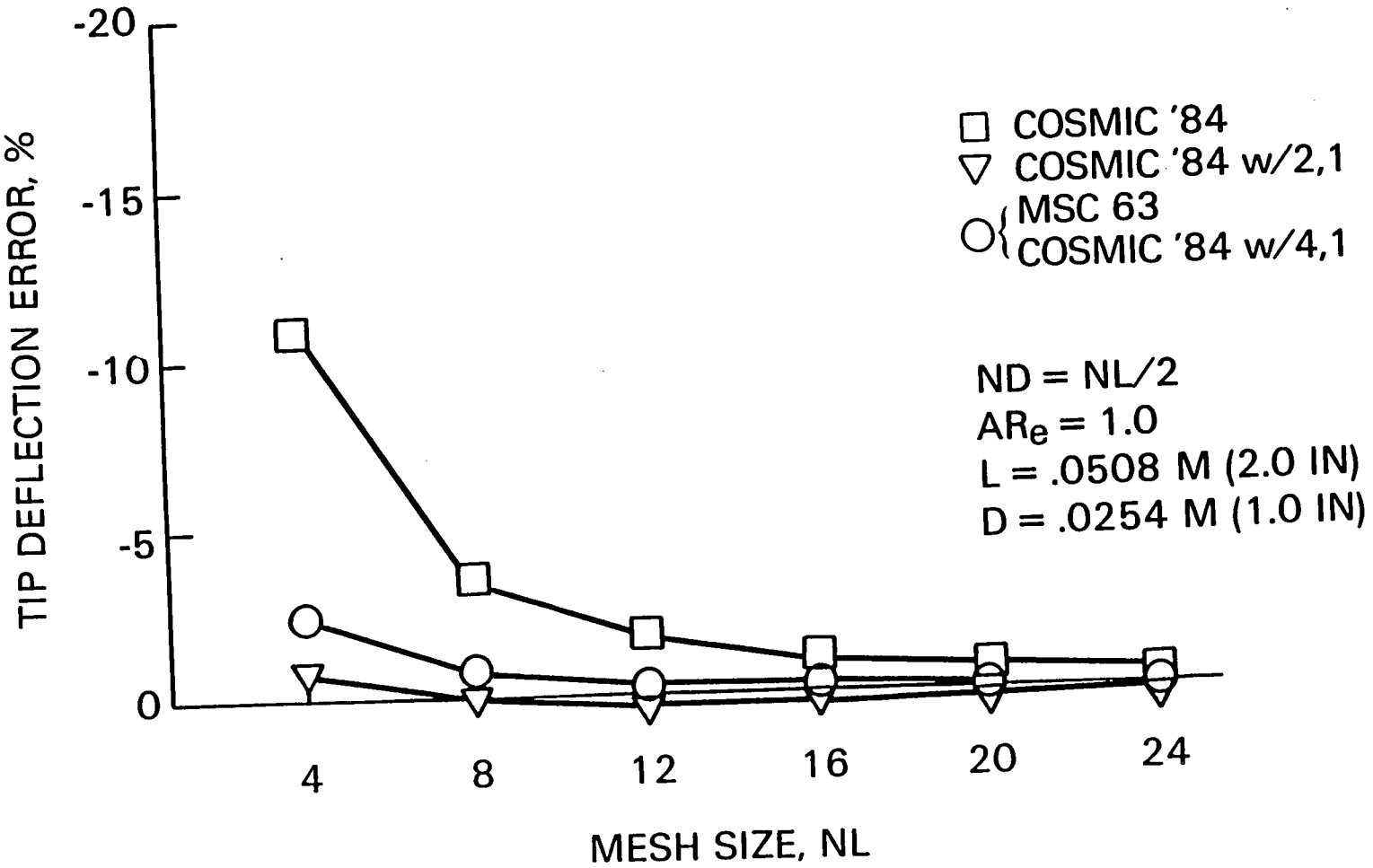

FIG. 5
TIP DEFLECTION ERROR
DEEP BEAM-END SHEAR LOADING
(MESH SIZE STUDY)

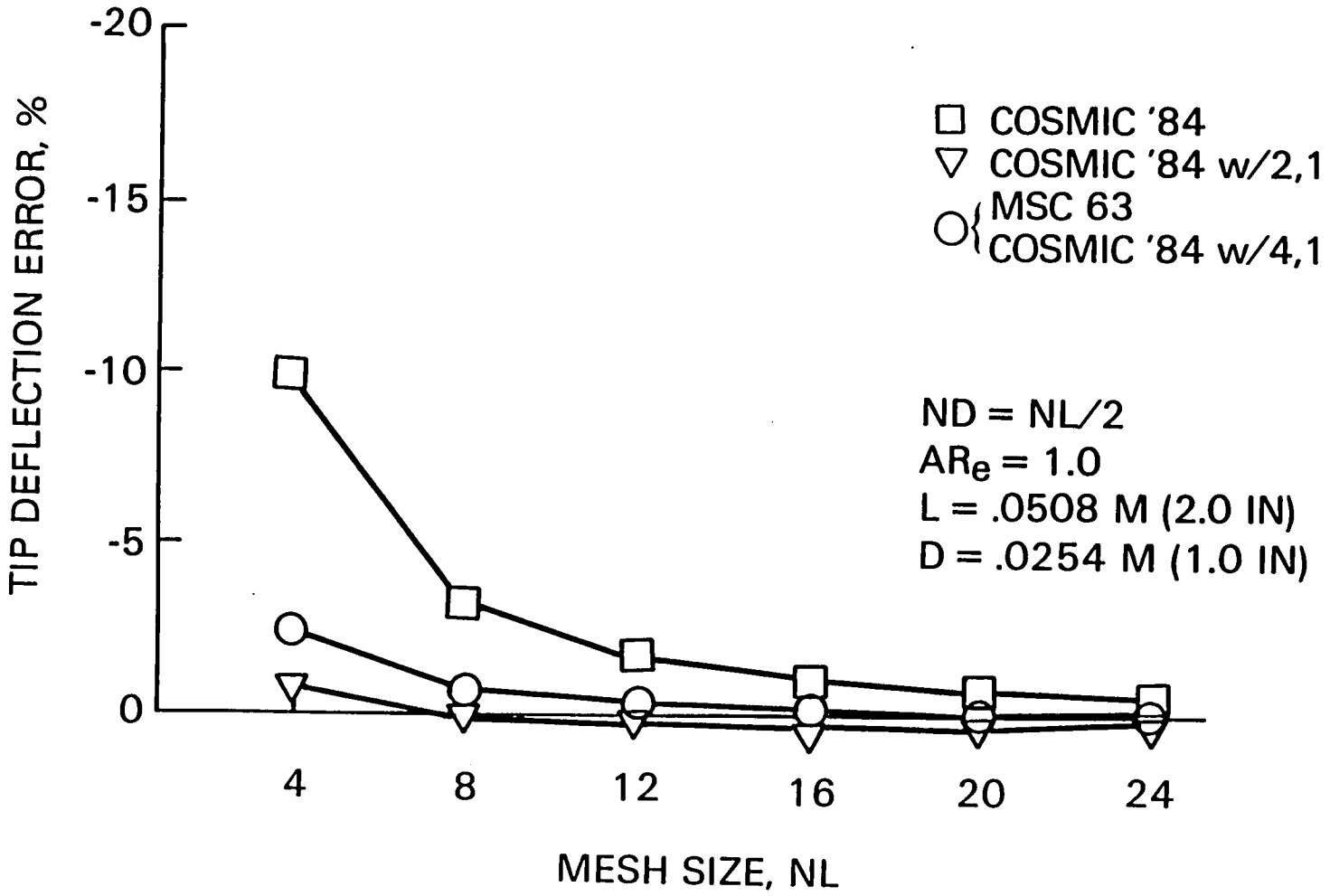

FIG. 6
DIRECT STRESS ERROR
DEEP BEAM-END MOMENT AND END SHEAR LOADING
(MESH SIZE STUDY)

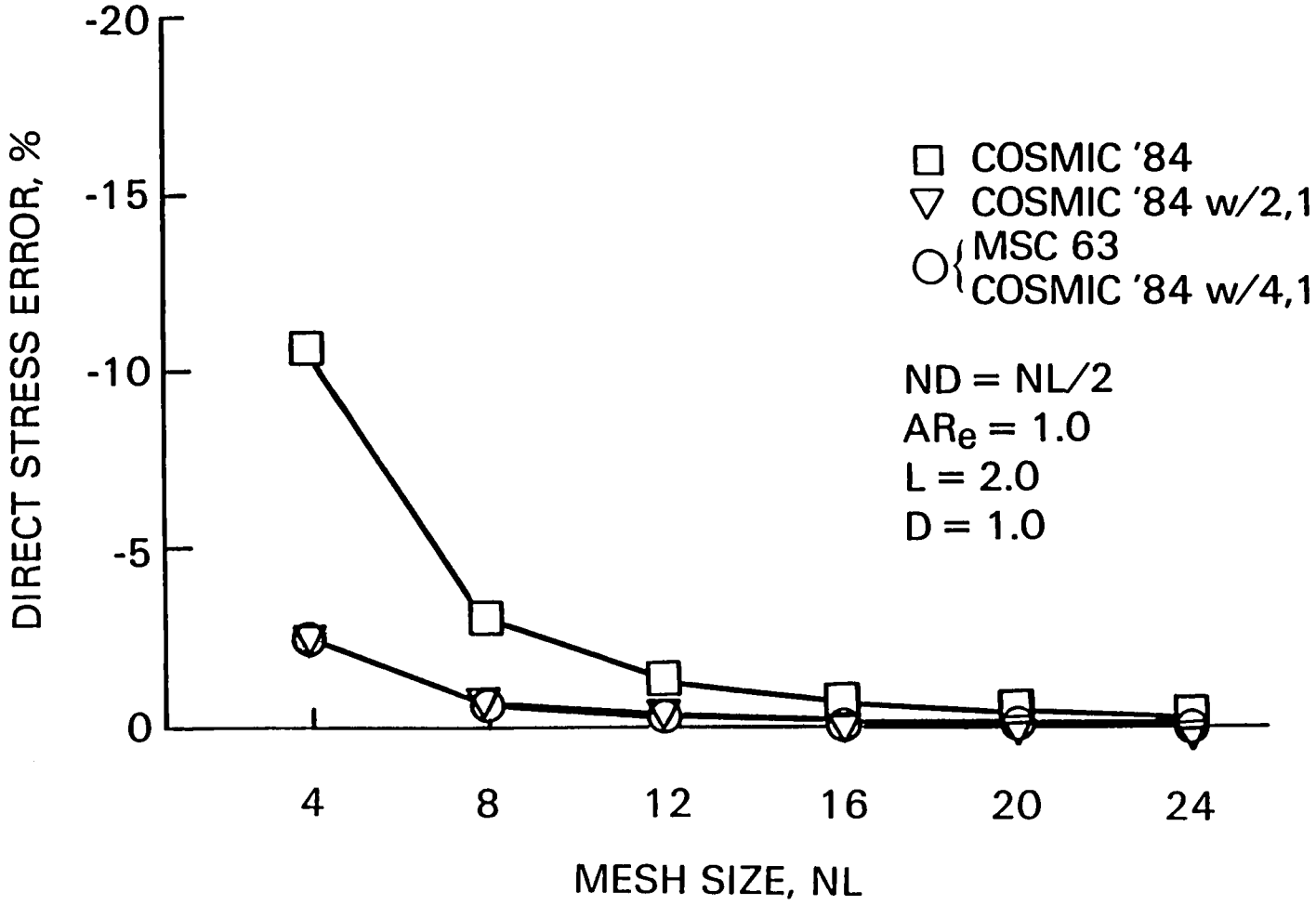

FIG. 7
SHEAR STRESS ERROR
DEEP BEAM-END SHEAR LOADING
(MESH SIZE STUDY)

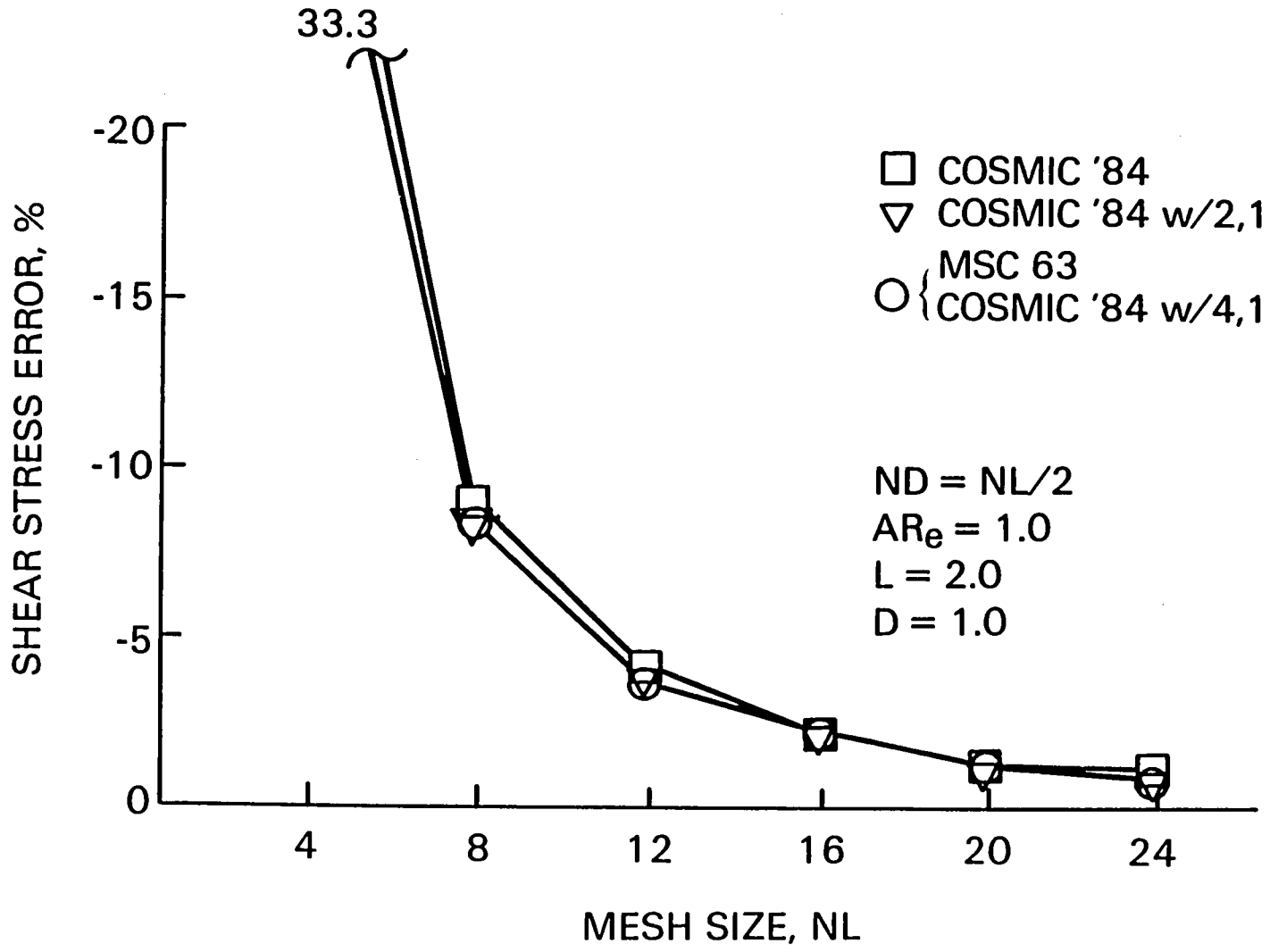

FIG. 8
TIP DEFLECTION ERROR
VARIABLE BEAM-END MOMENT LOADING
(ASPECT RATIO STUDY)

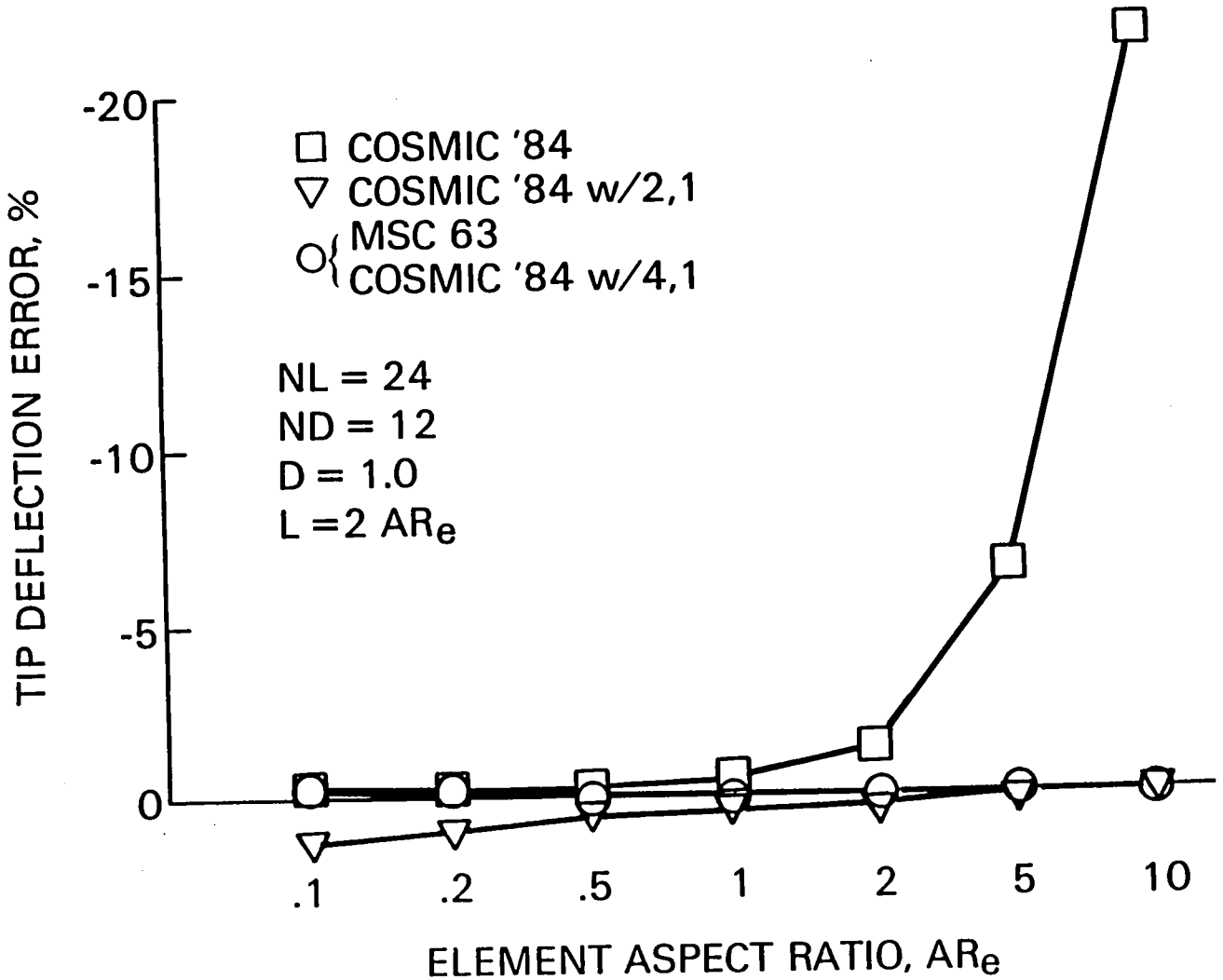

FIG. 9

8 NODE HEX ELEMENT GEOMETRY

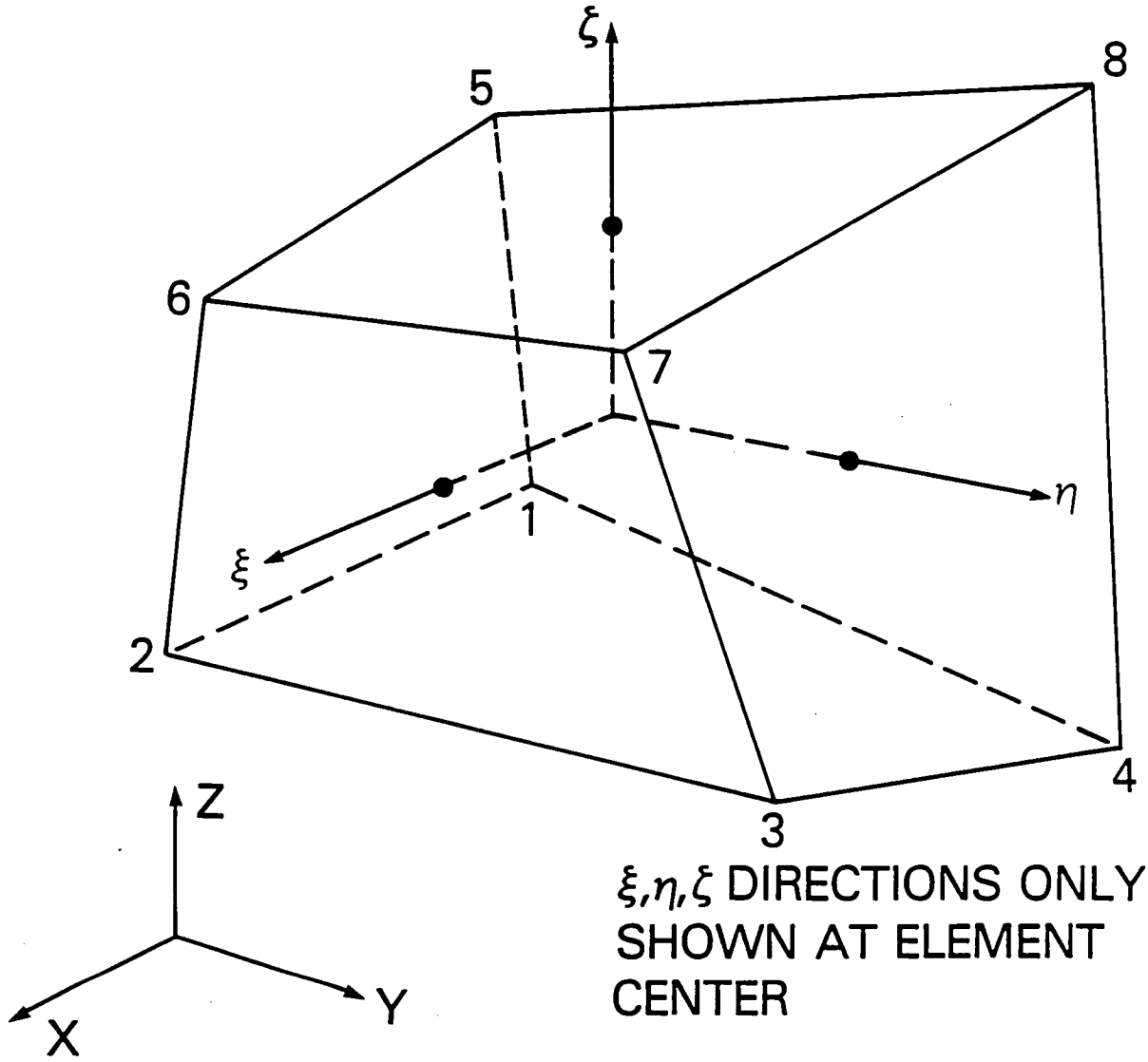

FIG. 10

TEST PROBLEM - SOLID ELEMENTS

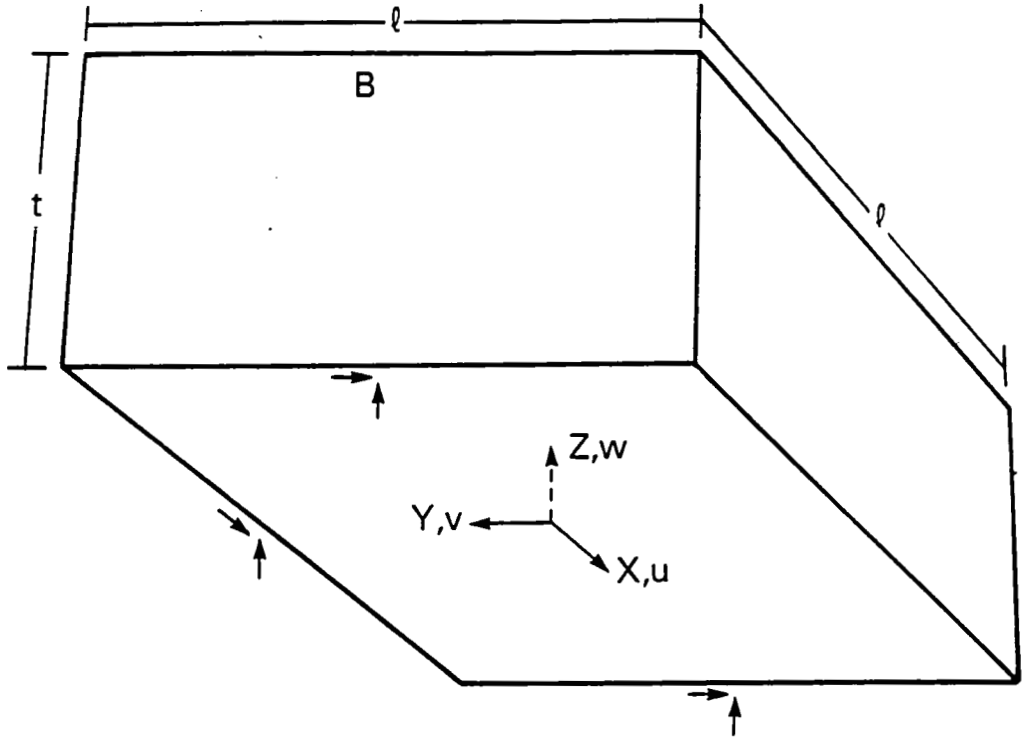

↑ INDICATES DEGREE OF FREEDOM CONSTRAINED FOR KINEMATIC MOUNTS

$v = w = 0$ AT $Y = Z = 0$, $X = \pm \ell/2$

$u = w = 0$ AT $X = Z = 0$, $Y = \ell/2$

A = (0.,0.,t)

B = (ℓ/2,0.,t)

MATERIAL INFORMATION (ALUMINUM)

$E = 6.89 \times 10^{10}$ N/M^2 (10×10^6 LB/IN^2)

$\rho = 2.71 \times 10^3$ KG/M^3 (.098 LB/IN^3)

$a = 22.7 \times 10^{-6}$ /K

$\upsilon = .33$

FIG. 11

ELEMENT TYPES

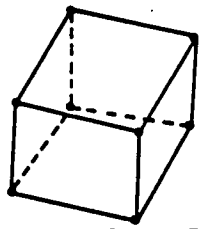

8 NODES

CHEXA2 10 TETRAHEDRA (COSMIC)

CIHEX1 LINEAR ISOPARAMETRIC (COSMIC)

CHEXA LINEAR ISOPARAMETRIC (MSC)

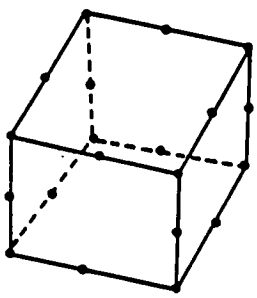

20 NODES

CIHEX2 QUADRATIC ISOPARAMETRIC (COSMIC)

CHEXA QUADRATIC ISOPARAMETRIC (MSC)

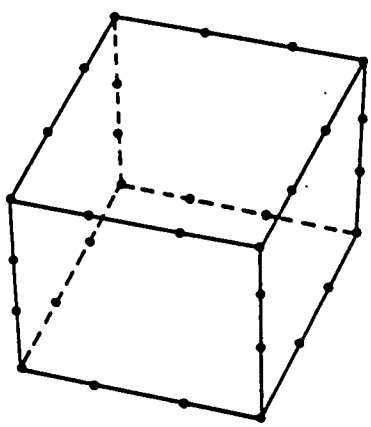

32 NODES

CIHEX3 CUBIC ISOPARAMETRIC (COSMIC)

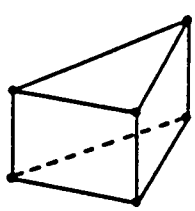

6 NODES

CWEDGE 3 TETRAHEDRA (COSMIC)

CPENTA LINEAR ISOPARAMETRIC (MSC)

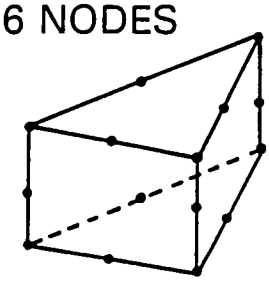

15 NODES

CPENTA QUADRATIC ISOPARAMETRIC (MSC)

FIG. 12

MESH GEOMETRY

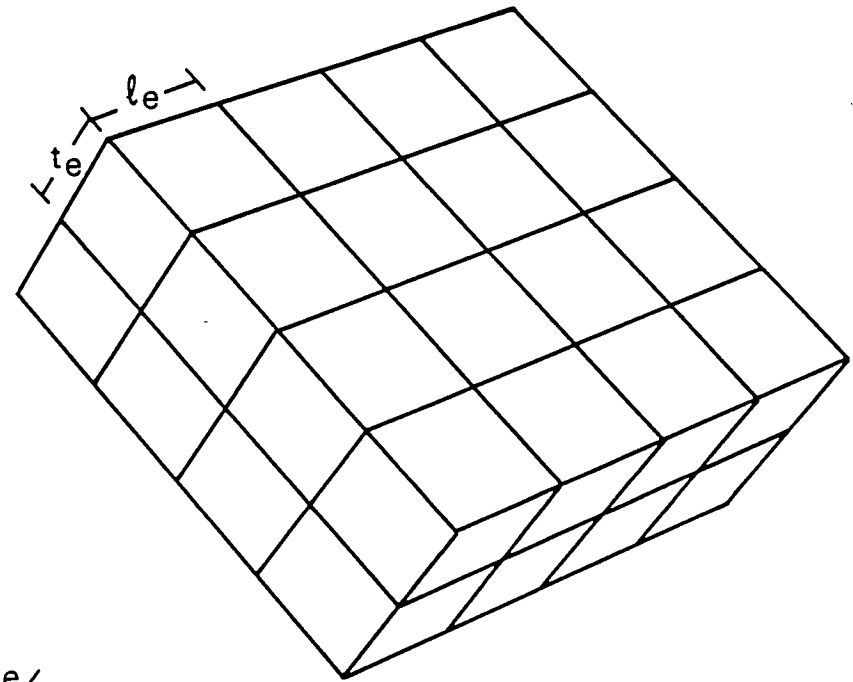

$AR_e = \ell_e / t_e$

$AR = \ell / t$

HEXAHEDRAL PATTERN

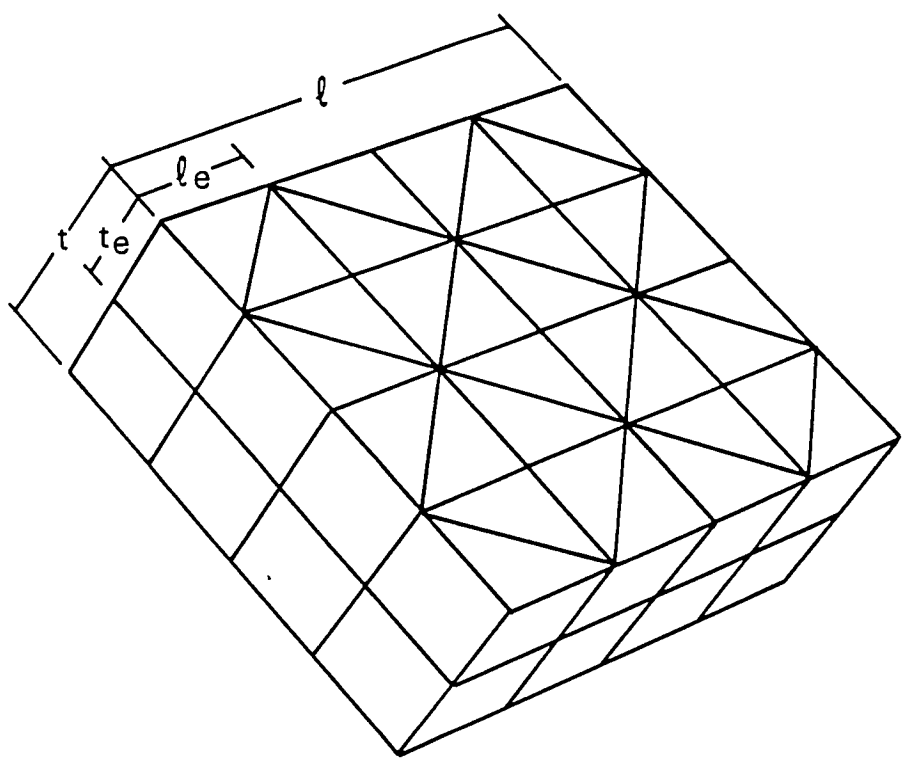

WEDGE PATTERN

FIG. 13

Z DISPLACEMENT ERROR AT (A)

THICK SLAB—LINEAR TEMPERATURE GRADIENT (MESH SIZE STUDY)

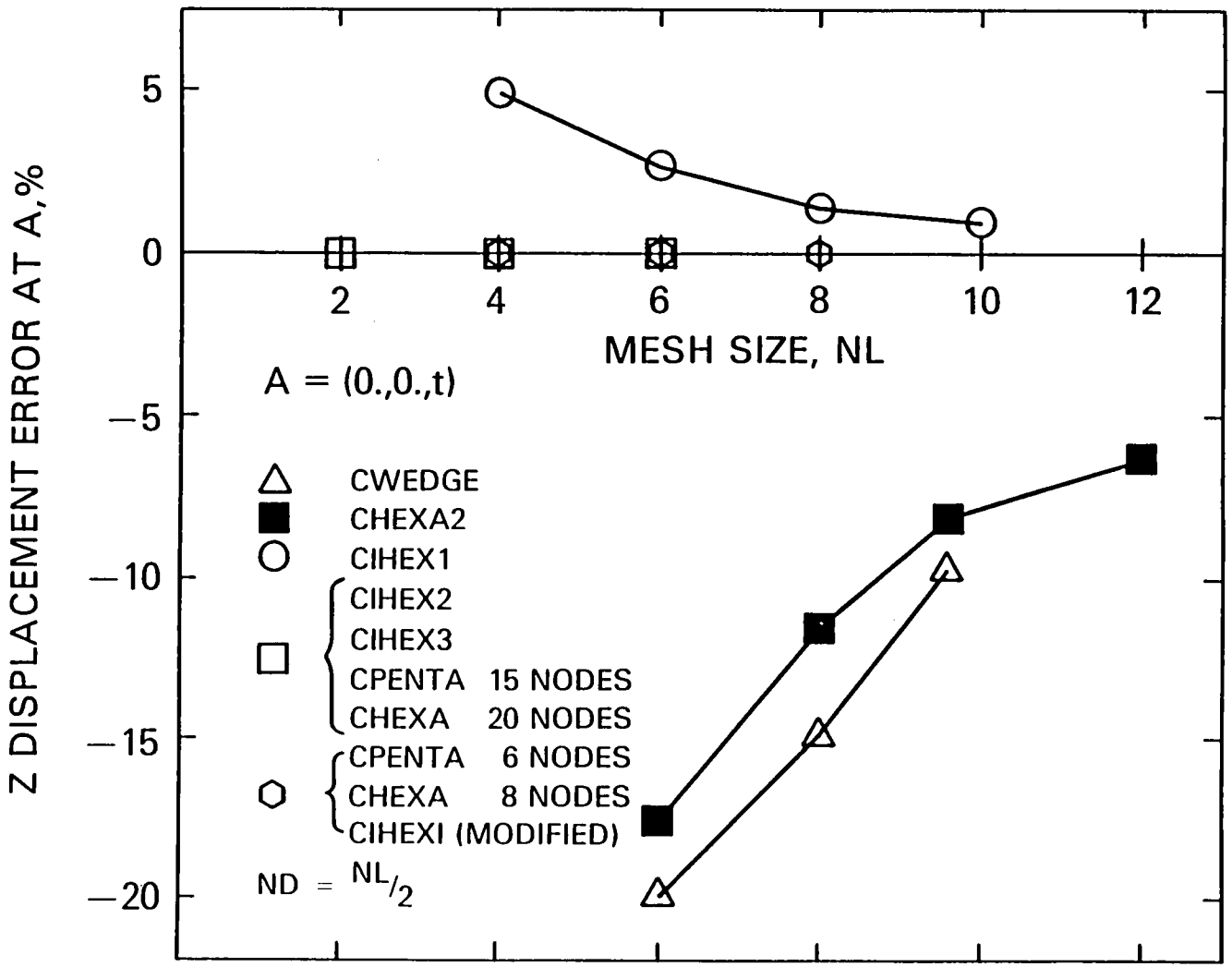

FIG. 14

Z DISPLACEMENT ERROR AT (A)

LINEAR TEMPERATURE GRADIENT (ASPECT RATIO STUDY)

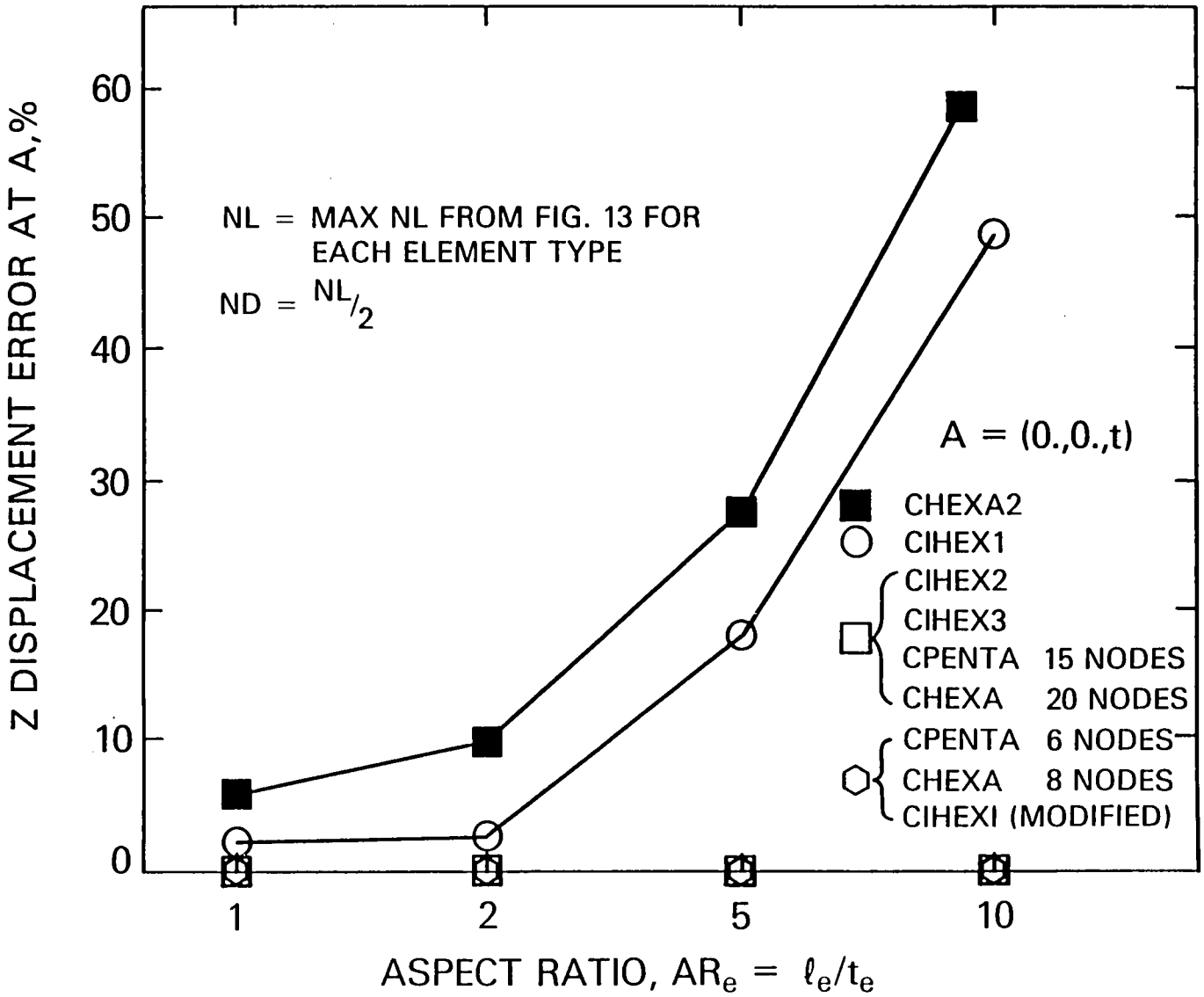

FIG. 15

Z DISPLACEMENT AT (A)

THICK SLAB — GRAVITY

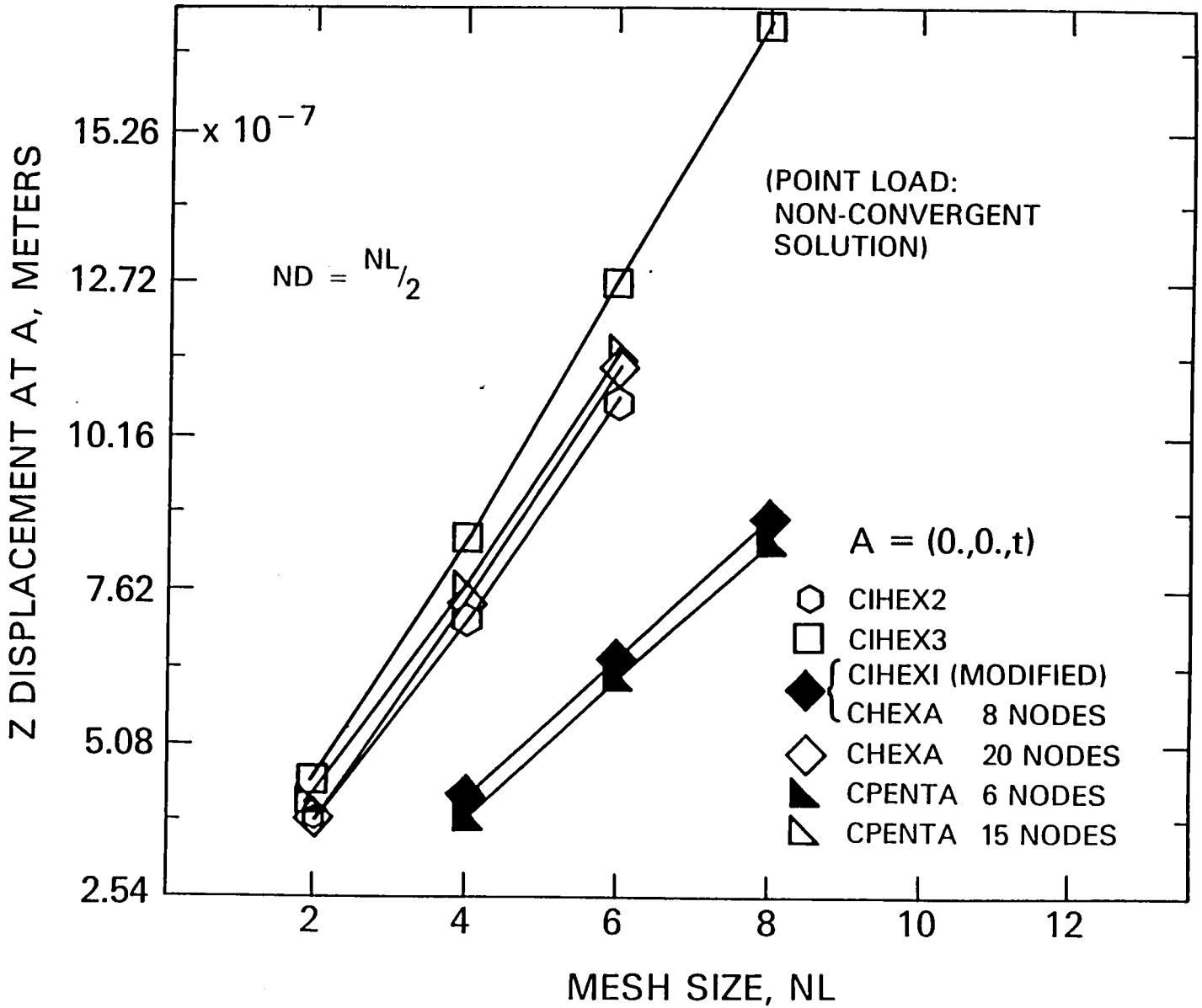

DYNAMIC AND AEROELASTIC ANALYSES OF TURBOSYSTEMS IN NASTRAN

by

V. Elchuri
Aerostructures
Arlington, Virginia

and

P. R. Pamidi
RPK Corporation
Columbia, Maryland

SUMMARY

Several new capabilities dealing with the dynamic and aeroelastic analyses of turbosystems have been added as standard features to the April 1986 release of NASTRAN. This paper gives a brief description of these capabilities and outlines their implementation in NASTRAN.

INTRODUCTION

In a series of related efforts over the past few years, NASA's Lewis Research Center (NASA LeRC) has sponsored the development of a number of analytical capabilities addressing the static, dynamic and aeroelastic problems of axial-flow turbosystems (References 1-10). To benefit from the state-of-the-art structural modeling and analyses techniques, these analytical developments were implemented in the general purpose finite element program NASTRAN. The capabilities are based on a unified approach to representing and integrating the structural and aerodynamic aspects of the turbomachinery problems.

The enhancements to NASTRAN developed under the above efforts can be grouped into two phases. The capabilities developed in the first phase (References 1-7) were incorporated into the UNIVAC Level 17.7 version of NASTRAN at NASA LeRC. These capabilities were subsequently expanded in the second phase (References 8-10) and made operational on RPK's CRAY version of the April 1984 release of NASTRAN at NASA LeRC. In order to make all of these enhancements available to the general NASTRAN user community, these capabilities have now been incorporated as standard features into the April 1986 release of NASTRAN.

DESCRIPTION OF THE NEW CAPABILITIES

Some of the new capabilities have been summarized in Reference 11. However, the authors feel it is very helpful and timely for NASTRAN users to have all of the new capabilities described in one paper presented to coincide with their incorporation in the April 1986 release of NASTRAN. Accordingly, the new capabilities are briefly described below. It is noted that all of the capabilities address tuned cyclic structures, that is, structures composed of cyclic sectors identical in mass, stiffness, damping and constraint properties.

1. Static Aerothermoelastic 'Design/Analysis' of Axial-Flow Compressors (References 1-3)

The non-linear interactive influences between the flexible structure of axial-flow compressor rotor or stator stage, and the steady state aerothermodynamics of the internal flow are addressed. The 'design' problem embraces the process of arriving at an 'as manufactured' blade shape to produce a desired design point pressure ratio, given the flow rate and the rotational speed. The subsequent process of analyzing the structural and aerothermodynamic performance at off-design operating points is termed the 'analysis' problem.

The three-dimensional aerothermodynamic theory discussed in Reference 12 is used. The capability also yields a differential stiffness matrix at the end of the iterative non-linear solution process for use in subsequent modal, flutter, dynamic and aerodynamic response analyses.

2. Modal Flutter Analysis of Axial-Flow Turbomachines (References 1-3)

Unstalled flutter boundaries of axial-flow turbomachines (compressors and turbines) can be determined using this capability. The aeroelastic stability of a given operating point of a given stage of the turbomachine is investigated in terms of modal families of several circumferential harmonic indices considered one at a time.

Two-dimensional cascade unsteady aerodynamic theories of Reference 13 (subsonic) and Reference 14 (supersonic) are used.

3. Forced Vibration Analysis of Rotating Cyclic Structures (References 4,5)

Cyclic structures rotating about their axis of symmetry, and subjected to sinusoidal or generally periodic loads moving with the structure are addressed. In addition, the axis of rotation itself is permitted translational oscillations resulting in inertial loads. Coriolis and centripetal acceleration effects are also included.

The problem is treated using the direct approach in NASTRAN.

4. Modal Flutter Analysis of Advanced Turbopropellers (References 6,7)

Unstalled flutter boundaries of multi-bladed advanced turbopropellers can be determined using this capability. Such propellers comprise thin blades of low aspect ratio and varying sweep. The analysis is similar to that for axial-flow turbomachines with the addition that the unsteady aerodynamics have been modified to recognize the blade sweep effects.

5. Modal Forced Vibration Analysis of Aerodynamically Excited Turbosystems (References 8-10)

Vibratory response of turbosystems subjected to aerodynamic excitation is addressed. Turbosystems such as single- and counter-rotating advanced turbopropellers with highly swept blades, and axial-flow compressors and turbines can be analyzed. The dynamic response problem is treated in terms of the normal modal coordinates of these tuned rotating cyclic structures. Both rigid and flexible hubs/disks are considered. Coriolis and centripetal accelerations, as well as differential stiffness effects, are also included.

Generally non-uniform steady inflow fields and uniform flow fields arbitrarily inclined at small angles with respect to the axis of rotation of the turbosystem are considered as the sources of aerodynamic excitation. Subsonic and supersonic relative inflows are addressed, with provision for linearly interpolating transonic airloads.

A stand-alone pre-processor program, independent of NASTRAN, has been additionally developed to compute the applied vibratory airloads on the blades of these turbosystems (Reference 10). This program, called AIRLOADS, is available separately from COSMIC.

NASTRAN IMPLEMENTATION

The incorporation of the new capabilities described above involved extensive changes to NASTRAN. These are outlined below.

1. Additions to the Rigid Format Data Base

The Rigid Format Data Base was expanded by the addition of two new rigid formats (DISP 16 for Static Aerothermoelastic Design/Analysis and AERO 9 for Cyclic Modal Flutter Analysis) and two new DMAP ALTER packages for the Forced Vibration Analysis of Rotating Cyclic Structures. Both of the ALTER packages represent DMAP ALTERs to the DISP 8 rigid format. One of the ALTER packages uses the direct approach and the other uses the modal approach. The latter one also allows for the effects of the generalized aerodynamic matrix due to oscillatory blade motions.

2. Additions to the Source Code

A total of 83 subprograms were added to NASTRAN in order to incorporate the new capabilities. These involve the following important additions.

A. Four new functional modules

ALG	---	Aerodynamic load generator (for use in the new DISP 16 rigid format)
APDB	---	Aerodynamic pool distributor for blades (for use in the new AERO 9 rigid format)
FVRSTR1	---	Forced vibration response analysis of rotating cyclic structures - Phase 1 (for use in the new DMAP ALTER packages)
FVRSTR2	---	Forced vibration response analysis of rotating cyclic structures - Phase 2 (for use in the new DMAP ALTER packages)

B. Two new bulk data cards

STREAML1 --- Defines grid points on a blade streamline from the leading edge to the trailing edge
STREAML2 --- Defines aerodynamic data for a blade streamline

C. Several new bulk data parameters (PARAMs)

3. Modifications to the Source Code

A total of 35 existing subprograms were modified in order to incorporate the new capabilities into NASTRAN.

CONCLUDING REMARKS

A brief description of a number of new capabilities added to the April 1986 release of NASTRAN for the dynamic and aeroelastic analyses of turbosystems has been presented. An outline of their implementation in NASTRAN is also given.

ACKNOWLEDGEMENTS

The authors take this opportunity to rightfully acknowledge the valuable contributions of Mr. A. Michael Gallo, Dr. G. C. C. Smith, Ms. B. J. Dale and Mr. S. C. Skalski, of Bell Aerospace Textron, to the development of the above-mentioned new capabilities in NASTRAN.

REFERENCES

1. Elchuri, V., Smith, G. C. C., Gallo, A. M., and Dale, B. J., "NASTRAN Level 16 Theoretical, User's, Programmer's, and Demonstration Manuals Updates for Aeroelastic Analysis of Bladed Discs," NASA CRs 159823-159826, March 1980.

2. Smith, G. C. C., and Elchuri, V., "Aeroelastic and Dynamic Finite Element Analysis of a Bladed Shrouded Disk," NASA CR 159728, March 1980.

3. Gallo, A. M., Elchuri, V., and Skalski, S. C., "Bladed-Shrouded-Disc Aeroelastic Analyses: Computer Program Updates in NASTRAN Level 17.7," NASA CR 165428, December 1981.

4. Elchuri, V., and Smith, G. C. C., "Finite Element Forced Vibration Analysis of Rotating Cyclic Structures," NASA CR 165430, December 1981.

5. Elchuri, V., Gallo, A. M., and Skalski, S. C., "Forced Vibration Analysis of Rotating Cyclic Structures in NASTRAN," NASA CR 165429, December 1981.

6. Elchuri, V., and Smith, G. C. C., "NASTRAN Flutter Analysis of Advanced Turbopropellers," NASA CR 167926, April 1982.

7. Elchuri, V., Gallo, A. M., and Skalski, S. C., "NASTRAN Documentation for Flutter Analysis of Advanced Turbopropellers," NASA CR 167927, April 1982.

8. Elchuri, V., "Modal Forced Vibration Analysis of Aerodynamically Excited Turbosystems," NASA CR 174966, July 1985.

9. Elchuri, V., and Pamidi, P. R., "NASTRAN Supplemental Documentation for Modal Forced Vibration Analysis of Aerodynamically Excited Turbosystems," NASA CR 174967, July 1985.

10. Elchuri, V., and Pamidi, P. R., "AIRLOADS: A Program for Oscillatory Airloads on Blades of Turbosystems in Spatially Non-Uniform Inflow," NASA CR 174968, July 1985.

11. Elchuri, V., and Gallo, A. M., "Four New Capabilities in NASTRAN for Dynamic and Aeroelastic Analyses of Rotating Cyclic Structures," Twelfth NASTRAN Users' Colloquium, NASA CP 2328, May 1984, pp. 239-256.

12. Hearsey, R. M., "A Revised Computer Program for Axial Compressor Design," ARL-75-0001, Vols. I and II, Wright-Patterson AFB, January 1975.

13. Rao, B. M., and Jones, W. P., "Unsteady Airloads for a Cascade of Staggered Blades in Subsonic Flow," 46th Propulsion Energetics Review Meeting, Monterey, California, September 1975.

14. Adamczyk, J. J., and Goldstein, M. E., "Unsteady Flow in a Supersonic Cascade with Subsonic Leading-Edge Locus," AIAA Journal, Vol. 16, No. 12, December 1978, pp. 1248-1254.

NASTRAN DATA DECK GENERATION ON THE PC

Robert J. Guyan
Space Transportation Systems Division
Rockwell International,Inc.

SUMMARY

Using two commercial programs an application has been developed to aid in generating a run-ready NASTRAN data deck on the PC. Macros are used to access relevant reference material and card files while editing the deck. The application can be easily customized to suit individual or group needs.

INTRODUCTION and BACKGROUND

Since 1984 I have been consulting on a project directed toward providing NASTRAN help on TSO. The initial task was to install documentation from the User's Manual. In the first year about 1200 panels of information, primarily data card descriptions and rigid format listings were generated. During this period I developed my own ideas of what the ultimate scope of this project might be.

Early in 1985 the IBM PC XT computer arrived in our engineering department with various application programs. Other software was available to cover almost any conceivable need. These programs demonstrate the true power of the PC and provide the user with great utility.

Also during this period I needed to monitor and submit TSO jobs from an off-site PC where the usual NASTRAN reference material was not available. This combination of events induced me to proceed with the NASTRAN application described in this paper.

DEFINING THE APPLICATION

Having appropriate commercial tools available for this project was instrumental to its undertaking. This software also defined its operational characteristics and limitations. The most important operational feature I wanted was the ability to edit the NASTRAN deck in one window and view the reference material in another. Other desirable features included: quick access to the reference material; full featured editor; and an application which would be easy to learn, use, and modify.

With the application tools selected only a minimum amount of programming would be required. Most of the development time would be spent selecting the reference material to be presented.

ORGANIZING THE REFERENCE DATA

The selection of reference data depends on the users to which the application is directed. Possible users include: general; members of a group or department; beginning; occasional; experienced; specific individual; or specific topic user.

For the prototype application described here the selection is generally for an intermediate experienced individual. References are also slanted to the type of work I do: modal analysis; frequency and transient response; DMAP; trouble shooting and feature verification using small problems.

Sources from which information can be drawn include: NASTRAN Manuals; symposium proceedings; handbooks; project reports; class notes; TSO files; and personal notes. Some of the most useful information which could be included here comes from the experienced user; NASTRAN bugs and idiosyncrasies and guidelines for effective analysis.

Organization of the reference data is best seen by the Main Menu in Figure 1 and the sub-menus in Figures 2 and 6. Examples of specific items included are given in the remaining figures. In general the items included are: job control language (JCL); NASTRAN card formats and examples; and help with regard to commands, i.e., any reference which may be required during deck generation.

IMPLEMENTATION

The software application tools selected for this project were Sidekick and Superkey, copyrighted products of Borland International (References 1 and 2). Both are "RAM resident" programs which means that once they are loaded into the computer they becomes active or inactive with a keystroke. Sidekick and Superkey are designed to work with each other and they make a good team.

Sidekick is composed of several utilities. The one called NOTEPAD is used here for the editor. NOTEPAD is a full screen editor with features more than adequate for this application. A few commands require three-key combinations but they quickly become very natural. Other commands have been assigned to the PC's special keys. The window size of NOTEPAD may be varied, but it is usually convenient to let it occupy the lower one half of the screen for this application.

Superkey's primary function is writing macros. Two types of macros are used: keyboard macros which allow a series of keystrokes to be assigned to a single key; and display macros which enable a keystroke to write a window of text to the screen. The macro file written for this development contains primarily display macros. A few keyboard macros are used to simplify the input of JCL cards. Some information on writing this macro file is given in Appendix B, with a full discussion in Reference 2. This file represents the programming effort required.

USING THE APPLICATION

The application is started by inserting the program diskette (see Appendix A) in drive A and starting the computer (booting up). After a minute or so the Main Menu and general instructions are presented in the top portion of the screen (Figure 1). Items from the Main Menu are selected by using the shifted function keys. To scroll a display use the PgUp/PgDn keys. Press Esc to remove a display before selecting another menu item.

The JCL and Bulk Data selections have sub-menus which access items using prefix keys Alt and Ctrl (Figures 2 and 6). From the JCL menu you may select card files to merge with the NASTRAN data. The last item on the JCL menu (Alt6) selects a display macro rather than a card file.

When activating NOTEPAD for the first time it is best to press Esc to clear the screen, then press CtrlAlt. From the Sidekick menu press N for NOTEPAD. The NASTRAN file is read in automatically (see Appendix A). To start a new file press F3 and enter a name for your data deck. When you exit NOTEPAD, which you must do to either scroll a display or select a new menu item, press CtrlAlt. Thereafter, the NOTEPAD window is toggled by CtrlAlt; passing through the Sidekick menu is not necessary.

NOTEPAD commands which are most useful in editing the NASTRAN deck, in addition to those listed at the bottom of the screen, are given under NOTEPAD Commands (ShftF10). The very useful operation of importing data from the display screen, initiated by pressing F4, is fully explained there and in Reference 1. Examples are shown in Figures 7 and 9. The Sidekick calculator utility is available while in NOTEPAD by pressing AltC.

Generating the NASTRAN data deck then consists of repeatedly editing and toggling the NOTEPAD window while either merging card files or viewing a display window until the data deck is complete. Save the file by pressing F2.

Finally you will want to send the completed deck to TSO and submit it to the mainframe for execution. If you have copied a communications program to the application diskette (see Appendix A) and your PC is connected by modem to TSO, switch to the COMM directory and logon. You may also want to examine the run results while on the PC.

CONCLUDING REMARKS

Generating a macro file is a relatively easy task; only a few Superkey commands are required to convert NASTRAN experience into a ready reference on the PC (or just to have available as a listing). The file is also easy to update as new experiences accumulate. And when one file is filled, additional ones can follow. These "database" files also serve to collect and organize NASTRAN data that frequently is misplaced or is generally distributed across many references and users.

REFERENCES

1. Sidekick Owners Handbook, Borland International, 1985.

2. Superkey Owners Handbook, Borland International, 1985.

```
MAIN MENU                NASTRAN AIDE - GENERAL INSTRUCTIONS

 ShftF1  Main Menu              Esc        Exit Menu
 ShftF2  JCL                    ShftFn     Menu Listed
 ShftF3  Executive Control      PgDn/PgUp  Scroll
 ShftF4  Case Control           CtrlAlt    Toggle NOTEPAD Editor
 ShftF5  Bulk Data              Altn       Read Card File into NOTEPAD
 ShftF6  DMAP Statements
 ShftF7  Alters & DMAP          Note: Examples are inserted in text
 ShftF8  Other (Card Replication)
 ShftF9  TSO Commands
 ShftF10 NOTEPAD Commands
```

```
A:\NASTRAN.                    Line 1    Col 1    Insert    Indent
You are now in NASTRAN MICROLAND.  Happy Hunting! Press F3 for a new file.
```

```
F1-help F2-save F3-new file F4-import data F9-expand F10-contract Esc-exit
```

Figure 1 Main Menu

```
JCL  CtrlAlt for NOTEPAD  Altn       Read Card File into NOTEPAD

 Alt1  IBM
 Alt2  IBM - data base; exec ctrl; case ctrl; optional plot
 Alt3  Cray - optional plot; sample run
 Alt4  FORTRAN Compilation and Linkedit
 Alt5  Create Load Module
 Alt6  Miscellaneous IBM JCL (display macro)
```

```
A:\NASTRAN.                    Line 1    Col 1    Insert    Indent
//YTT5068N JOB 'GUYAN R J B-01280205*04101720100          XXXXXX3    ',
//  REGION=1024K,TIME=5,MSGLEVEL=1,MSGCLASS=4,NOTIFY=YTT5068
//*MAIN  ORG=RM001          CASE1.CTL
//*FORMAT  PR,DDNAME=JESI0001,CONTROL=SINGLE
//NASTRAN  EXEC  @MSCNAST,DB1DISP=NEW,DB1CAT=KEEP,DB01='&CASE1'
//D.SYSIN  DD  *
NASTRAN  NLINES=35
ID       NASTRAN,CASE1
APP      DISP
SOL      63
```

```
F1-help F2-save F3-new file F4-import data F9-expand F10-contract Esc-exit
```

Figure 2 JCL Menu

```
EXECUTIVE CONTROL  Ctrl Alt for NOTEPAD  PgDn/PgUp  Scroll

NASTRAN              Optional - p 2.1-1a
ID       A1,A2 $     Required - Any legal alphanumeric field for problem ID
CHKPNT   A1,A2 $     A1=YES for checkpointing - default is NO checkpointing
                     A2=DISK if checkpoint file is on a direct access device
APP      A           A=DISP (default), =HEAT, =DMAP (default if DMAP seq-
                     quence is submitted)
SOL      K1          Required - K1= 3 Normal modes            p 2.2-4
                                K1= 5 Buckling
```

```
A:\NASTRAN.                          Line 12   Col 1   Insert    Indent
//NASTRAN  EXEC  @MSCNAST,DB1DISP=NEW,DB1CAT=KEEP,DB01='&CASE1'
//D.SYSIN  DD  *
NASTRAN  NLINES=35
ID       NASTRAN,CASE1
APP      DISP
SOL      63
TIME     5
DIAG     8
CEND
TITLE=MSC/NASTRAN CASE1
```

```
F1-help F2-save F3-new file F4-import data F9-expand F10-contract Esc-exit
```

Figure 3 Executive Control Window

```
CASE CONTROL  Ctrl Alt for NOTEPAD  PgDn/PgUp  Scroll

    SUB-SECTIONS

  OUTPUT CONTROL
  BULK DATA SELECTION
  OUTPUT SELECTION
  SUBCASE CONTROL
  STRUCTURAL PLOTTER
  XY PLOTTER
```

```
A:\NASTRAN.                          Line 17   Col 1   Insert    Indent
TITLE=MSC/NASTRAN CASE1
SUBTITLE=MODAL ANALYSIS
ECHO=BOTH
SPC=1
MPC=2
```

```
F1-help F2-save F3-new file F4-import data F9-expand F10-contract Esc-exit
```

Figure 4 Case Control Sub-sections

```
╔═══════════════════════════════════════════════════════════════════════════╗
║  XY PLOTTER                                                               ║
║                                                                           ║
║General format: XYCOM TYPE SUBCASE /a1(b1,c1),a2(b2,c2),etc/d1(e1,f1),etc  ║
║                                                                           ║
║XYCOM: XYPLOT, XYPRINT, XYPUNCH, XYPAPLOT                                  ║
║TYPE:  DISP, VELO, ACCE, ELFORCE, STRESS, OLOAD, SPCF, SDISP, SVELO, SACCE ║
║SUBCASE: Default is all                                                    ║
║                                                                           ║
║Example:  PLOTID=SAMPLE PROBLEM  I M ENGINEER RM001 DNY                    ║
║          OUTPUT(XYPLOT)                                                   ║
║          PLOTTER SC $                          Plot symbols: Cyclic for   ║
║          XGRID LINES=YES $                     multiple curves on same grid ║
║          YGRID LINES=YES $                     CURVLINE=1 (X) Default     ║
║          XAXIS=YES $                                 =2 (*)               ║
║          YAXIS=YES $                                 =3 (+)               ║
╚═══════════════════════════════════════════════════════════════════════════╝
╔    A:\NASTRAN.                      Line 23   Col 1   Insert    Indent     ╗
║  DISP=ALL                                                                 ║
║  ELFORCE=ALL                                                              ║
║  SPCFORCE=ALL                                                             ║
║  OLOAD=ALL                                                                ║
║BEGIN BULK                                                                 ║
╚═══════════════════════════════════════════════════════════════════════════╝
 F1-help F2-save F3-new file F4-import data F9-expand F10-contract Esc-exit
```

Figure 5 XY Plotter Sub-section Window

```
╔═══════════════════════════════════════════════════════════════════════════╗
║          BULK DATA  Ctrl Alt for NOTEPAD                                  ║
║                                                                           ║
║  Ctrl1  Geometry Definition                                               ║
║  Ctrl2  Element Connections                                               ║
║  Ctrl3  Properties & Materials                                            ║
║  Ctrl4  Mass                                                              ║
║  Ctrl5  Sets & Constraints                                                ║
║  Ctrl6  Loads                                                             ║
║  Ctrl7  Miscellaneous (EIGR,DYNRED,DMI,PLOTEL)                            ║
║                                                                           ║
╚═══════════════════════════════════════════════════════════════════════════╝
╔    A:\NASTRAN.                      Line 30   Col 1   Insert    Indent     ╗
║SUBCASE 1                                                                  ║
║  DISP=ALL                                                                 ║
║  ELFORCE=ALL                                                              ║
║  SPCFORCE=ALL                                                             ║
║  OLOAD=ALL                                                                ║
║BEGIN BULK                                                                 ║
║                                                                           ║
║ENDDATA                                                                    ║
║/*                                                                         ║
║//NS.FT04F001 DD SYSOUT=4                                                  ║
╚═══════════════════════════════════════════════════════════════════════════╝
 F1-help F2-save F3-new file F4-import data F9-expand F10-contract Esc-exit
```

Figure 6 Bulk Data Menu

```
    PROPERTIES & MATERIALS  Ctrl Alt for NOTEPAD  PgDn/PgUp  Scroll

PBAR,PID,MID,A,I1,I2,J,NSM,,+PB1   $ Shear stiffnesses are (K1)AG & (K2)AG
+PB1,C1,C2,D1,D2,E1,E2,F1,F2,+PB2  $ Form Factor K          Section
+PB2,K1,K2,I12                     $   .8333             Rectangular
                                   $   .90               Solid Circular
                                   $   .50               Thin-walled Circular
PROD,PID,MID,A,J,C,NSM             $ Shear stress = C*Moment/J (defines C)
PSHELL,PID,MID1,T,MID2,12*I/T**3,MID3,TS/T,NSM,+PS
+PS,Z1,Z2,MID4                     $ For plane strain analysis, MID2 = -1
```

```
    A:\NASTRAN.                      Line 30   Col 2   Overwrite Indent
SUBCASE 1
  DISP=ALL
  ELFORCE=ALL
  SPCFORCE=ALL
  OLOAD=ALL
BEGIN BULK

$PSHELL,PID,MID1,T,MID2,12*I/T**3,MID3,TS/T,NSM,+PS
$+PS,Z1,Z2,MID4                     $ For plane strain analysis, MID2 = -1
//NS.FT04F001 DD SYSOUT=4
```

F1-help F2-save F3-new file F4-import data F9-expand F10-contract Esc-exit

Figure 7 Properties and Materials Window

```
         DMAP  Ctrl Alt for NOTEPAD  PgDn/PgUp  Scroll

     SUB-SECTIONS

  MATRIX OPERATION
  UTILITY
  EXECUTIVE OPERATION
  GENERAL DMAP RULES

Default Values Shown for Parameters

TYPE=1  Single precision     FORM=2  General rectangular
TYPE=2  Double precision     FORM=6  Symmetric
```

```
    A:\NASTRAN.                      Line 13   Col 1   Insert    Indent
APP       DISP
SOL       63
TIME      5
DIAG      8

CEND
```

F1-help F2-save F3-new file F4-import data F9-expand F10-contract Esc-exit

Figure 8 DMAP Statements Sub-sections

```
PARTN    PHI,EM,/,,PHI1,/0 $  the lowest 25 after deleting 6 rigid body modes
MATGEN,  /ER/6/25/0/1/7/2/3/1/11 $ Row partitioning - select rows 1,9,10,14
PARTN    A,,ER/,A,,/1 $             of A for further processing
MERGE    A11,A21,A12,A22,CP,RP/A/V,Y,SYM=-1/V,Y,TYPE/V,Y,FORM $
                                              SYM LT 0 - CP is used for RP
                                              SYM GE 0 - CP & PR are distinct
MERGE,   ,,,,ES,/KAA/-1/2/6 $      Form symmetric null double precision
                            $      matrix of size the length of ES
MERGE,   ,PHIA,,,,RP1/1/2/2 $      Expand PHIA to g size where PHIA has only
         $   components 126 - RP1=(1.,1.,0.,0.,0.,1.,...repeating sequence)
TRNSP    A/X $
DIAGONAL A/B/C,Y,OPT=COLUMN/V,Y,POWER=1 $     OPT=COLUMN,SQUARE,WHOLE
READ     KAA,MAA,,,DYNAMICS,,CASECC/LAMA,PHIA,MI,OEIGS/MODES/S,N,NEIGV $
DUMMOD1  GPL,EQEXIN,USET,LAMA,PHIX,MXX,,/,,,,,,,/NTERMS $  KE requires link
```

```
A:\ZOFF.CTL                    Line 15   Col 1    Insert    Indent
TIME     5
DIAG     8,14
$MATGEN,  /ER/6/25/0/1/7/2/3/1/11 $ Row partitioning - select rows 1,9,10,14
$PARTN    A,,ER/,A,,/1 $             of A for further processing
CEND
TITLE=MSC/NASTRAN CASE1 - QUAD4 ZOFF CHECK
```

```
F1-help F2-save F3-new file F4-import data F9-expand F10-contract Esc-exit
```

Figure 9 DMAP Statements Window

```
4. DMAP - Modes & Kinetic Energy

BEGIN    $
GP1      GEOM1,GEOM2,/GPL,EQEXIN,GPDT,CSTM,BGPDT,SIL/S,N,LUSET/0/
         S,N,NOGPDT $
GP4      CASECC,GEOM4,EQEXIN,SIL,GPDT,BGPDT,CSTM/,,USET,ASET/LUSET/
         S,N,MPCF1/S,N,MPCF2/S,N,SINGLE/S,N,OMIT/S,N,REACT/S,N,NSKIP/
         S,N,REPEAT/S,N,NOSET/S,N,NOL/S,N,NOA/C,Y,SUBID $
INPUTT2  /K,M,,,/-1/11 $  (K & M from Rigid Format 3)
MATPRN   K,M,,,// $
READ     K,M,,,DYNAMICS,,CASECC/LAMA,PHIA,MI,OEIGS/MODES/S,N,NEIGV/1 $
OFP      OEIGS,LAMA,,,,// $
COND     FINIS,NEIGV $
MATPRT   PHIA// $
DUMMOD1  GPL,EQEXIN,USET,LAMA,PHIA,M,,/,,,,,,,/8 $
LABEL    FINIS $
```

```
A:\ZOFF.CTL                    Line 15   Col 1    Insert    Indent
CEND
TITLE=MSC/NASTRAN CASE1 - QUAD4 ZOFF CHECK
SUBTITLE=MODAL ANALYSIS
ECHO=BOTH
```

```
F1-help F2-save F3-new file F4-import data F9-expand F10-contract Esc-exit
```

Figure 10 DMAP Program Window

```
          TSO COMMANDS  Ctrl Alt for NOTEPAD  PgDn/PgUp  Scroll

     ATTRIBUTES

 attr a1 recfm(f b) lrecl(80) blksize(3120)      (cards)
 attr a1 recfm(f b) lrecl(6)  blksize(996)       (crt)
 attr a1 recfm(u)   lrecl(0)  blksize(32760)     (load)

     ALLOCATE

 alloc f(ft06f001) da(output.data) new space(5,5) track using(a1)  (general)
 alloc da(crt.case1.data) new space(5,5) track using(a1)           (crt)
 alloc da(msc.case1.data) new space(5,5) track                     (nastran)
 alloc da(msc.case1.load) new space(5,5) track dir(1) using(a1)    (load)
```

```
     A:\ZOFF.CTL                        Line 36   Col 1   Insert    Indent
$CQUAD4,EID,PID,G1,G2,G3,G4,THETA,ZOFFS,+CQ1
CQUAD2,1,1,1,2,4,3,,.5
=,*1,=,*2,*2,*2,*2,==
=2
PSHELL,1,1,.05,1,1.
```

F1-help F2-save F3-new file F4-import data F9-expand F10-contract Esc-exit

Figure 11 TSO Commands Window

```
          NOTEPAD COMMANDS  Ctrl Alt for NOTEPAD  PgDn/PgUp  Scroll

     CURSOR MOVEMENT

  Ctrl LtArrow/Ctrl RtArrow    Word left/Word right
  UpArrow/DnArrow              Line up/Line down
  Home/End                     EOL left/EOL right
  Ctrl Home/Ctrl End           Page top/Page bottom
  Ctrl PgUp/Ctrl PgDn          File top/File bottom
  Ctrl W/Ctrl Z                Scroll one line up/down
  PgUp/PgDn                    Scroll one page up/down
```

```
     A:\ZOFF.CTL                        Line 52   Col 1   Insert    Indent
FORCE,4,9,0,1000.,-1.,0.,0.
FORCE,4,10,0,1000.,-1.,0.,0.
ENDDATA
/*
//NS.FT04F001 DD SYSOUT=4
//NS.FT06F001 DD SYSOUT=4
//* NP.SYSOUTC DD DSN=YTTS068.CRT.CASE1.DATA,DISP=MOD
/*
```

F1-help F2-save F3-new file F4-import data F9-expand F10-contract Esc-exit

Figure 12 NOTEPAD Commands Window

APPENDIX A SETTING UP THE APPLICATION DISKETTE

Instructions for setting up the application diskette so that the program will run as described in the section on using the application are given here. The complete application can be placed on a single diskette. For a hard disk system the application components can be arranged similarly.

To make the diskette self booting format it with the system parameter s. Also copy the ANSI.SYS file from the DOS disk. Keep the programs and data files organized by using subdirectories for Sidekick, Superkey, the JCL card files, and a communications program. The contents of the application diskette should look like this.

A:\	A:\SK	A:\KEY	A:\CARDS	A:\COMM
AUTOEXEC.BAT	SK.COM	KEY.COM	JCL1.CRD	communications
IBMBIO.COM		AIDE.MAC	JCL2.CRD	program
IBMDOS.COM			JCL3.CRD	
COMMAND.COM			JCL4.CRD	
ANSI.SYS			JCL5.CRD	
CONFIG.SYS			...	
NASTRAN				

To load Sidekick and Superkey and display the main menu automatically the AUTOEXEC.BAT file should contain the following statements:

```
echo off
cd\key
key
cd\sk
sk
cd\key
key aide/ml
cd\
```

The root directory A:\ will then be the default directory and can be used for NASTRAN data decks. The ANSI.SYS file is needed by Superkey and is installed on start up if the CONFIG.SYS file is present and contains the line: DEVICE=ANSI.SYS.

Before copying Sidekick to the disk two things should be done to prepare SK.COM. First, run Sidekick and from the main menu select the Setup option. On the setup screen under Notefile enter NASTRAN for the Name and A:\ for the Directory. Save by pressing F4. Sidekick will now automatically read in the NASTRAN file when the NOTEPAD option is first selected. This file can act as a bulletin board prior to data deck generation.

Next, run the Sidekick program SKINST.COM, if you want to change the maximum file size of NOTEPAD. The default size is 8000 bytes which will hold about 180 lines. I use NOTEPAD to edit the macro file, AIDE.MAC, which is currently 729 lines (32355 bytes). I have it set to 40000. Use the size you anticipate needing up to 50000.

The Superkey program, KEY.COM, will also need to have it's maximum file size set with KEYINST.COM. Default size is 8000 bytes - maximum size is 60000. I use 40000 presently.

The JCLi.CRD files will depend on the mainframe in use and the job requirements. There are many communications programs available for the PC. All of the files listed above have now been mentioned. Other utility programs can be added. Neither of the help files for Sidekick and Superkey have been included because of disk space limitations. The necessary help may be placed in the macro file.

APPENDIX B WRITING THE SUPERKEY MACRO

The elements of the Superkey language which have been used to develop the macro file AIDE.MAC are listed here. See Reference 2 for a complete discussion of macros.

<BEGDISP><ShftF1>	Begin display macro for key ShftF1
<BEGDEF><Alt1>	Begin keyboard macro for key Alt1
<ENDDEF>	End macro
<TITLE>MAIN MENU<TITLE>	Associates macro key definition with a title in an auxiliary window (accessed by AltPrtsc)
<CTRLD>MAIN MENU<CTRLD>	Yellow foreground (border color)
<CTRLB>ShftF1<CTRLB>	White background/Black foreground
<AUTO>	Autostart a macro (used for MAIN MENU)
1 1 78 10.	Define display window (upper left corner at (1,1), 78 columns, and 10 rows

The display macro for the main menu reads like this:

```
<BEGDISP><ShftF1> 1 1 78 12. <TITLE>MAIN MENU<TITLE><AUTO>
<CTRLD>      MAIN MENU        NASTRAN AIDE - GENERAL INSTRUCTIONS<CTRLD>
<Ctrl B>ShftF1<Ctrl B>  Main Menu      <Ctrl B>Esc    <Ctrl B>Exit Menu
....
....
<Ctrl B>ShftF10<Ctrl B> NOTEPAD Commands
<ENDDEF>
```

Figure 1 shows the display resulting from these statements (except for color).

A keyboard macro for reading a JCL card file has the following form:

```
<BEGDEF><Alt1><TITLE>JCL1<TITLE><Ctrl K>RA:\CARDS\JCL1.CRD<ENTER>
<ENDDEF>
```

Ctrl KR is the command for reading a DOS file into NOTEPAD and A:\CARDS\JCL1.CRD is the pathname of the file to be read.

Superkey macros can be edited in NOTEPAD or an ASCII word processor. Since the length of macro lines can exceed the default right margin setting, reset the margin before editing these lines in NOTEPAD or some strange things may happen. Set the margin with Ctrl OR and enter 180.

Pre- and Post-Processing for Cosmic/NASTRAN On Personal Computers and Mainframes

by
H.A. Kamel, Anton V. Mobley, Ben Nagaraj, and K. W. Watkins
CASA/GIFTS, Inc.

Abstract

An interface between Cosmic/NASTRAN and GIFTS has recently been released, combining the powerful pre- and post-processing capabilities of GIFTS with Cosmic/NASTRAN's analysis capabilities. The interface operates on a wide range of computers, even linking Cosmic/NASTRAN and GIFTS when the two are on different computers. GIFTS offers a wide range of elements for use in model construction, each translated by the interface into the nearest Cosmic/NASTRAN equivalent; and the options of automatic or interactive modelling and loading in GIFTS make pre-processing easy and effective. The interface itself includes the programs GFTCOS, which creates the Cosmic/NASTRAN input deck (and, if desired, control deck) from the GIFTS Unified Data Base; COSGFT, which translates the displacements from the Cosmic/NASTRAN analysis back into GIFTS; and HOSTR, which handles stress computations for a few higher-order elements available in the interface, but not supported by the GIFTS processor STRESS. Finally, the versatile display options in GIFTS post-processing allow the user to examine the analysis results through an especially wide range of capabilities, including such possibilities as creating composite loading cases, plotting in color, and animating the analysis.

Introduction

The newly released interface between Cosmic/NASTRAN and GIFTS allows the user to combine GIFTS' pre- and post-processing capabilities with Cosmic/NASTRAN's analysis capabilities.

GIFTS pre-processors have a wide range of general-purpose capabilities for constructing and loading models interactively or automatically. Beam, spring, membrane, plate, shell, axisymmetric, and solid elements are available. Post-processing capabilities in GIFTS allow user-controlled display of displacements and stresses, beam shear and moment diagrams, deflected shapes superposed on undeflected, alphanumeric tables, and selected labels, element types, or portions of the model. GIFTS can also display plots in color and animate analysis results. The procedures for employing these capabilities are discussed below.

GIFTS and its interface with Cosmic/NASTRAN run on a wide variety of computers, including the IBM-PC AT and XT and their compatibles; larger IBM machines using CMS; VAX, Data General, and PRIME computers; and some UNIX implementations. It is possible to install both GIFTS and Cosmic/NASTRAN on the same computer (a VAX, for instance), or on different computers (say, a large IBM and a PC-AT). Thus the combination is well suited for networking.

The GIFTS-Cosmic/NASTRAN interface takes the form of two central programs: GFTCOS, to extract data from the GIFTS Unified Data Base and create ASCII input files for Cosmic/NASTRAN, and COSGFT, to return results obtained in Cosmic/NASTRAN to the GIFTS data base for post-processing. (A third program, HOSTR, assists with stress calculations for higher-order elements.) This interface supports many of Cosmic/NASTRAN's elements and features, and is scheduled for constant expansion updates to make use of new features in both Cosmic/NASTRAN and GIFTS. For instance, at present the interface supports both static analysis and vibrational mode extraction, with transient and buckling analysis expected in the next release.

Using the Interface

Before executing GFTCOS, the user constructs the desired model in GIFTS and assigns the desired loads and boundary conditions. The pre-processor BULKM (or BULKS for solid models) is used for efficient automatic mesh generation, with detailed editing capabilities available in EDITM (or EDITS). BULKF automatically suppresses degrees of freedom inappropriate to the model as constructed, and OPTIM optimizes the half-bandwidth, an essential step in preparing the model data for the interface. BULKLB and EDITLB (LOADS for solids) are then available for detailed application of loads, temperatures, and boundary conditions.

GFTCOS first examines the model for elements or material types not supported in the interface, notifying the user and terminating if it finds any. (See table below for correspondence between GIFTS elements and materials and their Cosmic/NASTRAN equivalents.) If the model is compatible with Cosmic/NASTRAN, GFTCOS then creates the Cosmic/NASTRAN input deck, producing two files in the process: the input file itself, named JOB.CNI, and a log file named JOB.CNL. The log file contains a record of all messages, prompts, and user responses executed while GFTCOS is running.

CORRESPONDENCE BETWEEN GIFTS AND COSMIC/NASTRAN ELEMENTS

GIFTS ELEMENT	TRANSLATED NASTRAN ELEMENT	GIFTS ANALYSIS
BEAM2	CBAR	YES
QA4	CTRAPRU	YES
QB4	CQUAD2	YES
QM4	CQDMEM1	YES
QM9	CIS2D8 (8 POINTS)	YES
ROD2	CROD	YES
SLD8	CIHEX1 (8 POINTS)	YES
SLD27	CIHEX2 (20 POINTS)	NO
SPRING	CELAS2	YES
TA3	CTRIARG	YES
TB3	CTRIA2	YES
TB6	CTRSHL	NO
TET4	CTETRA	YES
TM3	CTRMEM	YES
TM6	CTRIMG	YES
TSPRING	CELAS2	YES

CORRESPONDENCE BETWEEN GIFTS AND COSMIC/NASTRAN MATERIALS

GIFTS MATERIAL	TRANSLATED NASTRAN MATERIAL	GIFTS ANALYSIS
AALLOY	MAT1	YES
ELMAT	MAT1	YES
MSTEEL	MAT1	YES

The user can also choose to have GFTCOS create the Cosmic/NASTRAN control deck. In this case, the option of an eigen analysis is also offered, with the possibilities of using the determinant search, inverse power, givens, or modified givens method, and of normalizing the eigenvector with respect to the mass matrix, or using a selected point and freedom, or with the maximum deflection set to one.

Among the higher-order elements supported for the interface, GIFTS elements QM9 and SLD27 lack a direct counterpart in the Cosmic/NASTRAN library. Therefore, in translating GIFTS data into the Cosmic/NASTRAN input deck, GFTCOS transforms these elements into similar elements using fewer points (see element correspondence table) and notifies the user of the substitution via a message on the terminal screen. Local Cartesian, cylindrical, and spherical coordinate systems are preserved, as are prescribed displacements, loads, and temperatures. (Loads and temperatures are left untranslated when the user requests an eigen analysis.)

The Cosmic/NASTRAN input deck created by GFTCOS does not include an executive control deck; the user adds this after GFTCOS is run, by means of a text editor. At this time, the user can also edit the input deck itself, for instance by requesting output parameters in addition to the displacements handled by the interface.

The input deck is then submitted to Cosmic/NASTRAN for analysis. If GIFTS and Cosmic/NASTRAN are on different computers, of course the file must first be shipped across the link. The Cosmic/NASTRAN file produced at the end of analysis, containing displacements and stresses, must likewise be shipped back to the machine hosting GIFTS before COSGFT can be invoked.

COSGFT inserts the Cosmic/NASTRAN displacement results into the GIFTS data base. The stresses computed in Cosmic/NASTRAN are ignored, but the GIFTS post-processor STRESS can be called to recompute them for all elements fully supported in GIFTS. If the model contains other element types, such as higher-order solid and shell elements, the user can employ a special processor provided with the interface, named HOSTR, to compute approximate stress fields for them also.

The bulk of GIFTS' powerful post-processing capabilities are exercised via the post-processor RESULT. Here the user can examine all or any part of the model, labelling points, element or material types, and element sizing groups. Geometric entities and elements can be individually deleted from the plot and reactivated at will. Stress contours and vectors are available, as are shear, moment, and detailed cross-sectional plots of beams. Composite loading cases can be created and examined. A wide range of information commands allows tabular retrieval of selected subsets of data from the GIFTS data base. Color plotting permits especially clear, vivid display; and any display can be transferred to a hardcopy file. It is also possible to create animations of the analysis, for subsequent display with GIFTS post-processor VIDEO.

Example of Interface Applications

The following pages contain an example of a solid model constructed and loaded in GIFTS, analyzed in Cosmic/NASTRAN, and then examined in GIFTS. The structure is a pipe joint composed of solid elements and subjected to a combination of internal and external pressure. Printed here are the log file recording the interface procedure, the input file created from the GIFTS data base by the interface for use in Cosmic/NASTRAN, and a selection of plots from both pre- and post-processing in GIFTS. This example is only one demonstration of the way the GIFTS-Cosmic/NASTRAN interface turns GIFTS and Cosmic/NASTRAN into a single, complete general-purpose finite-element package which works on a number of computers, increasing the utility of both programs. Other interfaces are available to link GIFTS with still other programs, including many PC-based general drafting packages, thus expanding the user's capabilities still further.

```
$ SET NOVERIFY

Directory DUA1:[COSMIC]

L004.NID;1                170   5-FEB-1986 11:03

Total of 1 file, 170 blocks.
```

S O R T E D B U L K D A T A E C H O

CARD COUNT	. 1 ..	2 ..	3 ..	4 ..	5 ..	6 ..	7 ..	8 ..	9 ..	10 .
1-	CIHEX1	1	1	9	10	2	1	18	20	+H1
2-	+H1	21	19							
3-	CIHEX1	2	1	18	20	21	19	37	39	+H2
4-	+H2	40	38							
5-	CIHEX1	3	1	37	39	40	38	55	57	+H3
6-	+H3	58	56							
7-	CIHEX1	4	1	55	57	58	56	73	75	+H4
8-	+H4	76	74							
9-	CIHEX1	5	1	73	75	76	74	91	93	+H5
10-	+H5	94	92							
11-	CIHEX1	6	1	91	93	94	92	109	111	+H6
12-	+H6	112	110							
13-	CIHEX1	7	1	109	111	112	110	127	129	+H7
14-	+H7	130	128							
15-	CIHEX1	8	1	127	129	130	128	145	147	+H8
16-	+H8	148	146							
17-	CIHEX1	9	1	10	11	3	2	20	22	+H9
18-	+H9	23	21							
19-	CIHEX1	10	1	20	22	23	21	39	41	+H10
20-	+H10	42	40							
21-	CIHEX1	11	1	39	41	42	40	57	59	+H11
22-	+H11	60	58							
23-	CIHEX1	12	1	57	59	60	58	75	77	+H12
24-	+H12	78	76							
25-	CIHEX1	13	1	75	77	78	76	93	95	+H13
26-	+H13	96	94							
27-	CIHEX1	14	1	93	95	96	94	111	113	+H14
28-	+H14	114	112							
29-	CIHEX1	15	1	111	113	114	112	129	131	+H15
30-	+H15	132	130							
31-	CIHEX1	16	1	129	131	132	130	147	149	+H16
32-	+H16	150	148							
33-	CIHEX1	17	1	11	12	4	3	22	24	+H17
34-	+H17	25	23							
35-	CIHEX1	18	1	22	24	25	23	41	43	+H18
36-	+H18	44	42							
37-	CIHEX1	19	1	41	43	44	42	59	61	+H19
38-	+H19	62	60							
39-	CIHEX1	20	1	59	61	62	60	77	79	+H20
40-	+H20	80	78							
41-	CIHEX1	21	1	77	79	80	78	95	97	+H21
42-	+H21	98	96							

continues .....

S O R T E D B U L K D A T A E C H O

```
CARD
COUNT      .  1  ..  2  ..  3  ..  4  ..  5  ..  6  ..  7  ..  8  ..  9  .. 10  .
1387-      GRID   578     0      -21.00000.0     4.0000000      12456
1388-      GRID   579     0      -21.0000.97545774.9039260      1456
1389-      GRID   580     0      -21.0000.78034873.9231430      1456
1390-      GRID   581     0      -21.00001.9134234.6193950      1456
1391-      GRID   582     0      -21.00001.5307223.6955230      1456
1392-      GRID   583     0      -21.00002.7778574.1573440      1456
1393-      GRID   584     0      -21.00002.2222733.3258840      1456
1394-      GRID   585     0      -21.00003.5355403.5355280      1456
1395-      GRID   586     0      -21.00002.8284242.8284300      1456
1396-      GRID   587     0      -21.00004.1573532.7778430      1456
1397-      GRID   588     0      -21.00003.3258782.2222810      1456
1398-      GRID   589     0      -21.00004.6194021.9134080      1456
1399-      GRID   590     0      -21.00003.6955191.5307300      1456
1400-      GRID   591     0      -21.00004.903929.97544340      1456
1401-      GRID   592     0      -21.00003.923142.78035640      1456
1402-      GRID   593     0      -21.00005.0000000.0     0      13456
1403-      GRID   594     0      -21.00004.0000000.0     0      13456
1404-      MAT1   1       .15000E8.60000E7.25000000.0    0.0    0.0    0.0
1405-      MAT1   2       .30000E7.12500E7.20000000.0    0.0    0.0    0.0
1406-      PIHEX  1       1
1407-      PIHEX  2       2
1408-      PIHEX  3       1
1409-      PIHEX  4       2
           ENDDATA
```

*** USER INFORMATION MESSAGES FROM RESEQUENCING PROCESSOR - BANDIT (CRI= 1, MTH= 3, MPC= 2, DEP=-1, PCH=-1)

BEFORE RESEQUENCING - - -

BANDWIDTH	54
PROFILE	18011
MAX WAVEFRONT	54
AVG WAVEFRONT	30.322
RMS WAVEFRONT	32.604

AFTER RESEQUENCING BY GIBBS-POOLE-STOCKMEYER (GPS) ALGORITHM - - -

BANDWIDTH	46
PROFILE	17407
MAX WAVEFRONT	44
AVG WAVEFRONT	29.305
RMS WAVEFRONT	30.794

*** BANDIT SUMMARY ***

	BEFORE	AFTER
BANDWIDTH (B)	54	46
PROFILE (P)	18011	17407
MAXIMUM WAVEFRONT (C-MAX)	54	44
AVERAGE WAVEFRONT (C-AVG)	30.322	29.305
RMS WAVEFRONT (C-RMS)	32.604	30.794
NUMBER OF GRID POINTS (N)		594
NUMBER OF ELEMENTS (NON-RIGID)		256
NUMBER OF RIGID ELEMENTS PROCESSED		0
NUMBER OF MPC EQUATIONS PROCESSED		0
NUMBER OF COMPONENTS		1
MAXIMUM NODAL DEGREE		17
MINIMUM NODAL DEGREE		7
NUMBER OF UNIQUE EDGES		4553
MATRIX DENSITY, PERCENT		2.749
NUMBER OF POINTS OF ZERO DEGREE		0
BANDIT OPEN CORE		249412
CRITERION		RMS WAVEFRONT
METHOD USED		GPS
NO. OF SEQGP CARDS GENERATED		149

S Y S T E M G E N E R A T E D S E Q G P C A R D S,

SEQGP	1	2	2	4	3	6	4	8
SEQGP	5	10	6	12	7	14	8	18
SEQGP	9	1	10	3	11	5	12	7
SEQGP	13	9	14	11	15	13	16	15
SEQGP	17	17	18	19	19	20	20	21
SEQGP	21	22	22	23	23	24	24	25
SEQGP	25	26	26	27	27	28	28	29
SEQGP	29	30	30	31	31	32	32	16
SEQGP	33	33	34	34	35	35	36	36
SEQGP	37	37	38	38	39	39	40	40
SEQGP	41	41	42	42	43	43	44	44
SEQGP	45	45	46	46	47	47	48	48
SEQGP	49	49	50	50	51	51	52	52
SEQGP	53	53	54	54	55	55	56	56
SEQGP	57	57	58	58	59	59	60	60
SEQGP	61	61	62	62	63	63	64	64
SEQGP	65	65	66	66	67	67	68	68
SEQGP	69	69	70	70	71	71	72	72
SEQGP	73	73	74	74	75	75	76	76
SEQGP	77	77	78	78	79	79	80	80

continues .....

SEQGP	509	174	510	173	511	168	512	167
SEQGP	513	176	514	175	515	166	516	165
SEQGP	517	178	518	177	519	164	520	163
SEQGP	521	180	522	179	523	563	524	564
SEQGP	525	565	526	566	527	567	528	568
SEQGP	529	569	530	570	531	555	532	556
SEQGP	533	537	534	538	535	515	536	516
SEQGP	537	489	538	490	539	459	540	460
SEQGP	541	577	542	578	543	579	544	580
SEQGP	545	581	546	582	547	571	548	572
SEQGP	549	557	550	558	551	539	552	540
SEQGP	553	517	554	518	555	491	556	492
SEQGP	557	461	558	462	559	587	560	588
SEQGP	561	589	562	590	563	583	564	584
SEQGP	565	573	566	574	567	559	568	560
SEQGP	569	541	570	542	571	519	572	520
SEQGP	573	493	574	494	575	463	576	464
SEQGP	577	594	578	593	579	591	580	592
SEQGP	581	585	582	586	583	575	584	576
SEQGP	585	561	586	562	587	543	588	544
SEQGP	589	521	590	522	591	495	592	496
SEQGP	593	465	594	466				

NO ERRORS FOUND - EXECUTE NASTRAN PROGRAM

```
*** USER INFORMATION MESSAGE, TURN DIAG 38 ON FOR ADDITIONAL ELEMENT PROCESSING INFORMATION

*** USER FATAL MESSAGE 3302, IHEX1 ELEMENT NO.      116   ILLEGAL GEOMETRY, ALFA EXCEEDED.

*** USER FATAL MESSAGE 3302, IHEX1 ELEMENT NO.      124   ILLEGAL GEOMETRY, ALFA EXCEEDED.

*** USER FATAL MESSAGE 3302, IHEX1 ELEMENT NO.      213   ILLEGAL GEOMETRY, ALFA EXCEEDED.

*** USER FATAL MESSAGE 3302, IHEX1 ELEMENT NO.      221   ILLEGAL GEOMETRY, ALFA EXCEEDED.

*** USER FATAL MESSAGE 3302, IHEX1 ELEMENT NO.      221   ILLEGAL GEOMETRY, ALFA EXCEEDED.


***USER INFORMATION MESSAGE 3023--PARAMETERS FOR REAL   SYMMETRIC DECOMPOSITION OF DATA BLOCK KLL      ( N = 1596 )
              TIME ESTIMATE=  20586        C AVG =   81        PC AVG =    0   SPILL GROUPS =    0         S AVG =    1
            ADDITIONAL CORE=-227859        C MAX =  122        PCMAX =     0      PC GROUPS =    0  PREFACE LOOPS =    1


*** USER INFORMATION MESSAGE 3035

FOR LOAD    1 EPSILON SUB E =  1.2422739E-15
```

GIFTS LOAD CASE:1 SUBCASE 1

D I S P L A C E M E N T V E C T O R

POINT ID.	TYPE	T1	T2	T3	R1	R2	R3
1	G	0.0	0.0	-1.412810E-03	0.0	0.0	0.0
2	G	0.0	-8.293360E-05	-1.368316E-03	0.0	0.0	0.0
3	G	0.0	-1.434956E-04	-1.242397E-03	0.0	0.0	0.0
4	G	0.0	-1.666498E-04	-1.055474E-03	0.0	0.0	0.0
5	G	0.0	-1.495623E-04	-8.347788E-04	0.0	0.0	0.0
6	G	0.0	-1.023543E-04	-6.065379E-04	0.0	0.0	0.0
7	G	0.0	-4.450929E-05	-3.889870E-04	0.0	0.0	0.0
8	G	0.0	1.944273E-05	0.0	0.0	0.0	0.0
9	G	0.0	0.0	-1.379316E-03	0.0	0.0	0.0
10	G	0.0	-1.610228E-04	-1.318456E-03	0.0	0.0	0.0
11	G	0.0	-2.777156E-04	-1.149825E-03	0.0	0.0	0.0
12	G	0.0	-3.203591E-04	-9.107926E-04	0.0	0.0	0.0
13	G	0.0	-2.834938E-04	-6.502475E-04	0.0	0.0	0.0
14	G	0.0	-1.873774E-04	-4.133017E-04	0.0	0.0	0.0
15	G	0.0	-7.080255E-05	-2.277407E-04	0.0	0.0	0.0
16	G	0.0	2.224120E-05	-9.671461E-05	0.0	0.0	0.0
17	G	0.0	5.753958E-05	0.0	0.0	0.0	0.0
18	G	-6.841561E-05	0.0	-1.386334E-03	0.0	0.0	0.0
19	G	-5.449258E-05	0.0	-1.420199E-03	0.0	0.0	0.0
20	G	-6.868053E-05	-1.617761E-04	-1.325242E-03	0.0	0.0	0.0
21	G	-5.521253E-05	-8.346338E-05	-1.375516E-03	0.0	0.0	0.0
22	G	-6.941930E-05	-2.790896E-04	-1.155956E-03	0.0	0.0	0.0
23	G	-5.725115E-05	-1.444824E-04	-1.249049E-03	0.0	0.0	0.0
24	G	-7.048190E-05	-3.221241E-04	-9.159508E-04	0.0	0.0	0.0
25	G	-6.026979E-05	-1.679666E-04	-1.061282E-03	0.0	0.0	0.0
26	G	-7.166900E-05	-2.853871E-04	-6.542657E-04	0.0	0.0	0.0
27	G	-6.378039E-05	-1.510606E-04	-8.395361E-04	0.0	0.0	0.0
28	G	-7.278436E-05	-1.891781E-04	-4.161623E-04	0.0	0.0	0.0
29	G	-6.723651E-05	-1.039039E-04	-6.101293E-04	0.0	0.0	0.0
30	G	-7.367384E-05	-7.239363E-05	-2.295345E-04	0.0	0.0	0.0
31	G	-7.012354E-05	-4.602856E-05	-3.913739E-04	0.0	0.0	0.0
32	G	0.0	1.835273E-06	-1.884948E-04	0.0	0.0	0.0
33	G	-7.423946E-05	2.084744E-05	-9.756794E-05	0.0	0.0	0.0
34	G	-7.203059E-05	3.674250E-07	-1.896816E-04	0.0	0.0	0.0
35	G	-7.443262E-05	5.622514E-05	0.0	0.0	0.0	0.0
36	G	-7.269604E-05	1.799822E-05	0.0	0.0	0.0	0.0
37	G	-1.333498E-04	0.0	-1.405247E-03	0.0	0.0	0.0
38	G	-1.112928E-04	0.0	-1.440140E-03	0.0	0.0	0.0
39	G	-1.339938E-04	-1.636622E-04	-1.343518E-03	0.0	0.0	0.0
40	G	-1.127926E-04	-8.469930E-05	-1.394937E-03	0.0	0.0	0.0
41	G	-1.357890E-04	-2.824959E-04	-1.172427E-03	0.0	0.0	0.0
42	G	-1.170397E-04	-1.467525E-04	-1.266974E-03	0.0	0.0	0.0

continues .....

589	G	0.0	-1.015947E-03	2.145764E-04	0.0	0.0	0.0
590	G	0.0	-1.181167E-03	6.788397E-04	0.0	0.0	0.0
591	G	0.0	-1.383135E-03	4.928993E-05	0.0	0.0	0.0
592	G	0.0	-1.412404E-03	3.188860E-04	0.0	0.0	0.0
593	G	0.0	-1.520760E-03	0.0	0.0	0.0	0.0
594	G	0.0	-1.496575E-03	0.0	0.0	0.0	0.0

*** SYSTEM WARNING MESSAGE 3022

DATA BLOCK PLTPAR IS REQUIRED AS INPUT AND IS NOT OUTPUT BY A PREVIOUS MODULE IN THE CURRENT DMAP ROUTE.

*** SYSTEM WARNING MESSAGE 3022

DATA BLOCK GPSETS IS REQUIRED AS INPUT AND IS NOT OUTPUT BY A PREVIOUS MODULE IN THE CURRENT DMAP ROUTE.

*** SYSTEM WARNING MESSAGE 3022

DATA BLOCK ELSETS IS REQUIRED AS INPUT AND IS NOT OUTPUT BY A PREVIOUS MODULE IN THE CURRENT DMAP ROUTE.

* * * END OF JOB * * *

```
11:06:34          0.0 ELAPSED SECONDS       0.0 CPU SECONDS      SEM1  BEGN
11:06:40          6.0 ELAPSED SECONDS       3.0 CPU SECONDS      GNFI
11:06:41          7.0 ELAPSED SECONDS       3.0 CPU SECONDS      TTIO
11:08:01         87.0 ELAPSED SECONDS      74.0 CPU SECONDS      TTLP
11:09:23        169.0 ELAPSED SECONDS     155.0 CPU SECONDS      XCSA
11:09:39        185.0 ELAPSED SECONDS     168.0 CPU SECONDS      IFP1
11:09:43        189.0 ELAPSED SECONDS     171.0 CPU SECONDS      XSOR
11:12:12        338.0 ELAPSED SECONDS     305.0 CPU SECONDS      IFP   BEGN
11:14:02        448.0 ELAPSED SECONDS     407.0 CPU SECONDS      IFP   END
11:14:02        448.0 ELAPSED SECONDS     407.0 CPU SECONDS      XGPI
11:14:21        467.0 ELAPSED SECONDS     425.0 CPU SECONDS      BAND  IT  BEGN11:15:34        541.0 ELAPSED SECONDS     478.0 CPU
 SECONDS      BAND
  END
11:15:36        542.0 ELAPSED SECONDS     478.0 CPU SECONDS      SEM1  END
11:15:42        548.0 ELAPSED SECONDS     480.0 CPU SECONDS      LINK   1        END
11:15:42        548.0 ELAPSED SECONDS     480.0 CPU SECONDS      ----  --------  ----
11:15:55        561.0 ELAPSED SECONDS     485.0 CPU SECONDS      LINK   2        BEGN
11:15:55        561.0 ELAPSED SECONDS     486.0 CPU SECONDS         5  PARAM     BEGN
11:15:55        561.0 ELAPSED SECONDS     486.0 CPU SECONDS         5  PARAM     END
11:15:55        561.0 ELAPSED SECONDS     486.0 CPU SECONDS      XSFA      BEGN11:15:58        564.0 ELAPSED SECONDS     487.0 CPU
 SECONDS      XSFA
  END
11:15:59        565.0 ELAPSED SECONDS     487.0 CPU SECONDS         6  GP1       BEGN
11:17:01        628.0 ELAPSED SECONDS     536.0 CPU SECONDS         6  GP1       END
11:17:02        628.0 ELAPSED SECONDS     536.0 CPU SECONDS         7  PLTTRAN   BEGN
11:17:09        635.0 ELAPSED SECONDS     541.0 CPU SECONDS         7  PLTTRAN   END
11:17:09        635.0 ELAPSED SECONDS     541.0 CPU SECONDS         8  GP2       BEGN
11:17:14        640.0 ELAPSED SECONDS     544.0 CPU SECONDS         8  GP2       END
11:17:14        640.0 ELAPSED SECONDS     544.0 CPU SECONDS         9  PARAML    BEGN
11:17:14        640.0 ELAPSED SECONDS     544.0 CPU SECONDS         9  PARAML    END

 continues ........
20:16:09      32975.0 ELAPSED SECONDS   32388.0 CPU SECONDS           XSFA      BEGN
20:16:11      32977.0 ELAPSED SECONDS   32389.0 CPU SECONDS           XSFA       END
20:16:11      32977.0 ELAPSED SECONDS   32389.0 CPU SECONDS       140 SCAN      BEGN
20:16:11      32977.0 ELAPSED SECONDS   32389.0 CPU SECONDS       140 SCAN      END
20:16:12      32978.0 ELAPSED SECONDS   32389.0 CPU SECONDS       141 OFP       BEGN
20:16:12      32978.0 ELAPSED SECONDS   32389.0 CPU SECONDS       141 OFP       END
20:16:12      32978.0 ELAPSED SECONDS   32389.0 CPU SECONDS       142 OFP       BEGN
20:16:12      32978.0 ELAPSED SECONDS   32389.0 CPU SECONDS       142 OFP       END
20:16:12      32978.0 ELAPSED SECONDS   32389.0 CPU SECONDS       144 COND      BEGN
20:16:12      32978.0 ELAPSED SECONDS   32390.0 CPU SECONDS       144 COND      END
20:16:13      32979.0 ELAPSED SECONDS   32390.0 CPU SECONDS       149 COND      BEGN
20:16:13      32979.0 ELAPSED SECONDS   32390.0 CPU SECONDS       149 COND      END
20:16:13      32979.0 ELAPSED SECONDS   32390.0 CPU SECONDS       163 PURGE     BEGN
20:16:13      32979.0 ELAPSED SECONDS   32390.0 CPU SECONDS       163 PURGE     END
20:16:13      32979.0 ELAPSED SECONDS   32390.0 CPU SECONDS       164 EXIT      BEGN

Directory DUA1:[COSMIC]

Total of 50 files, 4444/4509 blocks.
  COSMIC       job terminated at  5-FEB-1986 20:16:39.84

  Accounting information:
  Buffered I/O count:          1757      Peak working set size:   512
  Direct I/O count:            6838      Peak page file size:    3253
  Page faults:                28863      Mounted volumes:           0
  Charged CPU time:     0 09:00:11.17    Elapsed time:     0 09:10:20.79
```

Input File For Use in Cosmic/NASTRAN

```
TITLE = GIFTS MODEL:L004
OUTPUT
   DISP = ALL
SUBCASE 1
   LABEL = GIFTS LOAD CASE:1
   LOAD = 1
BEGIN BULK
GRID     1       0       0.      0.      4.0000000       12456
GRID     2       0       0.      .78034873.9231430       1456
GRID     3       0       0.      1.5307223.6955230       1456
GRID     4       0       0.      2.2222733.3258840       1456
GRID     5       0       0.      2.8284242.8284300       1456
GRID     6       0       0.      3.3258782.2222810       1456
GRID     7       0       0.      3.6955191.5307300       1456
GRID     8       0       0.      4.0000000.      0       13456
GRID     9       0       0.      0.      5.0000000       12456
GRID     10      0       0.      .97545774.9039260       1456
GRID     11      0       0.      1.9134234.6193950       1456
GRID     12      0       0.      2.7778574.1573440       1456
GRID     13      0       0.      3.5355403.5355280       1456
GRID     14      0       0.      4.1573532.7778430       1456
GRID     15      0       0.      4.6194021.9134080       1456
GRID     16      0       0.      4.903929.97544340       1456
GRID     17      0       0.      5.0000000.      0       13456
GRID     18      0       -.8750000.      5.0000000       2456
GRID     19      0       -.8750000.      4.0000000       2456
GRID     20      0       -.875000.97545774.9039260       456
GRID     21      0       -.875000.78034403.9231440       456
GRID     22      0       -.8750001.9134234.6193950       456
GRID     23      0       -.8750001.5307173.6955250       456
GRID     24      0       -.8750002.7778574.1573440       456
GRID     25      0       -.8750002.2222713.3258860       456
continues .......
GRID     555     0       -19.01664.907369.95798270       456
GRID     556     0       -18.61203.930016.74496690       456
GRID     557     0       -19.00005.0000000.      0       3456
GRID     558     0       -18.50004.0000000.      0       3456
GRID     559     0       -20.12500.      5.0000000       2456
GRID     560     0       -20.12500.      4.0000000       2456
GRID     561     0       -20.1059.96650064.9057000       456
GRID     562     0       -20.0922.76348823.9264590       456
GRID     563     0       -20.08661.9035634.6234680       456
GRID     564     0       -20.05551.5103103.7039130       456
GRID     565     0       -20.06772.7721614.1611440       456
GRID     566     0       -20.01422.2085223.3350320       456
GRID     567     0       -20.04983.5353783.5356900       456
GRID     568     0       -19.96802.8255032.8313470       456
GRID     569     0       -20.03354.1609192.7725000       456
GRID     570     0       -19.91713.3313712.2140380       456
GRID     571     0       -20.01944.6233521.9038400       456
GRID     572     0       -19.86253.7028761.5128480       456
GRID     573     0       -20.00814.905668.96665020       456
GRID     574     0       -19.80603.926577.76288970       456
GRID     575     0       -20.00005.0000000.      0       3456
GRID     576     0       -19.75004.0000000.      0       3456
GRID     577     0       -21.00000.      5.0000000       12456
GRID     578     0       -21.00000.      4.0000000       12456
GRID     579     0       -21.0000.97545774.9039260       1456
GRID     580     0       -21.0000.78034873.9231430       1456
GRID     581     0       -21.00001.9134234.6193950       1456
GRID     582     0       -21.00001.5307223.6955230       1456
```

```
GRID    583     0       -21.00002.7778574.1573440       1456
GRID    584     0       -21.00002.2222733.3258840       1456
GRID    585     0       -21.00003.5355403 5355280       1456
GRID    586     0       -21.00002.8284242.8284300       1456
GRID    587     0       -21.00004.1573532.7778430       1456
GRID    588     0       -21.00003.3258782.2222810       1456
GRID    589     0       -21.00004.6194021.9134080       1456
GRID    590     0       -21.00003.6955191.5307300       1456
GRID    591     0       -21.00004.903929.97544340       1456
GRID    592     0       -21.00003.923142.78035640       1456
GRID    593     0       -21.00005.0000000.      0       13456
GRID    594     0       -21.00004.0000000.      0       13456
MAT1    1       .15000E8.60000E7.25000000.      0.      0.      0.
MAT1    2       .30000E7.12500E7.20000000.      0.      0.      0.
PIHEX   1       1
CIHEX1  1       1       9       10      2       1       18      20      +H1
+H1     21      19
CIHEX1  2       1       18      20      21      19      37      39      +H2
+H2     40      38
CIHEX1  3       1       37      39      40      38      55      57      +H3
+H3     58      56
CIHEX1  4       1       55      57      58      56      73      75      +H4
+H4     76      74
CIHEX1  5       1       73      75      76      74      91      93      +H5
+H5     94      92
CIHEX1  6       1       91      93      94      92      109     111     +H6
+H6     112     110
CIHEX1  7       1       109     111     112     110     127     129     +H7
+H7     130     128
CIHEX1  8       1       127     129     130     128     145     147     +H8
+H8     148     146
CIHEX1  9       1       10      11      3       2       20      22      +H9
+H9     23      21
CIHEX1  10      1       20      22      23      21      39      41      +H10
+H10    42      40
CIHEX1  11      1       39      41      42      40      57      59      +H11
+H11    60      58
CIHEX1  12      1       57      59      60      58      75      77      +H12
+H12    78      76
CIHEX1  13      1       75      77      78      76      93      95      +H13
+H13    96      94
CIHEX1  14      1       93      95      96      94      111     113     +H14
+H14    114     112
CIHEX1  15      1       111     113     114     112     129     131     +H15
+H15    132     130
CIHEX1  16      1       129     131     132     130     147     149     +H16
+H16    150     148
CIHEX1  17      1       11      12      4       3       22      24      +H17
+H17    25      23
CIHEX1  18      1       22      24      25      23      41      43      +H18
+H18    44      42
CIHEX1  19      1       41      43      44      42      59      61      +H19
+H19    62      60
CIHEX1  20      1       59      61      62      60      77      79      +H20
+H20    80      78
CIHEX1  21      1       77      79      80      78      95      97      +H21
+H21    98      96
CIHEX1  22      1       95      97      98      96      113     115     +H22
+H22    116     114
CIHEX1  23      1       113     115     116     114     131     133     +H23
+H23    134     132
```

```
CIHEX1  24      1       131     133     134     132     149     151     +H24
+H24    152     150
CIHEX1  25      1       12      13      5       4       24      26      +H25
+H25    27      25
CIHEX1  26      1       24      26      27      25      43      45      +H26
+H26    46      44
CIHEX1  27      1       43      45      46      44      61      63      +H27
+H27    64      62
 continued .......
CIHEX1  224     3       297     299     300     298     327     329     +H224
+H224   330     328
PIHEX   4       2
CIHEX1  225     4       489     490     492     491     443     444     +H225
+H225   446     445
CIHEX1  226     4       491     492     494     493     445     446     +H226
+H226   448     447
CIHEX1  227     4       493     494     496     495     447     448     +H227
+H227   450     449
CIHEX1  228     4       495     496     498     497     449     450     +H228
+H228   452     451
CIHEX1  229     4       497     498     500     499     451     452     +H229
+H229   454     453
CIHEX1  230     4       499     500     502     501     453     454     +H230
+H230   456     455
CIHEX1  231     4       501     502     504     503     455     456     +H231
+H231   470     469
CIHEX1  232     4       503     504     522     521     469     470     +H232
+H232   518     517
CIHEX1  233     4       443     444     446     445     401     402     +H233
+H233   404     403
CIHEX1  234     4       445     446     448     447     403     404     +H234
+H234   406     405
CIHEX1  235     4       447     448     450     449     405     406     +H235
+H235   408     407
CIHEX1  236     4       449     450     452     451     407     408     +H236
+H236   410     409
CIHEX1  237     4       451     452     454     453     409     410     +H237
+H237   412     411
CIHEX1  238     4       453     454     456     455     411     412     +H238
+H238   422     421
CIHEX1  239     4       455     456     470     469     421     422     +H239
+H239   466     465
CIHEX1  240     4       469     470     518     517     465     466     +H240
+H240   514     513
CIHEX1  241     4       401     402     404     403     363     364     +H241
+H241   366     365
CIHEX1  242     4       403     404     406     405     365     366     +H242
+H242   368     367
CIHEX1  243     4       405     406     408     407     367     368     +H243
+H243   370     369
CIHEX1  244     4       407     408     410     409     369     370     +H244
+H244   372     371
CIHEX1  245     4       409     410     412     411     371     372     +H245
+H245   378     377
CIHEX1  246     4       411     412     422     421     377     378     +H246
+H246   418     417
CIHEX1  247     4       421     422     466     465     417     418     +H247
+H247   462     461
CIHEX1  248     4       465     466     514     513     461     462     +H248
+H248   510     509
CIHEX1  249     4       363     364     366     365     329     330     +H249
+H249   332     331
```

```
CIHEX1  250     4       365     366     368     367     331     332     +H250
+H250   334     333
CIHEX1  251     4       367     368     370     369     333     334     +H251
+H251   336     335
CIHEX1  252     4       369     370     372     371     335     336     +H252
+H252   338     337
CIHEX1  253     4       371     372     378     377     337     338     +H253
+H253   374     373
CIHEX1  254     4       377     378     418     417     373     374     +H254
+H254   414     413
CIHEX1  255     4       417     418     462     461     413     414     +H255
+H255   458     457
CIHEX1  256     4       461     462     510     509     457     458     +H256
+H256   506     505
FORCE   1       1       0       85.76326-.557E-6-.098016-.995185
FORCE   1       2       0       170.7023-.533E-6-.195089-.980786
FORCE   1       3       0       170.7047-.73E-6 -.382681-.923881
FORCE   1       4       0       170.7053-.263E-7-.555568-.831471
FORCE   1       5       0       170.7053.5430E-6-.707106-.707107
FORCE   1       6       0       170.7052.4778E-6-.831470-.555570
FORCE   1       7       0       170.7045.8475E-6-.923880-.382683
FORCE   1       8       0       85.764160.      -.995185-.098016
FORCE   1       19      0       171.5260-.564E-6-.098016-.995185
FORCE   1       21      0       341.4041-.457E-6-.195089-.980786
FORCE   1       23      0       341.4094-.365E-6-.382680-.923881
FORCE   1       25      0       341.4116-.154E-6-.555568-.831471
FORCE   1       27      0       341.4119.3313E-6-.707106-.707107
FORCE   1       29      0       341.4111.6515E-6-.831470-.555570
FORCE   1       31      0       341.4094.8723E-6-.923880-.382683
FORCE   1       32      0       170.7033.4893E-6-.980785-.195090
FORCE   1       34      0       341.4060.5142E-6-.980785-.195090
FORCE   1       36      0       171.52750.      -.995185-.098016
FORCE   1       38      0       171.5251-.567E-6-.098015-.995185
FORCE   1       40      0       341.4031-.721E-6-.195088-.980786
FORCE   1       42      0       341.4097-.386E-6-.382679-.923882
FORCE   1       44      0       341.4128-.857E-7-.555568-.831471
FORCE   1       46      0       341.4136.1576E-6-.707107-.707107
FORCE   1       48      0       341.4121.7806E-6-.831470-.555569
FORCE   1       50      0       341.4097.7543E-6-.923881-.382681
FORCE   1       52      0       341.4043.2671E-6-.980785-.195089
FORCE   1       54      0       171.52600.      -.995185-.098015
FORCE   1       56      0       171.5242-.551E-6-.098014-.995185
FORCE   1       58      0       341.4021-.712E-6-.195087-.980786
FORCE   1       60      0       341.4099-.756E-6-.382679-.923882
FORCE   1       62      0       341.4141-.79E-7 -.555567-.831472
FORCE   1       64      0       341.4153.3313E-6-.707107-.707107
FORCE   1       66      0       341.4136.5689E-6-.831471-.555568
FORCE   1       68      0       341.4099.7344E-6-.923881-.382680
FORCE   1       70      0       341.4026.2472E-6-.980786-.195088
FORCE   1       72      0       171.52470.      -.995185-.098014
FORCE   1       74      0       171.5232-.551E-6-.098014-.995185
FORCE   1       76      0       341.4004-.45E-6 -.195086-.980786
FORCE   1       78      0       341.4102-.365E-6-.382677-.923882
FORCE   1       80      0       341.4153-.154E-6-.555567-.831472
FORCE   1       82      0       341.4172.3313E-6-.707107-.707107
FORCE   1       84      0       341.4153.6515E-6-.831472-.555567
FORCE   1       86      0       341.4099.8673E-6-.923882-.382679
FORCE   1       88      0       341.4009.5092E-6-.980786-.195087
FORCE   1       90      0       171.52350.      -.995185-.098013
FORCE   1       92      0       171.5222-.561E-6-.098013-.995185
FORCE   1       94      0       341.3994-.455E-6-.195086-.980786
FORCE   1       96      0       341.4104-.124E-6-.382677-.923882
FORCE   1       98      0       341.4165-.858E-7-.555566-.831472
```

continued ......

```
FORCE    1        528      0        370.4331.0021883.3695893.9291924
FORCE    1        530      0        399.7581.0022033.5467626.8372850
FORCE    1        532      0        424.6436.0011886.7063760.7078357
FORCE    1        534      0        441.6260-.319E-3.8368124.5474901
FORCE    1        536      0        448.7356-.001508.9298403.3679607
FORCE    1        538      0        446.4216-.001699.9830975.1830739
FORCE    1        540      0        222.4615-.001473.9959748.0896217
FORCE    1        542      0        167.17090.       .0926010.9957032
FORCE    1        544      0        345.1616.9513E-3.1894745.9818855
FORCE    1        546      0        370.0320.0021255.3739749.9274365
FORCE    1        548      0        394.7087.0020921.5499132.8352189
FORCE    1        550      0        417.1165.0011103.7070861.7071265
FORCE    1        552      0        435.1235-.32E-3 .8356379.5492803
FORCE    1        554      0        447.2412-.001432.9283869.3716130
FORCE    1        556      0        453.1758-.001653.9825720.1858730
FORCE    1        558      0        228.2964-.001469.9957484.0921032
FORCE    1        560      0        170.98220.       .0948008.9954963
FORCE    1        562      0        349.9470.9346E-3.1923786.9813204
FORCE    1        564      0        369.5327.0020654.3781974.9257224
FORCE    1        566      0        389.8376.0019884.5529263.8332276
FORCE    1        568      0        409.9722.0010391.7077617.7064510
FORCE    1        570      0        428.8962-.286E-3.8345078.5509961
FORCE    1        572      0        445.6563-.001361.9269736.3751231
FORCE    1        574      0        459.6250-.001610.9820634.1885440
FORCE    1        576      0        233.9797-.001465.9955221.0945179
FORCE    1        578      0        86.434690.       .0958782.9953930
FORCE    1        580      0        176.1477.9262E-3.1937943.9810417
FORCE    1        582      0        184.6307.0020354.3802702.9248732
FORCE    1        584      0        193.7235.0019373.5544077.8322430
FORCE    1        586      0        203.2462.0010048.7080938.7061177
FORCE    1        588      0        212.9244-.277E-3.8339486.5518419
FORCE    1        590      0        222.4211-.001327.9262747.3768466
FORCE    1        592      0        231.3876-.001590.9818138.1898394
FORCE    1        594      0        118.3921-.001463.9954097.0956946
ENDDATA
```

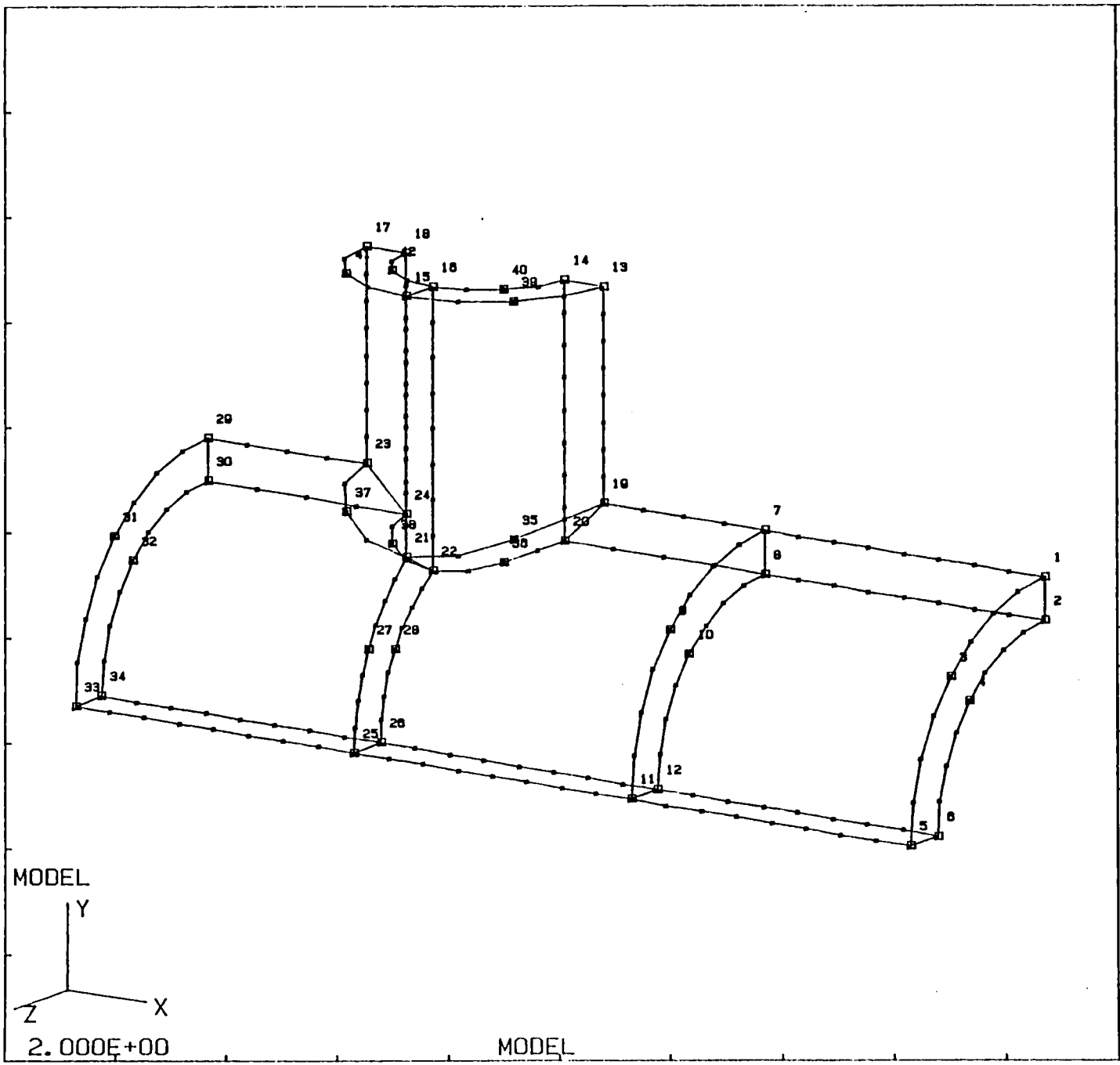

Pre-Processing: Key Points

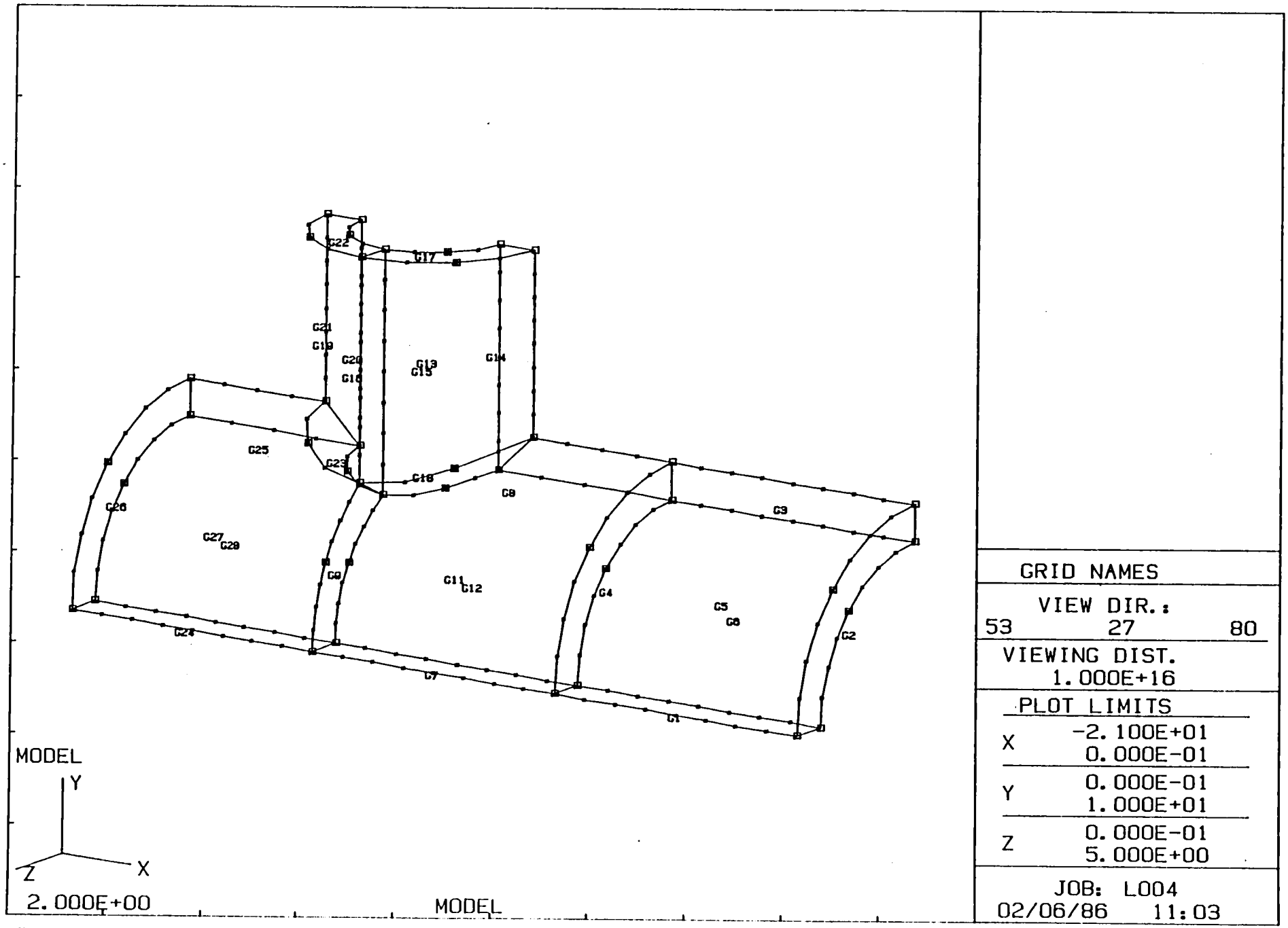

Pre-Processing: Grid Names

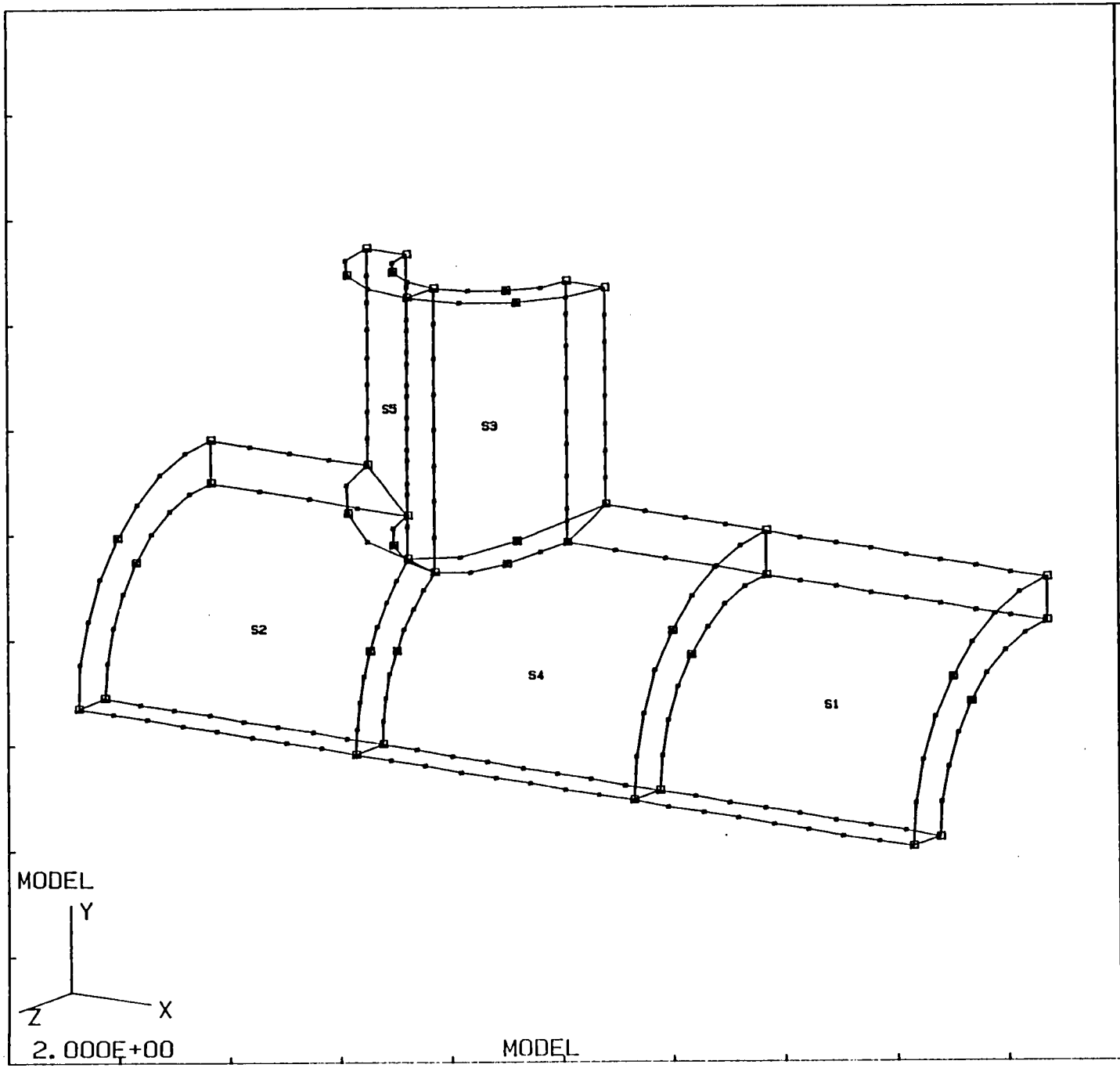

SOLID NAMES

VIEW DIR.:
53 27 80

VIEWING DIST.
1.000E+16

PLOT LIMITS

X	-2.100E+01 0.000E-01
Y	0.000E-01 1.000E+01
Z	0.000E-01 5.000E+00

JOB: L004
02/06/86 11:03

Pre-Processing: Solid Names

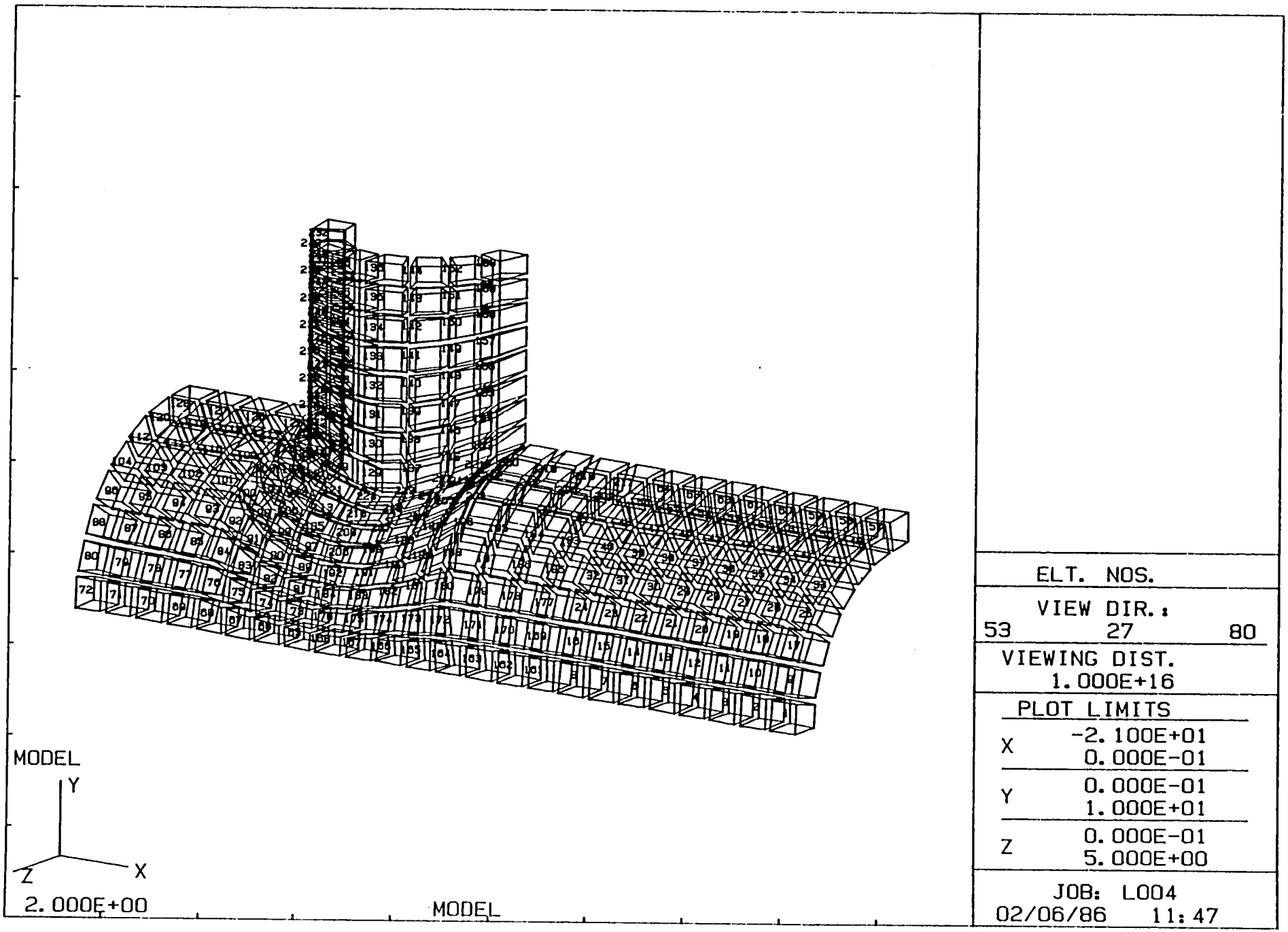

Pre-Processing: Element Slice With Element Numbers (Elements Shrunken 20% For Display)

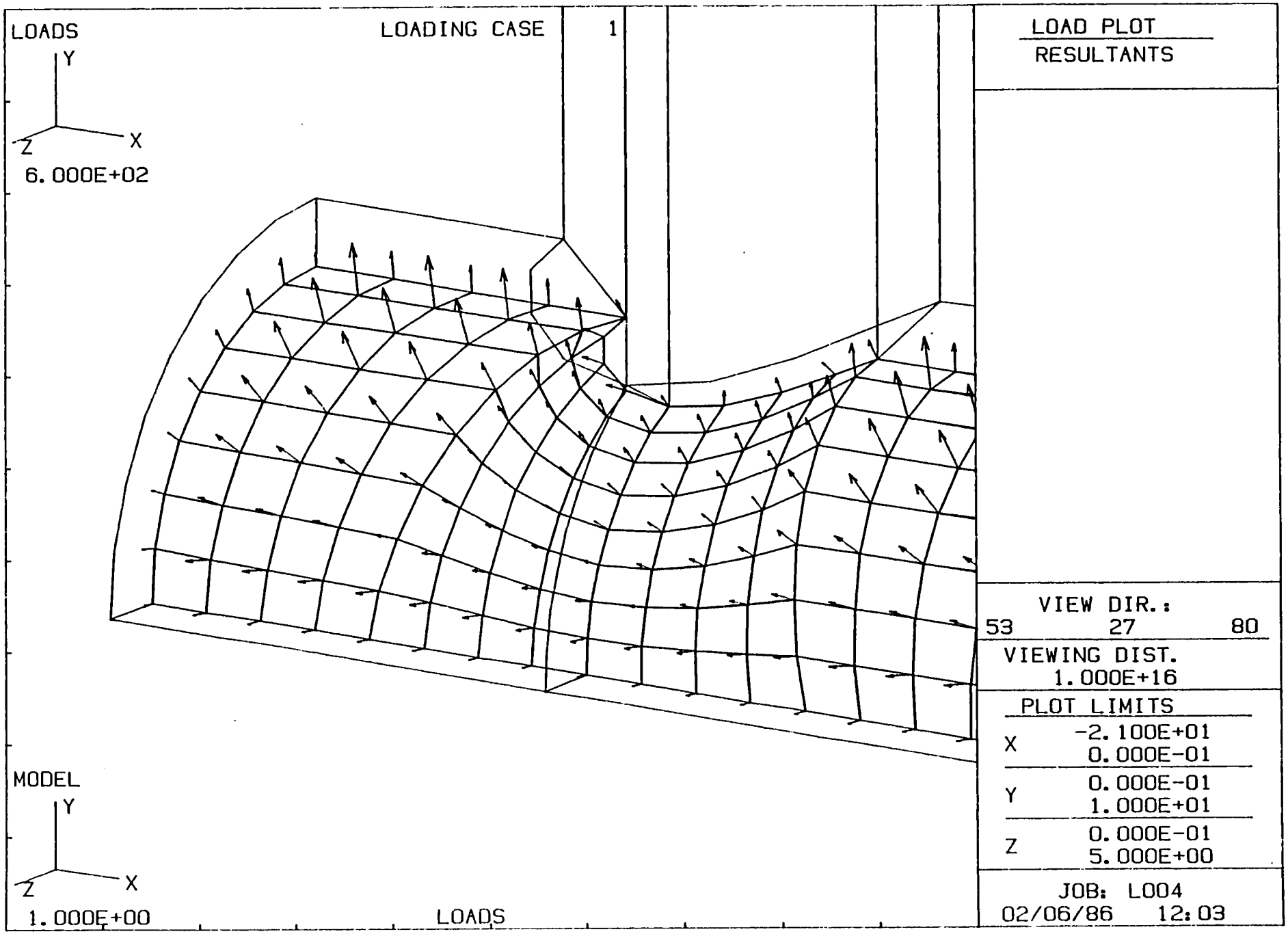

Pre-Processing: Window on Selected Load Vectors

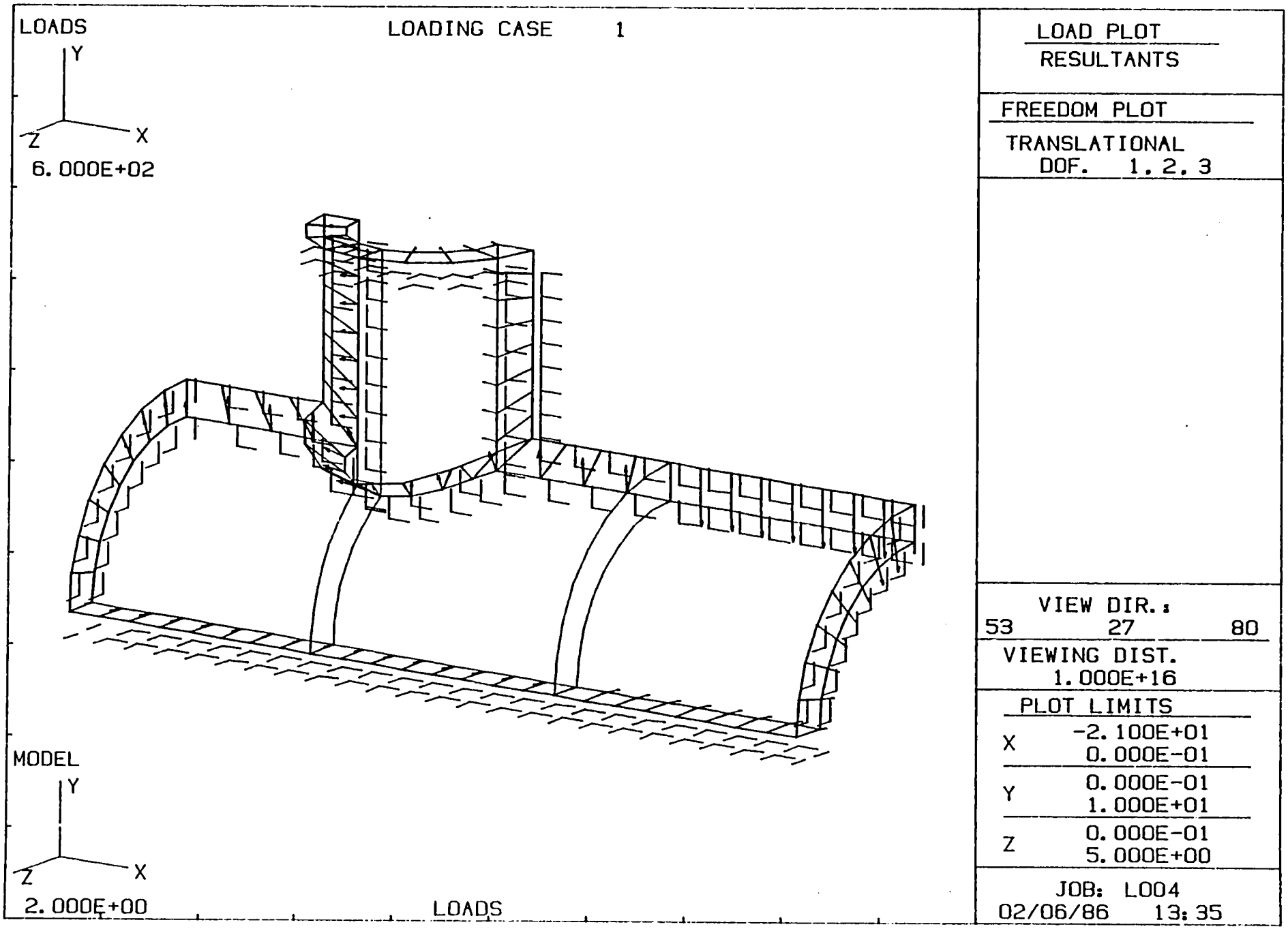

Pre-Processing: Translational Freedoms and Selected Load Vectors

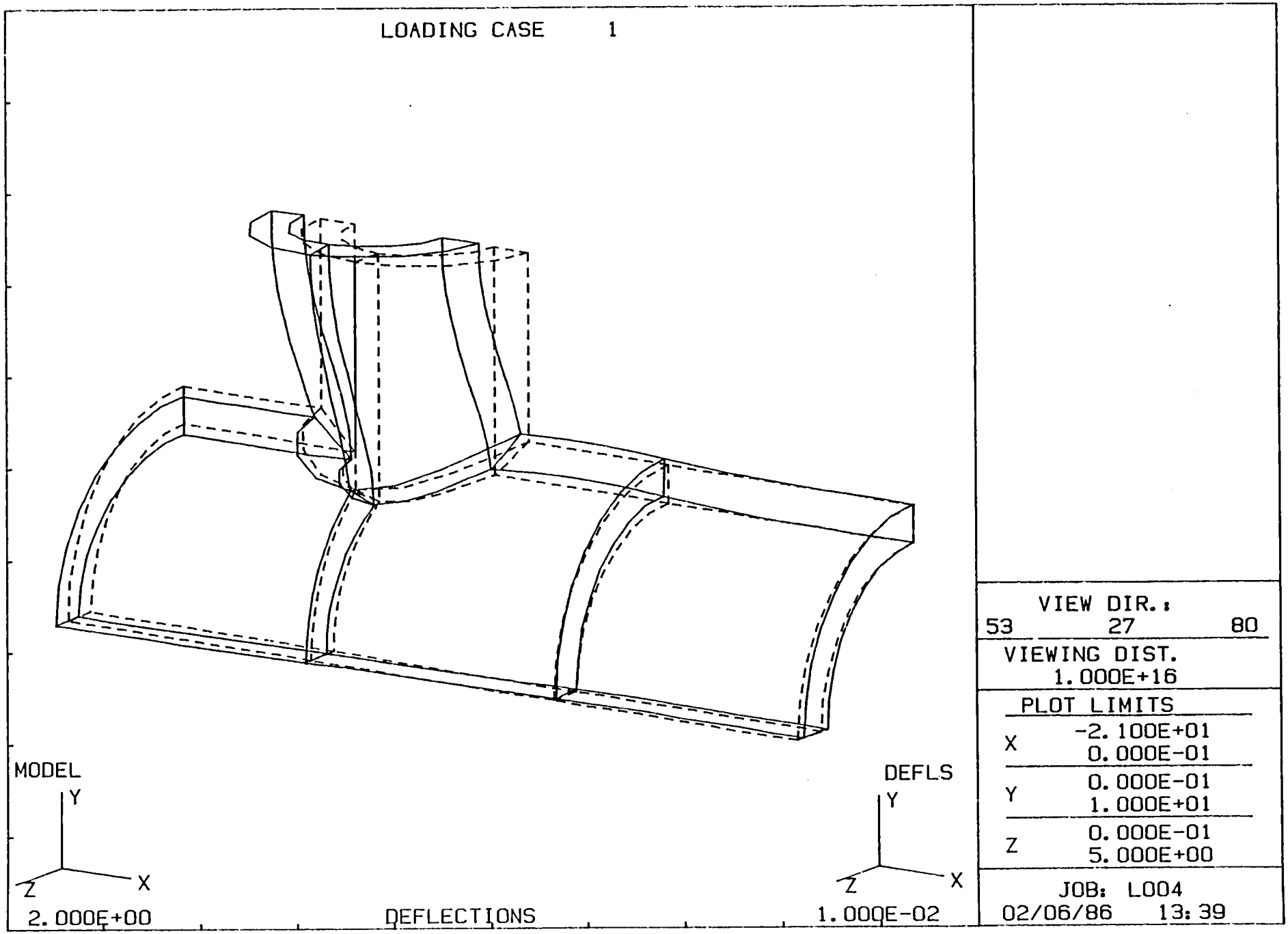

Post-Processing: Deflections Superposed on Undeflected Shapes

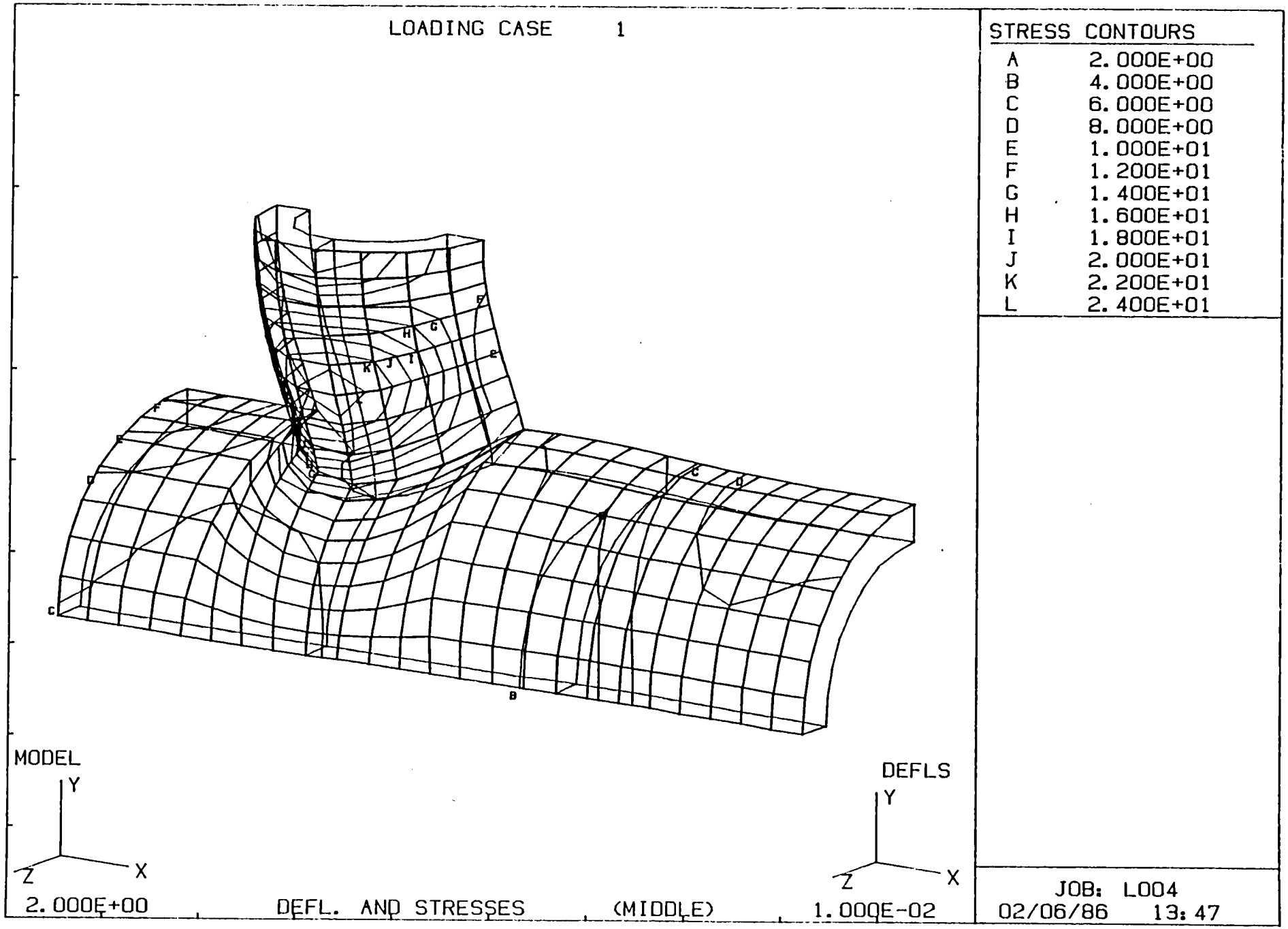

Post-Processing: Stress Contours on a Point Slice

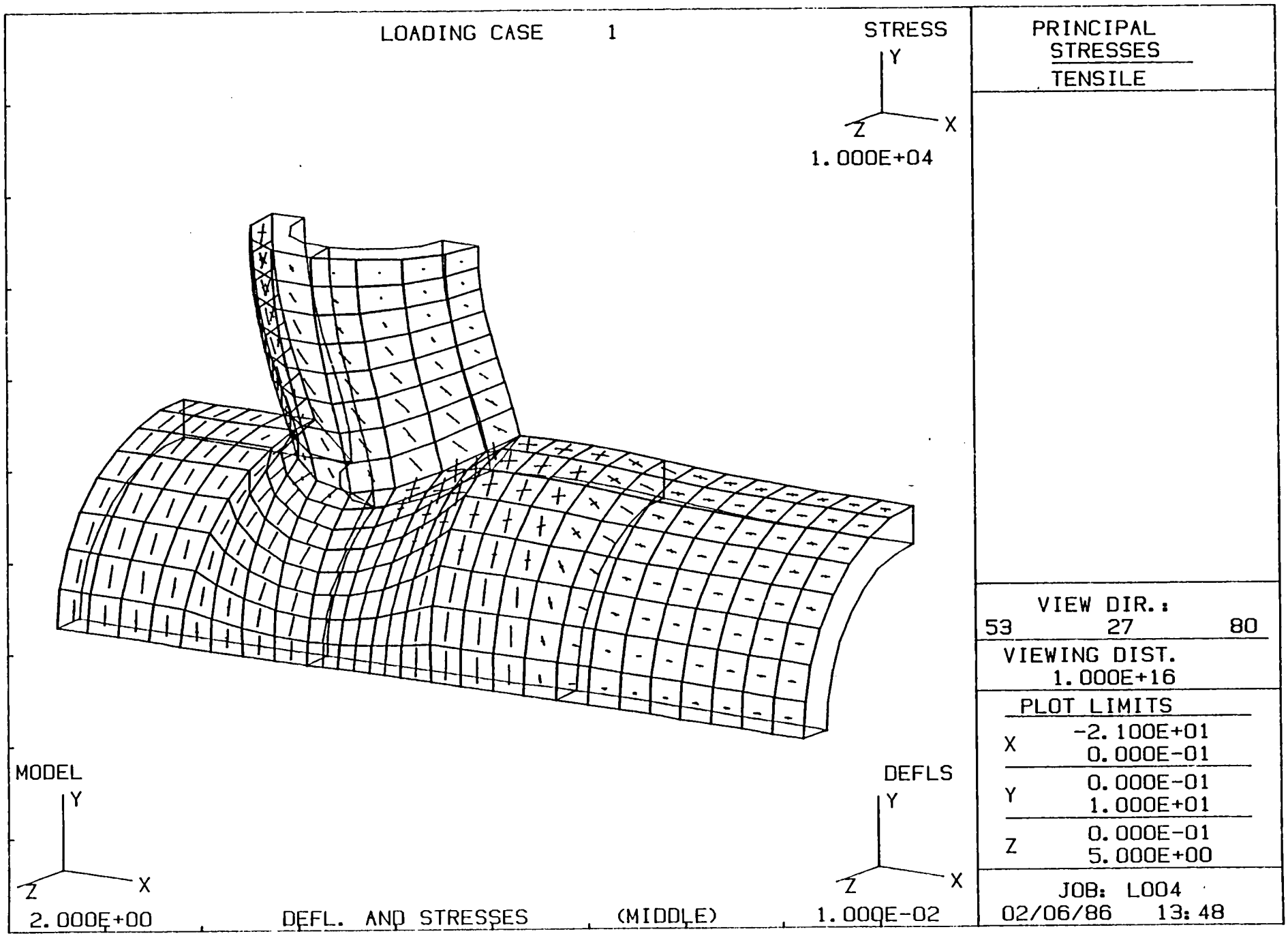

Post-Processing: Tensile Stresses on a Point Slice

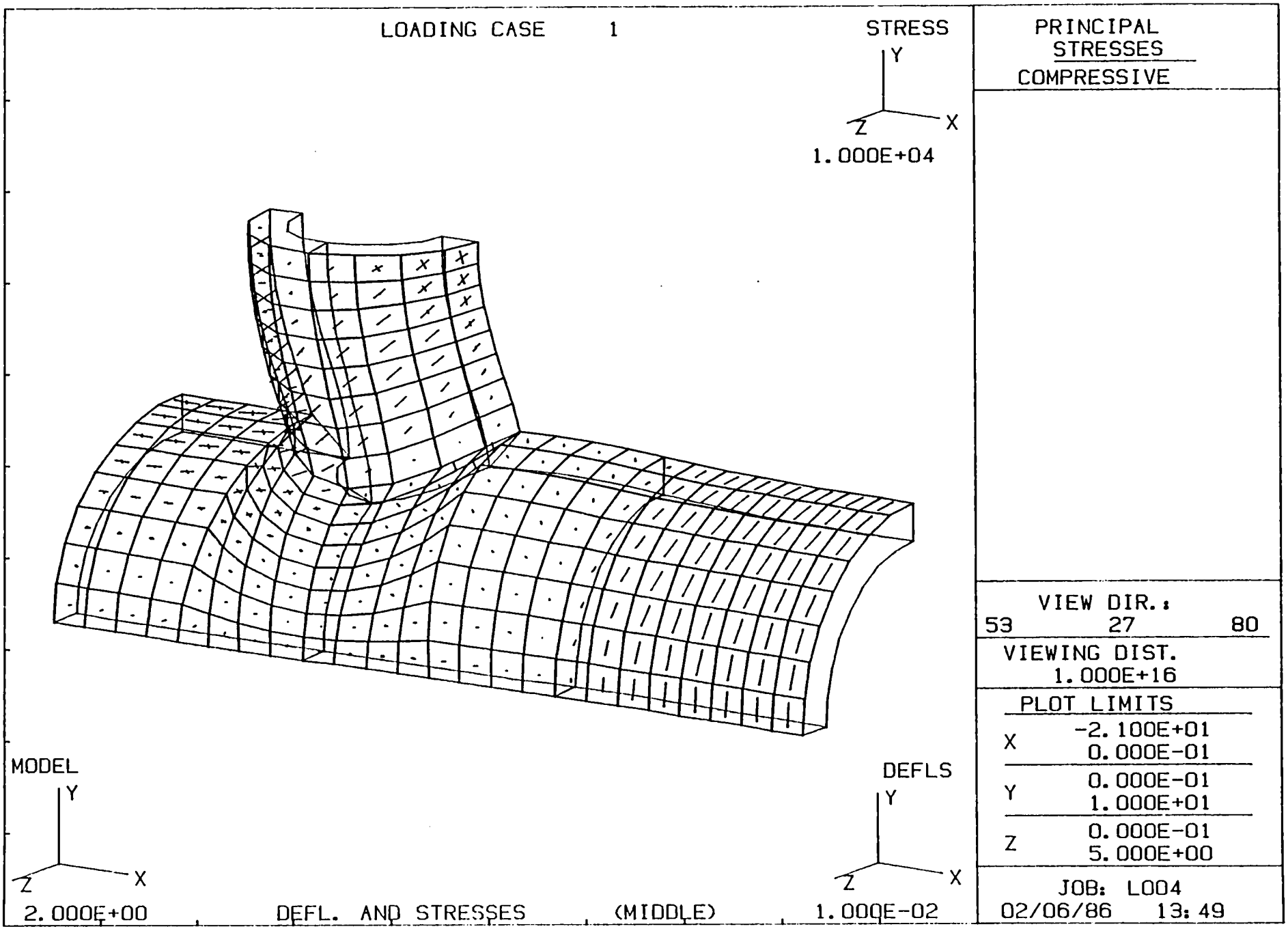

Post-Processing: Compressive Stresses on a Point Slice

```
INFG
JOB:L004                    02/06/86              11:40:58              PAGE  1
  NG   NAME      TYPE     BOUNDARY LINES          CNTR    SURF ELTS     STIFFNERS
                                                   PT     TYP  MN  TN DIR TYP  MN TN
   1 G1          GRID4    L56       L511                  NONE  0   0      NONE
                          L1112     L612
   2 G2          GRID4    L56       C15                   NONE  0   0      NONE
                          L12       C26
   3 G3          GRID4    L12       L17                   NONE  0   0      NONE
                          L78       L28
   4 G4          GRID4    L78       C711                  NONE  0   0      NONE
                          L1112     C812
   5 G5          GRID4    L17       C15                   NONE  0   0      NONE
                          L511      C711
   6 G6          GRID4    L28       C26                   NONE  0   0      NONE
                          L612      C812
   7 G7          GRID4    L1112     L1125                 NONE  0   0      NONE
                          L2526     L1226
   8 G8          GRID4    L78       L721                  NONE  0   0      NONE
                          L2122     L822
   9 G9          GRID4    L2122     C2125                 NONE  0   0      NONE
                          L2526     C2226
  10 G11         GRID4    C711      L721                  NONE  0   0      NONE
                          C2125     L1125
  11 G12         GRID4    C812      L822                  NONE  0   0      NONE
                          C2226     L1226
  12 G13         GRID4    L1521     C1315                 NONE  0   0      NONE
                          L1319     C1921
  13 G14         GRID4    L1920     L1319                 NONE  0   0      NONE
                          L1314     L1420
  14 G15         GRID4    C1416     L1420                 NONE  0   0      NONE
                          C2022     L1622
  15 G16         GRID4    L1516     L1521                 NONE  0   0      NONE
                          L2122     L1622
  16 G17         GRID4    L1314     C1315                 NONE  0   0      NONE
                          L1516     C1416
  17 G18         GRID4    C1921     L1920                 NONE  0   0      NONE
                          C2022     L2122
  18 G19         GRID4    L1723     C1517                 NONE  0   0      NONE
                          L1521     C2123
  19 G20         GRID4    L1622     C1618                 NONE  0   0      NONE
                          L1824     C2224
  20 G21         GRID4    L1718     L1723                 NONE  0   0      NONE
                          L2324     L1824

INFS
JOB:L004                    02/06/86              11:41:04              PAGE  1
  NS   NAME      TYPE              BOUNDARY GRIDS                          ELTYP NMAT
   1 S1          BRICK    G1        G3        G2        G5                  SLD8   1
                          G4        G6
   2 S2          BRICK    G24       G25       G9        G27                 SLD8   1
                          G26       G28
   3 S3          BRICK    G13       G15       G16       G18                 SLD8   2
                          G14       G17
   4 S4          BRICK    G7        G8        G4        G11                 SLD8   1
                          G9        G12
   5 S5          BRICK    G19       G20       G21       G23                 SLD8   2
                          G16       G22
```

Sample GIFTS Information Command Output
For Grids and Solids

NASTRAN Interfacing Modules Within the Integrated Analysis Capability (IAC) Program

by Harold P. Frisch

NASA / Goddard Space Flight Center

SUMMARY

The IAC program provides the framework required for the development of an extensive multidisciplinary analysis capability. Several NASTRAN related capabilities have been developed which can all be expanded in a routine manner to meet in-house unique needs. Plans are to complete the work discussed herein and to provide it to the engineering community through COSMIC in early 1987. Release is to be after the current IAC Level 2 contract work on the IAC executive system by Boeing Aerospace Company is completed and meshed with the interfacing modules and analysis capabilities under development at the GSFC.

INTRODUCTION

The Integrated Analysis Capability (IAC) program (ref. 1) has been under development at Boeing Aerospace Corporation (BAC) and the Goddard Space Flight Center (GSFC) since July 1979. During the development phase, several papers and seminars have been presented which define plans and usage at BAC and the GSFC, refs. 2-9. The first public release of the IAC through COSMIC was in July 1985 and is referred to as IAC Level 1.5. It contains most of the interfacing modules discussed herein, the others will be included in the next major update planned for spring 1987, IAC Level 2.0. The primary objective of the development team has been to create a computational environment in which multidisciplinary analysis can be carried out in a manner which makes optimum use of existing tried and true analysis procedures. Rather than create a family of new untested multidiscipline analysis programs, the IAC attempts to provide users with the computational tools required to generate, catalog, manipulate, query, and process data, and then to pass it from one program to another. This approach allows analysts to make use of well tested programs that they understand and trust. They must only convince themselves that the IAC data transfer and processing capabilities work to their satisfaction.

The initial thrust of the IAC development effort has been in the areas of structures, controls, thermal, and system dynamics. NASTRAN in its generic form has always been thought of as the prime analysis module to be used for structural analysis. For thermal analysis, NASTRAN is thought of as an option to be used if desired.

The objective of this paper is threefold: first to define what an IAC database and datastructure is and how they play a pivotal role in the ability to store, query, and process data; second to define purpose, function, and outline background theory for the DMAP programs and DMAP alters used to instruct NASTRAN to pass statics, dynamics, and thermal data to the outside world; lastly to define purpose, function, and outline background theory for the interfacing programs which read NASTRAN generated binary files, create the formal IAC datastructures, and then put them into an IAC database for follow-on multidiscipline analysis.

IAC DATASTRUCTURES AND DATABASES

Multidiscipline analysis to a major extent relies on the ability to pass data from one analysis module to another in a manner which is compatible with the output generation limitations of the first and the input requirements of the second. To the uninitiated, this is usually passed off as a trivial programming task; real workers know that the road to task completion can be exceedingly difficult and time-consuming. To ease the task, the IAC provides two formal datastructures: the RELATION and the ARRAY. The RELATION datastructure is used to store all data which is most naturally defined in a tabular format, the ARRAY datastructure is used to store all data which is most naturally defined as either a 2 or higher dimensional array. Within each datastructure, no restrictions are placed on the elements; they may be dimensioned quantities of any type. The datastructures are supported by an assortment of utilities which provide creating, loading, cataloguing, querying, getting, and putting capabilities. Getting and putting capabilities may be used in a variety of ways. At the highest level, interactive IAC commands are used; on a lower level, calls may be inserted into programs or subroutines which get datastructures from and put datastructures into an IAC database.

Physically, an IAC database is nothing more than a collection of user created IAC datastructures residing as binary files in a particular system subdirectory. In addition to these files, the subdirectory also contains the catalogue file IACCAT.IAC and the activities file IACACT.IAC of the database. The catalogue file is a RELATION datastructure which may be queried via IAC interactive commands. It contains the table of contents for the database along with other information such as IAC file name, title, keywords, creator, date of creation, etc. The activities file is created by the IAC executive and is used by it to implement the IAC's concurrent access capability, i.e., the ability for several users to simultaneously open the same database and access datastructures within it. There is no limit to the number of IAC databases that may reside in a user's account or across the entire system. The only restriction is that each database must reside by itself within a particular system subdirectory. Users are responsible for keeping track of use and purpose of each IAC database that they use and create. If project level IAC databases are established, users are responsible for knowing their location and purpose. The problem of keeping track of many databases in 1 or many systems is currently an active area of database management research and development. We are currently not adding that type of capability to the IAC; we are focusing on developing

software required to support computational analysis in a multidisciplinary project support environment. Conversely, we are cognizant of distributed database management systems and their ability to find, retrieve, and display data spread over many systems; we are of the opinion that the IAC can provide the high level analysis capability that these normally do not have..

Formal datastructures within the IAC are something more than just an ordered sequence of numeric and character data. Four examples are provided to illustrate the fact that they are designed in such a manner that they contain all information normally available from an annotated line printer listing. In addition to simply containing raw data, each datastructure has an accompanying descriptor. It contains all information needed by both system and user to query and then to output datastructure data to a user specified data file in a format compatible with user unique needs.

As an illustration, let TAPROD.NID be a bulk data file containing PARAM cards for the DMAP program NASDS. The IAC command

```
RUN CNASTRAN(F=TAPROD,RFA=NASDS)
```

is used to run the COSMIC/NASTRAN job. The output of the NASTRAN job is the standard .F06 file along with an OUTPUT2 file which is automatically placed in the file TAPROD.IO2. This OUTPUT2 file is to be read and processed by the interface module CINDA2. The IAC command

```
RUN CINDA2(FN=TAPROD.IO2,D=TAPROD:3)
```

will run the job. The program CINDA2 reads the OUTPUT2 file and automatically creates IAC datastructures for all recognized data blocks in the OUTPUT2 file TAPROD.IO2. Each datastructure created is given the file name TAPROD:3 when it is put into the database and catalogued. Once datastructures are in the database, users may query them and print all or part of their contents. They can also be used for follow-on analysis by any program containing the appropriate software commands. It should be noted that all IAC modules are run in a similar manner. RUN says run an IAC analysis module, the module name follows with a list of what we refer to as "run parameters." Run parameters allow users to communicate with either the module's command procedure or its executable. This approach is used to insulate users from all job control command procedures.

The following 2 examples of a RELATION datastructure descriptor are created by the interactive IAC command:

```
SHOW FILE TAPROD:3.LAMA, TAPROD:3.GPWG

DATASTRUCTURE=TAPROD:3.LAMA;1, CLASS=RELATION
TUPLES     NAME        DIMENSIONS TYPE   FORMAT
      75 EIGVAL                    R1     1X,E15.5
         RAD_SEC                   R1     1X,E15.5
         HZ                        R1     1X,E15.5
         GEN_MASS                  R1     1X,E15.5
         GEN_STIFF                 R1     1X,E15.5
```

```
DATASTRUCTURE=TAPROD:3.GPWG;1, CLASS=RELATION
TUPLES      NAME        DIMENSIONS TYPE  FORMAT
          1 REF_LOC     3          R1    1X,E11.4
            BODY_INER   6,6        R1    1X,E11.4
            S_TRANS     3,3        R1    1X,E11.4
            MASS_CG     4,3        R1    1X,E11.4
            CG_INER     3,3        R1    1X,E11.4
            PRN_INER    3          R1    1X,E11.4
            Q_TRANS     3,3        R1    1X,E11.4
```

Both examples were created automatically by the IAC interfacing program CINDA2. This program is designed to read an OUTPUT2 file containing the standard NASTRAN real eigenvalue table LAMA, the grid point weight generator table OGPWG, and many other tables and matrices generated during modal synthesis analysis via the DMAP program NASDS. The same datastructures can also be created by the module CINSA2 which is designed to read all data blocks that can be created by case control for rigid formats 1 and 3.

RELATIONs (tables) are characterized by tuples (rows) and attributes (columns). From the above examples, it should be obvious that the descriptor contains both the DATASTRUCTURE file name and its CLASSification (RELATION, ARRAY). To support more fully the needs associated with day-to-day parameter variation studies, we have found it most useful to introduce ":number" and to allow the IAC datastructure file name to be of the form

```
name:number.type;version
```

where:

```
number  - 10 digit integer (optional, default is 1)
type    - 10 character alphanumeric
version - 10 digit integer (optional)
```

The other data items contained in the descriptor are:

TUPLES - total number of tuples (rows) in the relation.

NAME - descriptive name to be associated with each attribute. It is convenient to utilize easily recognizable acronyms; in particular, one can notice that we have consistently tried to use NASTRAN .F06 file labels.

DIMENSIONS - actual dimension of data item. The above examples show scalar (blank) and multidimensional arrays. Variable single and multidimensional arrays are also allowed; these are symbolized by the * character.

TYPE - data type (I1-integer, R1-single precision real, R2-double precision, Z2-single precision complex, Z4-double precision complex, C*-variable length character string, Cn-character string of length n, L1-logical).

FORMAT - default output display format.

The following 2 examples of an ARRAY datastructure descriptor are created by the interactive IAC command:

```
SHOW FILE TAPROD.PHIG, TAPROD:4.EIGV
```

```
DATASTRUCTURE=TAPROD:1.PHIG;1, CLASS=ARRAY
INDEX  TUPLES     NAME        DIMENSIONS TYPE  FORMAT
0             5940 PHIG                    R2    1PD15.5
1              396 IN_DOF                  I1    1X,I10
                   EXT_GP                  I1    1X,I10
                   INT_GP                  I1    1X,I10
                   DOF                     C2    8X,A
2               15 CMID                    I1    1X,I10

DATASTRUCTURE=TAPROD:4.EIGV;1, CLASS=ARRAY
INDEX  TUPLES     NAME        DIMENSIONS TYPE  FORMAT
0             2100 MODES                   R2    1X,E15.5
1              140 COMPONENT               C8    3X,A8
                   EX_GRID_ID              I1    6X,I5
                   DOF                     C2    9X,A2
                   SIL_ID                  I1    6X,I5
2               15 MODE_ID                 I1    6X,I5
                   EIGVAL                  R2    1X,E15.5
                   RAD_SEC                 R2    1X,E15.5
                   HZ                      R2    1X,E15.5
```

The above 2 examples of an ARRAY datastructure descriptor were created to store eigenvector data. In the first example, the objective is to store the data block PHIG from the functional module SDR1, g-set eigenvectors along with sufficient information to associate rows with both internal/external grid point and DOF numbering sequences and columns with mode identification numbers. The objective of the second is to store eigenanalysis data obtained outside of NASTRAN using standard a-set mass and stiffness matrices or using the reduced order mass and stiffness matrices contained in a substructure operating file (SOF). In the latter case, eigenvector data associated with a substructure may be composed of physical and modal degrees of freedom which may span several components. INDEX 1 attributes provide both component and internal/external number sequence information. INDEX 2 attributes provide eigenvalue information. The name:number.EIGV datastructure is created by the module CIDRMX which reads all necessary input data directly from user specified datastructures. Again, note how easily recognized acronyms are used to define attributes. The only other data item contained in the ARRAY descriptor not found in that of the RELATION is:

INDEX - The ARRAY may be multidimensional; this is the identifier associate with each dimension. It should be noted that, in effect, a RELATION is associated with each index. In the above example, INDEX 0 is the core; the number of tuples here defines the total number of elements in the eigenvector matrix. INDEX 1 is asso-

ciated with the rows; a relation is provided to give more meaning to each row. INDEX 2 is associated with the columns; a relation is provided to give more meaning to each column. In general, there is no restriction on the number of INDEX's used. For each INDEX, TUPLES defines the number of tuples (rows) in the INDEX's associated relation.

For both the RELATION and ARRAY datastructure, the IAC provides an assortment of query and data manipulation utilities. Queries may be performed by using an assortment of relation operators (LT,LE,EQ,GE,GT,...) along with datastructure attribute names. We currently have a rather basic X,Y plot capability and a database management system (DBMS) designed primarily to support multidiscipline analysis needs. Our intent is to allow users to make use of the extensive plot and distributed DBMS capabilities currently available elsewhere. We provide the query capability to get the resultant analysis data needed to plot or store. At the GSFC, plot and DBMS programs are viewed as just other analysis modules which can be used via the IAC interactive command RUN.

INTERFACING CAPABILITY

NASTRAN users have at their disposal an extremely versatile program which can be used to solve standard problems via a host of rigid formats and non-standard problems via specially designed Rigid Format alters and DMAP programs. The interfacing capability within the IAC is designed to solve an equally broad range of data transfer problems (from NASTRAN OUTPUT2 binary file, to IAC datastructure, to an IAC database) in a manner which can be tailored by different user groups to meet their own unique in-house requirements.

IAC Level 2.0 will contain several NASTRAN to IAC interfacing capabilities. These are designed to read the binary files generated by the OUTPUT2 functional module of COSMIC and MSC NASTRAN. The objective is to read NASTRAN table and matrix data blocks generated via standard functional modules, place the data into an IAC datastructure, and then automatically place it into a user specified IAC database.

The driving force behind the interfacing capabilities currently contained in the IAC has been the controls/structure interaction analysis needs of the Guidance and Control Branch at the GSFC. Briefly, these are summarized as:

- Read any data block associated with statics or normal modes analysis which can be generated via standard case control commands.
- Do above in a manner compatible with extension to thermal and other NASTRAN analysis capabilities.
- Obtain all data required for the follow-on controls and system dynamics analysis programs DISCOS (refs. 10, 11), SAMSAN (ref. 12), INCA (refs. 5, 13), and DADS (refs. 14, 15, 16).

- o Place NASTRAN output data into IAC database. Use standard NASTRAN .F06 file acronyms as attribute names in datastructure descriptor.

- o Develop MSC/NASTRAN to COSMIC/NASTRAN interface. Provide capability to use finite elements of MSC/NASTRAN and substructure analysis capability of COSMIC/NASTRAN. Implement via an interface module designed to read MSC written OUTPUT2 files and then write COSMIC compatible INPUTT2 files.

- o Extract sufficient structure or substructure grid point location and analysis set mass and stiffness matrix information to enable one to perform eigenanalysis, modal synthesis, and post-processing analysis outside of NASTRAN in accordance with user unique needs.

INTERFACE MODULE CINSA2 FOR STRUCTURAL ANALYSIS RIGID FORMATS

The most common means of using NASTRAN is via use of one of its rigid formats. For example, rigid format 1 is used for statics analysis, and rigid format 3 is used for normal modes analysis. The following trivial DMAP alters may be used to write an OUTPUT2 file containing all data blocks generated via case control command; if the data block is not requested via case control, the OUTPUT2 functional module will ignore it. Both alters are to be placed just after the LABEL FINIS $ statement in their respective rigid formats.

O2S01.RFA

```
$  COSMIC/NASTRAN OUTPUT2 ALTER FOR RIGID FORMAT 01
$            STATIC ANALYSIS
$
$  CREATE OUTPUT2 FILE TO BE PROCESSED BY
$              IAC PROGRAM CINSA2
$
ALTER 156
OUTPUT2  GPL,BGPDT,USET,ECT,EST//C,N,0/C,N,11 $
OUTPUT2  OGPWG,MGG,UGV,PGG,QG//C,N,0/C,N,11 $
OUTPUT2  OPG1,OQG1,OUGV1,OES1,//C,N,0/C,N,11 $
OUTPUT2  OEF1,ONRGY1,OGPFB1,//C,N,0/C,N,11 $
ENDALTER
```

O2S03.RFA

```
$  COSMIC/NASTRAN OUTPUT2 ALTER FOR RIGID FORMAT 3
$            NORMAL MODES ANALYSIS
$
$  CREATE OUTPUT2 FILE TO BE PROCESSED BY
$              IAC PROGRAM CINSA2
$
ALTER 98
OUTPUT2  GPL,BGPDT,USET,MGG,ECT//C,N,0/C,N,11 $
OUTPUT2  OGPWG,LAMA,PHIG,OPHIG,//C,N,0/C,N,11 $
ENDALTER
```

These 2 DMAP alters write binary OUTPUT2 files which contain all data requested via case control. The program CINSA2 will read the OUTPUT2 file, create IAC datastructures, and automatically place them into the database that the user has opened via the IAC interactive command OPEN.

The program CINSA2 has a general modular type framework. It is able to read an arbitrary OUTPUT2 file of COSMIC/NASTRAN data blocks. A companion program INSA2 is available to read an arbitrary OUTPUT2 file of MSC/NASTRAN data blocks. After each data block is read, a search for known data block names is made. If the data block name is recognized, the data block is processed accordingly. If it is not recognized, a message is provided and the program proceeds to read the next data block on the OUTPUT2 file.

The following data blocks are currently recognized by the program CINSA2:

*** TABLES (INTEGER & REAL*4) ***

GPL - GRID POINT LIST
BGPDT - BASIC GRIP POINT DEFINITION TABLE
USET - DISPLACEMENT SET DEFINITION TABLE
OGPWG - GRID POINT WEIGHT GENERATOR OUTPUT TABLE
LAMA - REAL EIGENVALUE TABLE
OPHIG - OUTPUT EIGENVECTOR REQUESTS TABLE
ECT - ELEMENT CONNECTION TABLE *
EST - ELEMENT SUMMARY TABLE *
OQG1 - SINGLE-POINT CONSTRAINT FORCE REQUESTS
OPG1 - LOAD VECTOR REQUESTS
OUGV1 - DISPLACEMENT VECTOR REQUESTS
OEF1 - ELEMENT FORCE REQUESTS *
OES1 - ELEMENT STRESS REQUESTS *

* IAC datastructure for associated table data not yet defined.
These will be developed in tandem with need at the GSFC.

*** MATRICES (REAL*4 & REAL*8) ***

MGG - MASS MATRIX, G-SET
PHIG - MATRIX OF EIGENVECTORS, G-SET
UGV - DISPLACEMENT VECTOR MATRIX, G-SET
QG - SINGLE-POINT CONSTRAINT FORCES, G-SET
PGG - STATIC LOAD, G-SET

The data contained in the above datablocks is used to construct the following set of IAC datastructures with user specified [name:number]:

DS_1 DATASTRUCTURE = name:number.GRID, CLASS = RELATION
CONTENTS: Grid point numbering, location, and lumped inertia information.

```
DS_2 DATASTRUCTURE = name:number.DOF,      CLASS = RELATION
     CONTENTS:  Degree of freedom related information

DS_3 DATASTRUCTURE = name:number.GPWG,     CLASS = RELATION
     CONTENTS:  Grid Point Weight Generator table, rigid body mass
                and inertia properties

DS_4 DATASTRUCTURE = name:number.LAMA,     CLASS = RELATION
     CONTENTS:  Real Eigenvalue Table

DS_5 DATASTRUCTURE = name:number.OPHIG,    CLASS = ARRAY
     CONTENTS:  g-set single precision output eigenvector data

DS_6 DATASTRUCTURE = name:number.ODISP,    CLASS = ARRAY
     CONTENTS:  g-set single precision output displacement vector data

DS_7 DATASTRUCTURE = name:number.OLOAD,    CLASS = ARRAY
     CONTENTS:  g-set single precision output load vector data

DS_8 DATASTRUCTURE = name:number.OSPC,     CLASS = ARRAY
     CONTENTS:  g-set single precision output forces of single point
                constraint data

DS_9  DATASTRUCTURE = name:number.PHIG,    CLASS = ARRAY
      CONTENTS:  g-set double precision output eigenvector data

DS_10 DATASTRUCTURE = name:number.DISP,    CLASS = ARRAY
      CONTENTS:  g-set single double precision output displacement
                 vector data

DS_11 DATASTRUCTURE = name:number.LOAD,    CLASS = ARRAY
      CONTENTS:  g-set double precision output static load vector data

DS_12 DATASTRUCTURE = name:number.SPCF,    CLASS = ARRAY
      CONTENTS:  g-set double precision output forces of single point
                 constraint data
```

NASTRAN/SAMSAN/DISCOS DMAP PROGRAM NASDS AND INTERFACING MODULE CINDA2

Control/structure interaction analysis often requires that the system to be controlled must be modeled as a system of interconnected flexible bodies. In these situations, multibody analysis programs such as DISCOS or DADS must be used. If either of these programs are used, flexible body input data must be obtained in a format compatible with the program's requirements.

General multi-flexible body theory requires that several resultant mode dependent parameters be created by a preprocessor. This is true for either DISCOS, DADS, or any other multi-flexible body program.

Irrespective of program, the parameters necessary for the definition of the effects of flexibility on total system rigid and flexible body dynamics are definite integrals which depend upon mass distribution, grid point location, and eigenvector displacement. Furthermore, if any of the flexible bodies in the multibody system have 2 or more bodies attached, modal synthesis methods are required to generate the modes needed for follow-on multibody dynamics analysis. If modal synthesis methods are not used, an unreasonable number of free-free modes will usually be required and numerical precision and computational speed problems will yield a computationally impractical simulation. NASDS is designed to provide a variety of modal synthesis options and then to write an OUTPUT2 file with all data required for follow-on control structure interaction analysis. Users direct computation flow through NASDS with PARAM cards. The OUTPUT2 file created by NASDS is processed by the IAC interfacing module CINDA2.

NASDS is applicable for any structure for which a full g-set model is practical to obtain. If the model is extremely large or substructure analysis methods have been used, interfacing modules CINMSC, CINSOF, and CIDRMX may have to be utilized. These modules are designed to provide the interface between reduced order a-set or substructure analysis data and user post-processing needs. The objective of interface module CIDRMX is to compute necessary mode dependent parameters from reduced order mass, stiffness, and grid point location information.

Users of the DMAP program NASDS and the interface module CINDA2 may obtain the following NASTRAN data blocks and associated datastructures:

o GRID POINT LOCATION AND DISPLACEMENT SET DATA

All ARRAY datastructures containing displacement data or state vector coefficient matrices have either grid point or degree of freedom numbering information provided as INDEX (row/column) attributes. Unless specifically directed otherwise, the following data blocks are always written into the OUTPUT2 data file:

```
BGPDT  - BASIC GRID POINT DEFINITION TABLE
GPL    - GRID POINT LIST
USET   - DISPLACEMENT SET DEFINITION TABLE
```

If these data blocks are available, interface module CINDA2 will write the following datastructure:

```
DATASTRUCTURE = name:number.DOF,     CLASS = RELATION
CONTENTS: All degree of freedom related information, same as
          DS_2 generated by CINSA2.
```

To inhibit the above, use the PARAM card:

```
PARAM   PCHGD   -1
```

o GRID POINT WEIGHT GENERATOR AND EIGENANALYSIS TABLE DATA

If normal modes are generated, users normally call for NASTRAN to print the grid point weight generator table, the real eigenvalue table, and at times the real eigenvector table. For follow-on controls analysis, it is almost always necessary to obtain rigid body mass properties and to have direct access to the single precision eigenanalysis data in the associated data block tables. If the following PARAM cards are placed into the bulk data file:

```
PARAM   PCHGPWG   1
PARAM   PCHLAMA   1
PARAM   PCHPHIG   1
```

NASDS will write the following data blocks into the OUTPUT2 file:

```
OGPWG  - GRID POINT WEIGHT GENERATOR TABLE
LAMA   - REAL EIGENVALUE TABLE
OPHIG  - REAL EIGENVECTOR TABLE
```

If these data blocks are available, interface module CINDA2 will write the following datastructure:

```
DATASTRUCTURE = name:number.GPWG,     CLASS = RELATION
CONTENTS: Grid Point Weight Generator table, same as DS_3
          generated by CINSA2

DATASTRUCTURE = name:number.LAMA,     CLASS = RELATION
CONTENTS: Real Eigenvalue Table, same as DS_4 by CINSA2.

DATASTRUCTURE = name:number.OPHIG,    CLASS = ARRAY
CONTENTS: g-set single precision output eigenvector data,
          same as DS_5 generated by CINSA2.
```

o STANDARD NORMAL MODES ANALYSIS

This is the default computation path through NASDS. If the user does nothing other than provide a standard normal modes bulk data file, NASDS will, in addition to the above, write the following data blocks to the OUTPUT2 file:

```
MGG    - LUMPED MASS MATRIX, G-SET
PHIG   - MATRIX OF EIGENVECTORS, G -SET
BHH    - MODAL DAMPING MATRIX
KHH    - MODAL STIFFNESS MATRIX
MHH    - MODAL MASS MATRIX
```

Diagonal modal mass and stiffness matrices are constructed from known generalized mass and stiffness information within the system. Modal damping is obtained by the matrix triple product of a-set eigenvectors (PHIA), its transpose, and the a-set dynamic damping matrix which includes both viscous and the viscous equivalent of structural damping effects.

Users may inhibit writing the above matrices of double precision data to the OUTPUT2 file by using the following PARAM cards in their bulk data file:

```
PARAM   PCHGD   -1  DO NOT OUTPUT2 GRID POINT LOCATION AND DISPLACEMENT
                    SET DATA
PARAM   PCHMG   -1  DO NOT OUTPUT2 LUMPED MASS DATA
PARAM   PCHMD   -1  DO NOT OUTPUT2 (EIGENVECTOR) MODE SHAPE DATA
PARAM   PCHMM   -1  DO NOT OUTPUT2 MODAL MASS, STIFFNESS, AND DAMPING
                    MATRICES
```

If these data blocks are available, interface module CINDA2 will write the following datastructures:

```
      DATASTRUCTURE = name:number.GRID,     CLASS = RELATION
      CONTENTS:  Grid point numbering, location, and lumped inertia
                 information, same as DS_1 generated by CINSA2.

      DATASTRUCTURE = name:number.PHIG,     CLASS = ARRAY
      CONTENTS:  g-set double precision output eigenvector displacement
                 data, same as DS_9 generated by CINSA2.

DS_13 DATASTRUCTURE = name:number.MGG,      CLASS = ARRAY
      CONTENTS:  The g-set mass matrix

DS_14 DATASTRUCTURE = name:number.MMASS,    CLASS = ARRAY
      CONTENTS:  The modal mass matrix

DS_15 DATASTRUCTURE = name:number.MSTIF,    CLASS = ARRAY
      CONTENTS:  The modal stiffness matrix

DS_16 DATASTRUCTURE = name:number.MDAMP,    CLASS = ARRAY
      CONTENTS:  The modal damping matrix
```

o MASS, STIFFNESS, DAMPING, AND CONSTRAINT MATRICES

If follow-on application requires use of g-set coefficient matrices, these may be written to an OUTPUT2 file by the inclusion of the PARAM card

```
PARAM   MKMAT   1
```

in the bulk data file. If this card is used, computation within NASTRAN will terminate after the processing of all multipoint constraint data. The following data blocks will, in addition to GPL, BGPDT, and USET, be written to the OUTPUT2 file:

```
MGG - MASS MATRIX, G-SET
KGG - STIFFNESS MATRIX, G-SET
BGG - VISCOUS DAMPING MATRIX, G-SET
K4GG - STRUCTURAL DAMPING MATRIX, G-SET
RG - MULTIPOINT AND RIGID ELEMENT CONSTRAINT EQUATION
     MATRIX, G-SET TO M-SET
```

GM - MULTIPOINT AND RIGID ELEMENT TRANSFORMATION MATRIX
M-SET TO N-SET
GTOMN - PARTITIONING VECTOR, 1.0 IMPLIES N-SET WHILE
0.0 IMPLIES M-SET. UNION IS G-SET.

If these data blocks are available, interface program CINDA2 will write the following data structures:

DATASTRUCTURE = name:number.MGG, CLASS = ARRAY
CONTENTS: The g-set mass matrix, same as DS_13 defined above.

DS_17 DATASTRUCTURE = name:number.KGG, CLASS = ARRAY
CONTENTS: The g-set stiffness matrix

DS_18 DATASTRUCTURE = name:number.BGG, CLASS = ARRAY
CONTENTS: The g-set damping matrix

DS_19 DATASTRUCTURE = name:number.K4GG, CLASS = ARRAY
CONTENTS: The g-set structural damping matrix

DS_20 DATASTRUCTURE = name:number.RG, CLASS = ARRAY
CONTENTS: The multipoint and rigid element constraint equation matrix g-set to m-set

DS_21 DATASTRUCTURE = name:number.GM, CLASS = ARRAY
CONTENTS: The multipoint and rigid element transformation matrix m-set to n-set

o REDUCED MASS AND STIFFNESS MATRIX DATA

If the follow-on analysis activity is modal synthesis outside of NASTRAN, it is frequently necessary to work with reduced order mass and stiffness matrices. To obtain a-set mass and stiffness matrices, users of NASDS need only include the PARAM card

PARAM RMX 1

in the bulk data file. If this card is used, computation within NASTRAN will terminate after processing a-set mass and stiffness data blocks. The following data blocks will be written to the OUTPUT2 file:

MAA - MASS MATRIX, A-SET
KAA - STIFFNESS MATRIX, A-SET

If both MAA and KAA are on the OUTPUT2 file, the program CINDA2 assumes that the user desires to proceed with follow-on analysis via the interface program CIDRMX. The program CIDRMX was designed to read datastructures containing substructure operating file (SOF) data items and then proceed with necessary analysis outside of NASTRAN. Equivalent datastructures can be constructed from a-set information obtainable from NASDS. The following datastructures are identical to those produced by the interface program CINSOF. They are compatible with the input data requirements of CIDRMX.

DS_22 DATASTRUCTURE = name:number.KMTX, CLASS = ARRAY
CONTENTS: The a-set stiffness matrix

DS_23 DATASTRUCTURE = name:number.MMTX, CLASS = ARRAY
CONTENTS: The a-set mass matrix

DS_24 DATASTRUCTURE = name:number.EQSS, CLASS = RELATION
CONTENTS: External/internal grid point equivalence data identical to that associated with substructure analysis

DS_25 DATASTRUCTURE = name:number.BGSS, CLASS = RELATION
CONTENTS: Basic grid point coordinates data identical to that associated with substructure analysis

o FINE TO COARSE MESH MODELING

All multibody programs which accept flexible bodies require that resultant mode dependent parameters be obtained. These parameters are to be computed via the evaluation of a series of definite integrals. The integrals involve mass distribution, grid point location, and modal amplitude over the entire volume. For very large finite element models, it is computationally impractical to backtransform all eigenvectors from the a-set to the g-set. This capability was an attempt to provide sufficient data for a mass distribution interpolation program (never written) which could be used to reduce problem order. Data blocks written and datastructures created have rarely been needed; details are in the comment cards of the programs NASDS and CINDA2.

Recent theoretical developments have uncovered a means for obtaining all required mode dependent parameters directly from the full a-set mass matrix, grid point locations, and modal amplitudes. This work is implemented in the interfacing module CIDRMX.

o MODAL OBSERVABILITY AND CONTROLLABILITY

If follow-on modal analysis is the objective, one must always face the problem of deciding which modes to retain and which to discard. Both modal observability and controllability matrices may be computed within NASDS. Relative to the g-set, NASDS tells NASTRAN to set up the following matrix equation:

$$MGG * X'' + KGG * X = BMAT * U$$

$$Y = CMAT * X$$

where X is the state vector, U is the input vector, and Y is the output vector. If NASDS users insert the PARAM card

PARAM MODOBCL 1

the program will accept both matrices BMAT and CMAT via user supplied DMIG bulk data input. Normally, they are composed of simply 1's and 0's. The 1's define which DOF's are controllable and which are observable; the 0's define which are not. If this card is used, datablocks are written to the OUTPUT2 file which CINDA2 then reads and uses to create the following datastructures:

```
DS_26 DATASTRUCTURE = name:number.BMATG,     CLASS = ARRAY
      CONTENTS:  Input coefficient matrix BMAT compatible with g-set
                 eigenvector matrix PHIG

DS_27 DATASTRUCTURE = name:number.CMATG,     CLASS = ARRAY
      CONTENTS:  Output coefficient matrix CMAT compatible with g-set
                 eigenvector matrix PHIG

DS_28 DATASTRUCTURE = name:number.MODCTL,    CLASS = ARRAY
      CONTENTS:  Modal controllability matrix
            MODCTL = BMATG**T * PHIG      (**T - matrix transpose)

DS_29 DATASTRUCTURE = name:number.MODCSS,    CLASS = ARRAY
      CONTENTS:  Steady state modal controllability matrix
            MODCSS = MODCTL * diag(square root generalized
                                   stiffness inverse)

DS_30 DATASTRUCTURE = name:number.MODOBS,    CLASS = ARRAY
      CONTENTS:  The modal observability matrix
            MODOBS = CMATG * PHIG

DS_31 DATASTRUCTURE = name:number.MODOSS,    CLASS = ARRAY
      CONTENTS:  The steady state modal observability matrix
            MODOSS = MODOBS * diag(square root generalized
                                   stiffness inverse)
```

o AUGMENTED BODY MODES

If the flexible bodies in a multibody system have 2 or more contiguous bodies; that is, if the bodies have more than 1 hinge point, modal synthesis techniques are normally required to obtain a best set of modes. One approach is to create augmented body modes. Two augmented body options are available; the user may, via DMIG cards in the bulk data, add either lumped mass and/or lumped stiffness at each of the hinge points. The resultant modes are referred to as augmented body modes within NASDS, see ref. 17. Stiffness may be augmented without need of a PARAM card. To augment mass, the PARAM card

```
PARAM   AUGMOD    1
```

must be used. If this PARAM card is used, the program will compute all eigenvectors with the augmented mass matrix and modal mass with the non-augmented mass matrix. Modal mass will be non-diagonal. If the PARAM card is not used, modal mass will be computed with respect to the augmented

mass matrix and be diagonal. Modal stiffness is always computed with respect to the augmented stiffness matrix and hence is always diagonal. Datastructures created are the same as those created via standard modal analysis procedures. The above PARAM card is also needed to tell the system to write the non-augmented mass matrix into the OUTPUT2 file; follow-on multibody dynamics analysis requires this.

o FIXED-INTERFACE METHOD, CRAIG BAMPTON MODAL DATA

If the flexible bodies in a multibody system have 2 or more contiguous bodies, that is, if the bodies have more than 1 hinge point, modal synthesis techniques are normally required to obtain a best set of modes. Another modal synthesis technique commonly used is the Craig-Bampton fixed-interface method. Within NASDS, there is the capability to compute what we refer to as stage 1, stage 2, and stage 3 Craig-Bampton modes. The 3 stages are an outgrowth of the need to isolate the 6 rigid body modes within the set of constraint modes. Most multibody formulisms require only deformation modes; in fact, they require that rigid body modes be removed from the set of input modes. This is a problem with standard Craig-Bampton modes since rigid body modes cannot be simply partitioned out of the set of constraint modes. Stage 1 modes, within the context of NASDS, are standard Craig-Bampton modes; Stage 2 modes are obtained by a transformation which isolates the 6 rigid body modes; and Stage 3 modes are obtained via the setup and solution of a new eigenproblem which yields diagonal modal mass and stiffness matrices. The original multistage theory as used within NASDS was developed by Bodley and Park at Martin Marrietta, ref. 18. Reference 19 by Craig and Chang contains background ideas for Stage 2 and 3 modes in their sections devoted to the "Guyan reduction of junction (hinge) coordinates" and "Modal reduction of junction coordinates." Comment cards within NASDS, ref. 20, contain all necessary theory.

Users of this capability must adhere to certain setup rules defined completely in NASDS source code and explained by example in the programs accompanying documentation. The following PARAM cards are required if this capability is desired

```
PARAM   CB1MODS  1  Craig-Bampton stage 1, 2, or 3 desired
PARAM   CB2MODS  2  Craig-Bampton stage 2 or 3 desired
PARAM   CB3MODS  3  Craig-Bampton stage 3 desired
```

In addition to the PARAM cards, additional data is required to define which grid points are to be designated to be hinge (boundary) points. All points defined on bulk data SUPORT cards are by defintion boundary points; all others are by definition interior points. For stage 2 and 3 modes, one of the boundary points must be designated as a reference point; this is done by user specification of partitioning vectors via DMI bulk data input. The introduction of the reference point within the set of boundary points allows for the isolation of the 6 rigid body modes via a Guyan reduction step. If these cards are used, datablocks are written to the OUTPUT2 file which CINDA2 then reads and uses to create the following datastructures:

```
DS_32 DATASTRUCTURE = name:number.PHIGi,     CLASS = ARRAY
      CONTENTS:  g-set stage i (i=1,2,3) Craig-Bampton modal data.

DS_33 DATASTRUCTURE = name:number.MCBi,      CLASS = ARRAY
      CONTENTS:  Modal mass matrix for stage i (i=1,2,3) Craig-
                 Bampton modes

DS_34 DATASTRUCTURE = name:number.BCBi,      CLASS = ARRAY
      CONTENTS:  Modal damping matrix for stage i (i=1,2,3) Craig-
                 Bampton modes

DS_35 DATASTRUCTURE = name:number.KCBi,      CLASS = ARRAY
      CONTENTS:  Modal stiffness matrix for stage i (i=1,2,3)
                 Craig-Bampton modes
```

o FREE-INTERFACE METHODS

NASDS does not currently contain code to generate modal data associated with any of the free-interface methods discussed in the literature, see ref. 19. On the surface, the inclusion of the required DMAP statements to provided a free-interface method option, appears straight-forward.

MSC TO COSMIC/NASTRAN INTERFACE MODULE CINMSC

At the GSFC, there is a definite need to translate contractor supplied MSC/NASTRAN bulk data files to COSMIC/NASTRAN compatible format. The capability is primarily needed to mesh the work of various contractors via COSMIC/NASTRAN's substructure analysis capability into a complete system structural model. Rather than attempt the automated translation of bulk data files, the program CINMSC is designed to read a MSC/NASTRAN written OUTPUT2 file and to then write a COSMIC/NASTRAN compatible INPUTT2 file.

We have circumvented the bulk data translation problem by inserting OUTPUT2 statements within MSC/NASTRAN rigid formats and the appropriate INPUTT2 statements within the analogous COSMIC/NASTRAN rigid format. The module CINMSC accounts for unformatted file differences between the 2 versions of NASTRAN. It is designed to translate both table and matrix data blocks. It is not currently coded to translate complex matrix data blocks. This procedure allows the COSMIC job to be run with all MSC element cards removed from the bulk data file; they need only be replaced by a dummy mass and elastic element card. The dummy elements create the data blocks which will be filled at the appropriate time in the DMAP sequence by INPUTT2.

CAUTION!!! Lack of a sparse matrix OUTPUT2 capability within COSMIC can lead to extremely large files. It is common for COSMIC files to be 10 to 100 times larger than MSC files. Moderate size MSC files (5000 blocks) frequently translate into files which exceed total system free storage limits. This problem has limited the usefulness of interface module CINMSC.

INTERFACE MODULE CINSOF, READ SUBSTRUCTURE OPERATING FILE (SOF) DATA

Control/structure interaction analysis needs for space station and other very large systems will require use of substructure analysis techniques. Experience has shown that there is no guarantee that the structural analyst and the controls analyst will take the same modeling view of a large space structure; furthermore, there is no guarantee that a structural analyst will be available to merrily write DMAP to keep the controls analyst happy. This capability has been developed to allow follow-on controls analysis groups the ability to extract the basic data that they need from the SOF file and then process it as they desire outside of NASTRAN. The need for this capability occurs when the controls analyst attempts to develop a controller for large angle relative orientation of a pair of hinged flexible bodies. The SOF file contains mass and stiffness matrices for each component and eigenanalysis data associated with the analysis process used to obtain composite system modes and frequencies. The controls analyst needs eigenanalysis data for each body alone. The interface module CINSOF provides the ability to retrieve data for each component or substructure of components, while the interface module CIDRMX provides the ability to process it as needed.

Data for the program CINSOF is most effectively prepared via the submission of a stand alone substructure phase 2 job of the following form:

```
NASTRAN FILES=INPT
$
$  FILES=INPT establishes the specific NASTRAN permanent file
$  INPT as an executive file.  This file has the FORTRAN logical
$  unit FOR014.  Use CNASTRAN RUN parameter ASG to point to a
$  file containing the DCL statement
$
$             $ ASSIGN 'F'.EIO FOR014
$
$  This assigns a user specified file name to the NASTRAN permanent
$  file INPT and overrides its automatic deletion at job end.
$
ID READ,SOF
APP DMAP,SUBS
BEGIN  $ DMAP PROGRAM TO READ SOF FILE AND OUTPUT SELECTED ITEMS
$
$   Initialize error code DRY
PARAM    //*ADD*/DRY/1  /0  $
$
$   PRINT SOF TABLE OF CONTENTS (TOC)
SOFUT    //DRY/*TOC     */*SOFP*/0  /* */* */* */* */
               * */* */* * $
$
$  Use functional module EXIO to copy selected items from SOF
$  external file
$
```

```
$    FUNCTIONAL MODULE EXIO (EXTERNAL INPUT/OUTPUT FOR SOF)
$
$  PARAMETER #  USE      EXPLANATION
$       1       DRY      Integer code for error occurrence check
$       2       780      VAX 11/780 machine in use
$       3       DISK     EXIO file to be written will be on disk
$       4       INPT     Unit where EXIO file is to be located
$       5       INTERNAL  Internal file written with GINO
$       6       SOFOUT   Copy from the SOF to the external file
$       7       REWIND   Use in first EXIO statement
$               EOF      Use thereafter
$       8       xxxx     Data items on SOF to be copied
$       9       aaaa     Name of subucture whose items copied
$      10       bbbb     Name of substructure whose items copied
$      11       cccc     Name of substructure whose items copied
$      12       dddd     Name of substructure whose items copied
$      13       eeee     Name of substructure whose items copied
$
$       See programmer's manual page 4.130-1 for more detail
$
EXIO      //DRY/C,N,780/C,N,DISK/C,N,INPT/C,N,INTERNAL/
          C,N,SOFOUT/C,N,REWIND/*EQSS*/*WHOLESOF*/* */* */* */* * $
EXIO      //DRY/C,N,780/C,N,DISK/C,N,INPT/C,N,INTERNAL/
          C,N,SOFOUT/C,N,EOF/*BGSS*/*WHOLESOF*/* */* */* */* * $
$
$              etc.
$
END       $
TIME 30
CEND
SUBSTRUCTURE PHASE2
SOF(1)=FT20,500
PASSWORD=ABCD
$
ENDSUBS
$
TITLE = COPY SELECTED ITEMS FROM SOF TO USER FILE
BEGIN BULK
GRID,1
ENDDATA
```

The interface program CINSOF provides the ability to read the data contained in the unformatted data file produced by the functional module EXIO. The output of this program is intended for the use of experienced NASTRAN users. Users are expected to know what data is actually stored within the numerous SOF data items that are processed as standalone data blocks. Extremely large matrices will not be processed. The IAC currently requires all arrays to be stored in a dense format. A sparse format is currently under development.

The following substructure operating file data items are recognized and processed by interface program CINSOF:

```
TOC  - Substructure operating file table of contents
EQSS - External grid point and internal point equivalence data
BGSS - Basic grid point coordinates
CSTM - Local coordinate system transformation matrices
LODS - Load set identification numbers
KMTX - Stiffness matrix
MMTX - Mass matrix
PVEC - Load vectors
POVE - Load vectors on points omitted during matrix reduction
UPRT - Partitioning vector used in matrix reduction
HORG - H or G transformation matrix
UVEC - Displacement vectors or eigenvectors
QVEC - Reaction force vectors
SOLN - Load factor data or eigenvalues used in solution
       *WARNING* load factor data from statics not processed,
                 attributes refer to eigenanalysis data.
                 Program may error out for statics analysis data.
PAPP - Appended load vectors
POAP - Appended load vectors on omitted points
LOAP - Load set identification numbers for appended load vectors
LMTX - Decomposition product of REDUCE operation
GIMS - G transformation matrix for interior points in modal reduction
PHIS - Eigenvector matrix
LAMS - Eigenvalue data for modal reduction operation
K4MX - Structural damping matrix
BMTX - Viscous damping matrix
```

Data contained in the above data blocks are used to construct the following set of IAC datastructures with user specified [name:number]:

```
      DATASTRUCTURE = name:number.EQSS,     CLASS = RELATION
      CONTENTS:  External grid point and internal point equivalence
                 data, same as DS_24 generated by CINDA2

      DATASTRUCTURE = name:number.BGSS,     CLASS = RELATION
      CONTENTS:  Basic grid point coordinates data, same as DS_25
                 generated by CINDA2

      DATASTRUCTURE = name:number.KMTX,     CLASS = ARRAY
      CONTENTS:  a-set stiffness matrix, same as DS_22 generated by
                 CINDA2

      DATASTRUCTURE = name:number.MMTX,     CLASS = ARRAY
      CONTENTS:  a-set mass matrix, same as DS_23 generated by CINDA2

DS_36 DATASTRUCTURE = name:number.XXXX,     CLASS = ARRAY
      CONTENTS:  The SOF file matrix data item XXXX,
                 XXXX = K4MX,BMTX,GIMS,UPRT,PHIS,LMTX,PAPP,LMTX,
                        PAPP,PVEC,POAP,POVE,QVEC,UVEC,HORG
```

DS_37 DATASTRUCTURE = name:number.XXXX, CLASS = RELATION
CONTENTS: The SOF file data item XXXX,
XXXX = SOLN,LAMS,CSTM,LODS,LOAP

INTERFACE MODULE CIDRMX, NASTRAN - DISCOS/DADS INTERFACE PROGRAM

The interface program CIDRMX is designed to accept as input data the information contained in the following data structures:

DATASTRUCTURE = name:number.KMTX, DS_22
DATASTRUCTURE = name:number.MMTX, DS_23
DATASTRUCTURE = name:number.EQSS, DS_24
DATASTRUCTURE = name:number.BGSS, DS_25

The origin of these datastructures is of no concern to CIDRMX; currently they may be written by either CINDA2 or CINSOF. The objective of CIDRMX is to obtain all mode dependent parameters required by DISCOS, DADS, or any other multi-flexible body program from reduced order models. The starting point is a-set mass and stiffness matrices obtained via the DMAP program NASDS or from the reduced order mass and stiffness matrices of any substructure defined on an SOF file along with all grid point location and numbering information associated with all degrees of freedom in the associated state vector.

The capability contained within CIDRMX contains a fixed dimension for matrix order. There is a PARAMETER card in the source code of CIDRMX which requires all reduced order matrices to be less than order 300. This limit corresponds to the general rule of thumb within the GSFC and most other NASTRAN groups that in real world application eigenanalysis should never be done with matrices of order greater than about 250. CIDRMX contains 5 different eigenanalysis options; these correspond to the 5 capabilities provided in the EISPACK library, ref. 21. A variety of options are provided to give users some computational options. These are:

1. Default, compute all eigenvalues and eigenvectors by the QL method. Use if more than 25 percent of eigenvalues/vectors required.
2. Some eigenvalues/vectors. Determined by the method of bisection applied to the Strum sequence. Recommended if less than 25 percent of all eigenvalues/vectors required. User must specify the upper eigenvalue bound; the lower limit is set slightly negative to pick up all 0.0's.
3. Some eigenvalues/vectors. Determined by the method of bisection applied to the Strum sequence. Recommend if less than 25 percent of all eigenvalues/vectors required. User must specify index of the upper eigenvalue bound; lower bound is 1.
4. All eigenvalues and some eigenvectors. Determines all eigenvalues by using the implicit QL-method. User must specify index of the upper eigenvalue bound for which an eigenvector is desired. Lower limit is 1.

5. All eigenvalues and eigenvectors. To be used when matrix "B" is not positive definite. Results obtained via use of the general QZ algorithm applied to real symmetric matrices.

All modal data is currently obtained via a standard application of eigenanalysis procedures. Plans are currently underway to include various modal synthesis procedures in CIDRMX.

In multibody theory, the body fixed reference translates and rotates relative to the inertial reference frame at a rate that cannot be ignored. The mode dependent parameters required for follow-on multi-flexible body dynamics stem from the need to express state vector derivative in the kinetic energy expression of each flexible body relative to an inertially fixed reference frame. That is,

$$T = 1/2 \; [\dot{Na}] * [MAA] * (\dot{Na})$$

where

T - flexible body kinetic energy
MAA - reduced order mass matrix
Na - reduced order state vector, it may contain both physical and modal degrees of freedom
. - derivative relative to inertial frame

Let

R - position vector from inertial reference to body reference point
W - inertial angular velocity vector of body reference frame
Ni - deformed position and orientation of reference frame at grid point i
Pi - position vector from body reference point to undeformed position of grid point i
Di - elastic translational deformation at grid point i
Mj - j-th modal degree of freedom
o - derivative relative to body fixed reference frame

Then for each grid point associated with physical degrees of freedom

$$\dot{Ni} = \dot{R} + W \times (Pi + Di) + \overset{o}{Ni}$$

and for each modal degree of freedom

$$\dot{Mj} = \overset{o}{Mj}$$

Construct for each grid point i a 6x12 transformation matrix which can be used to express the inertial derivative of each grid point position vector Ni in terms of the body reference frame inertial rate and the grid point frame relative rate. This transformation, when accumulated for all grid points associated with all physical degrees of freedom, provides all information needed to define the transformation from inertial derivative of reduced state vector Na to inertial rate of the body fixed frame and relative rate of each grid point frame. To arrive at the actual transformation to be used, simply remove all rows associated with all DOF's

not in the set of physical DOF's in the reduced state vector, then add rows to account for modal DOF's. Eigenanalysis provides the final step, the transformation from relative deformation at grid points to modal coordinates. The fully assembled transformation is then substituted into the kinetic energy expression.

The above steps provide the transformation to a state vector composed of rigid body and modal degrees of freedom. The next step is to analytically form the matrix triple product between transformation matrix, its transpose, and the reduced mass matrix. Further manipulation leads to the time dependent reduced mass matrix expressed as a summation of time independent coefficient matrices and generalized displacement coordinates. The summation includes terms which are independent, linear, and quadratic in the generalized displacement coordinates. The Lagrange solution to the multibody equations of motion used in both DISCOS and DADS require this so that partial derivatives of the mass matrix can be formed with respect to generalized displacement coordinates. Rather than store large coefficient matrices, both formulations require mode dependent vectors and tensors. The programs use these in a computationally efficient manner to define only non-zero terms. The definition of each of the mode dependent parameters can be found in refs. 11 and 15. The equations differ only by notation. Complete specification of the unraveling steps and associated equations is planned for inclusion in the program documentation of IAC Level 2.0.

The following datastructures are created by CIDRMX:

DATASTRUCTURE=name:number.GPWG, CLASS = RELATION
CONTENTS: Grid Point Weight Generator table; standard data provided in the NASTRAN GPWG table. All data provided here is derived directly from the reduced order mass matrix MMTX and the gird point location information in EQSS & BGSS. It should be noted that within NASTRAN, GPWG data is not available beyond the phase 1 component definition step in substructure analysis. The same as DS_3.

DATASTRUCTURE=name:number.LAMA, CLASS = RELATION
CONTENTS: Real eigenvalue table; eigenvalues, natural frequencies generalized mass and stiffness data. The same as DS_4

DS_38 DATASTRUCTURE=name:number.EIGV, CLASS = ARRAY
CONTENTS: Real eigenvector data. Contains modes used for computation of all resultant mode dependent data. Modes may be standard orthogonal modes from unaltered eigenanalysis or non-orthogonal modes associated modal synthesis techniques used for interior flexible bodies. INDEX 1 attributes associate internal/external sequences of DOF's. INDEX 2 attributes associate eigenvalues.

DATASTRUCTURE=name:number.MMASS, CLASS = ARRAY
CONTENTS: Modal mass matrix. Same as DS_14.
MODES**T * MASS(MATRIX) * MODES.

DATASTRUCTURE=name:number.MSTIFF, CLASS = ARRAY
CONTENTS: Modal stiffness matrix. Same as DS_15.
MODES**T * STIFFNESS(MATRIX) * MODES.

For follow-on multibody analysis, one is expected to obtain all rigid body mass and inertia from the grid point weight generator datastructure DS3, name:number.GPWG. All mode dependent data is contained in the datastructures name:number.FLMX1 and name:number.FLMX2.

DS_39 DATASTRUCTURE=name:number.FLMX1, CLASS = RELATION
CONTENTS: The following mode dependent parameters dependent upon 1 mode:

A0 - Coupling terms between rigid body translational motion and modal velocity for the component of the full mass matrix which is independent of deformation. These are modal masses formed by the integral of modal deflection times mass distribution d-volume. One vector per mode.

D0 - Coupling terms between rigid body rotational motion and modal velocity for the component of the time dependent mass matrix which is independent of deformation. These are modal mass moments formed by the integral of grid point position vector cross grid point modal deflection vector times mass distribution d-volume. One vector per mode.

B1 - Component of the deformed body 3x3 moment of inertia dyadic which is linearly dependent upon modal deformation. These are formed by an integral of dyads formed by grid point position vector and modal deflection vector times mass distribution d-volume. One dyadic per mode.

A1 - Component of the deformed body 3x3 mass moment dyadic which is linearly dependent upon modal deformation. One dyadic per mode.

DS_40 DATASTRUCTURE=name:number.FLMX2, CLASS = RELATION
CONTENTS: The following mode dependent parameters dependent upon 2 modes:

C1 - Coupling terms between rigid body translational motion and modal velocity for the component of the full mass matrix which are linearly dependent upon modal deformation. One vector per mode pair.

C2 - Component of the deformed 3x3 body moment of inertia tensor which has a quadratic dependence on modal deformation. One dyad per mode pair.

Preliminary investigations with the interface module CIDRMX have convinced the author that the question of whether or not reduced order models contain sufficient fidelity to accurately produce all required mode dependent cross coupling terms must be more fully investigated. Early work

leads the author to believe that rigid body properties can be accurately obtained; however, mode dependent term accuracy must be more fully investigated. Current plans are to more fully understand this problem and to then include modal synthesis procedures before IAC Level 2 is released in early 1987.

INTERFACE MODULE INSAT
INTERFACE NASTRAN STATICS ANALYZER FOR THERMAL DATA

The program INSAT is designed to read a MSC/NASTRAN bulk data file which has been set up for a structural statics run and an array of nodal temperature data from a datastructure in an IAC database. INSAT then creates an enhanced bulk data file by generating cards which define thermal load sets and a table which correlates time values with solution subcases id's. This module was written by BAC for MSC/NASTRAN and has not yet been modified to work with COSMIC/NASTRAN.

INTERFACE MODULE INSAM
INTERFACE NASTRAN STATICS ANALYZER FOR MODAL DATA

The program INSAM is designed to read a MSC/NASTRAN bulk data file which has been set up for a structural statics run and an array of mode shape definitions. INSAM then creates an enhanced bulk data file by automatically generating cards which define nodal-to-modal conversion. The net result is the ability to compute nodal and modal displacements, stresses, etc. This module was written by BAC for MSC/NASTRAN and has not yet been modified to work with COSMIC/NASTRAN.

REFERENCES:

1. Vos, R. G., Beste, D. L., Gregg, J., Frisch, H. P., and Sanborn, J.A., "Integrated Analysis Capability (IAC) Program Level 1.5," COSMIC Program GSC-12992, COSMIC, Barrow Hall, Suite 112, University of Georgia, Athens, GA 30602.

2. Young, J. P., Vos, R. G., Frisch, H. P., and Jones, G. K., "Integrated Analysis Capability (IAC) Activity," SECOND CHAUTAUQUA on productivity in Engineering and Design THE CAD REVOLUTION, Nov 15-17, 1982.

3. Vos, R. G., Walker, W. J., Beste, D. L., Price, G. A., Young, J. P., and Frisch, H. P., "Development and Use of an Integrated Analysis Capability," AIAA/ASME/ASCE/AHS Structures, Structural Dynamics and Materials Conference, May 1983, Lake Tahoe, NV, AIAA Paper 83-1017.

4. Bossi, J. A., Price, G. A., and Winkleblack, S. A., " Flexible Spacecraft Controller Design Using the Integrated Analysis Capability (IAC)," AIAA Guidance and Control Conference, August 1984, Also IEEE Control Systems magazine, November 1985.

5. Bauer, F. H., Frisch, H. P., and Downing, J. P., "Integrated Control System Design Capabilities at the Goddard Space Flight Center," Pro- ceedings of the 2nd IEEE Control Systems Society Symposium on Computer- Aided Control System Design (CACSD), Santa Barbara, California, March, 13-15 1985.

6. Frisch, H. P. "Integrated Analysis Capability (IAC) for Structures, Controls, and Thermal Analysis," Seminar presented at the 13th NASTRAN Users' Colloquium, May 6-10, 1985.

7. Vos, R. G. "IAC level 0 Program Development," Large Space Systems Technology 1981, NASA Conference Publication 2215, Nov 16-19, 1981.

8. Bossi, J. A., Price, G. A., and Winkleblack, S. A., "Design of Multivariable Controllers Using the Integrated Analysis Capability," Proceedings of JPL Workshop on Identification and Control of Flexible Space Structures, San Diego, June 1984.

9. Walker, W. J., Vos, R. G., Price, G. A, and Brogren, E. W. "IAC Executive Summary," NASA Contractor Report 175196, May 1984.

10. Bodley, C. S., Devers, A. D., Park, A. C., and Frisch, H. P. "A Digital Computer Program for the Dynamic Interaction Simulation of Controls and Structure (DISCOS)," COSMIC Program GSC-12810.

11. Bodley, C. S., Devers, A. D., Park, A. C., and Frisch, H. P. "A Digital Computer Program for the Dynamic Interaction Simulation of Controls and Structure (DISCOS)," NASA Technical Paper 1219, Vols 1 and 2, May 1978.

12. Frisch, H. P. and Bauer, F. H. "Numerical Methods for Classical Sampled- System Analysis," COSMIC Program GSC-12827.

13. Bauer, F. H. and Downing, J. P. "INCA - Interactive Controls Analysis," COSMIC Program GSC-12998.

14. For information on "DADS - Dynamics Analysis and Design Systems" contact CADSI, P.O.Box 203, Oakdale, Iowa 52319.

15. Yoo, W. S. and Haug, E. J., "Dynamics of Articulated Structures, Part I: Theory," Journal of Structural Mechanics, to appear.

16. Yoo, W. S. and Haug, E. J., "Dynamics of Articulated Structures, Part II: Computer Implementation and Applications," Journal of Structural Mechanics, to appear.

17. Macala, G. A., "A Modal Reduction Method for use with Nonlinear Simulations of Flexible Multibody Spacecraft," AIAA/ASS Astrodynamics Conference, Aug 20-22, 1984, Seattle, WA, AIAA Paper 84-1989.

18. Gehling, R. N. "Model Reduction Technique for use with the Dynamic Interaction Simulation Controls and Structures (DISCOS) Computer Program," Martin Marietta Report MCR-85-534, Feb 1985.

19. Craig, R. R and Chang, C. "Substructure Coupling for Dynamic Analysis and Testing," NASA Contractor Report NASA CR-2781, Feb. 1975.

20. Frisch, H. P. "NASTRAN/DISCOS/SAMSAN DMAP Bridging Program," COSMIC Program GSC-12902.

21. Smith, B. T., Boyle, J. M., Dongarra, J. J, Garbow, B. S., Ikebe, Y., Klema, V. C., and Moler, C. B, "Matrix Eigensystem Routines - EISPACK Guide," Vol 6, Springer-Verlag, 1976.

A SYSTEM APPROACH TO DESIGN - ANALYSIS

Gil White
Intergraph Corporation
Huntsville, Alabama

SUMMARY

Today, the increased use of Finite Element Analysis coupled with computer graphics interfaces presents the analyst with many alternatives. The drive toward automation has resulted in the creation of many modeling and post-processing systems that are in use today throughout the world. Many of these systems exist as islands of technology. The need for fully integrated systems is being met by Intergraph Corporation today.

INTRODUCTION

Intergraph's Rand-MICAS (IRM), a computer-aided design and analysis system, runs on DEC VAX and VAX-compatible equipment. The system includes a pre-processor for model development, a complete analysis capability and a post-processor for displaying and managing analysis results. IRM can interface to the majority of major analysis systems including COSMIC NASTRAN.

The system is designed to operate in the design-analysis environment where quick model development and editing are required. Repeated analysis can be done realtime during the design-analysis session.

PURPOSE

The purpose of this paper is to describe an integrated approach to the design process from concept to manufacturing. An attempt will be made to demonstrate the cohesive properties of Intergraph's total system. The foundation of which are graphics and non-graphics data bases operating simultaneously under the VAX/VMS system architecture. The paper will center around the analysis of a retractable automobile headlamp assembly. A static stress analysis of the headlamp will be discussed.

MODEL DEVELOPMENT

Creation of the finite element model is done graphically from any of Intergraph's workstations. Working in a graphics design file and a data management file simultaneously, the analyst creates the model by selecting commands from a graphics menu (Figure 1A and 1B). Integration between design and analysis is achieved through the use of a reference file. The reference file is a read only file that can be viewed by the analyst and used as a guide during model creation. Figure 2 shows the headlamp reference file that was

used during model development. The modeling process begins with the selection of a model type from the model type/units tutorial (Figure 3). Dimensional units default to those of the design file. From the active parameters tutorial various modeling, loading, and post-processing parameters are established (Figure 4). Mesh generation is accomplished through the use of any of several meshing routines. Meshing capabilities include mapping to three dimensional "B-Spline" surfaces in addition to various project and sweep commands. All major element types are supported including mid-side node elements, gap elements, and super elements.

Figure 5 shows the completed model of the headlamp. Loading was applied to the front face of the headlamp using a fence pressure command. Fence commands allow the analyst to operate on groups of elements by defining a graphic fence. All real Eigenvalue extraction data is defined at the graphics workstation and becomes resident in the data base.

MODEL EDITING

Editing of the finite model is accomplished while at the graphics workstations. From the graphics environment, the data base can query and information obtained about any model component. Deletion and changes can be made and all associativity maintained. As in the model creation, changes to elements, nodes, loads and boundary conditions can be made one at a time or in a variety of group operations. Editing can be done from an alpha terminal as well as the graphics workstation. Figure 6 shows the model of the headlamp after editing.

ANALYSIS

After completion of the modeling process, the analyst has the option of doing the analysis on many third-party analysis packages or using the internal analysis capability of IRM. Analysis is using third-party packages is accomplished through the use of individual translators. These translators create the complete input deck to any major analysis package. In the case of COSMIC NASTRAN, the executive control deck, case control deck, and bulk data deck are all created. See Figure 7 and Figure 8.

The Intergraph Rand-MICAS analysis system consists of a basic module and six model type options. The basic module contains the data base functions as well as all of the model description and analysis processing capabilities. Included are node, element, load, and application generators. The analysis options include linear static, limited non-linear static and modal dynamic processing capabilities. Material properties include orthotropic as well as isotropic properties. IRM addresses a variety of boundary conditions including: restrained degrees of freedom, specified displacements, springs, gap spring to ground, distributed gap springs to ground, hook springs to ground, and distributed hook spring to ground.

Load type options (global or local) that are applied include:

- **Distributed**
- **Projected surface**
- **Pressure**
- Body force
- Nodal force and moment
- Concentrated
- Partially distributed
- Triangular
- Perimeter surface
- Wind (pressure and velocity)
- Thermal loads

The analysis system addresses general and specific translational masses as well as rotational masses.

In addition to the modeling capabilities offered through the graphics workstation environment, the user can access the same routines from the alpha environment. Both methods operate on the same data base, therefore, continuity is assured.

POST PROCESSING

Using IRM post-processing the analyst can display, manipulate and manage analysis results from the graphics environment. Results are viewed and saved in the working design file. Features of Intergraph Rand-MICAS post-processing are as follows:

- Contouring of any single value or scaler nodal function. The most common being stress, displacements and moments.
- Deformed shape plot including projection of scaler functions.
- Linear combination of load case results and other mathematical operations.
- Vector display of any nodal vector function. The most common being principal stress, velocity and acceleration.
- Color coding of elements for various parameters.
- Animation of displacements including dynamic modal analysis output.

As in the model creation process, the post-processing commands are selected from a graphics screen menu (Figure 9). The user has the option to write any results permanent to the design file or display them in a transient mode. Analysis output is managed and manipulated from the post-processing parameters tutorial (Figure 10). Post-processed results for the headlamp are shown in Figures 11, 12, and 13.

LIST OF FIGURES

1A Pre-Processing Menu (Page 1)

1B Pre-Processing Menu (Page 2)

2 Reference File of Headlamp

3 Model Type Tutorial

4 Active Parameters Tutorial

5 Completed Finite Element Model

6 Finite Element Model showing Editing

7 COSMIC NASTRAN Interface Tutorial

8 COSMIC NASTRAN Input Generated by Translator

9 Post-Processing Menu (Page 3)

10 Post-Processing Parameters Tutorial

11 Plot of Stress Contours

12 Plot of Displacement

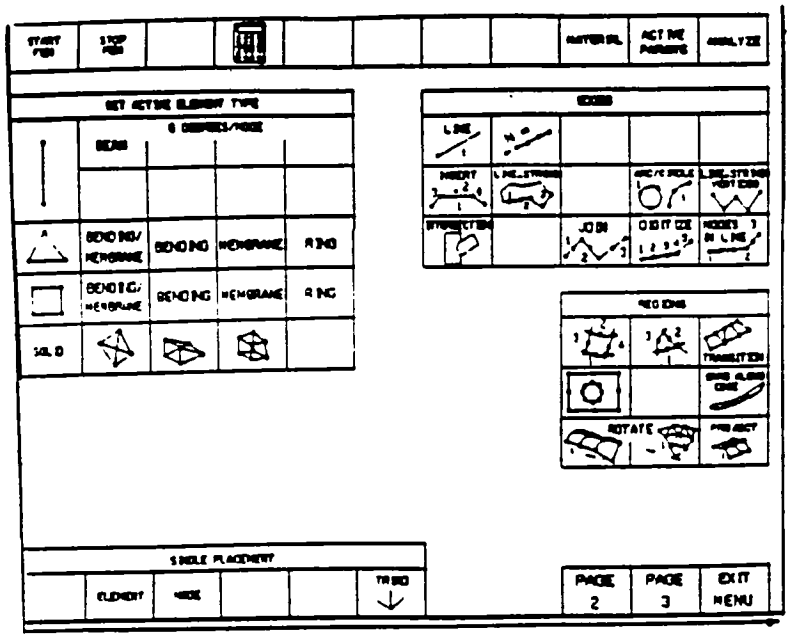

Fig. 1A - Pre-Processing Menu (Page 1)

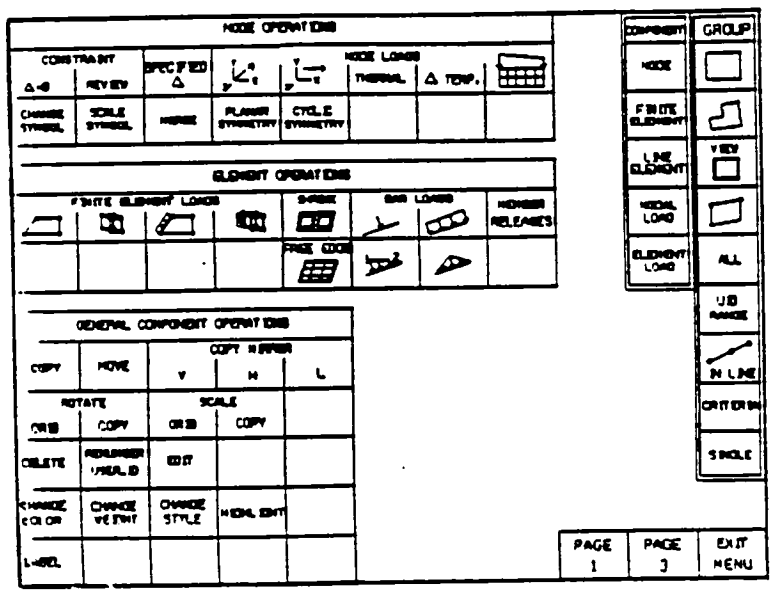

Fig. 1B - Pre-Processing Menu (Page 2)

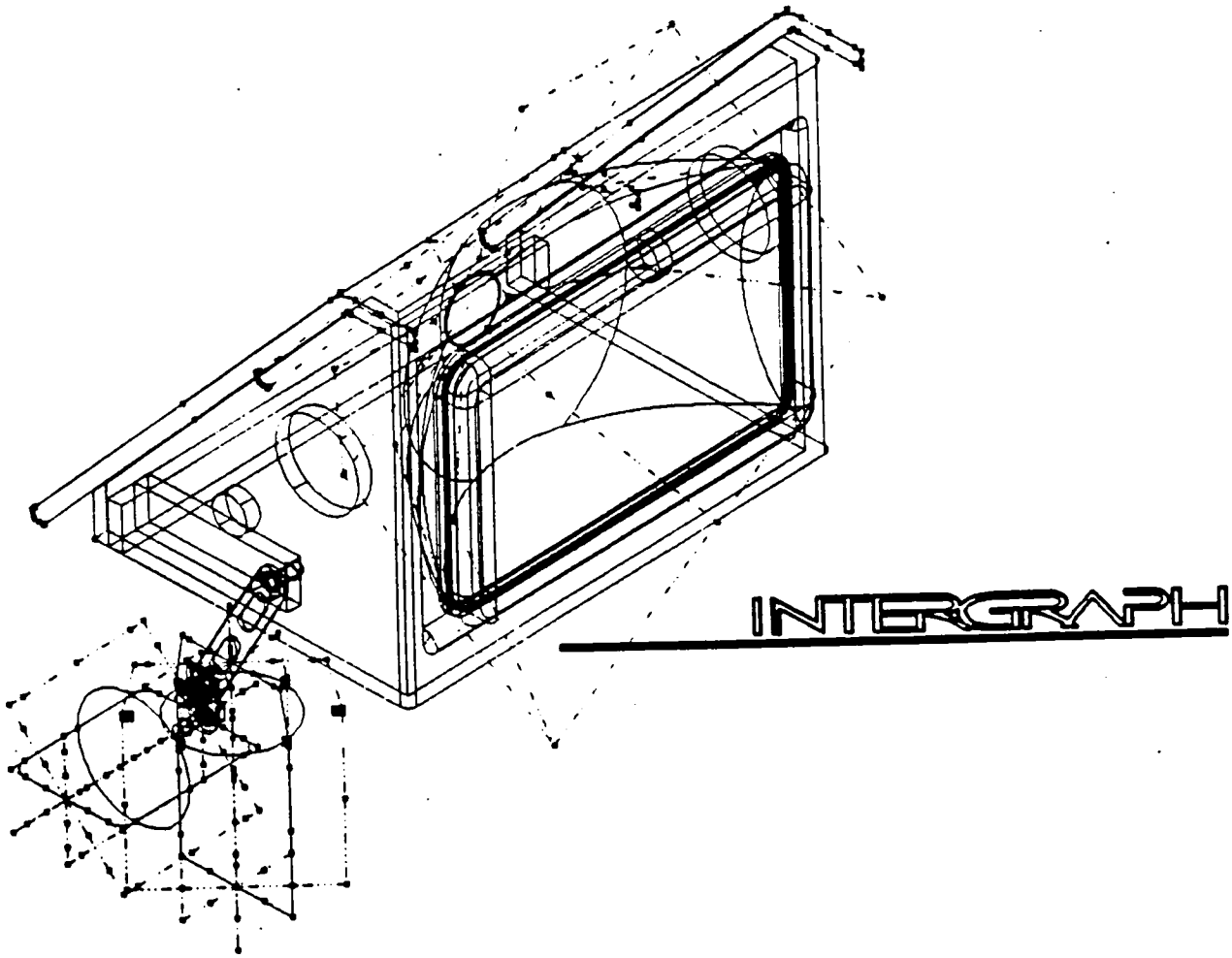

Fig. 2 - Reference file of Headlamp

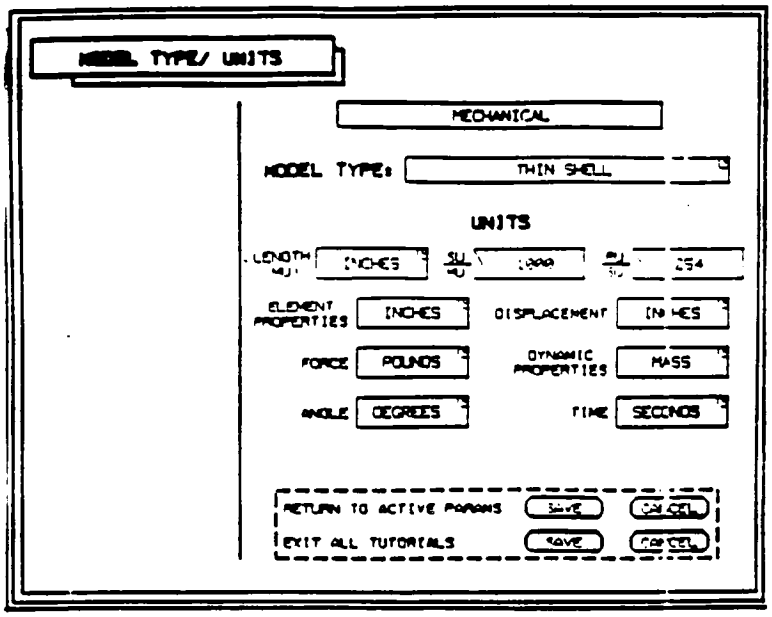

Fig. 3 - Model-Type Tutorial

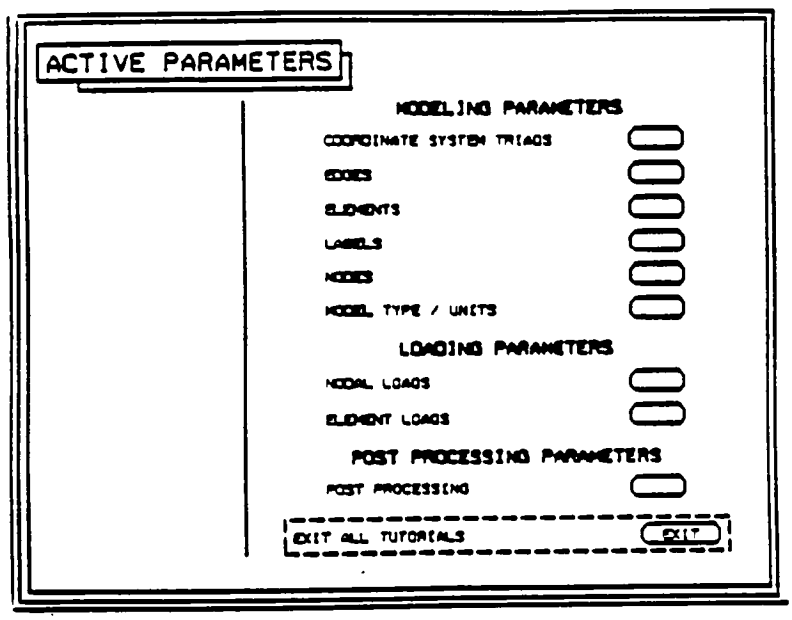

Fig. 4 - Active Parameters Tutorial

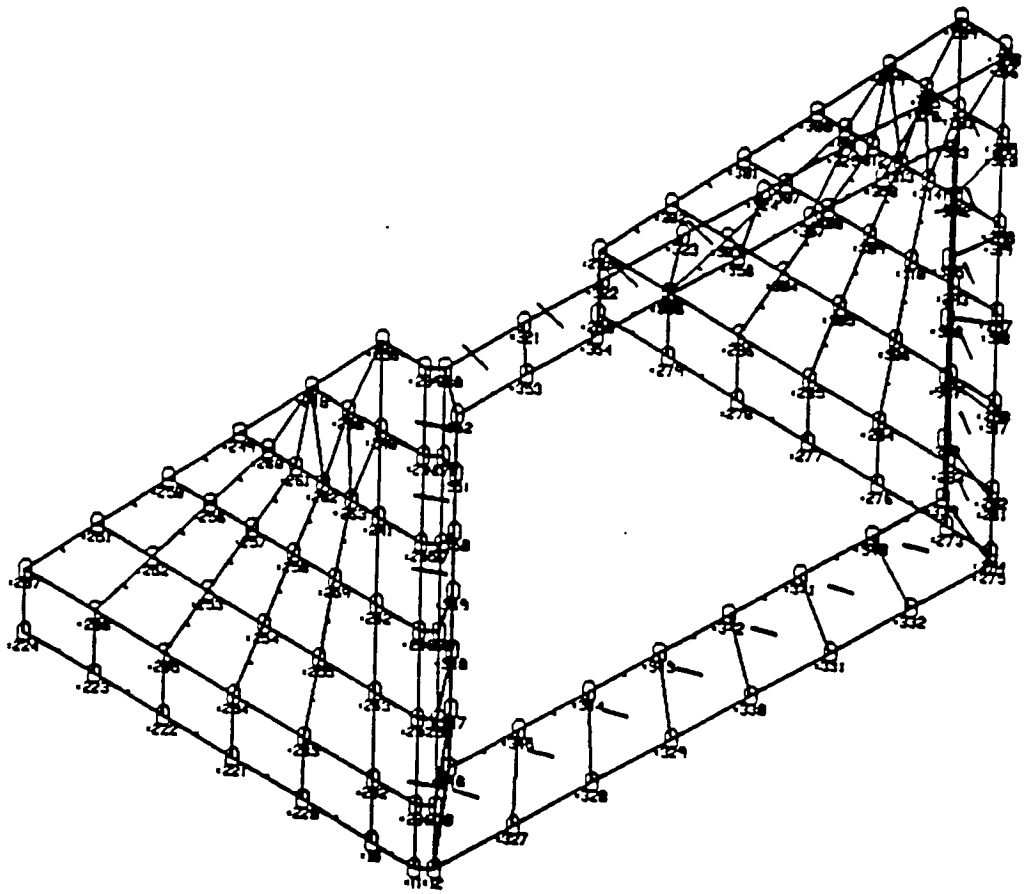

Fig. 5 - Completed Finite Element Model

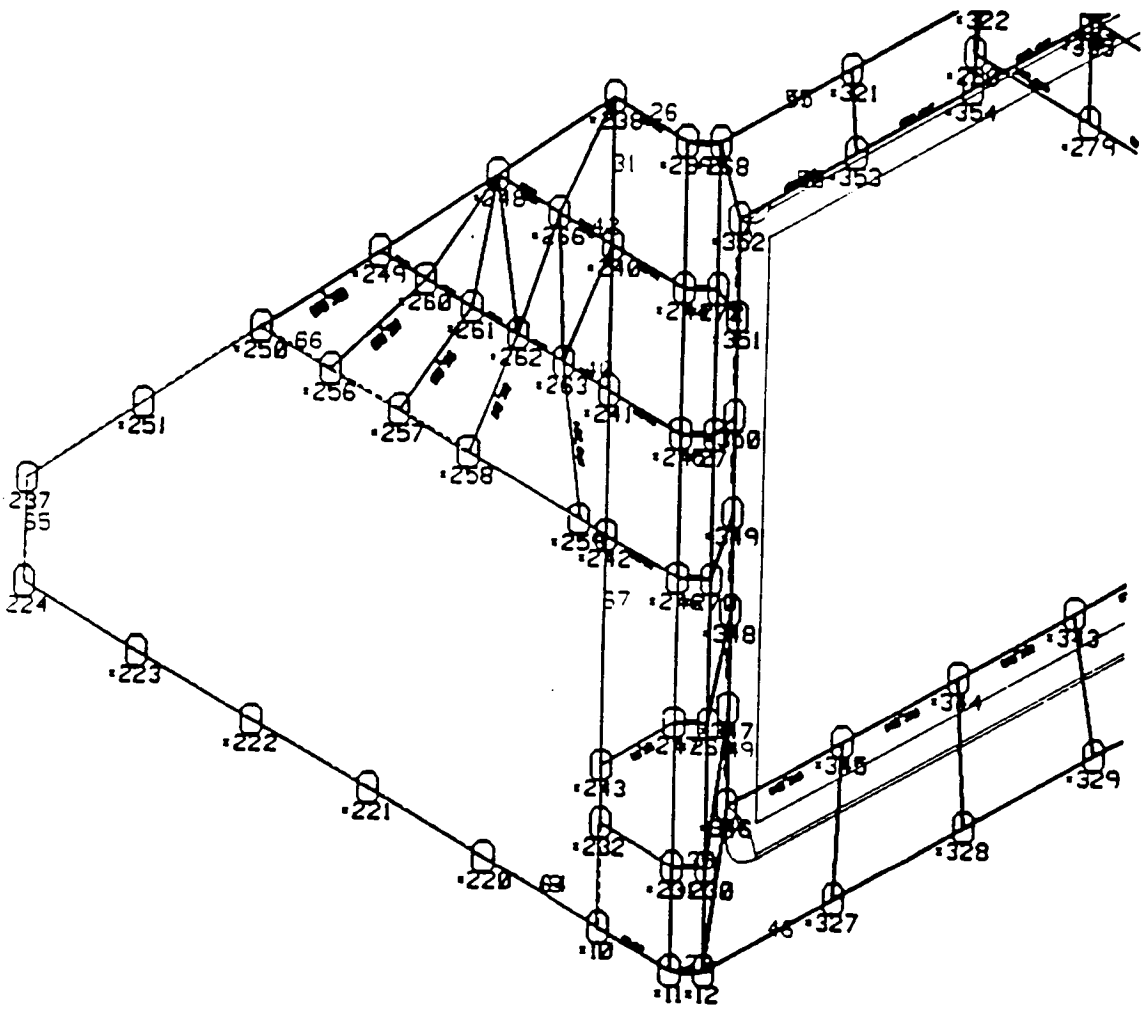

Fig. 6 - Finite Element Model Showing Fairing

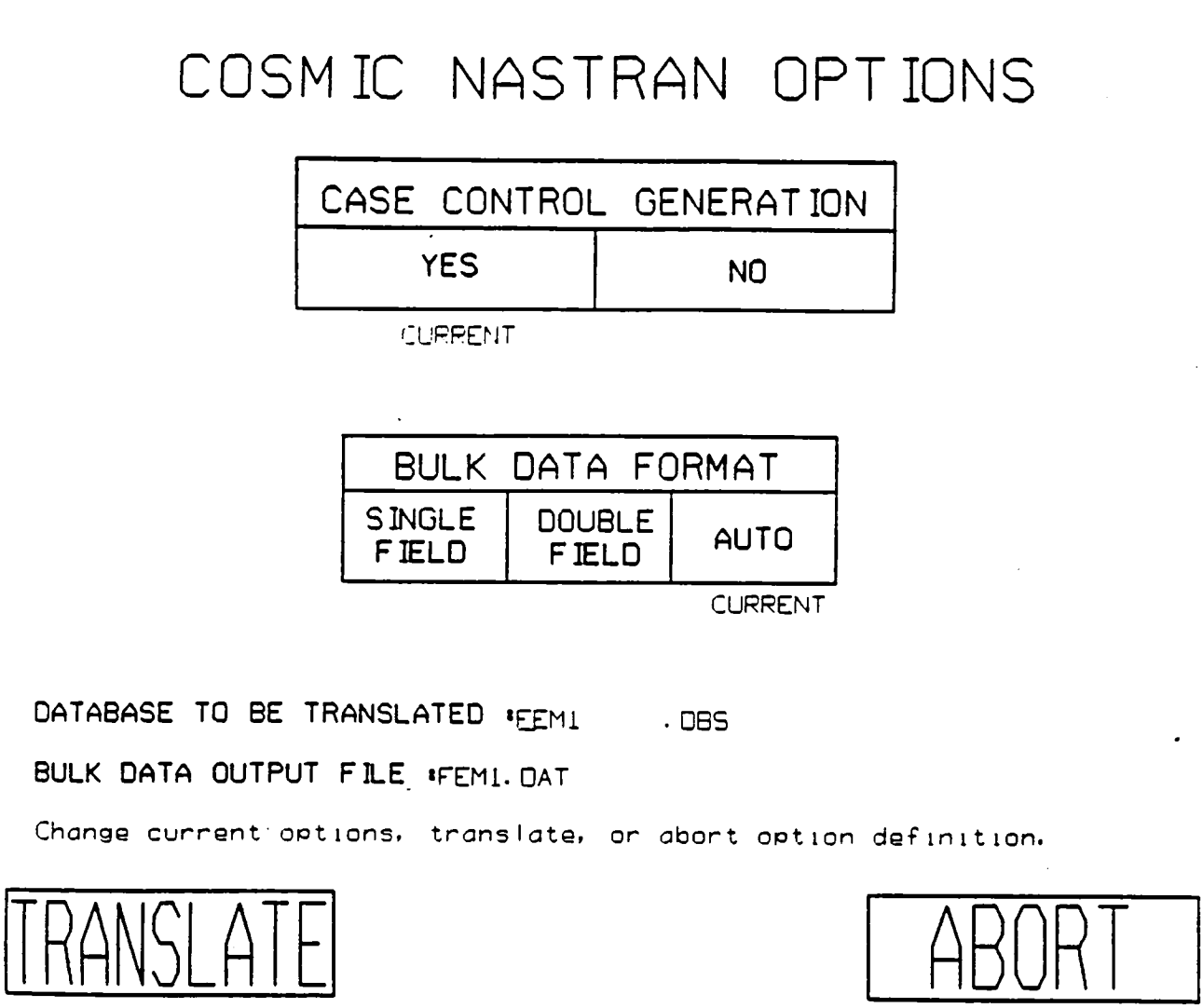

Fig. 7 - COSMIC NASTRAN Interface Tutorial

```
2       SUBTITLE= MODELLED WITH INTERGRAPH FEMS SYSTEM
3       LABEL= ANALYZED BY MSC/NASTRAN
4       ECHO= SORT
5       DLOAD= ALL
6       GPSTRESS = ALL
7       DISPLACEMENT(PRINT,PUNCH)= ALL
8       ELSTRESS(PLOT)= ALL
9       SUBCASE     1
10      LABEL= LOAD SET NUMBER     1
11      LOAD=      1
12      SPC =      1
13      OUTPUT(POST)
14      SET 10 = ALL
15      SURFACE 1 SET 10 FIBRE Z1 NORMAL X3 TOPOLOGICAL
16      BEGIN BULK

          INPUT BULK DATA CARD COUNT =    4047
```

MODELLED WITH INTERGRAPH FEMS SYSTEM

SORTED BULK DATA ECHO

CARD COUNT	. 1 ..	2 ..	3 ..	4 ..	5 ..	6 ..	7 ..	8 ..	9 ..	10 .
1-	CQUAD4 1	1	1	2	22	21				
2-	CQUAD4 2	1	21	22	23	20				
3-	CQUAD4 3	1	20	23	12	11				
4-	CQUAD4 4	1	2	3	24	22				
5-	CQUAD4 5	1	22	24	25	23				
6-	CQUAD4 6	1	23	25	13	12				
7-	CQUAD4 7	1	3	4	25	24				
8-	CQUAD4 8	1	24	26	27	25				
9-	CQUAD4 9	1	25	27	14	13				
10-	CQUAD4 10	1	4	8	28	26				
11-	CQUAD4 11	1	26	28	29	27				
12-	CQUAD4 12	1	27	29	15	14				
13-	CQUAD4 13	1	8	9	30	28				
14-	CQUAD4 14	1	28	30	31	29				
15-	CQUAD4 15	1	29	31	16	15				
16-	CQUAD4 16	1	9	10	19	30				
17-	CQUAD4 17	1	30	19	18	31				
18-	CQUAD4 18	1	31	18	17	16				
19-	CQUAD4 19	1	11	12	705	706				
20-	CQUAD4 20	1	12	13	704	705				
21-	CQUAD4 21	1	13	14	703	704				
22-	CQUAD4 25	1	36	35	34	33				
23-	CQUAD4 26	1	34	41	44	33				
24-	CQUAD4 27	1	33	44	45	32				
25-	CQUAD4 28	1	32	45	5	6				
26-	CQUAD4 29	1	41	40	46	44				
27-	CQUAD4 30	1	44	46	47	45				
28-	CQUAD4 31	1	45	47	4	5				
29-	CQUAD4 32	1	40	39	48	46				
30-	CQUAD4 33	1	46	48	49	47				
31-	CQUAD4 34	1	47	49	3	4				
32-	CQUAD4 35	1	39	38	50	48				
33-	CQUAD4 36	1	48	50	51	49				

Fig. 8 - COSMIC NASTRAN Input Generated by Translator

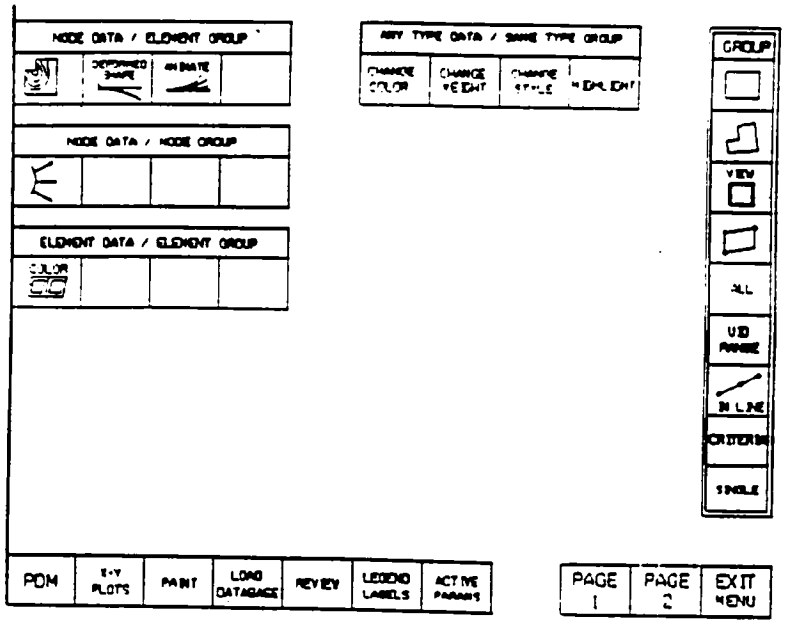

Fig. 9 - Post-Processing Menu

(Page 3)

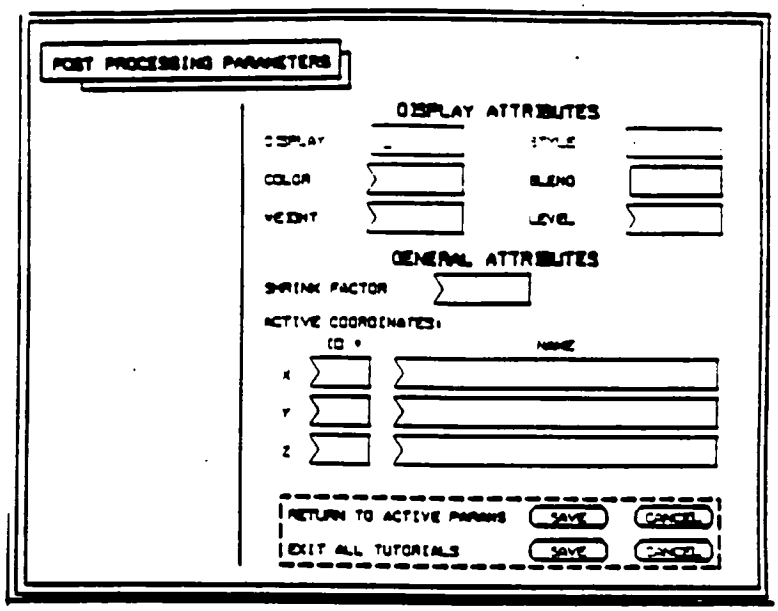

Fig. 10 - Post Processing Parameters Tutorial

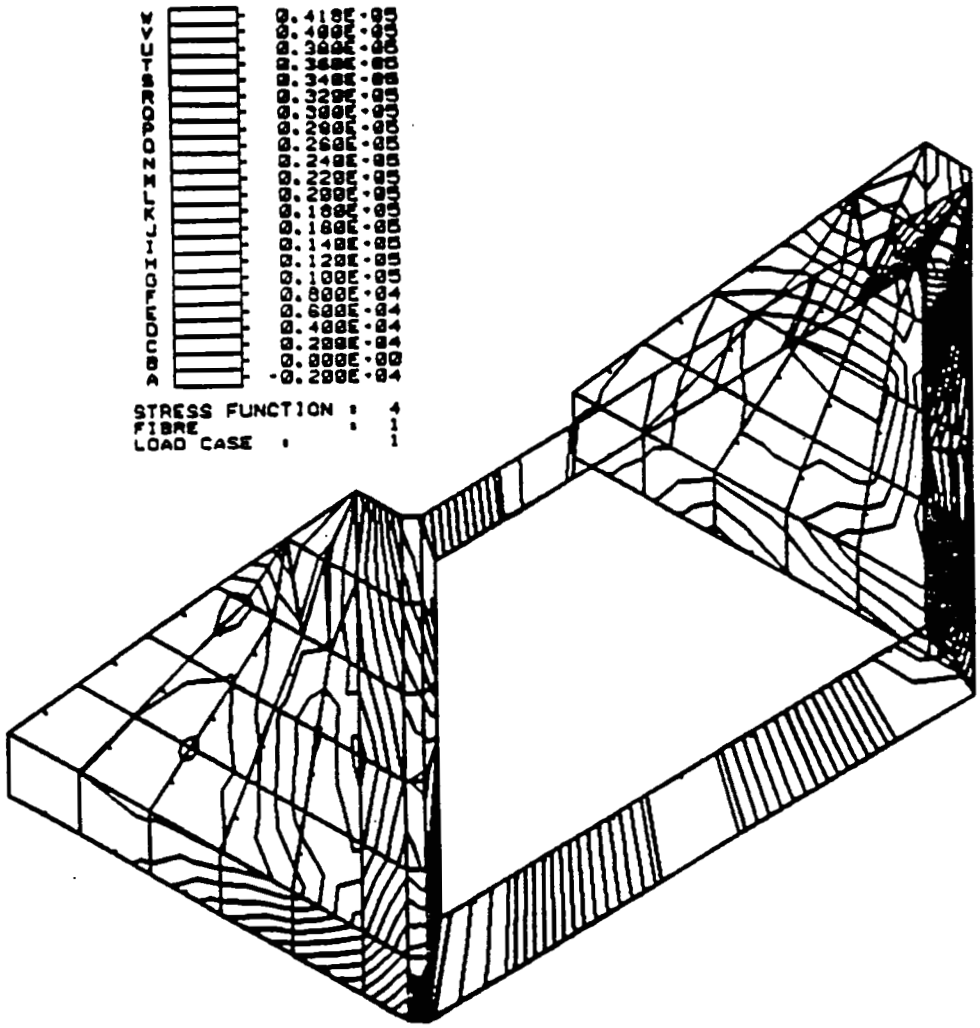

Fig. 11 - Plot of Stress Contours

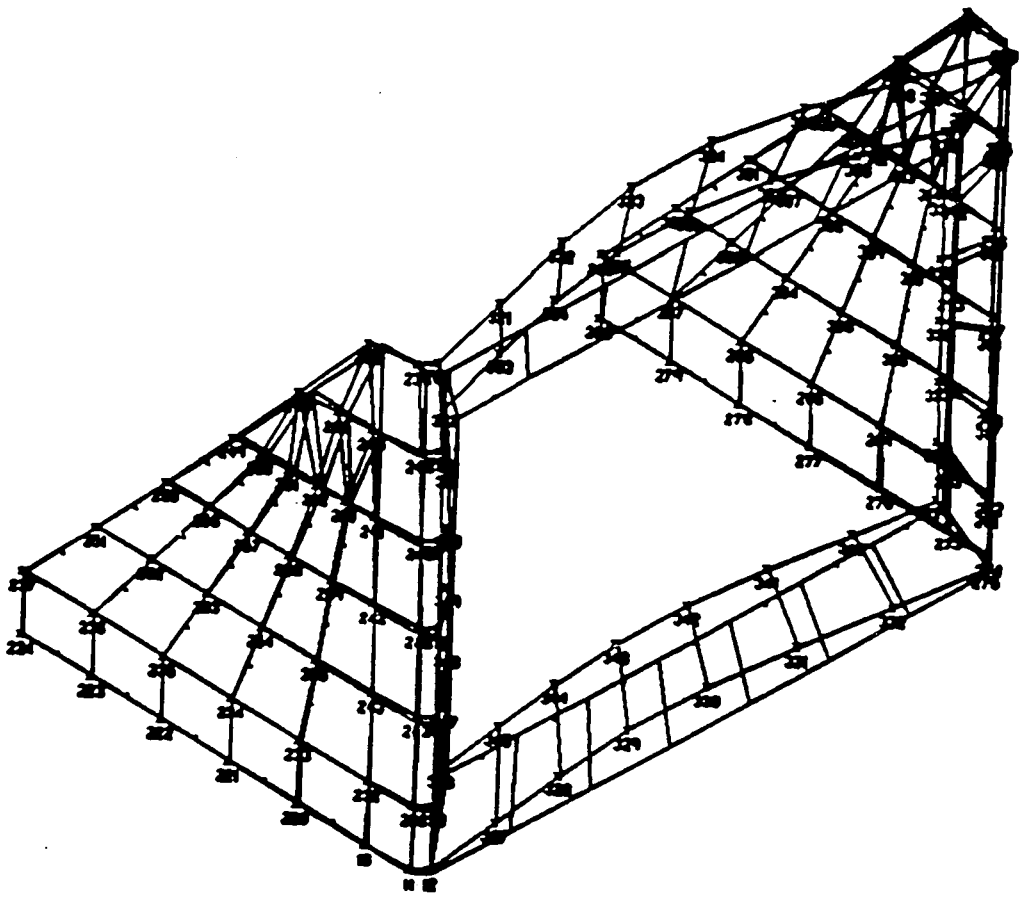

Fig. 12 - Plot of Displacement

EXPERIENCES WITH NASTRAN IN A MULTIDISCIPLINARY OPTIMIZATION ENVIRONMENT

Myles M. Hurwitz

David W. Taylor Naval Ship Research and Development Center

SUMMARY

NASTRAN and COPES/CONMIN were used in the early-stage design optimization of a propeller and shaft. The work was undertaken, in part, to assess the performance of these programs for such a task. While the optimization was successful, some drawbacks to the approach surfaced and are discussed.

INTRODUCTION

For almost 25 years, the finite element method (FEM) has been the premier technique used in the field of structural analysis. The FEM has enjoyed this popularity because of its generality, ease of use, and obvious physical relationship with the structure to be analyzed. With the advent of NASTRAN in 1970, engineers had a comprehensive and easily accessible program for taking advantage of this popular technique. NASTRAN and FEM technology, in general, have now had 10-15 years to mature, while users of the FEM have become very sophisticated in their use of such programs. In fact, usage of finite element programs has now extended far beyond structural analyses; heat transfer, aerodynamics, electricity, magnetism, and acoustics are but a few of the disciplines finite element programs now address.

Finite element analyses are now so routine that natural scientific inquiry leads to the question, "Now that I can analyze the structure so easily, can the structure be modified to make it better?" This question leads immediately to another: "What is meant by 'better'?" This question can usually be answered with adjectives such as lighter, cheaper, faster, more efficient, etc. Taking this process a step further, if the analyst (now a designer?) wants a lighter structure, a lighter material may mean larger deflections, which may not be allowable. Therefore, the engineer often has a conflict; he/she has an objective, e.g., the lightest structure possible to do the job, but the situation may call for constraints, e.g., stress, deflection, which conflict with the objective. The goal then is to minimize or maximize some objective function subject to imposed constraints. The subject area which attempts to solve this problem is called "optimization."

The objective of the work was, in part, to assess the performance of NASTRAN for early-stage design optimization. For this paper, the details of the specific structure being optimized are not important, but it should be noted that the optimization was very successful. So, the remainder of the paper will briefly present the optimization problem in mathematical terms and then describe (1) our experiences in attempting to solve an optimization problem which had constraints in fluid mechanics, structural mechanics, and acoustics; and (2) NASTRAN's role in the solution process.

OPTIMIZATION

The general mathematical constrained optimization problem can be described as (reference 1):

Minimize: $F(\bar{X})$

Subject to: $G_j(\bar{X}) \leq 0,\ j = 1, \ldots, m$

and $x_i^{\ell} \leq x_i \leq x_i^{u},\ i = 1, \ldots, p$

where

$\bar{X} = [x_1, x_2, \ldots, x_n]^T$ is the vector of design variables, i.e., those parameters in the problem whose values can change in order to achieve a "better structure";
F = the objective function to be minimized;
G_j = the jth constraint on the solution; and,
x_i^{ℓ}, x_i^{u} = lower and upper bounds on the ith design variable.

A simple example from reference 1 will clarify these concepts. Assume that the cantilever beam in the following sketch is to be optimized as follows:

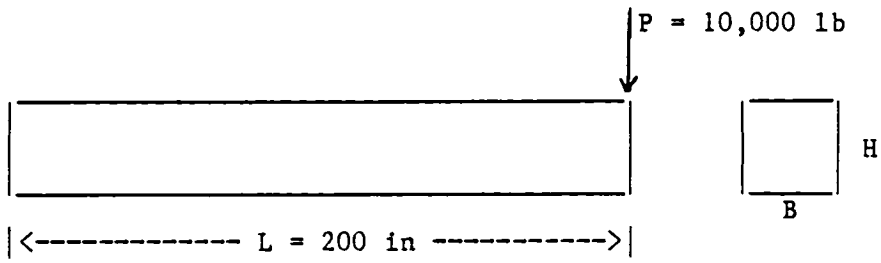

Minimize Volume = B•H•L (design variables are B and H, i.e., $\bar{X} = [B\ H]^T$ subject to the following constraints:

(1) Bending stress $\sigma_b \leq 20{,}000$ psi

$$\sigma_b = \frac{Mc}{I} = \frac{6PL}{BH^2} \leq 20{,}000, \text{ or } G_1(\bar{X}) \equiv \frac{6PL}{BH^2} - 20{,}000 \leq 0$$

where M is the moment, c is the distance from the neutral axis, and I is the moment of inertia of the section.

(2) Shear stress $\upsilon \leq 10{,}000$ psi

$$\upsilon = \frac{3}{2}\frac{P}{A} = \frac{3P}{2BH} \leq 10{,}000, \text{ or } G_2(\bar{X}) \equiv \frac{3P}{2BH} - 10{,}000 \leq 0$$

where A is the cross-sectional area BH.

(3) Deflection $\delta \leq 1.0$ in.

$$\delta = \frac{PL^3}{3EI} = \frac{4PL^3}{EBH^3} \leq 1.0, \text{ or } G_3(\bar{X}) \equiv \frac{4PL^3}{EBH^3} - 1.0 \leq 0$$

where E, Young's Modulus, is assumed to be 30×10^6 lb/in^2.

(4) $0.5 \leq B \leq 5.0$

(5) $1.0 \leq H \leq 20.0$

(6) $\frac{H}{B} \leq 10.0$

For a simple two-design variable problem such as this, the constraints and volume contours can be easily represented on a two-dimensional plot as in Figure 1. The cross-hatching of Figure 1 represents the violated sides of constraints. The shaded area represents the region of feasible designs, i.e., the only region which contains acceptable combinations of B and H. This region is enlarged in Figure 2, where the optimum design is at the circled point, which is B = 1.82 in., H = 18.2 in., and VOL = 6608 in^3.

For a problem with many design variables, a numerical, rather than graphical, method is required to obtain the optimal solution. The program used in the present work was the Control Program for Engineering Synthesis/Constrained Minimization (COPES/CONMIN) (references 1 and 2). (The optimization portion of the program has since been succeeded by the code Automated Design Synthesis (ADS), so that the current designation of the complete program is COPES/ADS, reference 3). Along with the numerical optimization program which computes new values of the design variables, and hence develops a new design, a program is needed to analyze the new design. The analysis program must compute the values of the objective function and constraints for the new design. These values are then passed back to the optimization program, which will develop still another design in an attempt to minimize the objective function while satisfying the constraints. This procedure is repeated until convergence has been achieved or until a predetermined number of iterations has been performed.

The analysis program can be linked to COPES/CONMIN in two ways: (1) the analysis program can be a subroutine within COPES/CONMIN, or if that is not possible, (2) the analysis program is kept separate from COPES/CONMIN, but linkage programs between the two must be provided. The second method requires

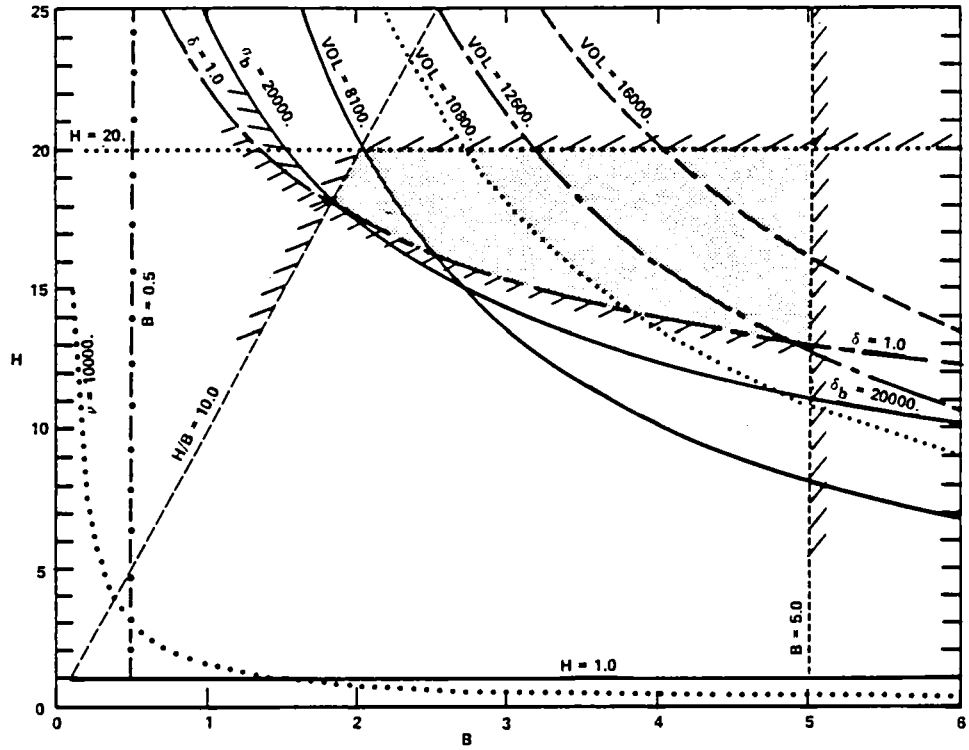

Figure 1 - Two-Dimensional Design Space

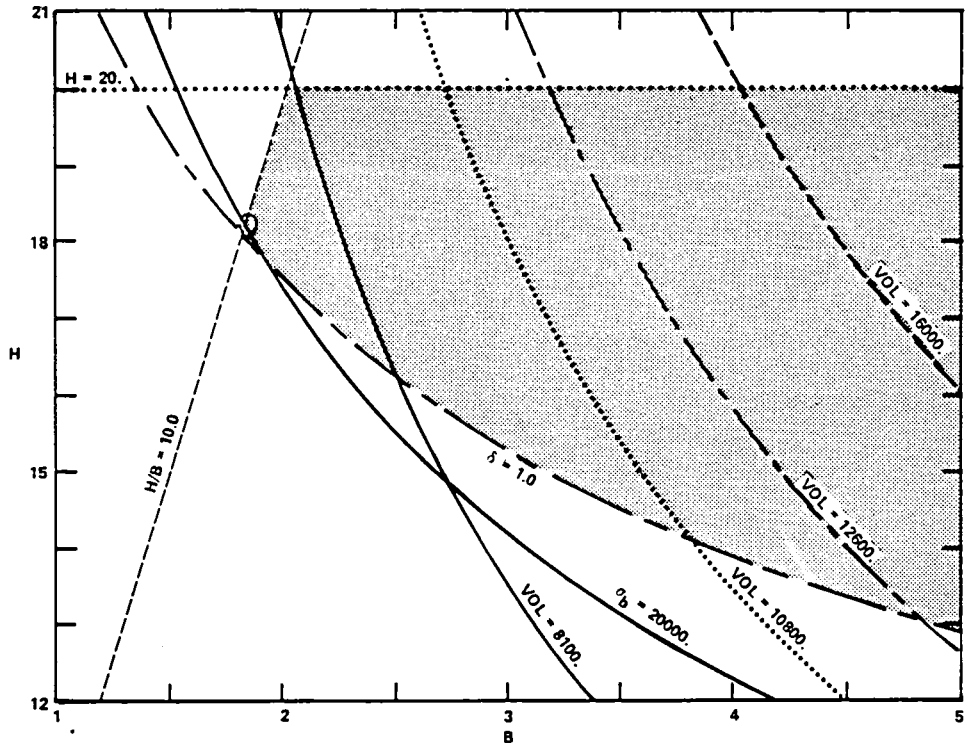

Figure 2 - Two-Dimensional Design Space (Enlarged)

either a special optimization procedure within COPES/CONMIN or a restart procedure, since COPES/CONMIN is not in memory while the analysis program is running. If NASTRAN is the analysis program, then the second method must be used.

THE PROBLEM

The structure to be optimized was a propeller and its associated shaft. The problem was to optimize the weight (or some other chosen function) of the system, which was subjected to hydrodynamic, structural, and acoustic constraints. Because the propeller design would influence the shaft design, but not vice versa, the problem was divided into two phases. First, the propeller was optimized; then, with the propeller design in hand, the shaft was optimized.

Propeller Optimization

Several propeller designs were generated corresponding to various objective functions such as weight, efficiency, tip speed, or combinations of these functions. The propeller designs had to meet a number of hydrodynamic and acoustic constraints. Therefore, hydrodynamic and acoustic analysis programs had to be linked to COPES/CONMIN. The relatively small hydrodynamic analysis program could be linked directly with COPES/CONMIN. However, a part of the input to the acoustic analysis program were results from a NASTRAN forced response analysis. Therefore, the acoustic analysis could not be linked directly to COPES/CONMIN, but made use of the second method described in the last section. Because of this complication and because of the strong desire to link the hydrodynamic analysis program to COPES/CONMIN directly, the analyses were separated as follows. An optimized hydrodynamic design was computed first, followed by an acoustic analysis of the optimized design. If the acoustic constraint was not met, tighter hydrodynamic constraints were imposed and the hydrodynamic optimization repeated. The purpose of the tighter hydrodynamic constraints was to modify the design variables so that the acoustic constraint would be met, as would the original hydrodynamic constraints. A flowchart of the process is shown in Figure 3. The linkage program represented in Figure 3 used COPES/CONMIN results to generate a NASTRAN data deck. This process continued until all constraints were met, at which point the shaft optimization was begun.

Shaft Optimization

The shaft optimization involved the design of the inner and outer diameters of two shaft sections. The weight of the shaft was to be minimized subject to various structural constraints; some were static; others, specifically, natural frequencies, were dynamic. Since NASTRAN was used as the analysis program, two NASTRAN runs were necessary: one for statics, another for natural frequencies. A flowchart of the process is shown in Figure 4. Each linkage program used data output from the preceding program to generate input for the following program.

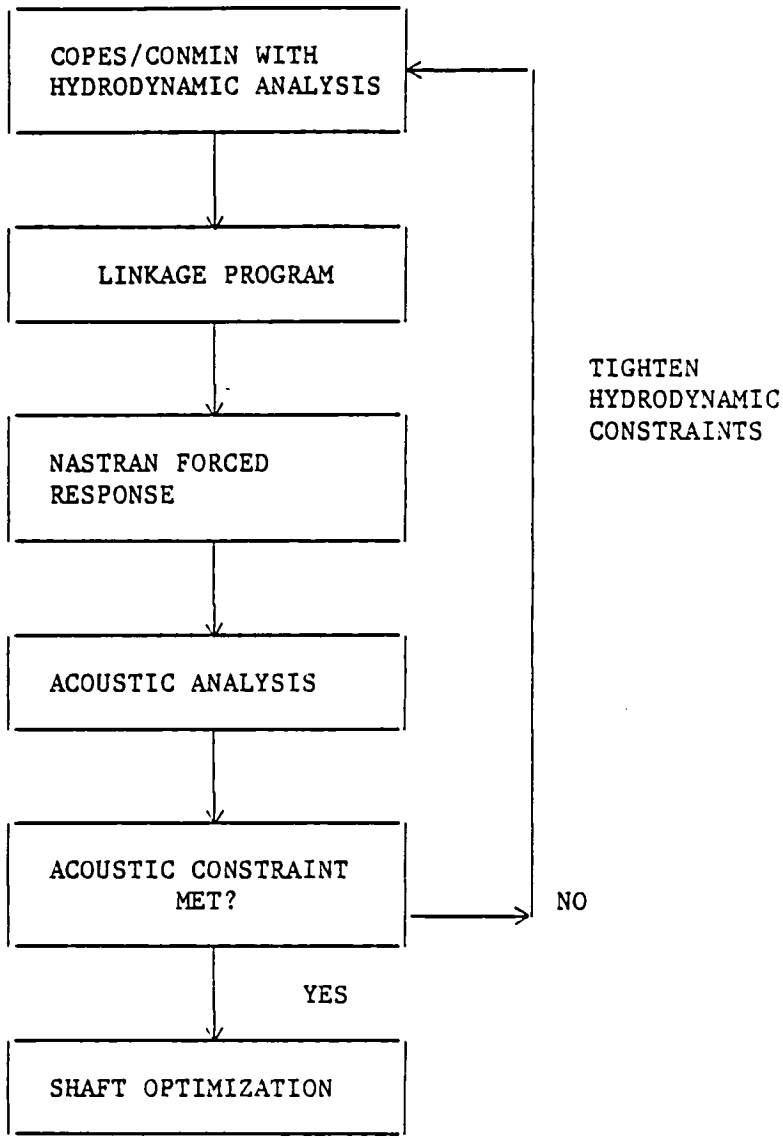

Figure 3 - Propeller Optimization Procedure

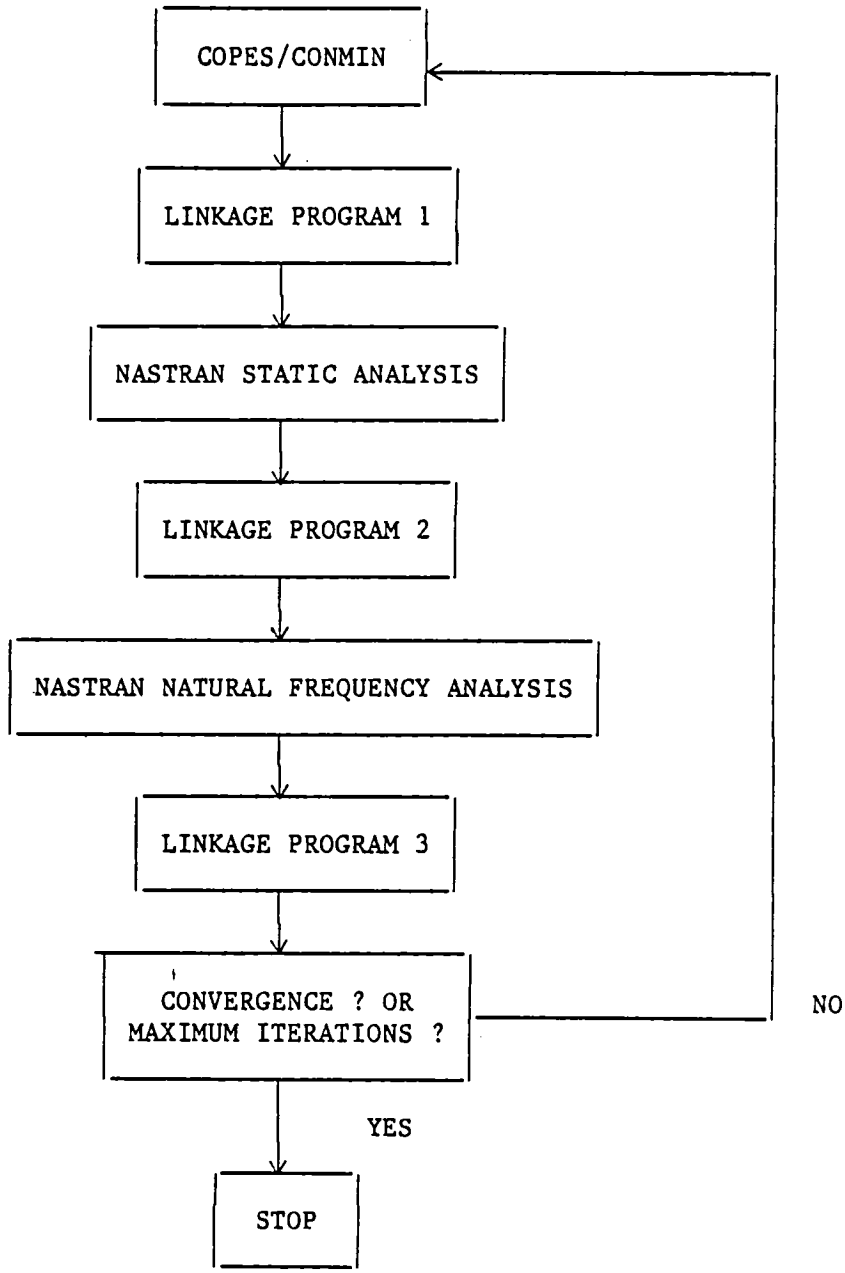

Figure 4 - Shaft Optimization Procedure

DISCUSSION

One of the purposes of this work was to explore the usefulness of NASTRAN in an early-stage design optimization procedure. The conclusions from the study were mixed. NASTRAN was very helpful in that all the required analyses (statics, natural frequencies, and forced response) were available in one program. Also, it was very easy to make changes to the basic structure when needed. However, there were a number of drawbacks to using NASTRAN. First, and perhaps most important, NASTRAN, because of its size, could not be made a subroutine within COPES/CONMIN. This meant that (1) the standard optimization procedures of COPES/CONMIN could not be used, and (2) linkage programs had to be written. Unless linkage programs are written for the very general case, changes to the structure and resulting finite element model require changes to the linkage programs. Since such changes are frequent in early-stage design, much time was spent in modifying the linkage programs. Another drawback was the cost of the optimization-analysis iterations. Although the finite element model was simple (34 CBAR elements, 35 grid points), the cost of one complete iteration was approximately $35.00 on the DTNSRDC computers. For the approximately 30 iterations run, the total cost was $1,000.00. While this is not an exorbitant sum for a large finite element analysis, for those engineers who usually work in early-stage design, $1,000.00 is a significant amount for computer runs. On the other hand, for that sum of funds, a complete, optimized design was achieved for the conditions given. The emphasis of the last phrase was made to indicate that, in early-stage design, conditions can change frequently, which could give rise to a number of optimization runs.

(Two parenthetical points can be made here. First, had NASTRAN been linked to COPES/CONMIN as a subroutine, the costs probably would have been higher. The reason is that, in that case, the standard optimization of COPES/CONMIN would have been used, necessitating NASTRAN to compute gradients of the constraints and objective function at each iteration, which would have been expensive. Since NASTRAN cannot be so linked to COPES/CONMIN, optimization based on approximation techniques was used, perhaps requiring more iterations but at less cost per iteration. The second point relates to the costs of optimization in early-stage versus detailed design. As was stated, in early-stage design, conditions change frequently, necessitating several optimization runs. In detailed design, where conditions have usually been set, the model is more complex and the number of design variables increases, thereby also increasing computer costs.)

CONCLUDING REMARKS

NASTRAN was used with COPES/CONMIN to, in part, assess the program's performance in early-stage design optimization for ship components. While an optimization of a propeller and shaft was successfully completed, the costs incurred have raised some questions as to the applicability of the approach for early-stage ship design. These costs were primarily due to developing and modifying linkage programs and to running multiple NASTRAN cases. An alternative is to develop special purpose programs which can be linked directly with

COPES/CONMIN, but such development costs would increase with the changing conditions of early-stage design and with the requirement to develop such programs for different structures. These trade-offs will require more study in order to reach "optimal" conclusions for the ship design process.

REFERENCES

1. Madsen, L.E., and G.N. Vanderplaats: COPES - A FORTRAN Control Program for Engineering Synthesis. Naval Postgraduate School, Monterey, California, NPS69-81-003, Mar 1982.

2. Vanderplaats, G.N.: CONMIN - A FORTRAN Program for Constrained Function Minimization, User's Manual. National Aeronautics and Space Administration, NASA Report TMX-62282, Aug 1973.

3. Vanderplaats, G.N.: COPES/ADS - A FORTRAN Control Program for Engineering Synthesis Using the ADS Optimization Program. Naval Postgraduate School, Monterey, California, NPS69-84-009, Jun 1984.

STRESS CONCENTRATION INVESTIGATIONS USING NASTRAN †

M. C. Gillcrist and L. A. Parnell
Naval Ocean Systems Center, San Diego, CA

ABSTRACT

Parametric investigations are performed using several two-dimensional finite element formulations to determine their suitability for use in predicting extremum stresses in marine propellers. Comparisons are made of two NASTRAN elements (CTRIM6 and CTRIA2) wherein elasticity properties have been modified to yield plane strain results. The accuracy of the elements is investigated by comparing finite element stress predictions with experimentally determined stresses in two classical cases: (1) tension in a flat plate with a circular hole; and (2) a filleted flat bar subjected to in-plane bending. The CTRIA2 element is found to provide good results. The displacement field from a three-dimensional finite element model of a representative marine propeller is used as the boundary condition for the two-dimensional plane strain investigations of stresses in the propeller blade and fillet. Stress predictions from the three-dimensional analysis are compared with those from the two-dimensional models. The validity of the plane strain modifications to the NASTRAN element is checked by comparing the modified CTRIA2 element stress predictions with those of the ABAQUS plane strain element, CPE4.

INTRODUCTION

It is common practice in stress analyses of marine propellers to create a three-dimensional (3-D) finite element model of the blade without hub or fillet and apply a rigid boundary condition at the blade-hub interface. The stresses nearest the hub are normally the largest. For this reason it is important to know what influence the absence of the hub and fillet have on the predicted stresses.

One approach to this problem is to perform a full 3-D finite element analysis of the blade, hub and fillet, a costly and time consuming computational effort. An alternate approach, used at the David Taylor Naval Ship Research and Development Center (DTNSRDC), is to perform a 3-D finite element analysis of the clamped blade model (i.e., without hub or fillet) and apply the computed displacements as a boundary condition for a two-dimensional (2-D) plane strain model of the blade with hub and fillet. This paper takes the DTNSRDC approach to investigate stress concentrations in the fillet region of a marine propeller blade.

ELEMENT SELECTION

The first step in the finite element analysis is to choose appropriate elements from NASTRAN's element library (ref. 1,2). The 20-node hexahedron, CIHEX2, is the obvious choice for the 3-D portion of the analysis. For the 2-D plane strain analysis, the 6-noded and 3-noded triangular plate elements, CTRIM6 and CTRIA2 respectively, were selected as probable candidates because of the ease with which triangular elements can be meshed to irregular geometries.

† This work was supported by the Naval Sea Systems Command (NAVSEA 63R5).

The formulation of the triangular plate elements in NASTRAN is based on the assumption of 'plane stress'. A 'plane strain' solution can be obtained however, by modifying the elasticity coefficients as described by Schaeffer (ref. 3). The validity of the plane strain modifications to NASTRAN is checked by comparing the stress predictions of the modified NASTRAN element with those of the ABAQUS plane strain element, CPE4 (ref. 4).

VERIFICATION OF ELEMENT ACCURACY

Success in performing numerical stress calculations by the finite element method depends on the choice of element and the layout of the element mesh. When properly formulated, the finite element solution should converge to the exact analytical solution if progressively finer meshes are used. For the circular hole and fillet geometries investigated in this paper, mesh size can be represented by the dimensionless ratio, l/r, where l is the length of an element (in the region of interest) and r is the radius of the circular hole or fillet. Laura, Reyes and Rossi (ref. 5) tried to assess the accuracy of the constant strain triangular element in regions of high stress concentration. Finite element predicted stress concentration factors were compared with photoelastically determined values at the boundary of a slot in a plate subjected to uniaxial stress. For element meshes with l/r equal to 0.13, the difference between numerical and experimental results was on the order of 10%.

In order to gauge the accuracy of the NASTRAN triangular elements for a given mesh size, comparisons are made between stress results obtained by the finite element method and those obtained by experimental or other analytical techniques. Two stress concentration cases are selected for the comparisons: (1) a flat rectangular plate with a small circular hole subjected to a uniform tension, σ , in the x-direction; and (2) a filleted bar subjected to in-plane bending. For the case of an infinite plate with a circular hole, Timoshenko (ref. 6) found that the stress in the x-direction is 3σ at the edge of the hole and quickly drops to σ away from the hole. For a finite plate with width no less than 4 times the hole diameter, Timoshenko found that the stresses produced should be within 6% of those produced in the infinite plate, that is, between 2.82σ and 3σ.

For the sake of comparison, a finite element analysis was performed on a flat square plate with the ratio of plate width to hole diameter of approximately 12 to 1. The applied stress is σ and the theoretical value of σ_x at the hole edge should be between 2.82σ and 3σ . Results for the NASTRAN CTRIA2 element are presented in table 1. Mesh fineness in the region of interest is represented in terms of the nondimensional ratio, l/r, where l is the length of an element and r is the radius of the circular hole. Table 1 shows that predicted stresses using the CTRIA2 element are within 6% of the theoretical value when mesh size values, l/r, of less than 40% are used. The CTRIM6 element yields surprisingly poor results. Nodal stresses at the edge of the hole range from 1.3σ to 4.3σ for very fine meshes (l/r less than 30%). Averaged nodal stresses yield better results; however, due to the disparity in nodal stresses from contributing elements, there is little confidence in the CTRIM6 predictions. This element is given no further consideration.

Hartman and Leven (ref. 7) used photoelastic techniques to determine stress concentrations in filleted bars subjected to in-plane bending as illustrated in figure 1. Stress concentrations of 1.2 to 3.0 were obtained for r/d values ranging from 0.03 to 0.50, where r is the fillet radius and d is the depth of the bar. The stress concentration factor, k, is defined as the ratio of the maximum stress at the fillet to the nominal stress computed by the flexure formula: $\sigma_{nom} = Mc/I$, where $c = d/2$, I = area moment of inertia and M = applied bending moment. Table 2 presents NASTRAN CTRIA2 stress predictions in the fillet region of a flat bar identical to one tested by Hartman and Leven. For this particular case ($r/d = 0.2$),

Hartman and Leven determined the stress concentration to be k = 1.53. The NASTRAN predicted k value of 1.58 presented in table 2 is in excellent agreement with this, differing by only 3.3% from the experimentally determined value.

THE 3-D DISPLACEMENT FIELD AS A BOUNDARY CONDITION

The 2-D plane strain finite element analysis of the blade with hub and fillet is predicated on the hypothesis that the displacement field predicted by the 3-D finite element model can be applied as a boundary condition to the 2-D model. This technique, which is supported by unpublished numerical experiments, is illustrated by the case of a thick plate in bending. A thick rectangular plate lying in the x-z plane is subjected to out-of-plane bending by the application of a moment along one edge while the opposite edge is fixed; that is, the plate is cantilevered and a moment applied to the free end as illustrated in figure 2. Using sixteen CIHEX2 isoparametric brick elements, a 3-D finite element model is constructed and solved for displacements and stresses. A 2-D model in the x-y plane is created using CTRIA2 elements. Displacements computed by the 3-D model at nodes 5 through 7 are applied as a displacement boundary condition to the corresponding nodes in the 2-D model. Stresses are then computed using the 2-D model. Table 3 presents stress predictions from both models at nodes 1, 2, 3 and 4 along the top surface of the plate. With the exception of node 1 located on the rigid boundary, stress predictions from the two models differ by less than 2%. Similar results are obtained for the bottom surface of the plate. Since the 3-D model composed of isoparametric brick elements can be expected to yield reasonable stress predictions at locations away from the boundary, these results support the assertion that the 3-D displacement predictions can be applied as a boundary condition to the 2-D model in order to obtain reasonable stress predictions.

PROPELLER MODELS

A 3-D and 2-D finite element propeller blade model are constructed for the purpose of analyzing the stresses in the blade root region. The 3-D blade model without hub or fillet consists of 40 CIHEX2 brick elements and is presented in figure 3. Figure 4 shows a 2-D model of a blade, hub and fillet cross section composed of 243 CTRIA2 elements. Maximum stress is usually developed at the base of the blade in the midchord region. For this reason, the 2-D analysis is based on a planar slice through the blade, hub and fillet in the vicinity of the midchord. The plane of interest is illustrated in figure 3 by superposition of a 2-D model on the 3-D model. R is the propeller radius measured from the center of the hub. Nodes 1, 2 and 3, located at approximately 0.36R, correspond to nodal points on both the 3-D and 2-D finite element models. Hydrodynamic and centrifugal loads are applied to the 3-D finite element model in order to predict the displacements at nodes 1, 2 and 3. These displacements are then applied to corresponding nodes on the 2-D planar model as a displacement boundary condition, ensuring that all out-of-plane degrees-of-freedom are constrained.

Several 2-D plane strain propeller models are analyzed in order to investigate the sensitivity of root stresses to fillet radius. The propeller under consideration has a fillet of constant radius, r, which is approximately one half the blade thickness, d. Table 4 presents stress predictions from both NASTRAN and ABAQUS 2-D analyses of the blade with hub and fillet. The extremum stresses (those of greatest absolute value) are the compression stresses developed in the fillet on the low-pressure face of the blade (see figure 4). The stress values presented in the table vary less than 4% over a range in r/d values from 0.37 to 0.56. The 3-D NASTRAN analysis of the clamped blade without hub or fillet predicts a maximum

stress value within 3% of the 2-D NASTRAN predictions and within 4% of the 2-D ABAQUS prediction. This technique of combining the 2-D and 3-D finite element analyses to predict fillet stresses is predicated on the assumption that the plane strain condition exists in the region of the 2-D planar slice. It is reassuring to note that the 3-D analysis predicts out-of-plane displacements an order of magnitude smaller than the in-plane displacements. This result lends credence to the assumption of plane strain.

SUMMARY AND CONCLUSIONS

Parametric investigations were performed using several two-dimensional finite element formulations to determine their suitability for use in predicting root stresses in marine propellers. Comparisons were made of two NASTRAN elements, CTRIM6 and CTRIA2, wherein elasticity properties were modified to yield plane strain results. The accuracy of the elements was investigated by comparing stress results obtained by the finite element method with those obtained by experimental or analytical techniques for two stress concentration cases: (1) a flat rectangular plate with a small circular hole subjected to uniform tension, and (2) a filleted bar subjected to in-plane bending. For both cases, the CTRIA2 element was found to provide stress predictions within about 5% of the expected value (experimental or theoretical) so long as the mesh size parameter, l/r, did not exceed about l5%. Furthermore, it was discovered that when the CTRIM6 element was used, the solution did not appear to converge. The plane strain modification to the NASTRAN element was checked by comparison with the ABAQUS plane strain element, CPE4. NASTRAN and ABAQUS 2-D plane strain analyses were performed on a propeller model yielding stress predictions which differed by only a few percent.

A combined 2-D and 3-D analysis of a thick plate in bending demonstrated the validity of applying predicted displacements from the 3-D analysis as a displacement boundary condition to the 2-D model in order to predict stresses in the plate. This technique was then applied to the analysis of root stresses in a marine propeller blade. It was found that extremum stresses develop in the fillet on the compression face of the blade and that these stresses are rather insensitive to small changes in the fillet radius. Furthermore, it was demonstrated that there is no significant difference in the extremum stresses predicted by the 3-D clamped blade analysis and the 2-D blade-hub-fillet analysis. Although the close proximity of the fixed displacement boundary condition in the 3-D model may distort the stress field in the root region, it does not appear to adversely affect the prediction of extremum stress.

REFERENCES

1. The NASTRAN Users Manual, Vol. 1, NASA Scientific and Technical Information Office, Washington, D.C., June 1985.

2. The NASTRAN Theoretical Manual, NASA Scientific and Technical Information Office, Washington, D.C., Jan 1981.

3. Schaeffer, H.G., MSC/NASTRAN Primer: Static and Normal Modes Analysis, Wallace Press, Inc., Milford, New Hampshire, Jan. 1982, pp 271-272.

4. ABAQUS User's Manual, Hibbit, Karlsson and Sorensen, Inc., May 1984.

5. Laura P.A., Reyes J.A. and Rossi R.E., Numerical Experiments on the Determination of Stress Concentration Factors, Strain, vol. 10, no. 2, Apr. 1974, pp 58-63.

6. Timoshenko, S.P. and Goodier, J.N., Theory of Elasticity, 3rd ed., McGraw-Hill, New York 1970, pp 90-92.

7. Hartman, J.B. and Leven, M.M., Factors of Stress Concentration for the Bending Cases of Fillets in Flat Bars and Shafts with Central Enlarged Section, Proceedings of the Society for Experimental Stress Analysis, vol. 9, no. 1, 1951, pp 53-62.

TABLE 1. STRESS AT THE EDGE OF A SMALL CIRCULAR HOLE IN A SQUARE FLAT PLATE SUBJECTED TO TENSION σ, IN THE x-DIRECTION.

Mesh size l/r	Stress† σ_x	Percent difference from infinite plate value
0.64	2.42σ	19.3
0.36	2.86σ	4.7
0.26	2.84σ	5.3
0.22	2.86σ	4.7

† NASTRAN predictions using triangular plate element CTRIA2.

l = element length
r = radius of hole
σ = applied stress
σ_x = stress in x-direction at the centroid of an element located at edge of hole

TABLE 2. STRESS CONCENTRATION IN A FILLETED BAR SUBJECTED TO IN-PLANE BENDING.

Mesh size l/r	Stress Concentration † k	Percent difference from experimental value*
0.140	1.46	4.9
0.025	1.58	3.3

† NASTRAN predictions using triangular plate element CTRIA2.

l = element length
r = fillet radius
* Experimental value = 1.53 (see reference 7).

TABLE 3. PLATE STRESSES PREDICTED BY NASTRAN 2-D AND 3-D MODELS

Node Number	Model	Dimensionless Stress*	Percent Difference
1	3D	1.221	14.0
	2D	1.392	
2	3D	1.106	0.8
	2D	1.096	
3	3D	1.011	0.4
	2D	1.015	
4	3D	1.000	1.2
	2D	1.012	

* The major principal stress at node 4 predicted by the 3D analysis has a dimensionless stress value of 1.000. The other stress values listed in the table are major principal stresses presented in terms of the unit stress at node 4.

TABLE 4. EXTREMUM STRESS PREDICTIONS BASED ON 2-D PLANE STRAIN ANALYSES OF THE BLADE, HUB AND FILLET.

Finite Element Code	Element Type *	Number of Elements	Mesh Size l/r	Fillet Size r/d	Extremum Stress **
NASTRAN	CTRIA2	243	0.03	0.37	0.985
NASTRAN	CTRIA2	243	0.03	0.46	0.974
NASTRAN	CTRIA2	243	0.12	0.56	1.00
ABAQUS	CPE4	136	0.40	0.46	0.968

r = fillet radius
d = blade thickness at hub
l = element length in region of extremum stress

* CTRIA2 refers to the NASTRAN CTRIA2 element modified for plane strain. CPE4 refers to the ABAQUS plane strain quadrilateral element.

** The extremum stress predicted by the 3-D blade model has a dimensionless stress value of 1.0. The stresses listed in the table are presented in terms of this unit stress.

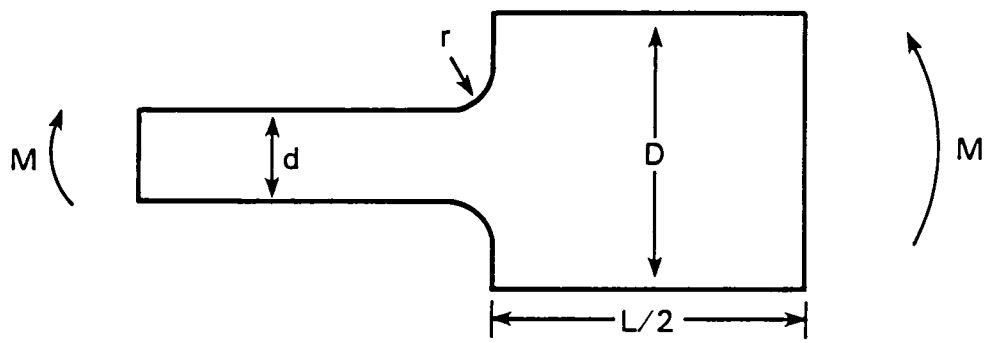

r/d = 0.2
L/D = 2
D/d = 3

K = 1.53 determined photoelastically by Hartman and Leven (ref. 7).

Figure 1. A filleted bar in a field of pure bending.

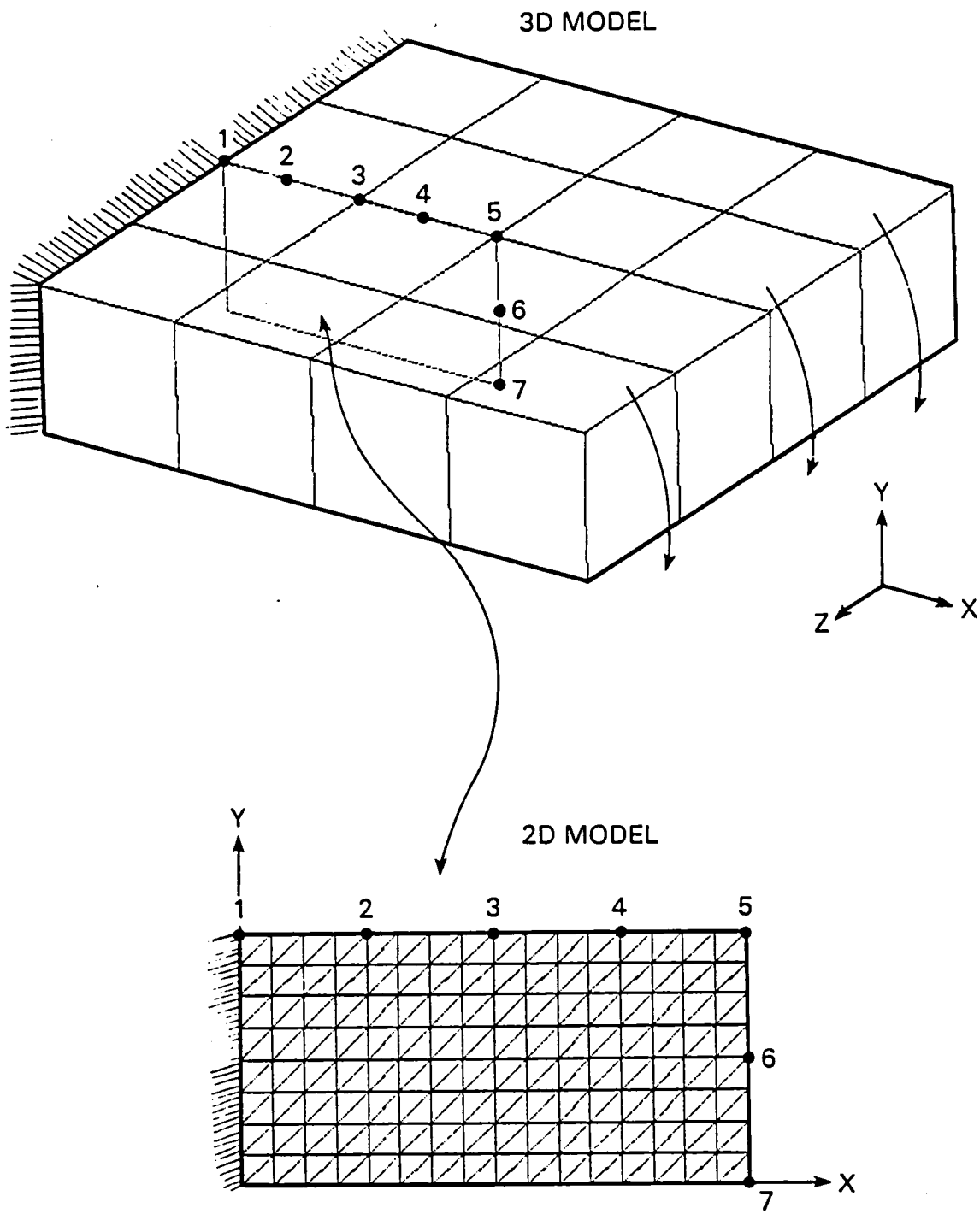

Figure 2. 3D and 2D thick-plate models.

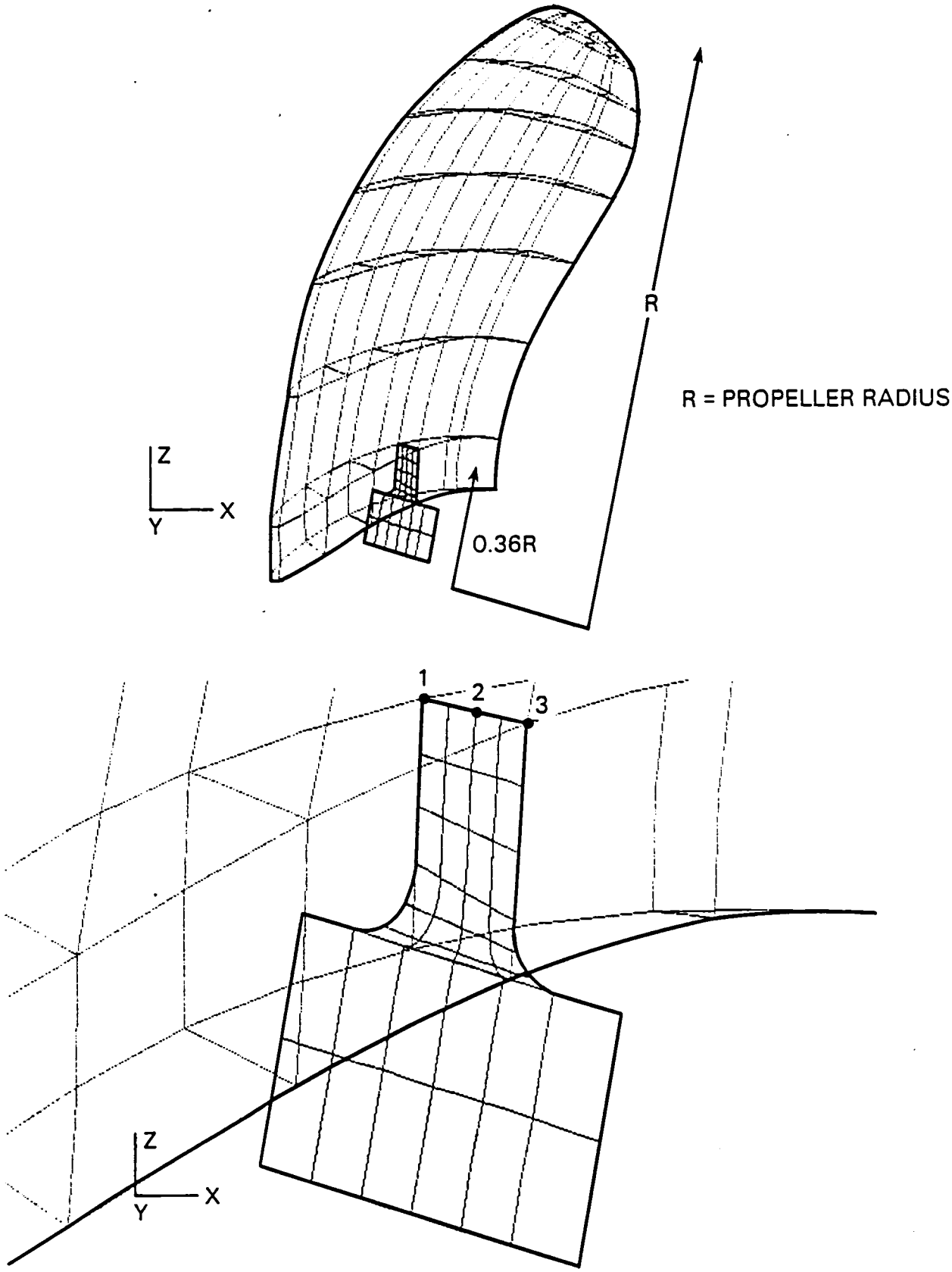

Figure 3. 2D blade, hub and fillet model superimposed on a 3D propeller blade model composed of 40 CIHEX2 elements.

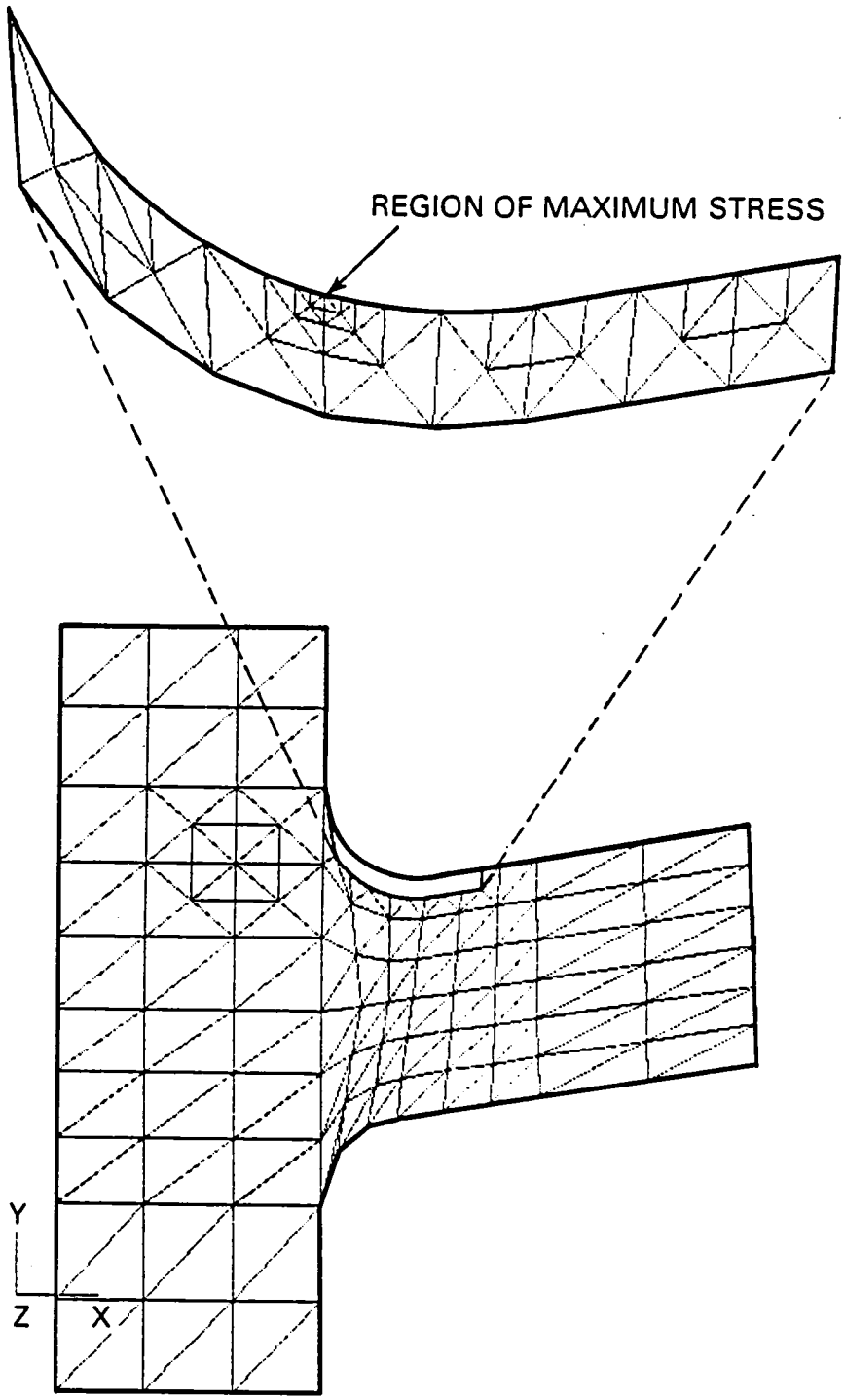

Figure 4. 2D Model of blade, hub and fillet showing detail of upper fillet. Model is composed of 243 CTRIA2 elements.

DIFFERENTIAL STIFFNESS EFFECTS

Ben H. Ujihara and Edward T. Tong
Space Transportation Systems Division
Rockwell International, Inc.

Differential stiffness as developed in NASTRAN is a linear change in stiffness caused by applied loads. Examples of differential stiffness are the stiffening effects of gravity forces in a pendulum, centrifugal forces in rotor blades, and pressure loading of shell structures. In cases wherein this stiffness caused by a load is destabilizing, the differential stiffness concept lends itself to nonlinear structural analysis. Rigid Formats 4 (static analysis with differential stiffness) and 13 (normal modes with differential stiffness) are specifically designed to account for such stiffness changes.

This paper clarifies how pressure loading may be treated in these rigid formats. This clarification resulted from modal correlation of ground vibration test (GVT) results for the empty and pressurized filament wound case (FWC) quarter-scale Space Shuttle solid rocket booster (QSSRB). A sketch of the QSSRB cantilevered to the floor by its external tank attachments is shown in Figure 1.

Correlation of GVT modal data with math model predictions for the FWC QSSRB showed frequency errors of 30 percent and 60 percent for fundamental pitch-roll and Z-bending modes (Table I).

To further isolate this discrepancy, a typical ring section of bars was extracted from the QSSRB model. Figure 2 is a sketch of this ring showing 2 of the 16 radial forces applied, representing discretized pressure forces obtained with the FORCE card.

Eigenvalues of this ring for unrestrained in-plane motion showed two zero frequencies for translation modes, and a rigid body rotational mode at a frequency that, instead of being zero, was nearly as high as the first elastic mode frequency. Examination of ring stiffness coefficients in cylindrical coordinates showed that although radial and rotational displacement coefficients were in balance, the tangential displacement coefficients had a moment unbalance equal to the radial force vector times the tangential displacement (for small displacements). Further, this restoring moment, converted to overall ring rotational stiffness, produced a rotational mode frequency matching the third eigenvalue.

Mathematical development of the differential stiffness concept is presented in the *NASTRAN Theoretical Manual.* Stated therein, externally applied loads, included in the computation of differential stiffness coefficients, are assumed to remain constant in magnitude and direction (CMD assumed). The limiting nature of this assumption is not always easily recognized. With hindsight, this rotational mode restoring moment is easy to predict by the CMD assumption, and is illustrated in Figure 3.

Clearly, if differential stiffness effects caused by pressure are to be modeled, representation by loading other than external forces are necessary. One such possible approach is the use of low stiffness rods with high initial strains, i.e., the rod stiffness should be low enough that overall structural characteristics remain unchanged. As a quantitative check, eigenvalues using Rigid Format 3 (normal modes without differential stiffness effects) for the structural configuration with and without the rods could be compared. The initial strains should be high enough that response displacements do not cause rod elastic forces to appreciably change the pressure preloads. Either DEFORM or TEMP cards could create these initial strains.

With some DMAP, a second possibility would be to store the computed differential stiffness matrix for recombination with nominal structure (without pressure rods) in a succeeding step. In the second approach, requirements for low stiffness and high strain would not exist.

Pressure rods used in a single cross section of the QSSRB and an overall view of all the rods are shown in Figure 4. An initial deformation of 50 radii was used for the radial rods. Contiguous rods along the body centerline provided the longitudinal pressure force. The common centerpoint of radial rods at each pressurized cross section also served as a joint in these longitudinal rods. Their total initial deformation was also 50 radii.

Frequencies obtained with these pressure rods are compared in Table II with those of Table I.

Based upon these results, PLOAD and FORCE cards used to apply pressure forces in Rigid Formats 4 and 13 will result in fictitious moment restraints. To circumvent this restriction, pressure forces may be regarded as a self-equilibrating system in the same way as forces arising from initial preload (DEFORM or TEMP card). For pressurized structures of arbitrary shape, the task of defining pressure rods along selected surface normals may not be easy. As a possible aid, MPC might be used to define a rigid platform of suitable shape from which pressure rods can be supported. Of course, this platform will remain in equilibrium if rod forces have been correctly applied. Further, depending upon magnitude of structural displacements, the condition of rod forces remaining normal to the surface may have to be addressed. The analysis would then be iterative.

Short of possible stiffness formulations at the element level, an automated treatment of pressure loading is needed to support the PLOAD and FORCE cards. Much of the needed capability, such as discretization of pressure forces, already exists. The automated definition of corresponding pressure rods, their properties, and initial strains is needed.

TABLE I.—INITIAL CANTILEVERED FWC QSSRB (EMPTY) FREQUENCIES (HZ) AT 500 PSI

Test	Pressure With PLOAD Card	Description
15.13	19.21	Pitch/roll mode
18.80	21.22	Y-bending
22.46	35.26	Z-bending
36.97	38.24	XY
49.61	50.04	
54.10	56.04	

TABLE II.—FINAL CANTILEVERED FWC QSSRB (EMPTY) FREQUENCIES (HZ) AT 500 PSI

Test	Pressure With PLOAD Card	Pressure With DEFORM Card	Description
15.13	19.21	14.94	Pitch/roll mode
18.80	21.22	18.53	Y-bending
22.46	35.26	22.16	Z-bending
36.97	38.24	37.55	XY
49.61	50.04	49.30	
54.10	56.04	53.90	

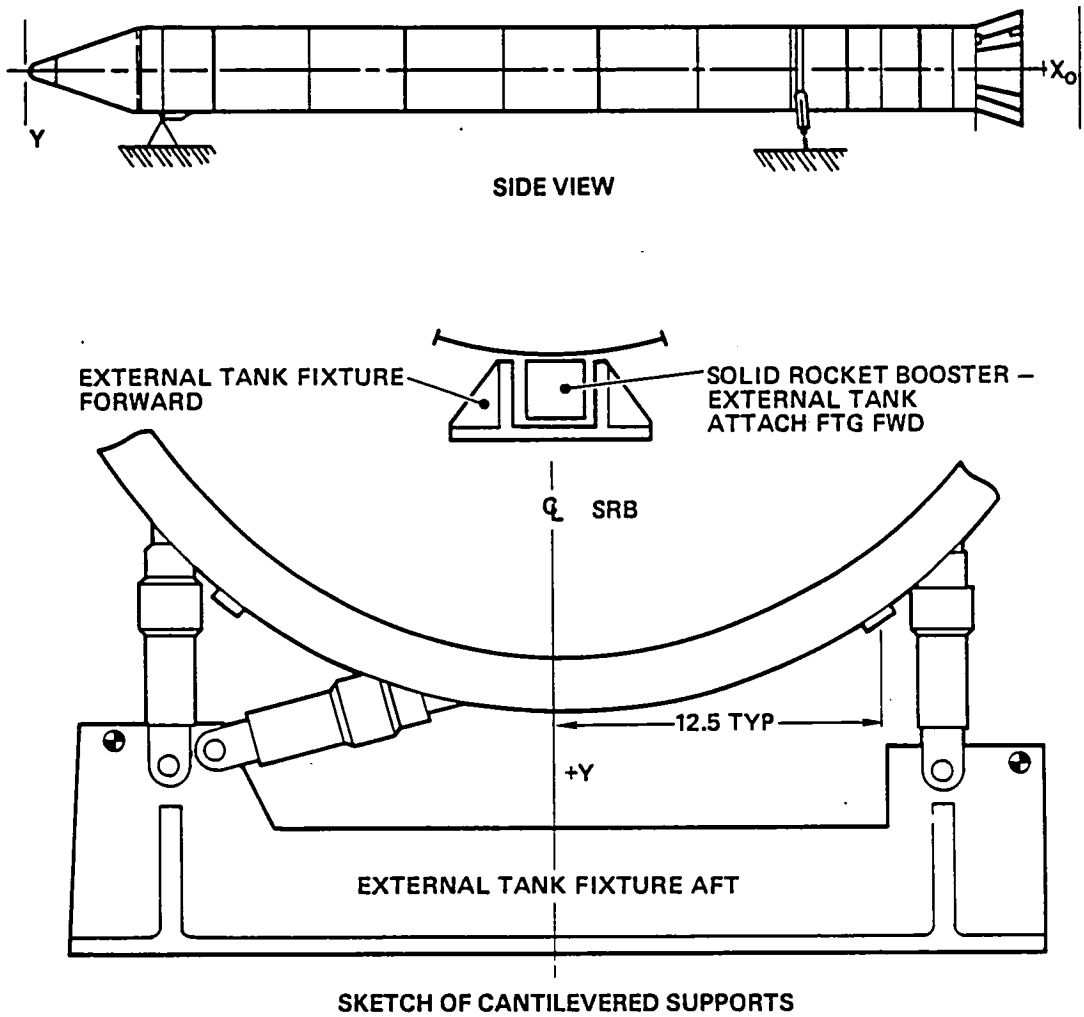

Fig. 1 QSSRB Cantilevered at External Tank Attachments

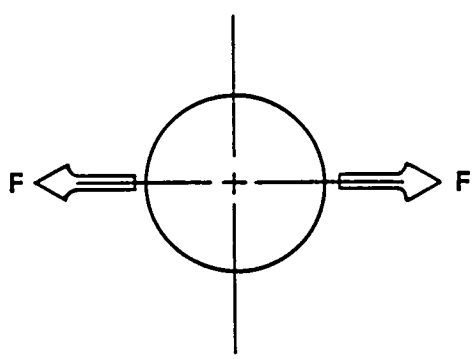

Fig. 2 Sketch of Pressurized Ring Showing 2 of 16 Discretized Pressure Forces

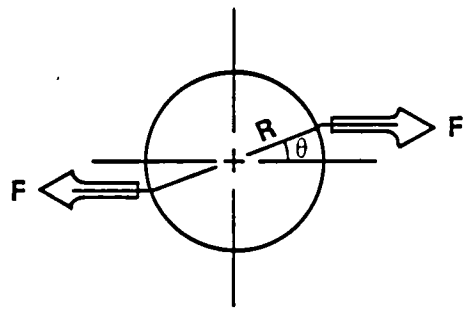

RESTORING MOMENT = 2RFθ

Fig. 3 Sketch of Pressurized Ring Showing Forces After Rotational Displacement

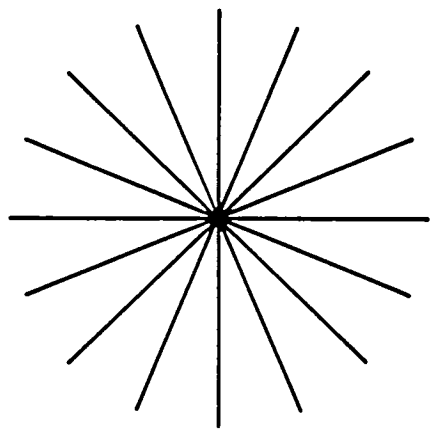

END VIEW

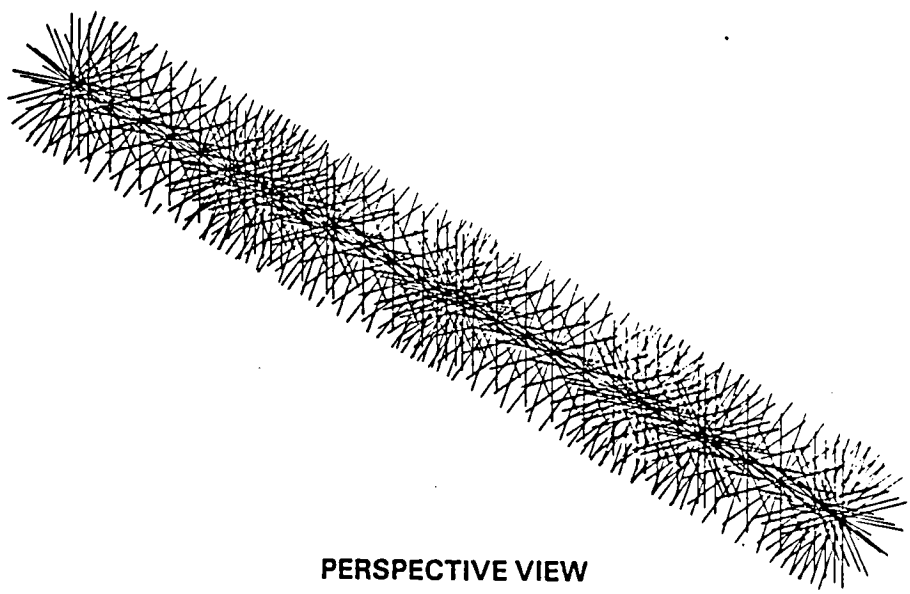

PERSPECTIVE VIEW

Fig. 4 Pressure Rods in QSSRB Model

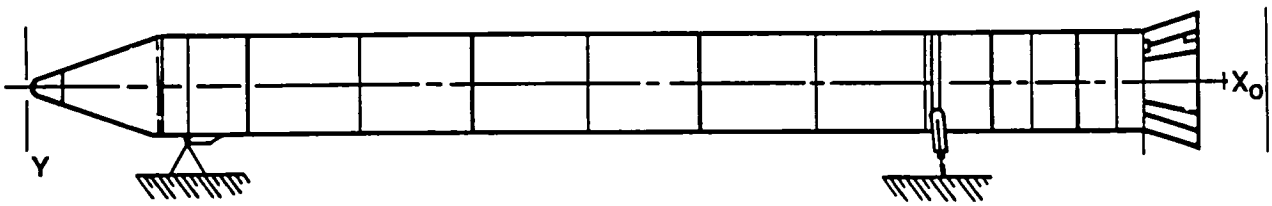

SIDE VIEW

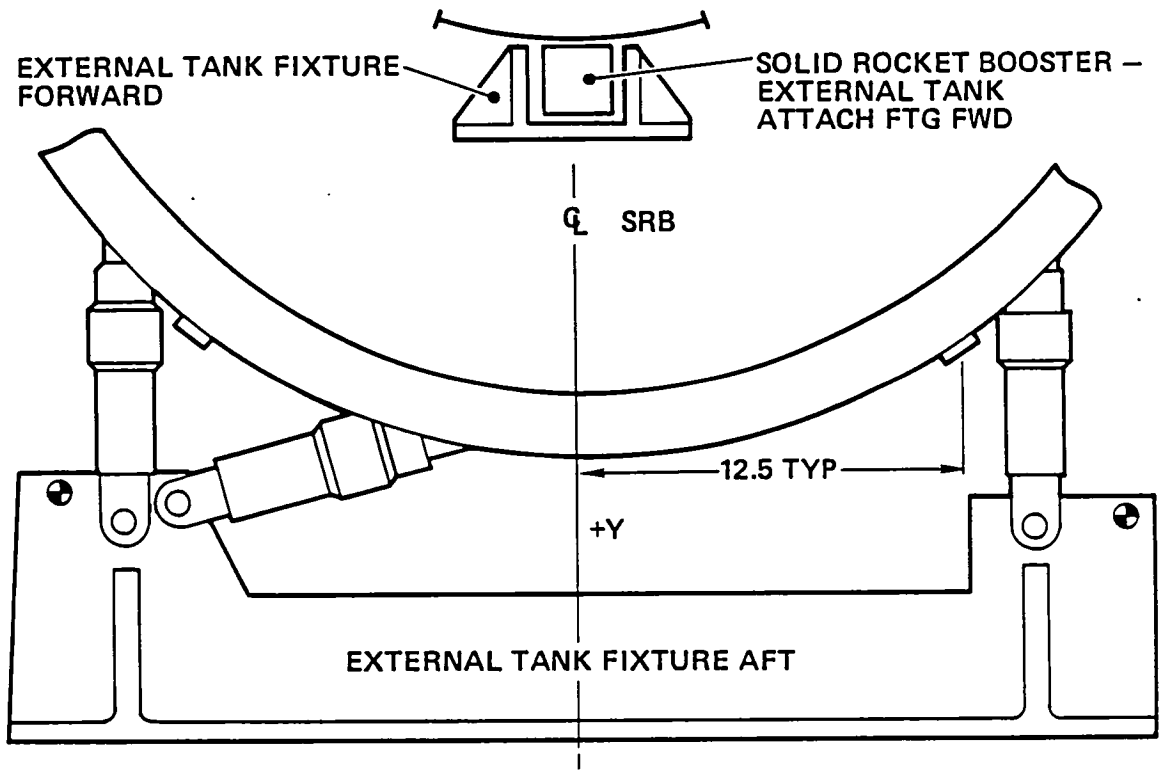

SKETCH OF CANTILEVERED SUPPORTS

Figure 1. QSSRB Cantilevered at External Tank Attachments

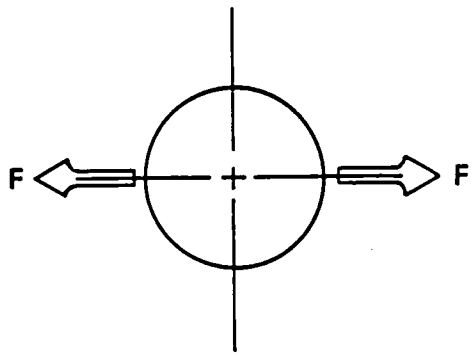

Figure 2. Sketch of Pressurized Ring Showing 2 of 16 Discretized Pressure Forces

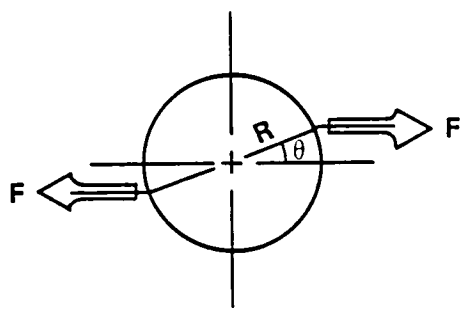

RESTORING MOMENT = 2RFΘ

Figure 3. Sketch of Pressurized Ring Showing Forces After Rotational Displacement

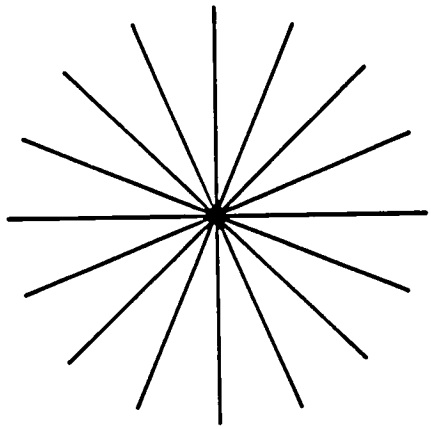

END VIEW

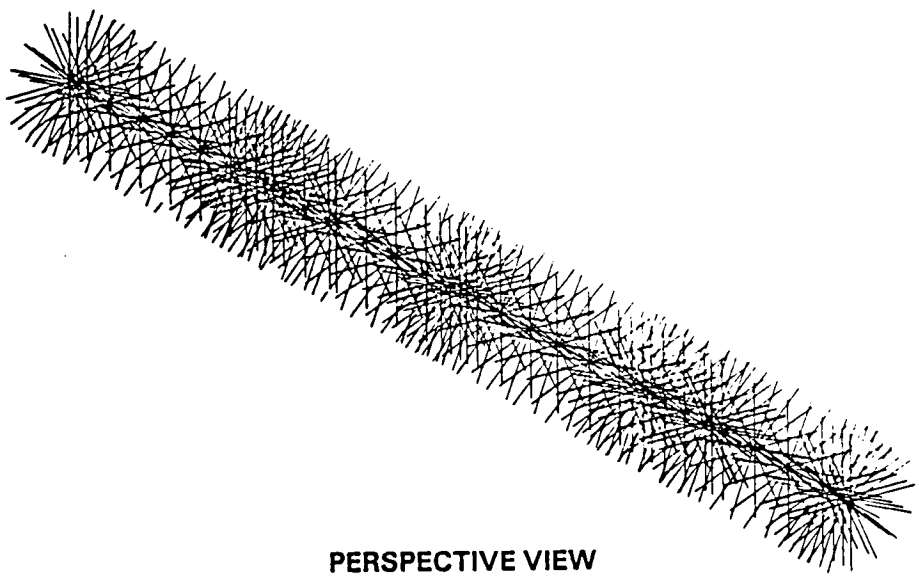

PERSPECTIVE VIEW

Figure 4. Pressure Rods in QSSRB Model

TEST VS ANALYSIS
A DISCUSSION OF METHODS

by

THOMAS G. BUTLER
BUTLER ANALYSES

INTRODUCTION

I write not as a sage with answers but as a confessor with questions. Exposure to this arena has left me with the impression that much needs to be learned about using existing methods, and we need to rely heavily on experience. Some techniques for comparing structural vibration data, determined from test and analysis are discussed. Orthogonality is a general category of one group, correlation is a second, synthesis is a third, and matrix improvement is a fourth. Advantages and short-comings of the methods are explored with suggestions as to how they can complement one another.

OBJECTIVE

The purpose for comparing vibration data from test and analysis for a given structure is to find out whether each is representing the dynamic properties of the structure in the same way. Specifically; whether

mode shapes are alike;
the frequencies of the modes are alike;
modes appear in the same frequency sequence;

and if they are not alike, how to judge which to believe.

PROCEDURE

The first task is to find out which modes from test correspond to ones from analysis. This is no trivial task over a spectral range for complex structures having hundreds or thousands of degrees of freedom. It is tempting to fall into the trap of declaring that two modes correspond when their frequencies are near to one another. It is however, absolutely necessary to determine correspondence based upon their mode shapes, first, and then see how close they are in frequency. The mere fact that their frequencies are not expected to be alike testifies to the notion that there must be variations between two companion mode shapes. The first problem then is learning to recognize likeness. Taking a simple open note of a violin string will illustrate how two eigenvectors may look different but represent the same mode.

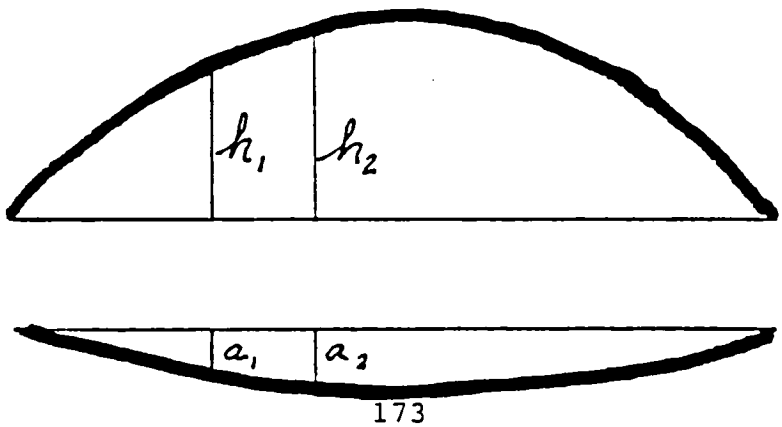

$$\frac{h_1}{h_2} = \frac{a_1}{a_2}$$

The amplitudes and the phase relationships at the instant of measurement are different, but they do represent the same mode; they will both have the same pitch (i.e. their frequencies are the same) but the top vector will sound louder than the bottom one. Extrapolating from this simple mode it is evident how necessary it is to agree on a set of rules as to how to compare modes.

This can be approached mathematically. The eigenvalue problem has one more unknown than equations, so an additional equation has to be supplied. A popular approach is to provide a scaling--that is arbitrarily declaring the magnitude of one displacement in the vector and then all other displacements in that vector will be scaled to this arbitrary value. This happens also in test, because one is free to select how much forcing to apply when exciting a mode. The problem in comparing results is to put the two sets of arbitrary amplitudes on a comparable footing. In analysis one usually sets one part to unity. This is called normalizing. One approach is to canvas a vector for its largest value and find the ratio of its trial value to 1.0 then scaling all other terms in the vector by the same ratio. Another approach is to isolate a reference point then set the trial value of its modal displacement there to unity followed by a like scaling of the rest. One that dynamicists often use is to scale a mode's generalized mass to unity; i.e. if the matrix product for the ith mode is

$$[\varphi_{si}]^T [M_{ss}] [\varphi_{si}] = k,$$

then scaling the ith vector by $\sqrt{k}$ will give the value 1.0 to this product. The net result is that every eigenvector has its individual scaling factor regardless of the method of normalizing. For comparing test with analysis pose the question, "Does the method of normalization have to be the same for both?" It will for some types of comparisons and others will have a built-in arbitrator so it might not.

Only rarely in a complex structure will a test mode match an analytical mode in every detail. There is a need to arbitrate as to when any two are comparable. One way, certainly, is to look at their plots and make a judgement as to whether they are similar enough. This doesn't quantify anything. Other ways are to compute certain properties and set ranges for such computed values as to their comparability. The next section will be devoted to various computations. The treatment will be organized according to first a discussion of the methods of making computations, then setting up a tabulation of (a) the operations that are entailed, (b) the utility of the computation for helping the analyst to make a judgement, and (c) the resources involved in the computation.

METHODS

Orthogonality Test-

Modes from test are multiplied into mass from analysis in the formula for generalized mass:

$$[\varphi_e]^T [M_a] [\varphi_e] = [G].$$

If the test vectors are normalized to the analytical mass then acceptability can be readily determined by comparing [G] with unity, [I]. It is usual that certain thresholds are assigned for acceptable departures from unity. This technique has been implemented by the author for NASTRAN and is described in reference (1). Raw test data is read from magnetic tape into a processor program called TAP2DMI to convert it into DMI bulk data format. The rest of the computation is done internally in NASTRAN by means of a DMAP ALTER packet. It normalizes the test vector to the analytical mass. Two different quantities are computed. The first is the matrix [G] shown above. The other will be discussed in the succeeding paragraph. The ALTER delivers [G] in standard MATPRN format. The diagonal of [G] will be unity because mass orthogonality forced it to be so, therefore the residue of off-diagonal terms constitutes the test. Ideally non-diagonal terms would be null. When g_{ij} $(i \neq j)$ are > a threshold, the test mode is declared to be mis-matched with the analytical model. It does not declare whether test or analysis is at fault, it just declares a mis-match. The value of the threshold is arbitrary. When a threshold is exceeded one needs to consult other data such as plots or correlation data to assess differences.

Cross-Orthogonality-

A product is formed from analytical mass, the matrix of mass normalized test vectors and, the matrix of mass normalized analytical modes.

$$[\phi_e]^T[M_a][\phi_a] = [H].$$

This is implemented in NASTRAN in the same DMAP ALTER packet of reference (1) that was mentioned above in the discussion of the orthogonality test. After the recovery of eigenvectors, $[\phi_a]$, the product of the first two matrices is multiplied into the analytical vectors to obtain [H]. Ideally [H] would be unity. Two criteria are used for acceptability; (a) diagonal terms h_{ii} should lie within a band of unity, i.e. $1-v < h_{ii} < 1+v$, and (b) off-diagonal terms should be less than a threshold c; i.e. $h_{ij} < c$ $(i \neq j)$. Failing either of these tests, classifies the test data as mis-matched with respect to analysis data. Once again plots and correlation are helpful in visualizing these differences.

Critique of Orthogonality and Cross-Orthogonality Tests-

Analysis can be condensed to test degrees of freedom in order to produce a mass matrix for normalization that is commensurable with the test vectors. Condensation to only instrumented points could be contrary to good dynamics practice, because points are chosen for measurement in test primarily on the basis of accessibility or on the expectation of being near antinodes, while the needs of analysis are to condense to significant mass locations to preserve kinetic energy. In using NASTRAN without a DMAP ALTER there is no alternative but to select the A-set based on instrumented locations only. If, however, a rational dynamic approach is taken to condensation which includes all instrumented points as a subset, then it would be possible to obtain reliable eigenvectors for the structure based on a generous

number of degrees of freedom. I came upon this idea only while writing this paper, so the idea is only sketched out and has not been checked. The scheme is this. Subsequent to the eigenvalue analysis the eigenvectors could be partitoned down from a reliably implemented eigenvalue analysis to the instrumented set as opposed to a condensation down to the instrumented set. In addition a second Guyan reduction from A-size to I-size (instrumented set size) could be performed using DMAP for partitioning the A-sized stiffness and mass into e-set (for elimination) and i-set (for instrumented) then calculating the $[K_{ee}]$ decomposition in preparation for determining the $[G_e]$ matrix from $[K_{ee}][G_e] = -[K_{ei}]$. Then the second Guyan reduction could be performed from the equation

$$[M_{ii}] = [\bar{M}_{ii}] + [G_e]^T[M_{ei}] + [M_{ei}]^T[G_e] + [G_e]^T[M_{ee}][G_e].$$

The partitioned PHII would need renormalizing with the $[M_{ii}]$ matrix. There is still some question as to how violent an effect this second Guyan reduction would have on the mass matrix; therefore it would be prudent to do an additional orthogonality check on just the analytical I-sized set. If this is acceptable, the I-sized mass matrix is ready to be used to normalize the test vectors and proceed with the orthogonality test. If the I-sized analytical set does not pass the orthogonality check, the I-sized mass matrix condensation should be modified until it does pass the analytical check before applying it to the test vectors. If no satisfactory condensation is achieved, then there should be a renegotiation of the test plan to include instumentation at some necessary mass locations to achieve compatibility between test and analysis.

Test data is not compromised (assuming modes are properly excited) by a relocation of instrumentation unless pick-ups are located too close to node lines. If the test structure is well instrumented and well excited and well mounted, the modal data represents the true vibration properties of the test article. (Aside--this does not imply that the test article necessarily represents the structure as designed.) Normalization of test data with a normalizing factor originating from analysis does not in any way prejudice the test data because each factor is distinct and arbitrary, regardless of origin, so the modal properties are preserved.

The two orthogonality tests diagnose all modes at once with a net result regarding the modes as a whole without any details within the modes. It provides no insight as to which source to suspect if there is a mismatch.

Correlation-

Since in a correlation computation, mode shapes are compared over their entire region with products, point by point - between the two sources, then averaged; a detailed examination is obtained and characterized by a single number. Correlation coefficients computing to 1.0 are exact. Comparable modes can be identified by the high value of their coefficients, and their frequencies can subsequently

be compared. Only shape data are considered, so no mass or stiffness data get involved explicitly. Theory behind the computation of correlation and the strategy for the algorithms was developed by personnel at Goddard Space Flight Center and was published in reference (2). The implementation of this technique was done at Goddard. Documentation of its application to a structure is explained in reference (3). The definition of the correlation coefficient copied from reference (3) is

$$r_{ab} = \frac{s_{ab}}{s_a \cdot s_b} \qquad \text{where,}$$

$$s_{ab} = (1/n)\sum_{i=1}^{n}(a_i-\bar{a})(b_i-\bar{b})$$

is the covariance between mode a and mode b having n degrees of freedom to define the mode shapes, and s_a or s_b are standard deviations which can be obtained by taking the square root of the variance, where the variance is

$$s_x^2 = (1/n)\sum_{i=1}^{n}(x_i - \bar{x})^2 \qquad \text{and} \qquad \bar{x} = (1/n)\sum_{i=1}^{n} x_i$$

is the mean value of a mode.

Differences-

As an auxilliary to correlation to find out where and by how much two sources differ, all points can be scouted in pairs by two methods as defined on pages 2-2 and 2-3 of reference (3) and repeated here.

(a) Relative Difference of the ith dof

$$rd_i = \frac{a_i}{s_a} - \frac{b_i}{s_b} \quad , \qquad \text{or}$$

(b) Scaled Difference of the ith dof

$$D_i = (Ca_i - b_i)/S \quad , \qquad \text{where}$$

$$C = \frac{\sum_{i=1}^{n} a_i\, b_i}{\sum_{i=1}^{n} a_i^2} \quad , \qquad \text{and}$$

$$S^2 = (1/n)\left(\sum_{i=1}^{n} b_i^2 - C^2 \sum_{i=1}^{n} a_i^2\right)$$

Critique of Correlation-

Correlation is done as a short-running post processor outside of NASTRAN, but depends on a DMAP ALTER from NASTRAN before it can execute. Full analytical fidelity of modes is preserved by first computing detailed modes before partitioning to instrumented points. Many more analytical modes than test modes may be involved if desired. No scaling of modes is required ahead of computing correlation because the formulas contain self-scaling by their own standard deviations.

The correlation coefficient can give evidence as to which modes are distinct and which have multiple similarities. Point by point comparisons are made. Data is sorted by user prescribed thresholds so the pertinent information is at hand without clutter. Localized evidence of differences allows the analyst to examine a point with respect to G-sized modes to see what structural factors could contribute to local disparities.

Correlation involves only displacement information and does not involve stiffness or mass, but since localized information is given over many anlytical modes, inferences can be drawn from such data as to the type of involvement.

The scaling coefficient C brings unscaled sources within the same average amplitude. The standard error scaling results in magnification of terms and allows separation of coefficients as they near unity.

Synthesis-

Since a large number of analytical modes are usually available and since they constitute an orthogonal set, they can logically be used as a basis for synthesizing test data in analytical terms thus avoiding the difficulties involved in scaling. This method was published by a team from Rockwell International in reference (4).

Expand the observed displacement y_i^k in mode k at instrumented location i in n analytical modes φ_{ij} that have been determined from a large set of points, but have been partitioned down to just the instrumented points. Y_i^k is the approximated expansion.

$$Y_i^k = \sum_{j=1}^{n} \varphi_{ij}\, b_j \quad \text{where } b_j\text{'s are unknown amplifiers.}$$

Sum the residuals over the m instrumented points i in the kth mode as

$$R^k = \sum_{i=1}^{m} (y_i^k - Y_i^k).$$

Rectify the residuals to develop an expression for the solution of b_j's.

$$RR^k = \sum_{i=1}^{m} (y_i^k - Y_i^k)^2.$$

Provide for the use of a weighting function such as: just the diagonals of the mass matrix, and substitute in the rectified residuals with the Y_i^k s expanded.

$$RR^k(M) = \sum_{i-1}^{m} M_i (y_i^k - \varphi_{i1} b_1^k - \varphi_{i2} b_2^k - \cdots\cdots - \varphi_{in} b_n^k)^2 .$$

Find the extremals of $RR^k(M)$ with respect to one b_j at a time.

$$\frac{1}{2}\frac{\partial RR^k(M)}{\partial b_j} = \sum_{i=1}^{m} M_i (-y_i^k \varphi_{ij} + \varphi_{ij}\varphi_{i1} b_1^k + \varphi_{ij}\varphi_{i2} b_2^k + \cdots\cdots + \varphi_{ij}^2 b_j^k +$$

$$\cdots\cdots + \varphi_{ij}\varphi_{in} b_n^k) = 0,$$

which when taken for all n b's compresses in matrix notation to

$$[\varphi_{ij}]^T [M_i][\varphi_{ij}]\{b_j^k\} = [\varphi_{ij}]^T [M_i]\{y_i^k\}.$$

Now $\{b_j^k\}$ can be solved for, because all else is known.

1. The b_j^k tell us how much of each of the n modes are going into simulating the kth test mode. Substitue b's into the original expansion to obtain the intended approximation Y_i's for every instrumented point of the kth test mode. Then construct R^k and $RR^k(M)$.

2. A simple mass weighted correlation coefficient differs from the Goddard one.

$$R_{kl} = \frac{\sum_{j=1}^{m} M_j (\varphi_{kj} - \bar{\varphi}_k)(\varphi_{lj} - \bar{\varphi}_l)}{\{[\sum_{j=1}^{m} M_j (\varphi_{kl} - \bar{\varphi}_k)^2][\sum_{j=1}^{m} M_j (\varphi_{lj} - \bar{\varphi}_l)^2]\}^{1/2}}$$

   where the φ's can be either analytical or test modes.

3. Multiple correlation coefficient in the kth mode of approximated vector to test vector. This has no corrolary with the Goddard approach.

$$R_k^2 = \sum_{j=1}^{m} M_j (Y_j^k - \bar{y}^k)^2 \Big/ \sum_{j=1}^{m} M_j (y_j^k - \bar{y}^k)^2$$

4. Compute the standard error S^k and use it to scale modal amplitudes b.

$$S^k = \{ \sum_{j=1}^{m} M_j (Y_j^k - y_j^k)^2 \}^{1/2}$$

$$T^k = b_j^k / S^k.$$

5. Compute spread of amplitudes over sampling points for an analytical mode W_i and the similar spread for the test mode W_j. Determine their relative influence

$$X(I) = \frac{b_i W_i}{W_j} .$$

6. Orthogonality with synthesized modes. First construct a matrix of all k of the synthesized modes.

$$[Y_{ik}] = [\phi_{ij}][b_{jk}].$$

$$[G] = [Y_{ik}]^T [M_{ii}][Y_{ik}] = [b_{jk}]^T [\phi_{ij}]^T [M_{ii}][\phi_{ij}][b_{jk}]$$

but since the analytical modes were normalized to mass this test reduces to

$$[G] = [b_{jk}]^T [I][b_{jk}].$$

This synthesized [G] can be compared to [I] as to how well analysis compares with test both in diagonal and off-diagonal terms.

Critique of Synthesis-

This is by far the most complete and most versatile of available codes for making comparisons. It would be worth the investment of purchasing the DUMMOD from Cosmic and spending time to sysgen it into one's NASTRAN executable. It operates entirely within a NASTRAN execution. Two kinds of local behavior are reported -- how much an analytical mode is participating in a test mode, and how much an approximation misses its test counterpart. Local behavior is further focused by the T value and the relative influence X(I). The simple correlation is quite similar to the Goddard one except its scaling, but it has the added advantage of diagnosing analysis alone. The multiple correlation is unique in that it gives well magnified measures for one mode at a time. Its generalized mass is more versatile than the usual orthogonality or cross-orthogonality tests and it is more efficient.

Matrix Improvement-

The premise in this technique is that test data has been certified, but analysis doesn't match. Analytical stiffness and mass matrices Kcomputed and Mcomputed are are assumed to be not too divergent but do need improvement. A method of applying incremental values to the analytical matrices was developed at Kaman Aircraft according to reference (5).

Given: Φ_T & Ω^2_T from test data and K_c & M_c from analysis, where c > T dof's.

Objective: Apply corrections to K_c & M_c to arrive at synthesized K_s & M_s.

Develop mass corrections first under these constraints:

$$[\Phi_s]^T[M_s][\Phi_s] = [I] \qquad \text{and} \qquad [K_s][\Phi_s] = [M_s][\Phi_s][\Omega^2_T]$$

Step 1. Expand $[\Phi_T]$ to c-size by setting up the eigenvalue equation in c-size for just one frequency at a time and partition it between test size and oversize = complement of c with respect to t.

$$\left[\begin{bmatrix} K_{tt} & K_{to} \\ K_{ot} & K_{oo} \end{bmatrix} - \omega_i^2 \begin{bmatrix} M_{tt} & M_{to} \\ M_{ot} & M_{oo} \end{bmatrix} \right] \begin{Bmatrix} \varphi_{Ti} \\ \varphi_{oi} \end{Bmatrix} = 0$$

Solve for the remnants of $\{\Phi_s\}$ mode by mode from

$$\{\varphi_{oi}\} = -[K_{oo} - \omega_i^2 M_{oo}]^{-1} [K_{to}^T - \omega_i^2 M_{to}^T]\{\varphi_{Ti}\}$$

Step 2. Find correction to $[M_c]$ by minimizing differences of $[M_c - M_s]$ while enforcing orthogonality. The resulting expresssion is based on approximating the correction for diagonal terms.

$$\epsilon = \| [M_c]^{-\frac{1}{2}} [M_s - M_c][M_c]^{-\frac{1}{2}} \| .$$

Set up equations in La Granqian multipliers

$$\Psi = \epsilon + \sum_{i=1}^{m}\sum_{j=1}^{m} \lambda_{ij} [\Phi_s^T M_s \Phi_s - I]_{ij}$$

Differentiate with respect to elements of unknowns $[M_s]$ and set to zero then solve for values of λ_{ij} which minimize ϵ. The resulting equation is

$$[M_s] = [M_c] + [M_c][\Phi_s][m_c]^{-1} [I - m_c][m_c]^{-1} [\Phi_s M_c] ,$$

where $[m_c] = [\Phi_s]^T[M_c][\Phi_s]$.

Step 3. Find correction to $[K_c]$ by applying the constraint equations to develop $[K_s]$.

$$[K_s][\Phi_s] - [M_s][\Phi_s][\Omega^2_T] = 0$$

$$[\Phi_s]^T[K_s][\Phi_s] - [\Omega^2_T] = 0$$

$$[K_s] - [K_s]^T = 0.$$

The resulting quantity to be minimized is

$$\epsilon = \| [M_S]^{-\frac{1}{2}} [K_S - K_C][M_S]^{-\frac{1}{2}} \|$$

Set up three sets of La Grangian multipliers for each of the three constraints. The result is

$$\psi = \epsilon + \sum_{i=1}^{n}\sum_{j=1}^{m} \Lambda_{K_{ij}} [K_S \Phi_S - M_S \Phi_S \Omega_T^2]_{ij}$$

$$+ \sum_{i=1}^{m}\sum_{j=1}^{m} \Lambda_{O_{ij}} [\Phi_S]^T [K_S][\Phi_S] - \Omega_T^2] + \sum_{i=1}^{n}\sum_{j=1}^{n} \Lambda_{S_{ij}} [K_S - K_S^T]_{ij}$$

Differentiating and setting the result to zero produces

$$[K_S] = [K_C] + [\Delta + \Delta^T] \quad \text{where}$$

$$[\Delta] = 1/2\ [M_S \Phi_S [\Phi_S^T K_C \Phi_S + \Omega_T^2] \Phi_S^T M_S - K_C \Phi_S \Phi_S^T M_S].$$

The resulting synthesized $[M_S]$ and $[K_S]$ satisfy all constraints and the increments in change can be tabulated element by element with respect to the original computed $[M_C]$ and $[K_C]$.

Critique of Matrix Improvement-

If the only object were to provide a systems analyst with a matrix that could act for a given component structure for the dynamic behavior of a total complex, this method would have good applications. Many times the need is for more than providing a surrogate, but to provide corrections to an existing model such that the resulting improved model will properly predict stresses and internal load paths and deformation behavior in the data recovery process after the results of the systems response is obtained. The interpretation of the incremental changes to the physical model is sometimes impossible, so that in spite of having an improvement it will not serve as a physical guide to model correction. With my limited experience in this area the one suggestion that I might make is to impose a further constraint on the admissable terms for applying the corrections. Null terms of $[K_C]$ and $[M_C]$ should be forced to remain null. I found extensive coupling in the $[K_S]$ and $[M_S]$ terms that defied physical justification. I also feel that this technique is workable during the very early stages of comparative analysis. For instance, it might be applied to the mass only and be tested for physical meaning so that possibly by increments it would act as a guide.

The following is a tabulation of the items described above giving a precis of the operation involved, its utility and its demand for resources.

OPERATION	UTILITY	RESOURCES
Orthogonality	Gives net modal check on test modes or analysis mass by severity in a single simple test.	Preprocess test vectors, into DMI format, then calculation is by DMAP ALTER. In public domain.
Cross-Orthogonality	Gives net modal checks on both test & analysis in a single simple test.	Continues with DMAP ALTER for 2 more steps. In public domain.
Cross-Correlation	Gives quantitative measures of net correspondence between test & analytical modes.	DMAP ALTER followed by a post processor program. Short running. In public domain.
Differences	Gives measures of isolated differences between test and analysis modes. Relates directly to actual positions in a model. Scaled differences give greater spread of results near unity.	An option of cross-correlation program. Short running.
Synthesis. Modal Amplifiers.	Gives measure of how much an analytical mode can behave like a test mode.	DUMMOD available from Cosmic. High memory requirements.
Synthesis. Residuals.	Can give individual also cumulative differences in shapes; test vs. analysis.	An option of synthesis.
Synthesis. Rectified Mass weighted residual	Gives magnified differences Weighting can help distinguish importances.	An option of synthesis. Part of another calculation so is neglible computer time.
Synthesis.Simple Correlation.	Single number to measure one mode with another. Helps evaluate analysis vs analysis; test vs analysis; and test vs test. Helps check self consistency of analytical model.	Correlates without averaging. DUMMOD must be sysgened into NASTRAN executable. The code is Cosmic catalog number (TU 1/80)
Synthesis. Multiple Correlation.	Single number measure one mode at a time. Gives greater spread near 1.0.	Relates to average test value of mode. Distinct differencing operations.

Synthesis. T value.	Gives greater focus of analytical similarity to test at individual points.	Scaling is fast after calculation of standard error function.
Synthesis. Relative Difference X(I)	Refined localized variation	It must canvas spreads overall instrumented points and all modes.
Synthesis. Generalized Mass	Gives equivalent of orthogonality test and cross-orthogonality test in a single matrix.	Quite direct and efficient.
Matrix Improvement. Dilated Test Vector.	Can be used for comparison with analytical mode to check on assumption of whether small changes can correct computed matrices.	Expensive Decomposition. Proprietary. Available only as service.
Matrix Improvement. Mass increments.	If Eqns 5, 6 & 7 were constrained to maintain null values, the lesser coupling might be easier to relate to model. Could be used in early liaison with test.	Simple multiplication.
Matrix Improvement. Stiffness increments.	Would be useful if a way were found to process new increments through data recovery modules so as to give direct connection to individual model elements.	Simple multiplication.

APPLICATION

These are the tools. Plots, Orthogonality, Cross-Orthogonality, Cross- Correlation, Differences, Relative Differences, Scaled Differences, Synthesized Modal Amplifiers, Residuals, Rectified Residuals, Simple Correlation, Multiple Correlation, T value, Relative Difference X(I), Generalized Mass, Improved Vector Dilation, Improved Mass, Improved Stiffness. How and what should be applied when?

The situation is usually this. Analysis has gone on for quite a while and a test plan has been drawn up during design development. So, frequencies, shapes, and plots of analytical eigenvectors are at hand. Test has been set up and liaison has established the set of corresponding instrument locations. The situation with respect to Orthogonality is this. Generally the analytical model has been condensed down to a logical A-set and not to the instrumented set. As soon as test liaison is established, the A-set should be modified to

include the complete set of instrumented freedoms as a sub-set. When this is done DMAP ALTER's should be considered for applying a second Guyan reduction for condensing the MAA matrix to MII size.

It makes good sense then to apply correlation as a first step after test results start to come in. DMAP ALTER packet, as defined in either TM 86081 or TM 86044, can conveniently be included in NASTRAN runs to create a TESET vector and to have modes partitioned to PHITE freedoms. This permits the identification of which analytical modes correspond to which test modes. It is a shock when correlation results are viewed for the first time. One has a stereotyped notion that there will be a few values in the .90 to .98 range and a cluster of values in the 0.0 to .08 range. The predominance of values in the .4 to .8 range takes one aback. The first impulse is to condemn correlation as being useless. It takes a fair amount of study to begin to realize the implications that are revealed by this plethora of data. Nothing is clear cut. Develop judgement as to relative magnitudes and remedies needed to home in on the anomolous parts of the model. If one analytical mode correlation coefficient $\lesssim 1.0$ and others are high, this can imply the one near unity is a match and the other modes with large coefficients (say > 0.4) have defects and should be flagged for location as to where model should be investigated. I have yet to talk to any structures man who considers himself to be an expert in assessing correlation results. One needs to develop experience by making interpretations; taking actions based on the initial interpretations; then revise the original interpretation by reacting to results produced by actions. I have never used synthesis, but I would expect that multiple correlation will help to isolate some effects. Test and analysis people should look over the correlation results together to see what is revealed. For instance, look for frequency disparities in the modes and check secondary correlation results for finding anomolous local involvements that might be corrected. Each discipline can then ask its own set of questions, such as

Analysis	Test
Are any moments of inertia wrong?	Is the structure being excited in
Do any joints need to be remodeled?	a poor place?
Is there a wrong exponent in a modulus of elasticity?	Are instruments reading in the right amplitude range?
Do any BAR elements have misplaced offsets?	Is the structure being supported improperly?
Are any of the modes spurious due to inadequate constraints?	Do pick-ups need to be remounted?
	Are any modes not being excited?

After test and analysis have applied remedies based on the first correlation results, another correlation check ought to be made based on analytical and test reruns. When all the obvious adjustments have been made after reruns, the orthogonality ALTER packet should be

included in a succeeding run in conjuction with a correlation process. If one uses orthogonality alone, information is too condensed to home in on discrepencies. With correlation, specific locations can be obtained for applying remedies. The two approaches can be included in a single run to take advantage of simultaneous data. Note should be made, immediately, as to whether a difference in correlation resulted from condensing the analytical model to the instumented points. If there is a great difference then no particular meaning can be gleaned from the orthogonality results. If the shift in correlation is acceptable, the orthogonality and cross-orthogonality results will show which modes are within threshold specification, and how far other modes are out of specification.

SUMMARY

Good tools for comparing vibration data from test and analysis are available in the public domain. The Goddard package is easy to get and quick to run. The Rockwell package is the best. It takes planning to get it operational. The Kaman service can be used as a guide or a position of last resort. In all cases, it takes much practice to use these tools well.

REFERENCES

(1) Internal OAO Report No. 4-85

(2) NASA Technical Memorandum 86081, "Statistical Correlation Analysis for Comparing Vibration Data from Test and Analysis", by T. G. Butler, R. F. Strang, L. R. Purves, and D. J. Hershfeld.

(3) NASA Technical Memorandum 86044, "Statistical Correlation of Structural Modes Shapes from Test Measurements and NASTRAN Analytical Values", by L. Purves, R. Strang, M. P. Dube, P. Alea, N. Ferragut, and D. Hershfeld.

(4) "LINWOOD as a NASTRAN Dummy Module for Modal Correlation with Test Data (A Least Squares Algorithm)", by B. H. Ujihara, R. J. Guyan, L. J. Van Hofwegen, and R. N. Heckenlaible, from the Proceedings of the First Chitauqua on Finite Element Modeling.

(5) "Improvement of a Large Analytical Model Using Test Data", by A. Berman and E. J. Nagy; AIAA Journal Volume 21, Number 8, Page 1168.

A COMPARISION OF NASTRAN (COSMIC) AND EXPERIMENTAL RESULTS FOR THE VIBRATION OF THICK OPEN CYLINDRICAL CANTILEVERED SHELLS*

Wayne L. Mindle+
Martin Marietta Orlando Aerospace

Peter J. Torvik°
Air Force Institute of Technology

SUMMARY

The natural frequencies and associated mode shapes for three thick open cantilevered cylindrical shells were determined both numerically and experimentally. The shells ranged in size from moderately to very thick with length to thickness ratios of 16, 8 and 5.6, the independent dimension being the shell thickness. The shell geometry is characterized by a circumferential angle of 142 degrees and a ratio of length to inner radii arc length near 1.0. The finite element analysis was performed using NASTRAN's (COSMIC) triangular plate bending element CTRIA2, which includes membrane effects. The experimental results were obtained through holographic interferometry which enables one to determine the resonant frequencies as well as mode shapes from photographs of time-averaged holograms.

In all, comparison between experimental and computational results were obtained for a total of 22 cases. In more than 77 percent of the cases the agreement was within 5 percent and for 45 percent of the cases within 2 percent. The largest percent error in frequency occured for all three shells in the first flexural mode, with 8.0, 18.8 and 20.1 percent errors with increasing thickness. There was also a 12.7 percent error in the second flexural mode for the thickest blade. In other cases, the differences between the computed and experimental results did not appear to be a result of changes in shell thickness. A contributing factor to the large error in the flexural modes is the difficulty in providing a true clamped end condition as the shell gets thicker, resulting in lower experimentally determined frequencies.

*Support for this work was provided by the Aero-Propulsion Laboratory, AFWAL/PO, Wright-Patterson Air Force Base.
+Joined Martin Marietta after completion of this work as a Post-Doctoral research Associate, Air Force Institute of Technology.
°Professor and Head, Dept. of Aeronautics and Astronautics.

INTRODUCTION

The free vibration frequencies and mode shapes were determined both numerically and experimentally for three thick open cylindrical cantilevered shells. The numerical results were computed using NASTRAN's (COSMIC) triangular plate bending element CTRIA2 which includes membrane effects. The experimental results were found using holographic interferometry. The shell dimensions are characterized by length to thickness ratios of 16, 8 and 5.6, with the independent dimensions being the shell thickness.

A review of the literature reveals no results for shells with the dimensional characteristics, ie. short, stubby, thick and nonshallow, of the ones considered in this study. However, the vibration characteristics of cantilevered shallow cylindrical shell segments has been addressed. Walker [1] developed a doubly curved right helicoidal shell finite element which he applied to several thin shallow shells. Gill and Ucmaklioglu [2] applied a three-dimensional isoparametric element to a curved fan blade. Their results were compared with experimental results as well as other finite element solutions. Leissa, Lee and Wang [3] used shallow shell theory and the Ritz Method to solve a range of cantilevered shell problems for a range of aspect, shallowness and thickness ratios. In a recent paper, Lee, Leissa and Wang [4] applied the procedure developed in [3] to the problem of cylindrical shell segments with chordwise taper.

A similar type of investigation was reported in a series of papers by MacBain, Kielb and Leissa [5,6]. Their study considered the vibration of twisted cantilever plates with rectangular planform. The characteristic dimensions for two of their cases are similar to those presented here. The theoretical results included 15 finite element, 2 shell theory and 2 beam theory solutions as well as 3-D elasticity solutions for 2 of the cases. The finite element results included solutions using the NASTRAN (COSMIC) CTRIA2 triangular plate element and the NASTRAN (MSC) CQUAD4 quadrilateral shell element.

EXPERIMENTAL INVESTIGATION

The three cylindrical shells chosen for this study were machined from 50.80 mm diameter steel rods of length 61.91 mm. The shells are only 25.40 mm in length, leaving the remaining portion of the rod to slide into the steel block as shown in Figure 1. The shells, labelled 1, 2 and 3, have the same inner radius of 11.43 mm and an arc length of 142 degrees with thicknesses of 1.59 mm, 3.18 mm and 4.57 mm, respectively. The holes shown on the base of the shell were drilled around the circumference of the cylindrical base at 90 degree intervals. Their

purpose being to seat setscrews used in mounting and to provide a consistent way of orienting the shells.

The excitation of the shells was accomplished with a piezoelectric shaker mounted to a steel block of dimensions 76.20 mm x 76.20 mm x 101.60 mm as shown in Figure 1. The block was secured to an optical table by four bolts, one at each corner of the block. A 50.8 mm diameter hole was bored through the top of the block to a sufficient depth to accomodate the base of each shell. Setscrews were then used to secure the shell in place. The total mass driven by the shaker was 232, 109 and 72 times the mass of the shells.

Real time holographic interferometry was used to find the resonant frequencies and mode shapes of the shells. Figure 2 shows the optical setup chosen for the investigation. A description of the procedure can be found in [7].

EXPERIMENTAL RESULTS

The search for the resonant mode shapes was accomplished with an accelerometer attached to the shells. This was done to insure that the observed response was at the first fundamental mode of the excitation, rather than at a harmonic component. Because the accelerometer introduces an added mass (0.35 grams), once the resonant frequencies were identified the accelerometer was removed and the shells retested. As expected, these final frequencies were slightly higher. The accelerometer caused no discernable changes in the mode shapes themselves.

Experimental results for the three shells without an accelerometer are presented in Figures 3-5 in the form of photographs of the time averaged holograms of the concave side of the shells. Resonant modes in the frequency range of 0 to 100 KHZ were sought, but were not found above 45 KHZ. The contour lines on the holographic images represent out-of-plane displacements. Which of the white areas are nodal lines or zones of zero displacement can be deduced from the fact that the lower edge is fixed. The magnitude of the displacement increases as fringes are crossed, moving away from a nodal line. The time averaged hologram does not distinguish between positive and negative displacements, although the relative direction can be determined by using the nodal lines to identify lines of zero displacement and noting that the displacement must have continuous derivatives across those lines.

Upon viewing the photographs of the shells, it is apparent that the far left interior portion of each shell is not visible. This is due to the curvature of the shells and the fact that it was not possible to position the object beam so that this area

could be illuminated. The photographs also indicate that the mode shapes are biased toward one side. Since the shells are symmetric about a vertical plane perpendicular to the plane of the paper, the modes should be totally symmetric or anti-symmetric. The reason that the modes are biased is most likely a slight asymmetry in the loading which can be attributed to imperfect clamping and/or misalignment of the shaker.

The first ten mode shapes for Shell 1, the thinnest of the shells, are presented in Figure 3. The frequency for each mode is also given in the figure. Among the ten modes are the first and second torsional modes (1T,2T) and the first flexural mode (1F). Modes at 10,973 HZ and 24,835 HZ represent chordwise bending. The mode at 22,770 HZ appears to be related to the first of these in that it has two veritcal nodal lines with the addition of a second horizontal nodal line. Modes at 24,835 HZ and 39,627 HZ are similarly related. The mode at 23,685 HZ represents an in-plane shear mode. The mode at 36,060 HZ defines a diaphragm type displacement and the mode at 44,300 HZ consists of many localized displacements along the free edges of the shell.

The six modes found for Shell 2 are presented in Figure 4. They include modes 1T, 1F, 2T, the two chordwise bending modes and an in-plane shear mode at 22,965 HZ. The meeting of the fringe pattern for the 1T mode at the line of symmetry means that the mode is not one of pure torsion. Some other component of displacement is also present. A rigid body rotation, caused by a slight looseness in clamping, is suggested. The fact that many less fringes were obtained for each mode of Shell 2 than for Shell 1 or Shell 3 suggests higher energy dissipation, as might be caused by slipping at a less than perfectly clamped end. The 1F mode might be expected to be especially vulnerable to a less than ideal end condition.

Figure 5 shows the six mode shapes found for Shell 3, the thickest of the shells. The observed modes include 1T, 2T, 1F, 2F, a symmetric chordwise bending mode, and an in-plane shear mode at 24,232 HZ. For this blade the lowest mode is the first flexural mode, whereas for the other two shells the fundamental mode was the first torsional. This is believed to be a consequence of the inability to create a completely clamped end. In this case the end may be well clamped, but clamped to a deforming object. This is the only blade for which the second flexural mode was seen.

NUMERICAL INVESTIGATION

A finite element analysis of the cylndrical shells was accomplished using NASTRAN's CTRIA2 element, which is a three

node triangular plate bending element that includes membrane effects. The element mesh, Figure 6, used to model Shell 1 consists of 24 and 21 nodes along the circumference and height, respectively. The mesh was refined for Shells 2 and 3 by increasing the number of nodes along the circumference to 26 and 27, respectively. All the eigenmodes should be symmetric or anti-symmetric since the shells are symmetric. However, because of the inherent asymmetry of the triangular elements, the mesh used in the analysis introduced a slight bias in the deformation pattern.

The mode shapes are presented in the form of contour plots of the out-of-plane displacement for comparison with the holographic results. Figures 7-9 show the mode shapes for the three shells. The bottom edges in the figures are the clamped ends.

A comparison of the computed and observed frequencies is given in Tables 1,2 and 3. The modes are listed sequentially according to the numerical results, with the experimental values placed by the corresponding mode shape. Note that all of the modes observed in the experiment were duplicated numerically. Also, the greatest difference in frequency occurs for the 1F modes. This is attributed to imperfect clamping of the shells in the experiments, giving rise to lower frequencies. This is most noticable for Shells 2 and 3, where the differences between computed and observed frequencies are around 20 percent. In general the agreement was very good. For Shells 1 and 2 the errors in the frequency for modes other than the first are all under 5 percent.

CONCLUDING REMARKS

The experimental procedure consisted of a test fixture which provided (approximately) a clamped end condition. The shells were excited by a small shaker exciting them in a direction perpendicular to the planform. The resonant frequencies and mode shapes were then determined using holographic interferometry.

The shells were modelled using NASTRAN's triangular plate bending element (CTRIA2) which includes membrane effects. The resulting mode shapes agree well with the mode shapes obtained by holographic means. The computed and measured frequencies were in very good aggreement, except for the flexural modes. This reflects the difficulty with experimentally providing a perfectly clamped boundary condition.

REFERENCES

1. K.P. Walker, "Vibrations of Cambered Helicoidal Fan Blades," J. Sound Vib., Vol. 59, No. 1, pp. 35-57 (1978).

2. P.A.T. Gill and M. Ucmaklioglu, "Isoparametric Finite Elements For Free Vibration Analysis of Shell Segments and Non-Axisymmetric Shells," J. Sound Vib., Vol. 65, No. 2, pp. 259-273 (1979).

3. A.W. Leissa, J.K. Lee and A.J. Wang, "Vibrations of Cantilevered Shallow Cylindrical Shells Having Rectangular Planform," J. Sound Vib., Vol. 78, No. 3, pp. 311-328 (1981).

4. J.K. Lee, A.W. Leissa and A.J. Wang, "Vibrations of Blades With Variable Thickness and Curvature by Shell Theory," J. of Engrg. For Gas Turbine and Power, Trans. ASME, Vol. 106, pp. 11-16 (1984).

5. J.C. MacBain, R.E. Kielb and A.W. Leissa, "Vibrations of Twisted Cantilevered Plates - Experimental Investigation," ASME Paper No. 84-GT-96 (1984).

6. R.E. Kielb, A.W. Leissa and J.C. MacBain, "Vibrations of Twisted Cantilever Plates - A Comparison of Theoretical Results," IJNME, Vol. 21, pp. 1365-1380 (1985).

7. W.L. Mindle, The Multiple Mode Phenomenon in the Vibration of Curved Cantilevered Blades, Air Force Institute of Technology, Report No. AFIT-TR-EN-85-5 (1985).

Table 1. Comparison of NASTRAN and Experimental Frequencies For Shell 1.

MODE NUMBER	FREQUENCY (HZ)		PERCENT ERROR
	NASTRAN	EXPERIMENT	
1	5,265	5,088	3.5
2	8,609	7,972	8.0
3	11,428	10,973	4.2
4	20,959	20,662	1.4
5	23,017	22,770	1.1
6	23,244	23,685	-1.9
7	25,257	24,835	1.7
8	37,827	36,060	4.9
9	39,892	39,627	0.7
10	45,693	44,300	3.1
11	47,060	------	---
12	48,420	------	---
13	50,922	------	---
14	56,797	------	---

Table 2. Comparison of NASTRAN and Experimental Frequencies For Shell 2.

MODE NUMBER	FREQUENCY (HZ)		PERCENT ERROR
	NASTRAN	EXPERIMENT	
1	7,799	7,948	-1.9
2	10,262	8,635	18.8
3	17,633	18,135	-2.8
4	23,644	22,965	3.0
5	31,466	30,414	3.5
6	35,497	------	---
7	41,331	41,227	0.3
8	45,020	------	---
9	50,950	------	---
10	56,636	------	---
11	62,520	------	---
12	72,007	------	---
13	73,613	------	---
14	77,978	------	---

Table 3. Comparison of NASTRAN and Experimental Frequencies For Shell 3.

MODE NUMBER	FREQUENCY (HZ)		PERCENT ERROR
	NASTRAN	EXPERIMENT	
1	9,963	9,909	0.5
2	11,207	9,330	20.1
3	22,363	22,694	-1.5
4	24,255	24,232	0.1
5	39,365	36,418	8.1
6	42,488	37,690	12.7
7	50,993	------	---
8	51,163	------	---
9	52,850	------	---
10	56,610	------	---
11	75,290	------	---

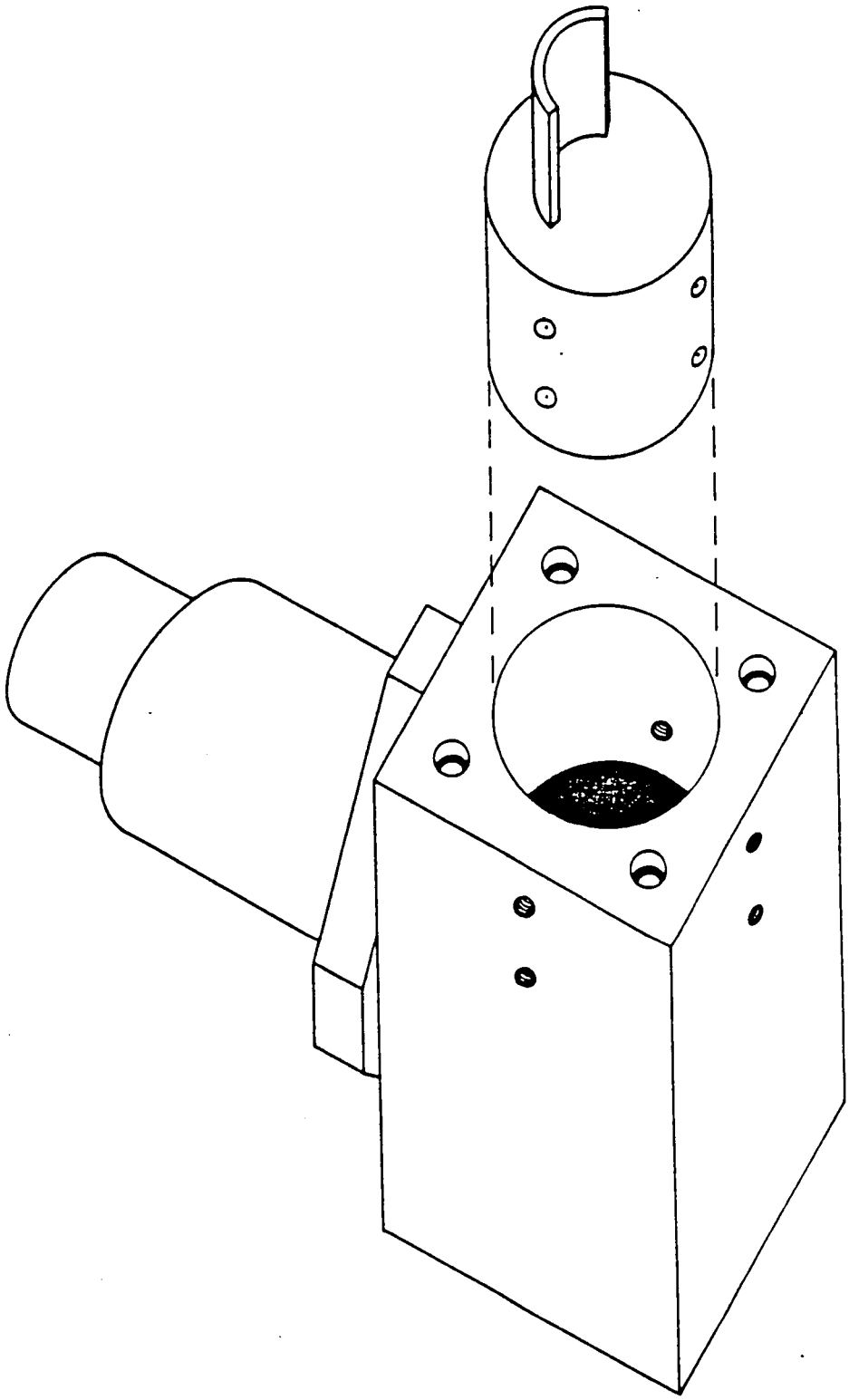

Figure 1. Vibration Test Fixture and Shell Assembly

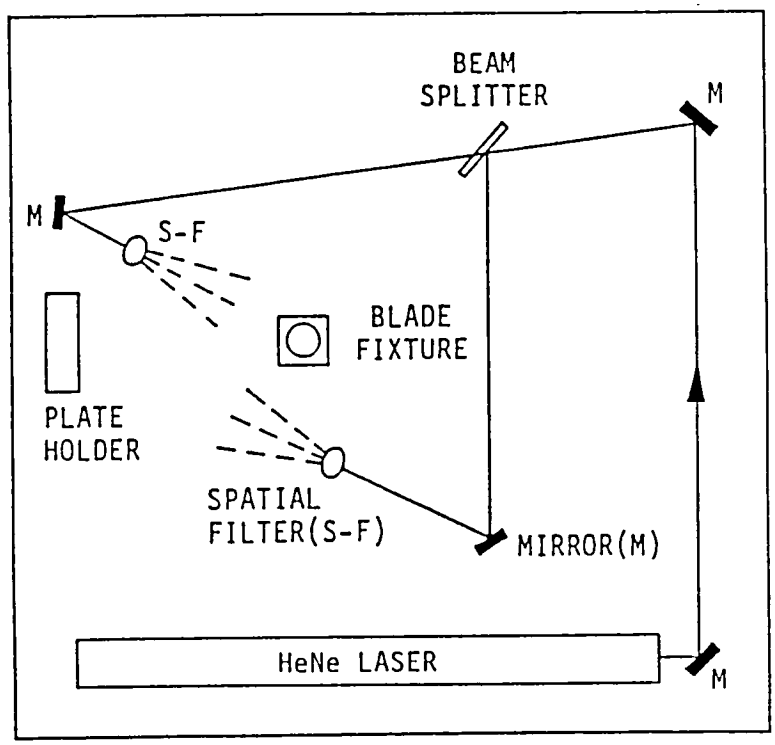

Figure 2. Optical Table Set-Up For Holographic Vibration Tests

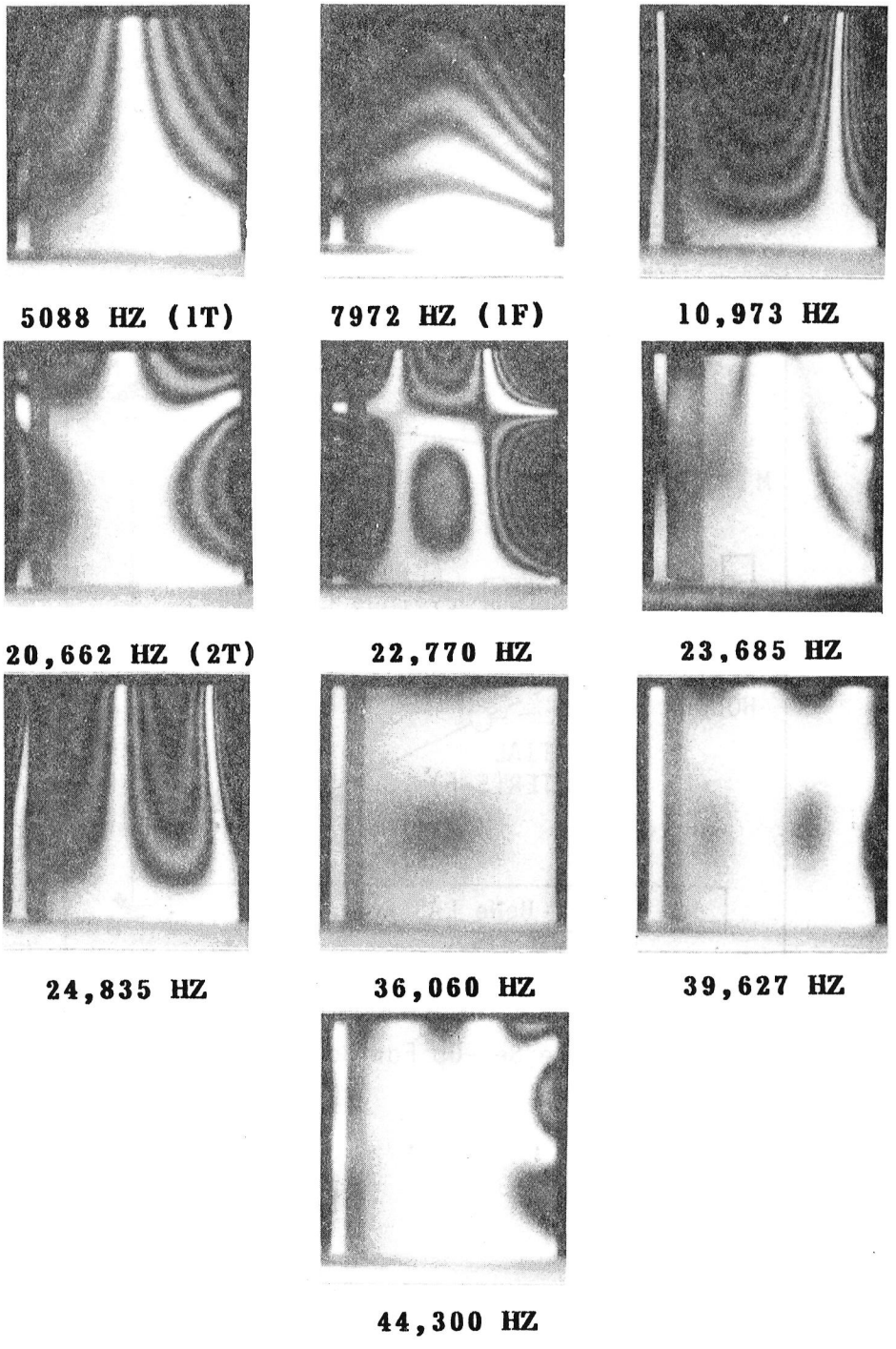

Figure 3. Holographic Vibration Test Results For Shell 1

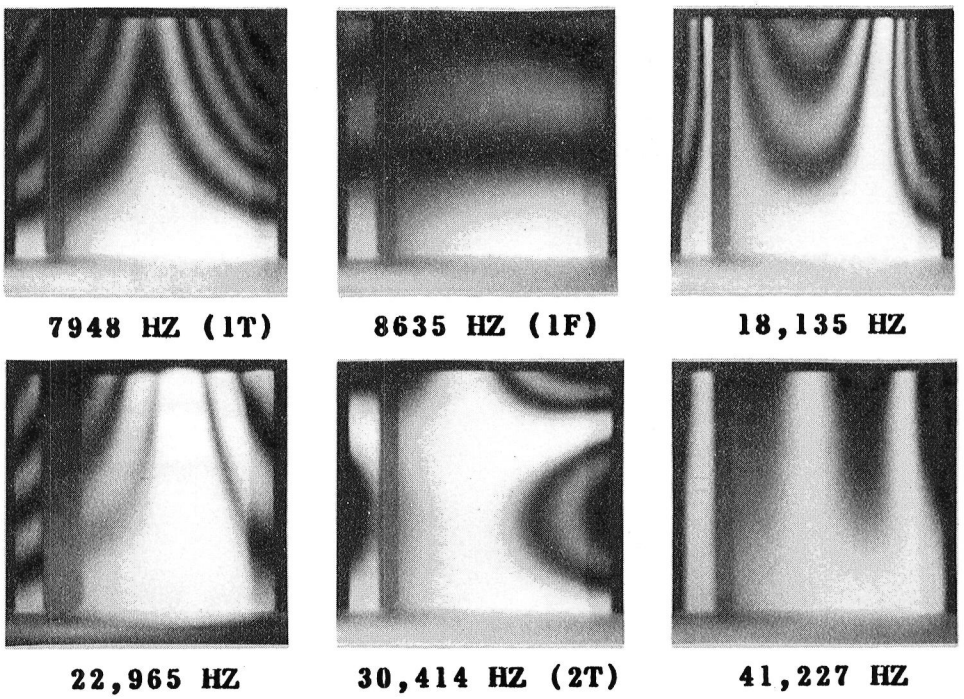

Figure 4. Holographic Vibration Test Results For Shell 2

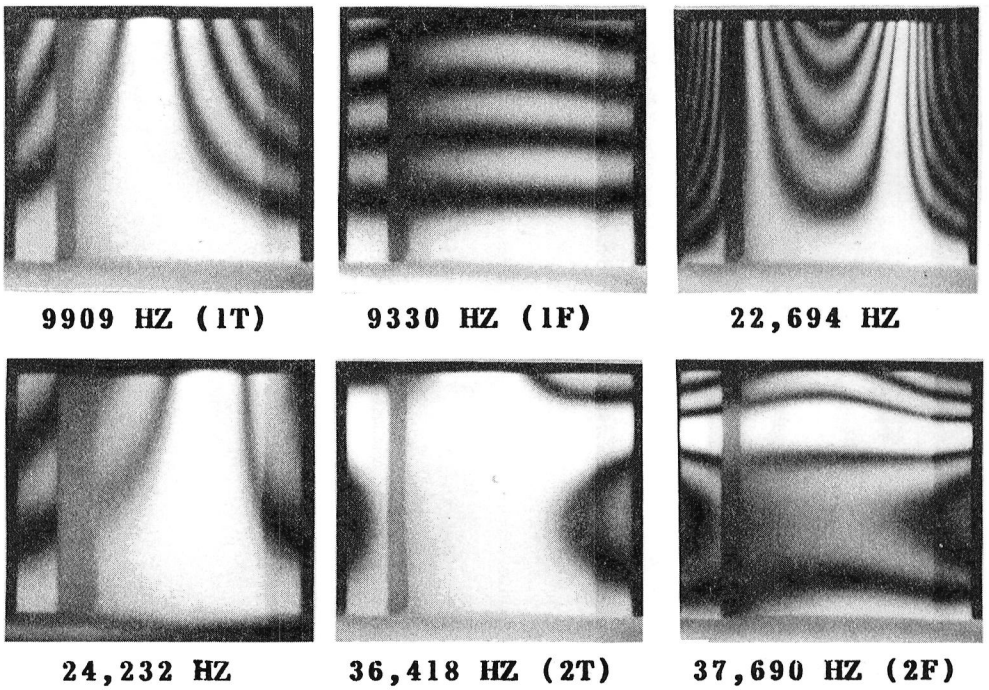

Figure 5. Holographic Vibration Test Results For Shell 3

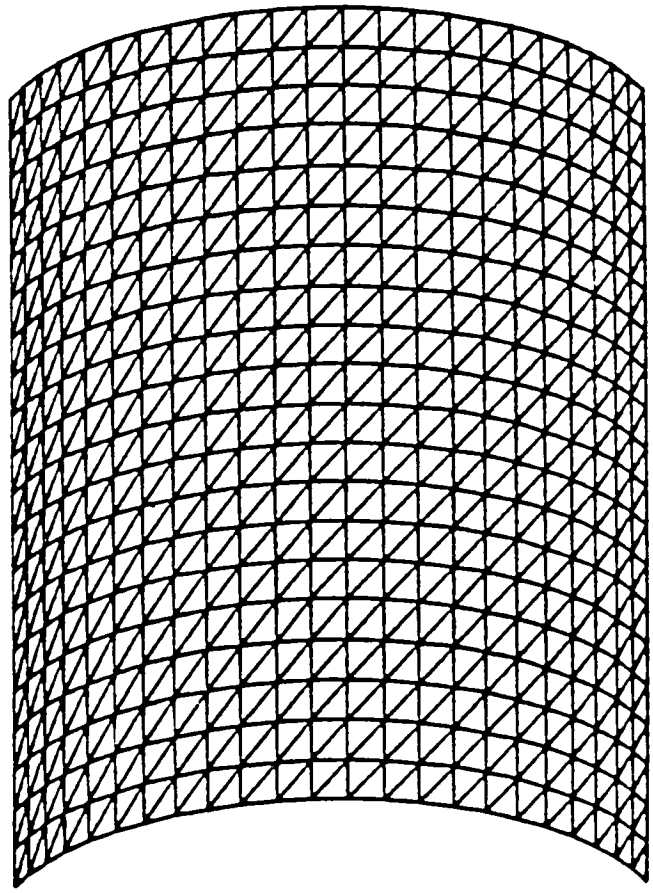

MASS DENSITY: 7.83×10^{3} KG/M^2 (7.32×10^{-4} (LB-SEC^2)/IN^4)
POISSON'S RATIO: 0.3
YOUNG'S MODULUS: 2.07×10^{11} N/M^2 (3.0×10^{7} LB/IN^2)

Figure 6. Finite Element Mesh For Shell 1

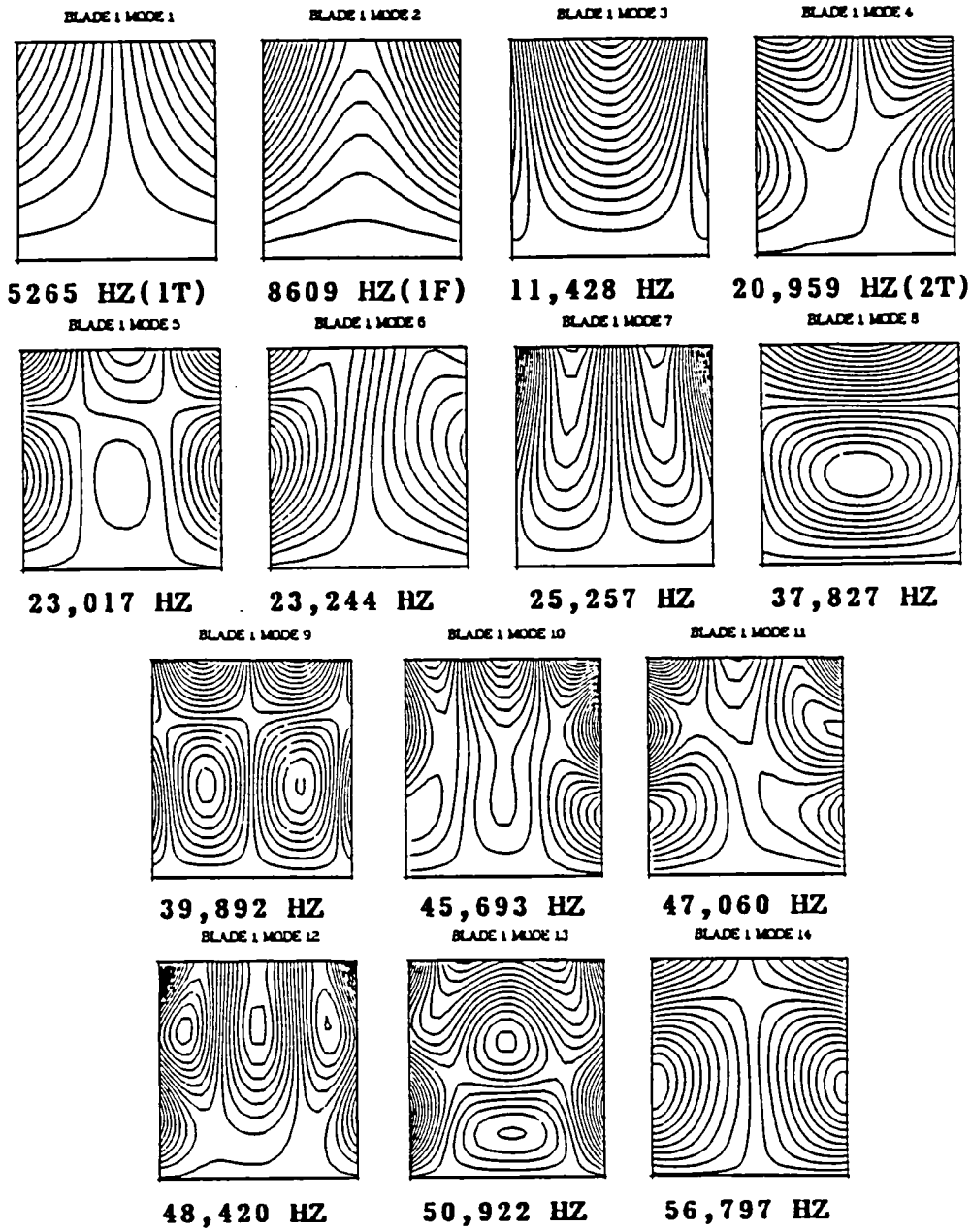

Figure 7. Resonant Mode Shapes From NASTRAN Solution For Shell 1 in the Form of Contour Plots of the Out-of-Plane Displacements

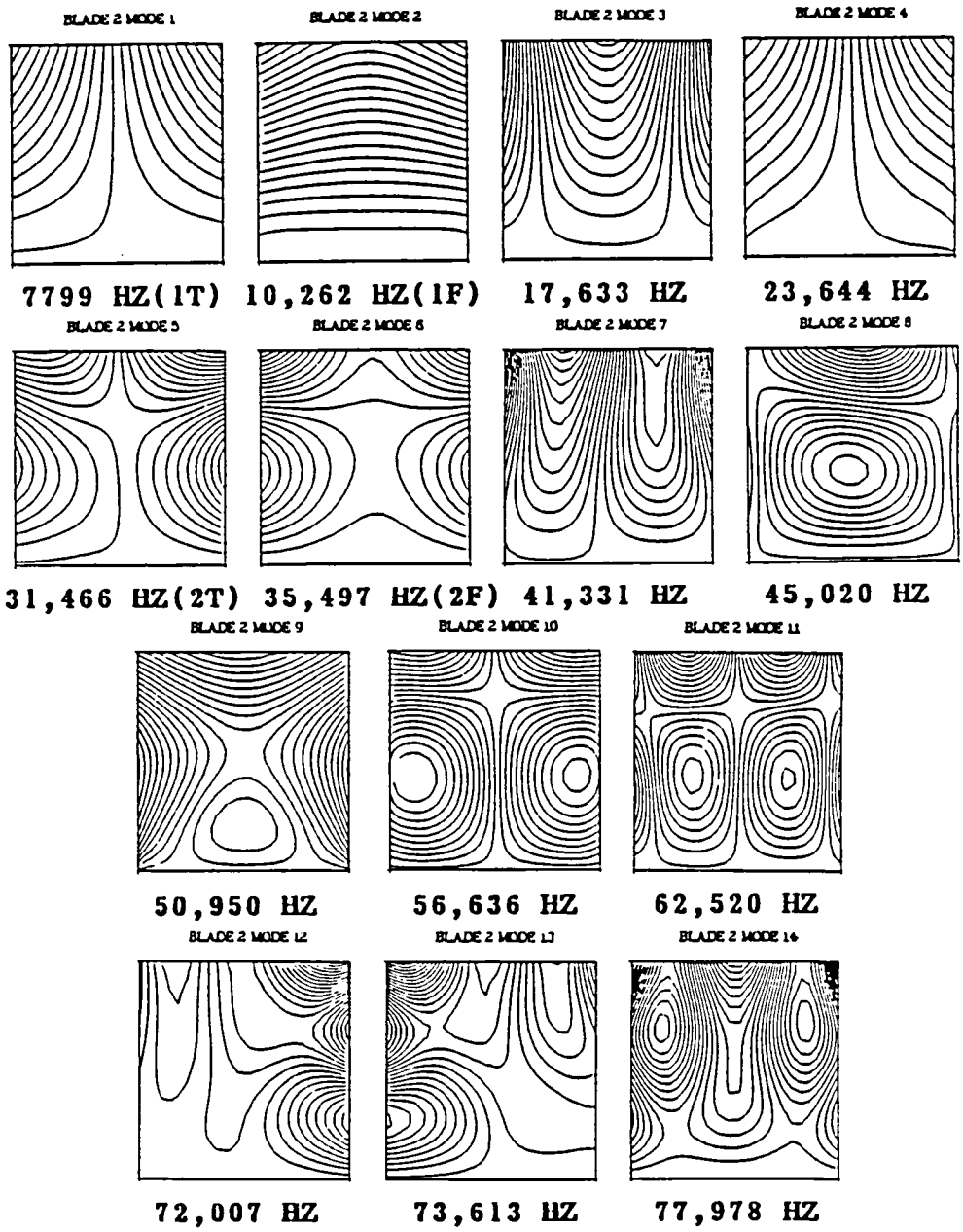

Figure 8. Resonant Mode Shapes From NASTRAN Solution For Shell 2 in the Form of Contour Plots of the Out-of-Plane Displacements

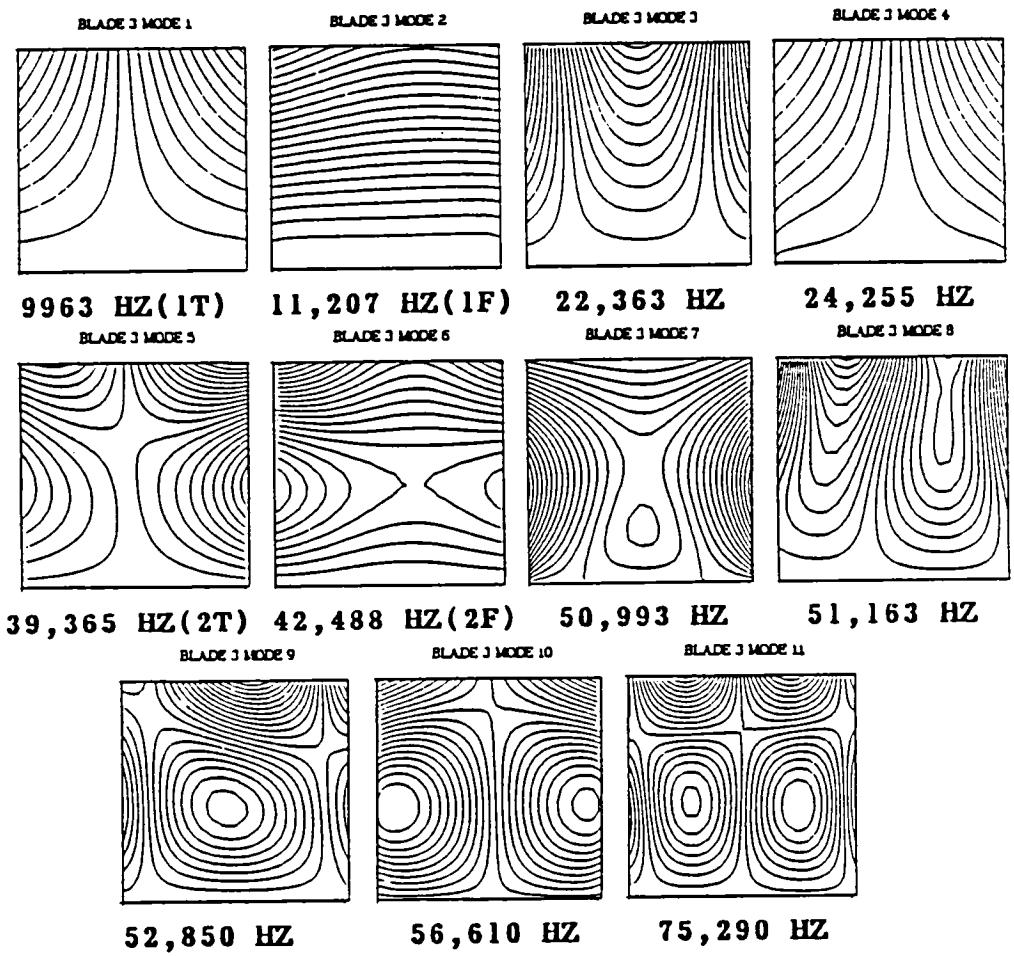

Figure 9. Resonant Mode Shapes From NASTRAN Solution For Shell 3 in the Form of Contour Plots of the Out-of-Plane Displacements

NASTRAN STRUCTURAL MODEL FOR THE LARGE GROUND ANTENNA PEDESTAL WITH APPLICTIONS TO HYDROSTATIC BEARING OIL FILM

CHIAN T. CHIAN

Jet Propulsion Laboratory, Pasadena, CA

SUMMARY

Investigations were conducted on the 64-meter antenna hydrostatic bearing oil film thickness under a variety of loads and elastic moduli. These parametric studies used a NASTRAN pedestal strutural model to determine the deflections under the hydrostatic bearing pad. The deflections formed the input for a computer program to determine the hydrostatic bearing oil film thickness. For the future 64-meter to 70-meter antenna extension and for the 2.2-meter (86-in.) haunch concrete replacement cases, the program predicted safe oil film thickness (greater than 0.13 mm (0.005 in.) at the corners of the pad). The effects of varying moduli of elasticity for different sections of the pedestal and the film height under distressed runner conditions were also studied.

INTRODUCTION

The upgrade of the large NASA Deep Space Network (DSN) antennas provide the necessary increase in earth-based space communication capability at the following three Deep Space Communication Complexes: Goldstone, California; Canberra, Australia; and Madrid, Spain. (Fig. 1)

The physical diameter of the three large antennas are extended from the existing 64 meters to 70 meters. (Fig. 2) The increase of the antenna aperture and the associated structural and mechanical modifications are needed in support of the Voyager 2 - Neptune encounter in August 1989 (Fig. 3), the Galileo-Jupiter mission (Fig. 4), and ongoing spacecraft communications in our solar system. Radio Astronomy and Search for Extraterrestrial Intelligence (SETI) scientific projects will also benefit from the enchancement.

The pedestal of the large antenna is a two-story, reinforced concrete building, which supports the movable structure of the antenna. (Fig. 5) The pedestal is under pressure loadings at the three hydrostatic bearing pads. A minimum hydrostatic bearing oil film of 0.13 mm (0.005 in.) is required to avoid any metal to metal contact between the pad and the runner and to accommodate any runner malfunctioning and placement tolerance.

This article reports on the static analysis and computer modeling for the large 64-meter antenna pedestal. NASTRAN Program was used to develop the pedestal structural model. The top surface deflection of the pedestal obtained from the NASTRAN model was used as an input to a separate computer program to determine the minimum oil film thickness between the hydrostatic bearing pad and the runner. The knowledge of the oil film thickness was necessary to conduct a variety of hydrostatic bearing rehabilition studies.

Three parametric studies were conducted to evaluate the performance of the hydrostatic bearing system. Effects on the oil film thickness due to the following factors were considered in each of the three parametric studies:

(1) The height of the new concrete in the pedestal haunch area.

(2) The different moduli of elasticity of the concrete in the pedestal wall and haunch area.

(3) The hydrostatic bearing pad load increase due to the planned antenna aperture extension from 64 meters to 70 meters.

The results of these parametric studies are presented in this report.

PEDESTAL DESCRIPTION

The azimuth hydrostatic bearing, set on the pedestal top, supports the full weight of the moving parts of the antenna and permits a very low friction azimuth rotation on a pressurized oil film. (Ref. 1) A cross-sectional diagram of the hydrostatic bearing is shown in Fig. 6.

Three movable pad-and-socket assemblies float on the oil film over a stationary runner and support the three corners of the alidade base triangle as shown in Fig. 7. The stationary runner for the bearing and the three bearing pads are completely enclosed in an oil reservoir. The three hydrostatic bearing pads are equidistant from the central axis of the pedestal as shown in Fig. 8.

The pedestal is 13.7 m (45 ft) tall, 25.3 m (83 ft) in diameter, with a diaphragm top which has a concrete collar in the center; the pedestal supports the movable structure of the antenna. The wall thickness is 1.1 m (3.5 ft).

The three principal forces from the antenna alidade which act on the pedestal are: (1) vertical forces from the azimuth hydrostatic bearing pads, (2) rotational forces from te azimuth drives, and (3) horizontal forces on the azimuth radial bearing.

The three hydrostatic bearing pads, made of carbon steel are 1.Ø16 m (4Ø in.) wide, 1.524 m (6Ø in.) long, and Ø.5Ø8 m (2Ø in.) deep. There are six recesses in the bottom of each pad as indicated in Fig. 9 with the two center recesses being larger than the corner recesses. According to the original design specification, the pedestal concrete is required to have a Young's modulus of elasticity E of $3.5 \times 1Ø^{10}$ N/m^2 ($5.Ø \times 1Ø^{6}$ psi). However, it is believed that the current Young's modulus of elasticity for the pedestal concrete is less than this value, and a reduced value, consistent with current core-sample measurements, is assumed for this report.

DESCRIPTION OF THE NASTRAN MODEL

All three pads are assumed to support the same amount of loads. Therefore, the pedestal is divided into three identical segments. Moreover, due to the symmetry with respect to the center line of the pad, each segment can be further divided into two segments.

As a consequence, a one-sixth segment of the pedestal, with angular span of 60°, is being developed in the present structural model as shown in Fig. 10. Appropriate boundary conditions are being applied to reflect the aforementioned symmetry: (1) zero slope at the points representing the centerline of the pad, and (2) zero slope at the ponts representing midposition between two pads.

The pedestal model is first considered as a cylinder of uniform wall thickness which comprises 630 six-sided solid elements (CHEXA2) with a total of 880 grid points. The actual haunch contour and the top slab is added in the pedestal model to provide additional stiffness on the pedestal wall.

The pedestal concrete is assumed to be homogeneous, with a reduced Young's modulus of elasticity E of 2.8×10^{10} N/m^2 (4.0×10^6 psi). The actual pressure profile of the oil under the hydrostatic bearing pad is exerted on the top pedestal surface (Fig. 11).

For simplicity, the pressure pattern of the oil under the pad is assumed to be symmetric with respect to the pad centerline in the NASTRAN pedestal model. Therefore, $p_1 = p_3$ and $p_4 = p_6$. Pad 3, which experiences the highest load among the three pads, is the one considered in our model. The values of the pad recess pressures are given in Table 1.

DESIGN CHARACTERISTICS

Two design characteristics are used to evaluate the sensitivity of the hydrostatic bearing pad operation to the modulus of elasticity. The first characteristic is the maximum pad out-of-flatness. Deflected shapes of the hydrostatic bearing pad and runner surface are illustrated in Fig. 12. Relative deflections within the hydrostatic bearing pad and within the runner surface (from centerline to edge of pad) are shown as Δ_p and Δ_r, respectively.

Design criteria (Ref. 1) require that the mismatch of deflected surfaces, $\Delta\delta$, be within 0.101 mm (0.004 in.). (This is the variation of the film height between the pad and the runner.) Out of this a maximum mismatch of deflected shapes of 0.076 mm (0.003 in.) was established as the allowance for creep during construction before the bearing pads could be moved. The remaining 0.025 mm (0.001 in.) was the design criteria for mismatch of elastic deformations. Since creep strains have been compensated for by releveling of the runner, the maximuum pad out-of-flatness, a $\Delta\delta$ of 0.101 mm (0.004 in.), can now all be accounted for by elastic deformations. These elastic deformations are part of the NASTRAN output.

The second characteristic used to evaluate the operability of the hydrostatic bearing is the minimum oil film thickness between the pad and the runner. Based on previous operational experience, a minimum oil film thickness, h, of 0.127 mm (0.005 in.) is considered necessary for safe operation. Figure 13 shows

a typical deflection map of the top pedestal surface under pad load. This deflection map is used as the input to the oil film height model to determine the minimum oil film thickness between the pad and the runner.

COMPARISON WITH FIELD MEASUREMENTS

The field measurements were conducted at the Goldstone, California (DSS-14) 64-meter antenna pedestal, and the load-deformation relationships of the pedestal were obtained.

Fig. 14(a) shows the locations of the gauges for deflection measurements. Instruments were installed to measure vertical deformations over a 1.27 m (50 in.) gauge length on the external surface of the haunch and the wall. Figure 14(b) is a schematic of the instrumentation used. As shown, small blocks were bonded to the structure at the preselected locations. A direct current differential transformer (DCDT) mounted in a fixture was attached to the upper block. A wire from the spring-loaded plunger of the DCDT was attached to the lower block. The output of the DCDT was continuously recorded during the time required for antenna Pad 3 to be moved across the instrumented location. This time is approximately 3 minutes.

Figures 15 and 16 show the good correlation between the field deflection measurements and the NASTRAN predicted values for two different locations: azimuth 49° and aximuth 96°.

PARAMETRIC STUDIES

Three parametric studies were conducted to evaluate the operability of the large 64-meter antenna:

(1) Effect on the oil film thickness due to the height variation of the new concrete in the pedestal haunch.

(2) Effect on the oil film thickness due to the variation of concrete elastic moduli in the pedestal wall and haunch area.

(3) Effect on the oil film thickness due to the pad load increase for an antenna aperture extension from 64 meters to 70 meters.

A. Height of New Concrete in the Pedestal Haunch

The pedestal concrete with an initial modulus of elasticity E of 2.1×10^{10} N/m^2 (3×10^6 psi) was replaced by a new concrete with the modulus of elasticity of 3.5×10^{10} N/m^2 (5×10^6 psi) at different heights from the top. Results of this parametric study are shown in Table 2 as well as in Fig. 17.

B. Variation of Concrete Elastic Moduli in the Pedestal Wall and Haunch Area:

The severity of the concrete deterioration with accompanying reduction in compressive strength and modulus of elasticity varies widely throughout the pedestal mass. Studies to date have shown that the most serious damage was in the haunch area. A height of 2.2 m (86 in.) of the concrete in the haunch area has been replaced as part of the rehabilitation efforts.

Portions of the remainng pedestal concrete not replaced have experienced moderate damage and are expected to drop further in strength and modulus of elasticity in the future since the alkali-aggregate reaction (the main reason of deteriorations) is continuous, and not fully understood. Therefore, this study was made to evaluate the operability of the hydrostatic bearing under these continuous deteriorations. The moduli of elasticity of the concrete in the pedestal wall and the haunch area were varied. This study was further subdivided into two parts:

(1) The new haunch area down to a depth 2.2 m (86 in.) was assigned a fixed modulus of elasticity of 3.5×10^{10} N/m^2 (5×10^6 psi), while the modulus of elastic ity of the remaining wall was taken to be 2.1×10^{10} N/m^2 (3×10^6 psi), 1.4×10^{10} N/m^2 (2×10^6 psi), and 0.7×10^{10} N/m^2 (1×10^6 psi), to simulate time deteriorations. Note that tests made on replaced concrete showed E larger than 3.5×10^{10} N/m^2 (5×10^6 psi).

(2) The pedestal wall was assumed to have a fixed modulus of elasticity of 1.4×10^{10} N/m^2 (2×10^6 psi), while the new haunch area was assigned a modulus of elasticity of 3.5×10^{10} N/m^2 (5×10^6 psi), 3.15×10^{10} N/m^2 (4.5×10^6 psi) and 2.8×10^{10} N/m^2 (4×10^6 psi) to simulate different values of the replaced concrete.

Results of this parametric study showing the effect on the oil film thickness due to the variation of concrete elastic moduli are summarized in Tables 3 and 4. Figures 18 and 19 also give the results of this study.

C. Pad Load Increase With an Antenna Aperture Extension From 64 meters to 70 meters

This study investigates the effects of the increased pad load of the antenna with an aperture extension from 64 meters to 70 meters on the pedestal deflection and the oil film thickness. Pad 3 was assumed to have a load of 1.1×10^6 kg (2.4×10^6 lb). In this study, four loads of 1.1×10^6 kg (2.4×10^6 lb.), 1.3×10^6 kg (2.8×10^6 lb), 1.45×10^6 kg (3.2×10^6 lb), and 1.6×10^6 kg (3.6×10^6 lb) were considered for pad 3, which correspond to load factors of 1.00; 1.17; 1.33; and 1.50, respectively, relative to the estimated original 64-meter pad 3 load. The modulus of elasticity was assumed to be 3.5×10^{10} N/m^2 (5×10^6 psi) for both the pedestal wall and the haunch area. The maximum film height variation, $\Delta\delta$, and the minimum film thickness, h, are given in Table 5 for the four loads considered. The results are also shown in Fig. 20.

CONCLUSIONS

In this study we reported on applications of the NASTRAN pedestal model to the hydrostatic bearing oil film for the large 64-meter antenna. The NASTRAN model gave as one result the top surface deflections of the pedestal. These deflections formed the input for the hydrostatic bearing oil film computer program to determine the minimum oil film thickness.

The knowledge of the minimum oil film thickness between the hydrostatic bearing pad and the runner was required to conduct a variety of hydrostatic bearing rehabilitation studies.

Based on results presented in this study, a height of 2.2 meters (86 in.) of concrete in the top-most pedestal haunch area has been replaced in the DSS 14, located in Goldstone, California, as part of the rehabilitation efforts. For a new concrete with the modulus of elasticity of 3.5×10^{10} N/m^2 (5×10^6 psi), the study predicted a safe oil film thickness of more than 0.13 mm (0.005 in.).

The effect on the oil film thickness due to the pad load increase for an antenna aperture extension from 64 meters to 70 meters was also investigated. For a pad load increase of up to 20%, the study predicted a safe oil film thickness.

REFERECE

1. TDA Technical Staff, "The NASA/JPL 64-Meter-Diameter Antenna at Goldstone, California: Project Report", JPL Technical Memorandum 33-671, Jet Propulsion Laboratory, Pasadena, CA, July 15, 1974.

Table 1. Pad 3 Recess Presures[a]

Recess presure	p_1	p_2	p_4	p_5
N/m^2	11,383,000	7,757,000	10,859,000	9,480,0000
psi	1651	1125	1575	1375

[a] Assume $p_1 = p_3 = \frac{1}{2}(p_1 + p_3)$ and $p_4 = p_6 = \frac{1}{2}(p_4 + p_6)$.

Table 2. Effect on the oil film thickness due to the height variation of the new concrete in the pedestal haunch.

Description, N/m^2 (psi)	Film height variation $\Delta\delta$, mm (in.)	Minimum oil film thickness h, mm (in.)
Entire pedestal: $E = 2.1 \times 10^{10}$	0.147	0.132
(3×10^6)	(0.0058)	(0.0052)
Top 1.4 m (56 in.): $E = 3.5 \times 10^{10}$	0.102	0.196
(5×10^6)	(0.0040)	(0.0077)
Remaining pedestal: $E = 2.1 \times 10^{10}$		
(3×10^6)		
Top 2.2 m (86. in.): $E = 3.5 \times 10^{10}$	0.097	0.191
(5×10^6)	(0.0038)	(0.0075)
Remaining pedestal: $E = 2.1 \times 10^{10}$		
(3×10^6)		

Table 3. Effect of varying the modulus of elasticity of the pedestal wall[a]

Modulus of elasticity of the pedestal wall, N/m^2 (psi)	Film height variation $\Delta\delta$, mm (in.)	Minimum oil film thickness h, mm (in.)
2.1×10^{10} (3×10^{6})	0.097	0.193
	(0.0038)	(0.0076)
1.4×10^{10} (2×10^{6})	0.102	0.191
	(0.0040)	(0.0075)
0.7×10^{10} (1×10^{6})	0.119	0.178
	(0.0047)	(0.0070)

a The modulus of elasticity of the top 2.2 m (86 in.) in the haunch is considered to be fixed at 3.5×10^{10} N/m^2 (5×10^{6} psi).

Table 4. Effect of varying the modulus of elasticity of the haunch area[a]

Modulus of elasticity of the top 2.2 m (86 in.) in the haunch, N/m^2 (psi)	Film height variation $\Delta\delta$, mm (in.)	Minimum oil film thickness h, mm (in.)
3.5×10^{10} (5×10^6)	0.102	0.191
	(0.0040)	(0.0075)
3.15×10^{10} (4.5×10^6)	0.112	0.152
	(0.0044)	(0.0060)
2.8×10^{10} (4×10^6)	0.125	0.152
	(0.0049)	(0.0060)

[a] The modulus of elasticity of the pedestal wall is assumed to be fixed at 1.4×10^{10} N/m^2 (2×10^6 psi).

Table 5. Effect of the pad load increase due to the antenna extension[a]

Pad (No. 3) load, kg (lb)	Load Factor	Film height variation, $\Delta\delta$, mm (in.)	Minimum oil film thickness, h, mm (in.)
1.09×10^6	1.00	0.089	0.185
(2.4×10^6)		(0.0035)	(0.0073)
1.27×10^6	1.17	0.104	0.152
(2.8×10^6)		(0.0041)	(0.0060)
1.45×10^6	1.33	0.119	0.122
(3.2×10^6)		(0.0047)	(0.0048)
1.63×10^6	1.50	0.135	0.086
(3.6×10^6)		(0.0053)	(0.0034)

[a] The entire pedestal is assumed to have a modulus of elasticity of 3.5×10^{10} N/m^2 (5×10^6 psi) in all cases.

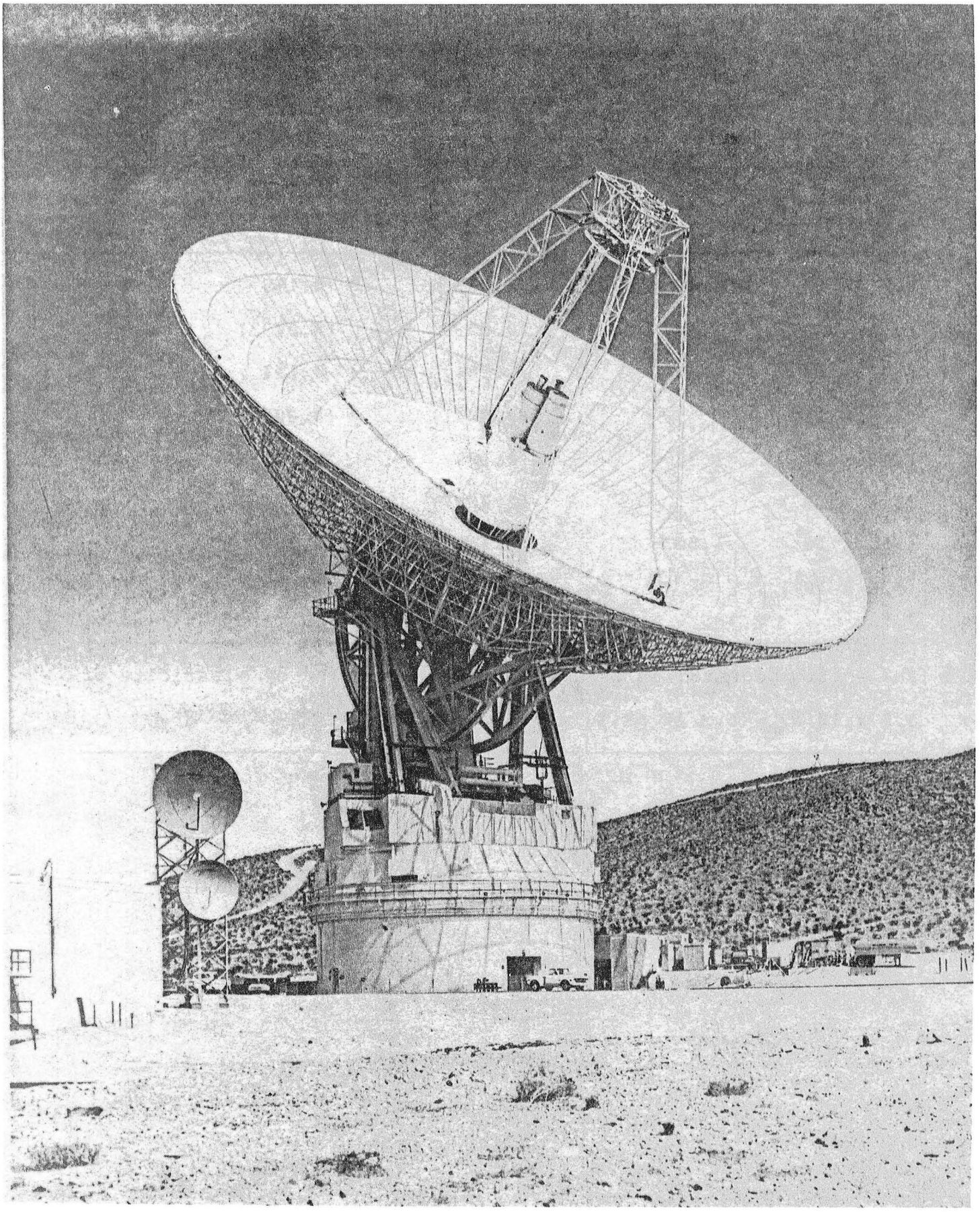

Fig. 1. Large 64-meter NASA Deep Space Network Antenna

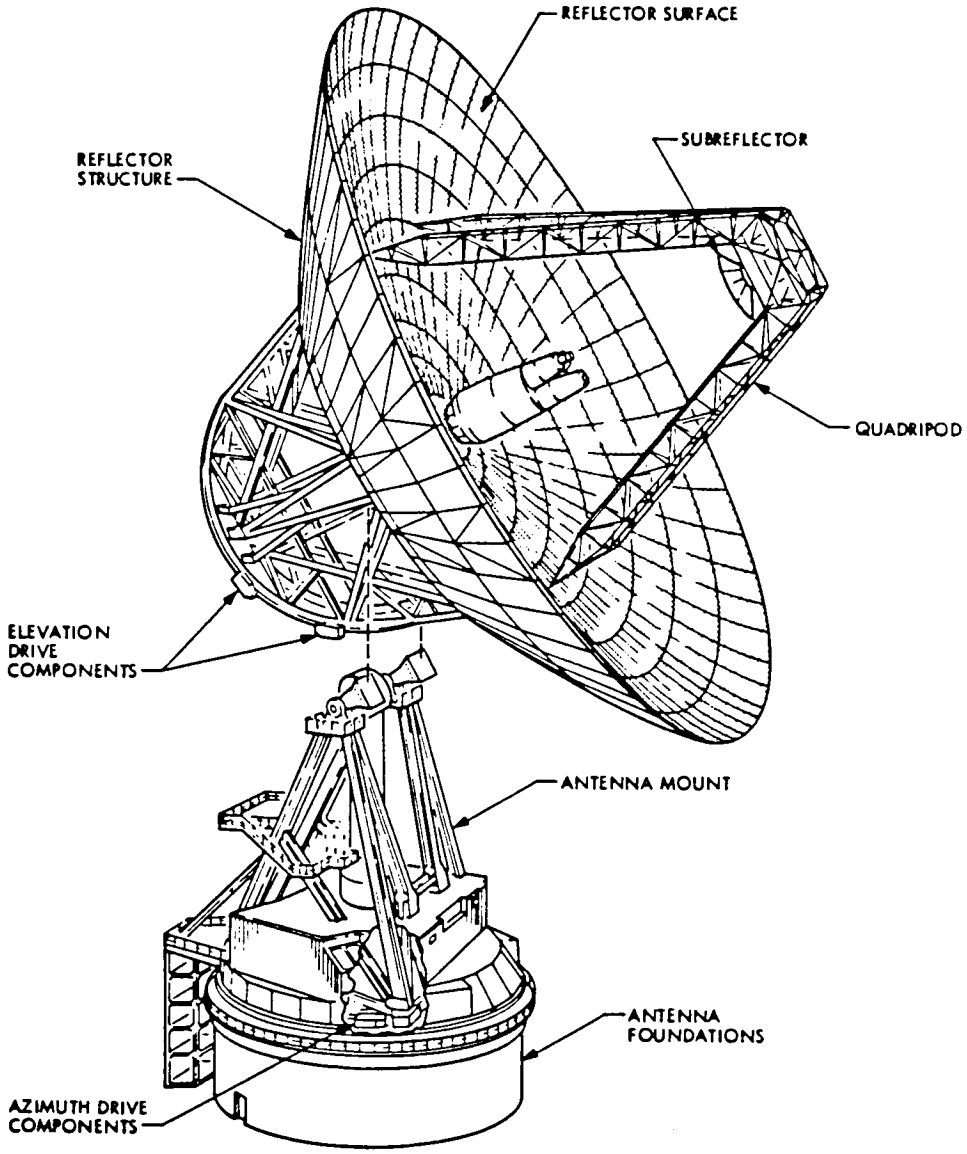

Fig. 2. Antenna Aperture Extension from 64 meters to 70 meters

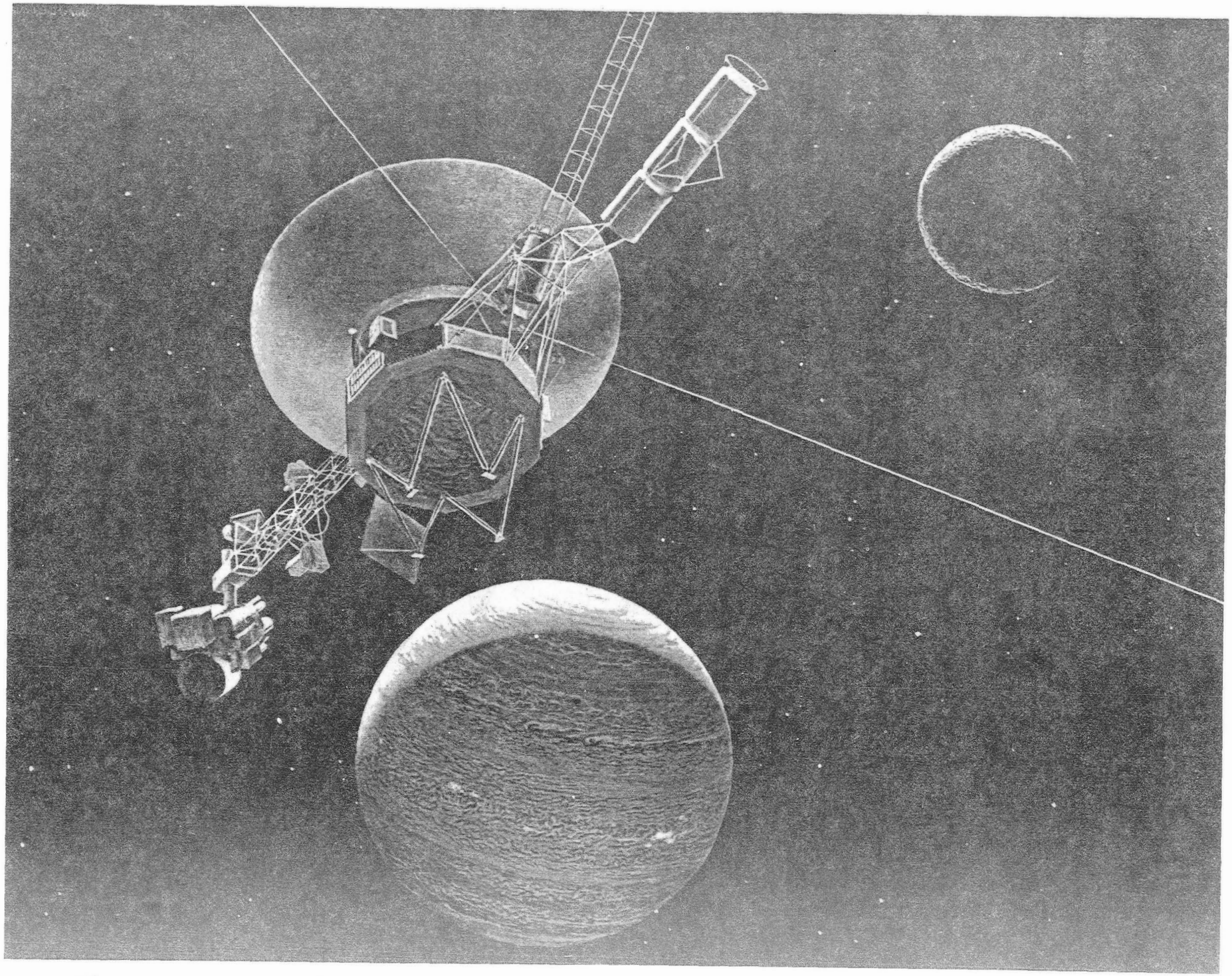

Fig. 3. Voyager 2 makes its closest Encounter with Neptune on August 24, 1989.

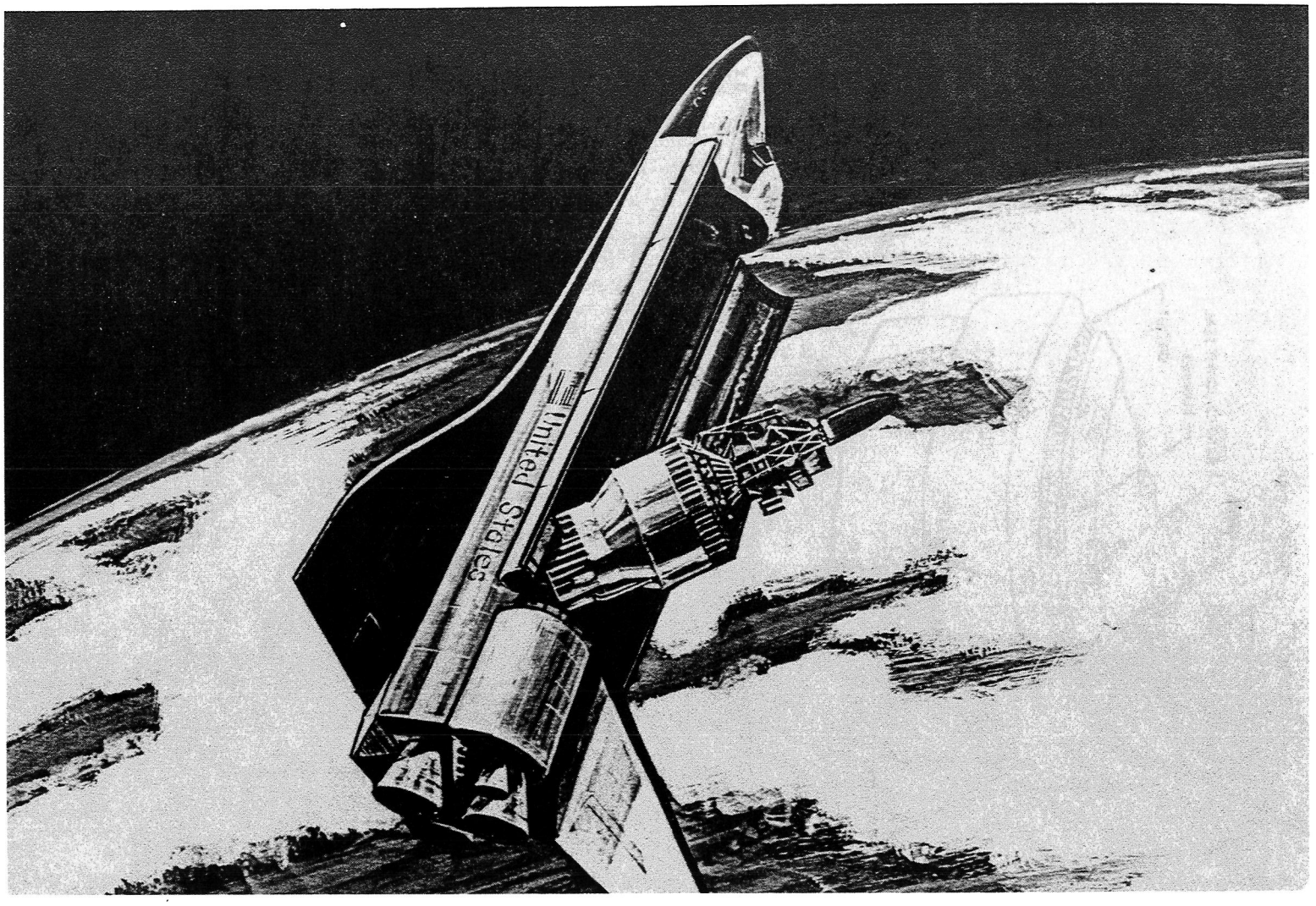

Fig. 4. Galileo Spacecraft to Jupiter is being launched from the space shuttle.

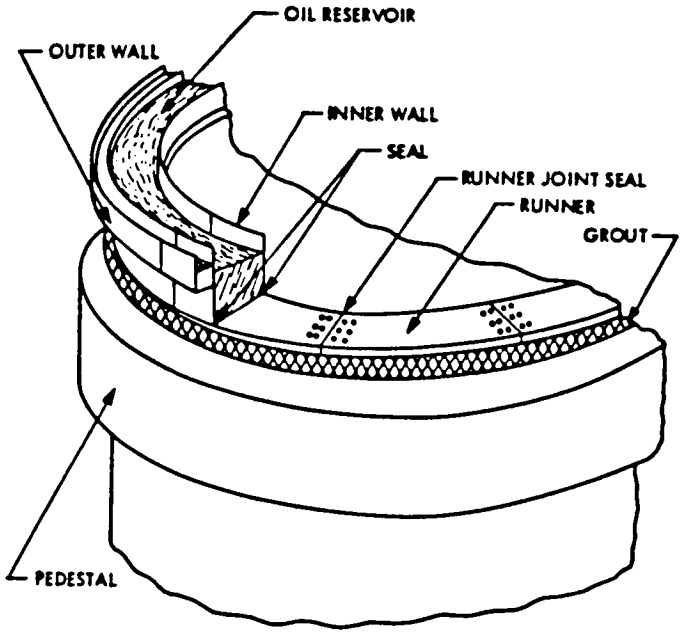

Fig. 5. General arrangement of 64-m antenna hydrostatic bearing

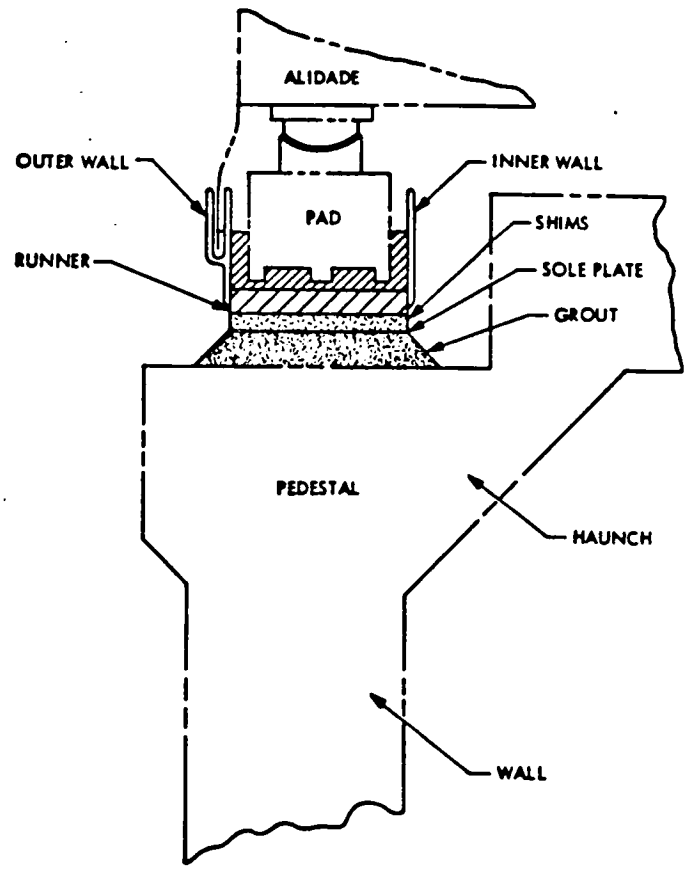

Fig. 6. Cross section of hydrostatic bearing system

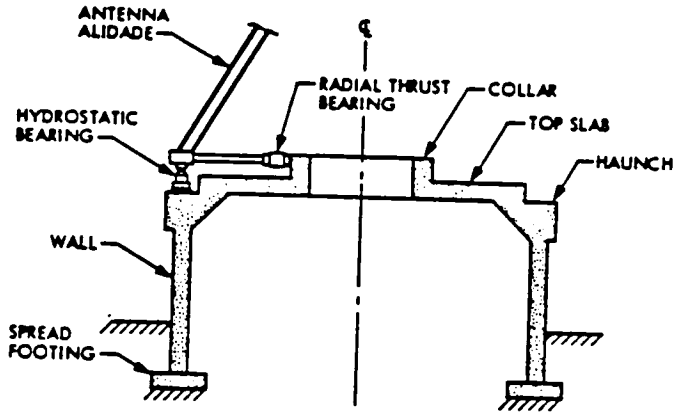

Fig. 7. Cross Section of Concrete Pedestal

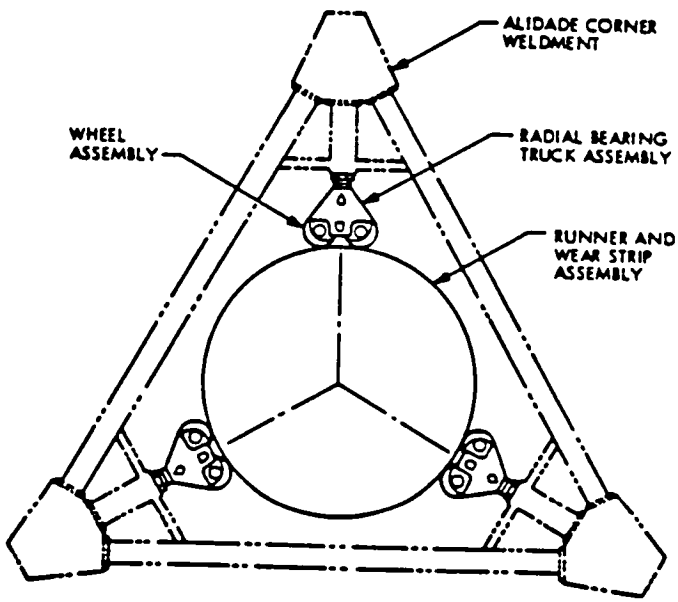

Fig. 8. Alidade base triangle and radial bearing assembly

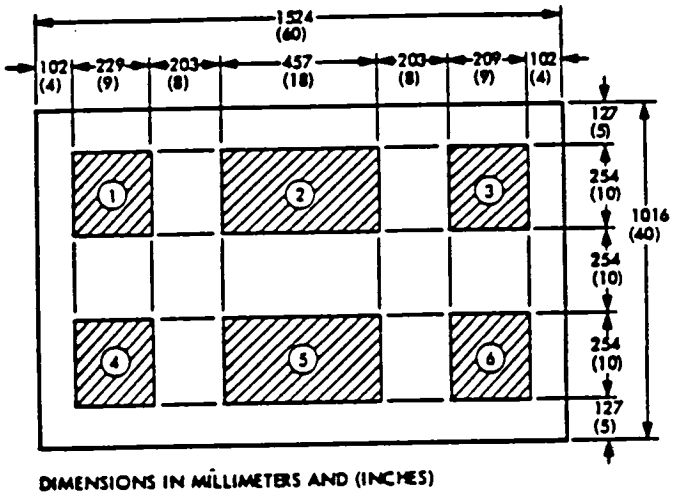

Fig. 9. Recess pattern of hydrostatic bearing pad

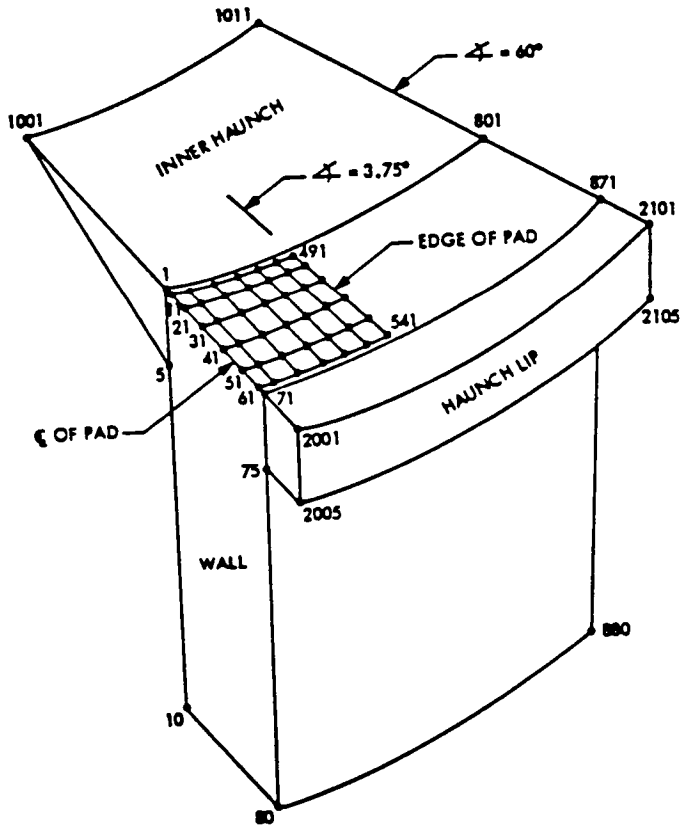

Fig. 10. NASTRAN pedestal model and nodal points

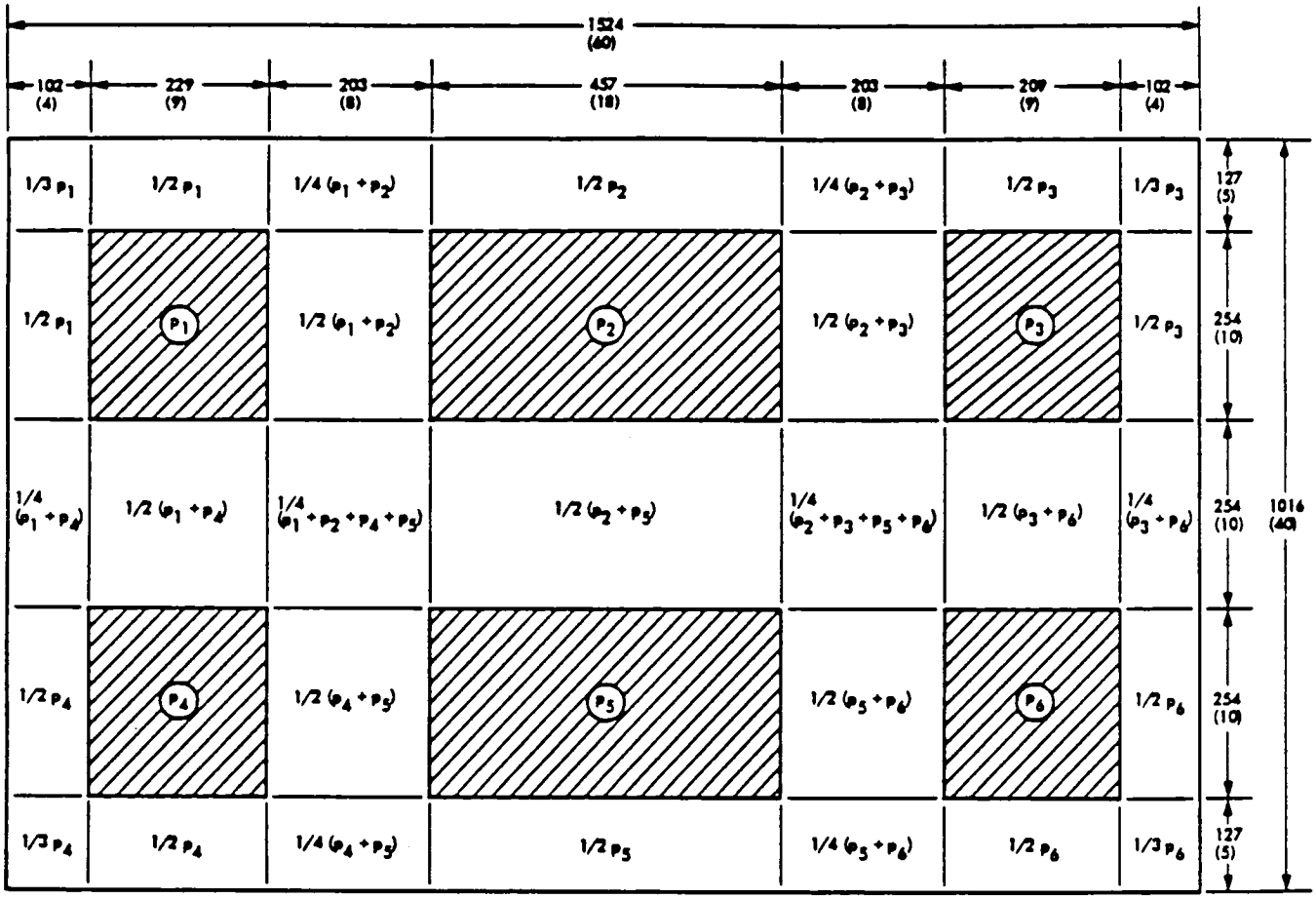

Fig. 11. Pressure profile of hydrostatic bearing pad

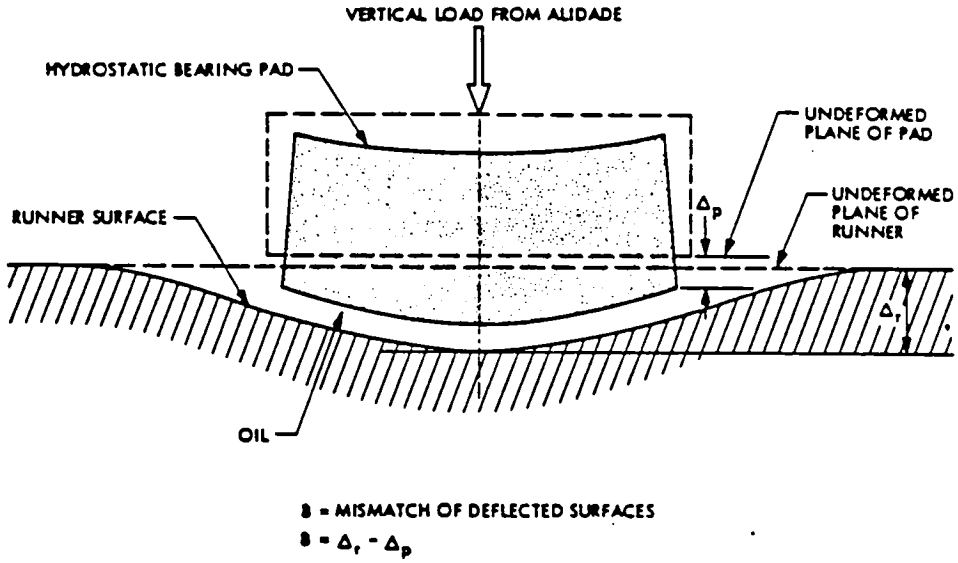

Fig. 12. Deflections of hydrostatic bearing pad and runner surface

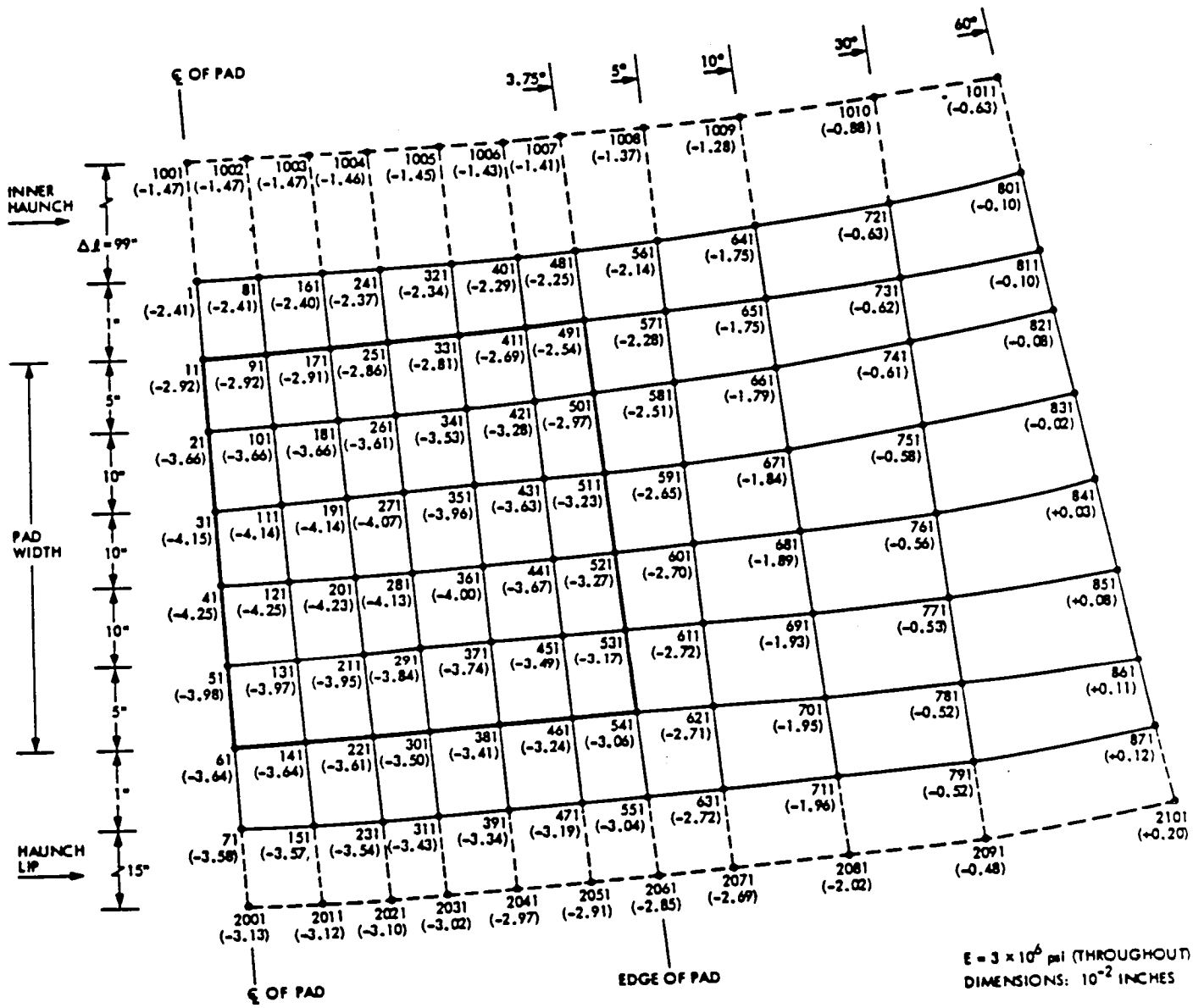

Fig. 13. Deflection map of the pedestal surface

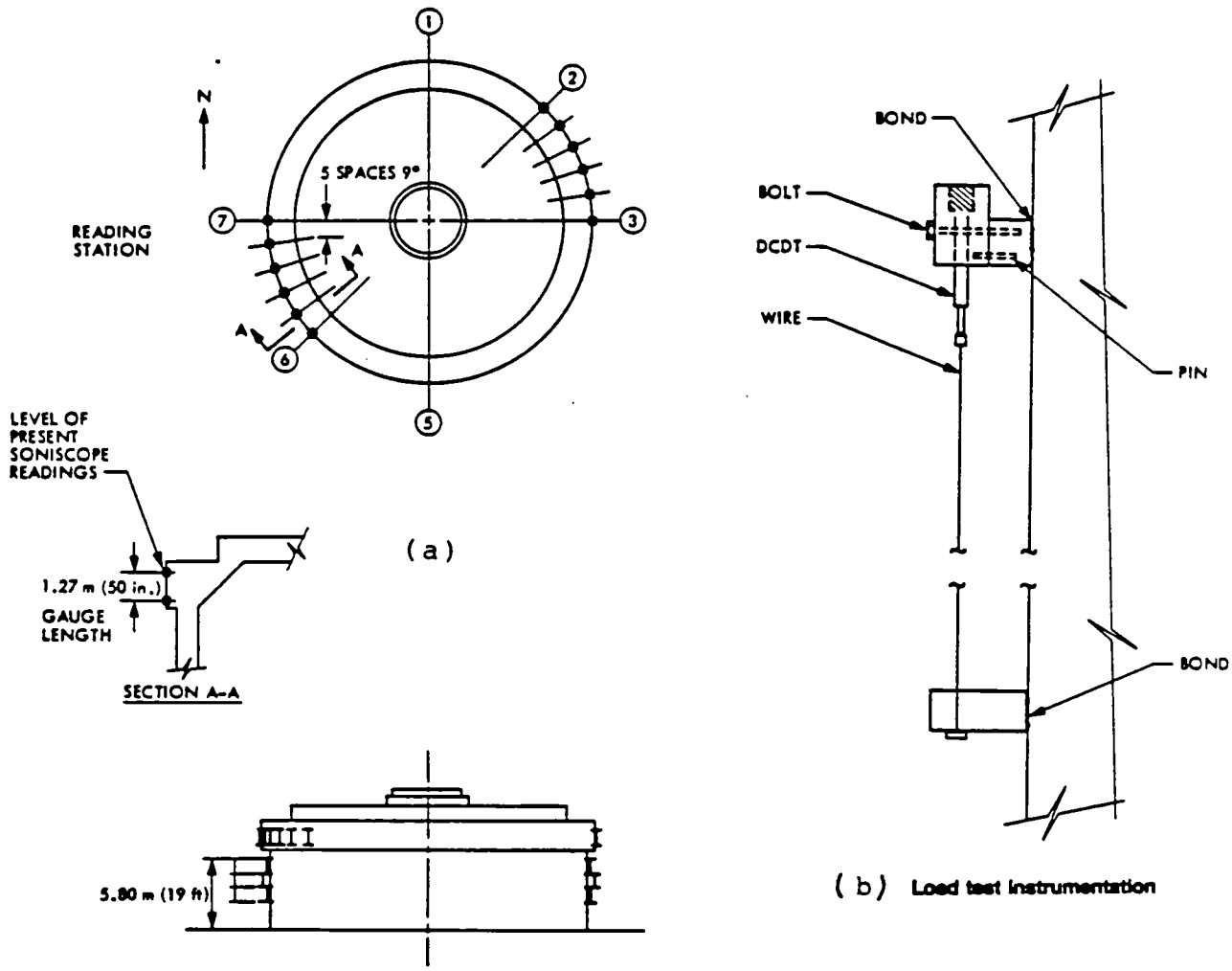

Fig. 14 Location of pad load tests

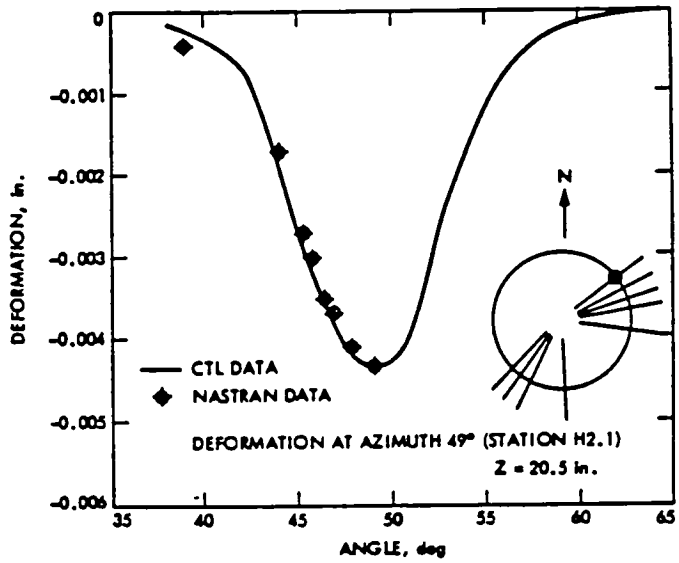

Fig. 15. Comparison of the NASTRAN mode results with field test data, azimuth = 49°

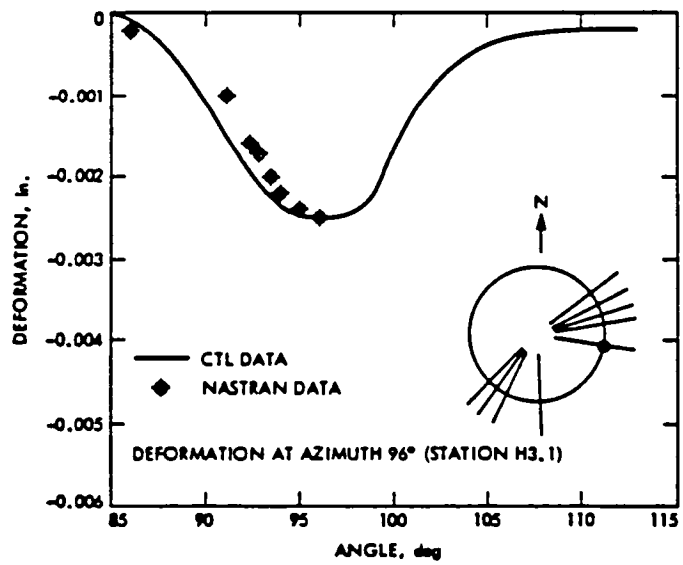

Fig. 16. Comparison of the NASTRAN model results with field test data, azimuth = 96°

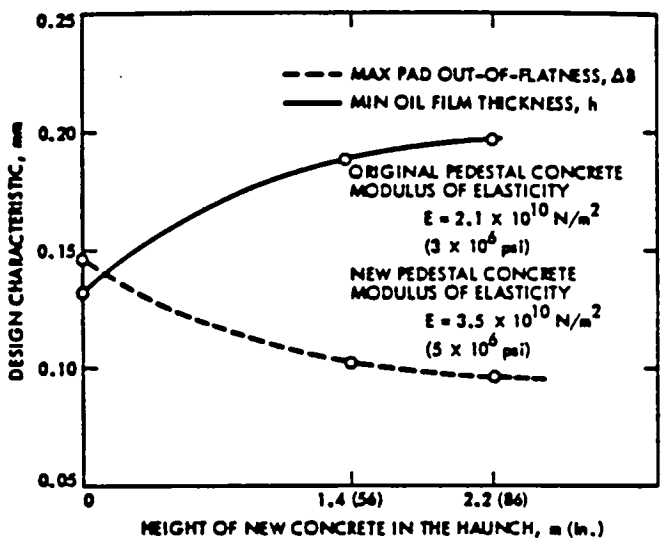

Fig. 17. Effect on the oil film thickness due to the height variation of the new concrete in the pedestal haunch.

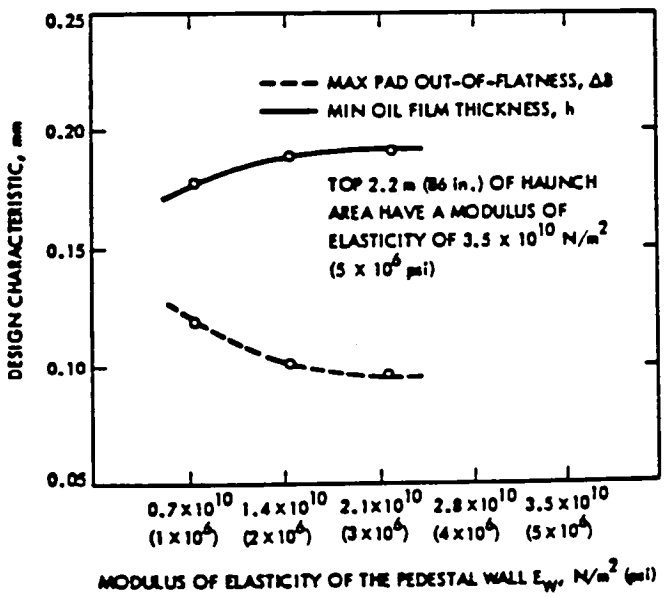

Fig. 18. Effect of varying the modulus of elasticity of the pedestal wall

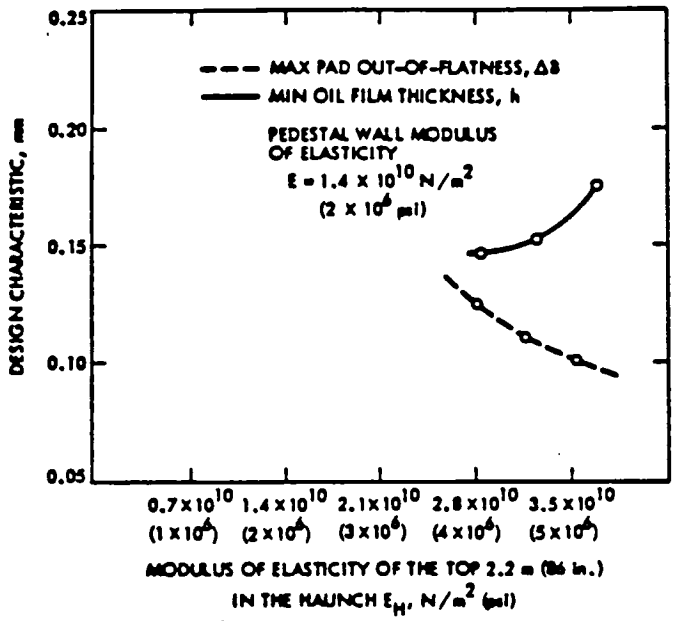

Fig. 19. Effect of varying the modulus of elasticity of the haunch area

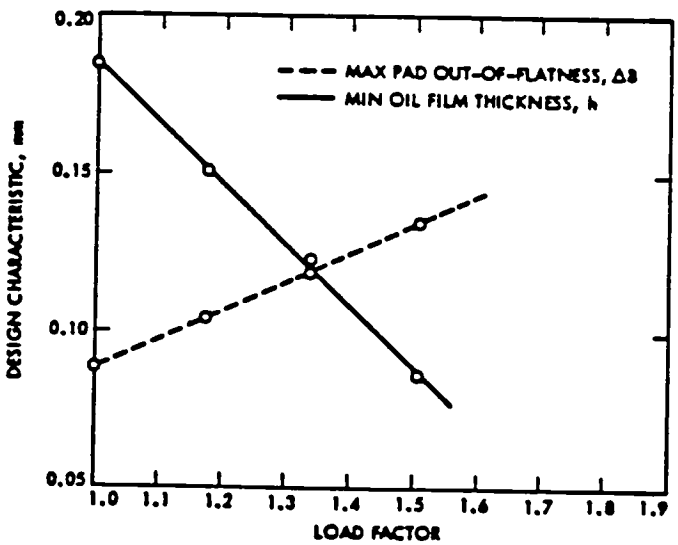

Fig. 20. Effect of the pad load increse due to the antenna extension

SOLVING LARGE-SCALE DYNAMIC SYSTEMS USING BAND LANCZOS METHOD IN ROCKWELL NASTRAN ON CRAY X-MP

Viney K. Gupta, Scott D. Zillmer,
and Robert E. Allison

Rockwell International,
North American Aircraft Operations,
Los Angeles, California 90009, USA.

SUMMARY

The improved cost-effectiveness using better models, more accurate and faster algorithms, and large-scale computing offers more representative dynamic analyses. The band Lanczos eigensolution method has been implemented in Rockwell's version of 1984 COSMIC-released NASTRAN finite-element structural analysis computer program to effectively solve for structural vibration modes including those of large complex systems exceeding 10,000 degrees of freedom.

The Lanczos vectors are re-orthogonalized locally using the Lanczos Method and globally using the modified Gram-Schmidt method for sweeping rigid-body modes and previously generated modes and Lanczos vectors. The truncated band matrix is solved for vibration frequencies and mode shapes using Givens rotations. Numerical examples are included to demonstrate the cost-effectiveness and accuracy of the method as implemented in ROCKWELL NASTRAN. The CRAY version is based on RPK's COSMIC/NASTRAN.

The band Lanczos method is more reliable and accurate and converges faster than the single vector Lanczos Method. The band Lanczos method is comparable to the subspace iteration method which is a block version of the inverse power method. However, the subspace matrix tends to be fully populated in the case of subspace iteration and not as sparse as a band matrix.

INTRODUCTION

With the objective of solving large-scale dynamic systems, several papers in recent years have presented a number of issues, of which we address, in particular, the following.

The improved cost-effectiveness with large-scale computing offers more extensive optimization (1-4), nonlinear capability (5), and more representative dynamic analyses(3-7), in addition to solution of fluid mechanics problems.

A cheaper solution to the larger numerical problem does not, however, eliminate the desire for solving the problems of proper formulation, modelling, and interpretation of results, using expert systems, in an effort to capture the finite-element modelling expertise of real-world aircraft structures, which involves decisions about mesh size, element selection, and constraint representation. Compatible system development is, however, the key to integrating software "black boxes" associated with the finite element analysis that generates most of the data, the data base management systems that handle and store the data, and the user-friendly interfaces that display the data; this, ideally, should be achieved by design rather than by adaptation. Grooms, Merriman, and Hinz (8) are developing an expert system for training structural engineers in modelling and analyses using ROCKWELL NASTRAN.

The correlation between a real physical structure and its mathematical finite element model (FEM) is premised on reasonable and defensible assumptions and idealizations. The agreement between experiment and theoretically predicted frequencies becomes weaker for the higher modes. With enough modelling elements, the FEM model for a complicated structure can, in principle, be made arbitrarily accurate. To achieve modal convergence, Hughes (9) computes modal coefficients of both momentum and angular momentum to identify dominant modes that must be retained when the number of Lanczos vectors is truncated . He analyzes a wrap-rib space antenna reflector by re-ordering modes, selecting only 9 dominant ones instead of the 26 suggested by the simple natural order modal truncation procedure based on experience with slender beam models. He found breathing modes to be important for the sake of convergence. Hughes' mode selection criteria tends to reduce the cost of dynamic response based on modal superposition.

The problem size or dimensionality can be reduced by Guyan reduction (10,11), e.g., at substructure level (5), and

component mode synthesis (12,13), by omitting unnecessary elastic degrees of freedom to suppress insignificant modes. For a large sparse system, dynamic condensation and associated loss of sparsity tends to increase eigensolution cost (14); the Lanczos method offers a superior alternative, since it does not rely on adhoc degree-of-freedom selection without apriori knowledge of modes to achieve reduced problem size. For a linear structural dynamic system, which is inertia invariant when the gross body motion is small, the frequency spectrum of the system transfer function is independent of time. A number of dominant modes of vibration can be retained, e.g., based on Fourier analysis of the frequency spectrum of the forcing function. The load-dependent basis of Ritz vectors, which are equivalent to Lanczos vectors, can be exploited to minimize the cost of dynamic analysis, linear (7,15,16) or nonlinear (17). However, the frequency content of the external forcing functions alone is not sufficient for predicting excitation of closely spaced modes in the system, if mass matrix changes or nonlinear effects cause inertia-induced reaction forces to excite higher modes. With damping, higher modes need to be retained only over short transients, not over the entire time interval. The static effect of higher modes can be accounted for by either including certain correction terms with modal superposition, as suggested by Shabana and Wehage (13), and Misel et al (6), or by peforming dynamic analysis in terms of Ritz or Lanczos vectors (7,15-17).

Local buckling of a conventional aircraft wing, preferrably based on a sufficiently detailed representation of the reinforcing stiffeners and any substantial features (e.g., access holes, mounting lugs, etc.), could result in a mesh of approximately 100,000 nodes - one order of magnitude beyond current practice. With multi-level substructuring, analyses of up to 500,000 degrees of freedom have been performed. The development of automated modelling and advanced hardware-software systems in the next ten years may lead to bigger analysis involving one to ten million degrees of freedom.

BAND LANCZOS METHOD

The band Lanczos method (18,19) is similar to the one called block Lanczos (20-22), or Subspace Iteration (15,16,23,24), or block Stodola (25), or Simultaneous Iteration (24), all involving simultaneous iteration using a block of trial vectors; their authors - Hestenes and Karush,

Bauer, Rutishauser, Jennings and Orr, Dong, Wolf, and Peterson, Bathe and Wilson - are referenced by Parlett (19), Bathe (24), or Dong (25). In contrast, classical Stodola-Vianello technique (also known as inverse power method) and simple Lanczos method (14,26-28) operate on one trial vector rather than a block of vectors. The band or block approach has been demonstrated to be effective and very efficient computationally when solving sparse algebraic system with large bandwidth for subset of the lowest eigenvalues and corresponding eigenvectors. Dong (25) has further extended the Block Stodola method to solve the complex, quadratic, and cubic eigenvalue problems.

Assume an algebraic eigensystem of the form: Ku = e Mu, where K and M cannot both be singular but both are symmetric and large and preferably narrowly banded, i.e., not involving damping, Coriolis effects and non-conservative forces which make K unsymmetric. The Lanczos method essentially reduces the rank of the algebraic eigensystem by an appropriate transformation. The starting vectors selected must span the dominant subspace eigenbasis in a relatively complete mathematical sense by not being orthogonal to this subspace. If the transformation T spans the dominant subspace completely, the eigenvectors are true and the solution is exact. The subset of eigenvectors in the original space is recovered by T. The band Lanczos method when applied to structural problems is similar to Ritz analysis in that eigenvalues are upper bounds and convergence will always be from above; the extent to which this frequency discrepancy is affected by Guyan reduction depends upon the degrees of freedom selected. Though not necessary in the case of band Lanczos method, Sturm sequence technique(29) has been suggested to ensure and verify convergence of all of the dominant eigenvalues with the subspace iteration technique, along with some shifting strategy (23). Frequency shifting accelerates convergence of modes near the shift frequency. Wilkinson (30) analogizes Lanczos method to the Stodola power iteration with shifts.

Shifted Block Lanczos Method has been implemented in MSC/NASTRAN (21,22) for Version 65. A procedure re-orthognalizes Lanczos vectors to maintain accuracy, while multiple frequency shifts permit spanning higher modes in the eigenspectrum. The decision to shift involves a trade-off between convergence error and the cost of triangular decomposition required at each frequency shift. Other performance tradeoffs by Grimes et al (22) show that the input/output cost will vary inversely as the block size, and the CPU cost will vary directly. Parlett (32) also recommends

the block approach with larger block size for problems that require more than available primary computer storage, as the input/output cost of reading and writing large matrices dominates the CPU cost.

Band Lanczos Algorithm

In an earlier paper(14), we described our implementation of the Lanczos-Householder algorithm in ROCKWELL NASTRAN (Level 17.5), based on simple Lanczos method (19,26,28) and Householder re-orthogonalization (31) with respect to all previously generated modes and Lanczos vectors. Weingarten (27) showed by three examples that this method "requires less CPU time than the standard subspace iteration and determinant search" techniques in SAP7. Parlett (32) compared explicitly vectorized versions of the simple Lanczos method and subspace iteration method on Cyber 205 and found the Lanczos method to be at least 10 times more CPU efficent. Several authors have demonstrated the block approach to be even more effective and efficient computationally when solving sparse algebraic eigensystems with large bandwidth for subset of the lowest eigenvalues and corresponding eigenvectors. We selected Parlett's (19) version of the band Lanczos method to enhance performance of the simple Lanczos algorithm in ROCKWELL NASTRAN on IBM and CRAY X-MP computers. However, a few modifications were made to improve the accuracy and cost-effectiveness of the algorithm in ROCKWELL's production version of the April 1984 COSMIC-released NASTRAN.

The modifications incorporated (14,26) are primarily concerned with the selection of starting trial vectors and block size, Householder/Gram-Schmidt re-orthogonalization (31,33,34), explicit/implicit vectorization on CRAY computer, dynamic core allocation, automatic restart with a new randomly generated vector when the Lanczos feed vector becomes null or dominated by numerical noise, and the truncation criteria to achieve the required number of converged eigenpairs.

Described as the FEER method in NASTRAN programmer's manual (28), the simple Lanczos method has been available in COSMIC-released NASTRAN since level 17.5 (1979), including Cholesky decomposition of the mass-shifted stiffnes matrix, forward-backward substitution, and recovery of the physical eigenvectors using Lanczos vectors to transform the truncated eigenvectors of the reduced eigenproblem. Cholesky decomposition is premised on a semi-positive definite matrix. The shift frequency is internally calculated, which permits

calculation of zero-order modes without making the resulting shifted matrix indefinite. Whether eigenvectors are ortho- or mass-normalized, the truncated band matrix is identical. The mathematical equations are well documented (14,26,28).

The band Lanczos method, as implemented in ROCKWELL NASTRAN, is useful for calculating modal frequencies near zero, particularly the fundamental frequencies and the lowest dominant modes. A built-in restart capability (14) assures convergence to maximum cut-off frequecy without a shift. For still higher-order interior modes, a frequency shift, if required, is possible using the simple Lanczos method or even the Inverse Power Method, by appending and sweeping out the modes previously calculated by the band Lanczos method.

Numerical Results

A series of numerical examples have been executed on ROCKWELL NASTRAN using IBM and CRAY versions to validate the Band Lanczos method for production use. Cray wall clock and CPU times are fraction of those for IBM. Rockwell's CRAY X-MP/14 (COS) has 4 million words of central memory to allow cost-effective solution of reasonably large dynamic problems.

The Band Lanczos method implementation affected NASTRAN READ Module subroutines FNXTVC, VALVEC, REIG, FEERBD, QRITER, and WILVEC, resulting in cost savings of 16% to 46% during READ Module execution over the FEER method, for different size problems. The COSMIC NASTRAN method FEER frequently fails to converge on a multiple root and the associated eigenvector. The reduced problem size necessary to determine q eigenpairs accurately was specified as (2q+10) for the FEER (simple Lanczos) method as well as the Band Lanczos method to assure convergence of q user-specified number of roots.

When Guyan reduction was used to reduce 2380 degrees of freedom to 494, the eigensolution time (READ module execution after triangular decomposition) to obtain 40 modes using the band Lanczos method was reduced from 203 CPU seconds to 176, whereas the overrall solution time including the cost of Guyan condensation increased from 211 to 550. A comparison of eigensolution times for FEER (simple Lanczos method) and band Lanczos method as implemented in Rockwell's enhanced version of RPK's April 1984 release of Cray COSMIC/NASTRAN is also presented in Table 1. Rockwell's Cray NASTRAN has been partly optimized to take advantage of the available central memory, dynamically.

CONCLUDING REMARKS

Following are some distinct advantages of using the band Lanczos algorithm as implemented in ROCKWELL NASTRAN:

1. multiple or closely clustered roots can be accurately determined without the risk of missing them or without the necessity of a Sturm sequence property check; this risk seemingly exists with the simple or single-vector Lanczos method as well as the subspace iteration method.

2. local Lanczos re-orthogonalization in Parlett's Band Lanczos algorithm assures purity of the resulting Band matrix (19).

The use of Lanczos vectors looks promising for performing linear and nonlinear dynamic analyses, involving substructuring, in the spirit of component mode synthesis.

REFERENCES

1. Isakson, G.; Pardo, H.; Lerner, E.; and Venkayya, V. B.: ASOP-3: A Program for the Optimum Design of Metallic and Composite Structures subjected to Strength and Deflection Constraints. 18th Structures, Structural Dynamics & Materials Conference, San Diego, Calif., Mar. 21-23, 1977, pp. 93-100.

2. Berke, L.; and Khot, N. S.: Use of Optimality Criteria Methods for Large-Scale Systems. AGARD Lecture Series on Structural Optimization, Oct. 10-18, 1974, AFFDL-TM-74-70-FBR, April 1974.

3. Gupta, V. K.; and Marrujo, F. G.: Minimizing Unbalance Response of the CRBRP Sodium Pumps. Trans. 5th International Conference on Structural Mechanics in Reactor Technology (SMiRT), Paper F8/1, Aug. 1979.

4. Sobieszczanski-Sobieski, J.: Recent Experiences in Multidisciplinary Analysis and Optimization. NASA Conference Publication 2327, April 1984.

5. Bayo, E.; and Wilson, E. L.: Numerical Techniques for the Evaluation of Soil-Structure Interaction Effects in the Time Domain. Report UCB/EERC-83/04, University of California, Berkeley, Feb. 1983.

6. Misel, J. E.; Nennon, S. B.; and Takahashi, D.: Transient Response Dynamic Module Modifications to include Static and Kinetic Friction Effects. 12th NASTRAN User's Colloquium, Orlando, Florida, May 10-11, 1984.

7. Nour-Omid, B.; and Clough, R. W.: Dynamic Analysis of Structures Using Lanczos Coordinates. Report PAM-186, University of California, Berkeley, Nov. 1983.

8. Grooms, H. R.; Merriman, W. J.; and Hinz, P. J.: An Expert/Training System for Structural Analysis. ASME PV&P Conf., New Orleans, Lousiana, June 23-27, 1985.

9. Hughes, P. C.: Space Structure Vibration Modes: How many exist? Which ones are important? Proceedings of the Workshop on Applications of Distributed System Theory to the Control of Large Space Structures, NASA JPL Publication 83-46, pp. 31-48.

10. Guyan, R. J.: Reduction of Stiffness and Mass Matrices. A.I.A.A. Journal Vol. 3, No. 2, 1965.

11. Fox, G. L.: Evaluation and reduction of Errors induced by the Guyan Transformation. 10th NASTRAN User's Colloquium, NASA Conference Publication 2249, May 1982, pp. 233-248. 509-518.

12. Benfield, W. A.; and Hruda, R. F.: Vibration Analysis of Structures by Component Substitution. AIAA Journal, Vol. 9, No. 7, July 1971, pp. 1255-1261.

13. Shabana, A.; and Wehage, R. A.: Dynamic Analysis of Large-Scale Inertia-Variant Flexible Systems. University of Iowa, Technical Report No. 82-7.

14. Gupta, V. K.; Cole, J. G.; and Mock, W. D.: A Cost-Effective Eigensolution Method for Large Systems with Rockwell NASTRAN. presented at CAFEM-7 Seminar, Chicago, Illinois, Aug. 29-30, 1983, published in Nuclear Engineering and Design 78, 1984.

15. Arnold, R. R.; Citerley, R. L.; Chargin, M., and Galant, D., "Application of Ritz Vectors for Dynamic Analysis of Large Structures. Computers & Structures Journal, 1984.

16. Wilson, E. L.; and Itoh, T.: An Eigensolution Strategy for Large Systems. Advances and Trends in Structural Solid Mechanics, A.K. Noor and J.M. Housner, eds., Pergamon Press, 1983, pp. 259-268.

17. Idelsohn, S. R.; and Cardona, A.: A Load-Dependent Basis for Reduced Nonlinear Structural Dynamics. Computers & Structures Journal, Vol. 20, No. 1-3, 1985, pp. 203-210.

18. Ruhe, A.: Implementation Aspects of Band Lanczos Algorithms for Computation of Eigenvalues of Large Sparse Symmetric Matrices. Mathematics of Computation, Vol. 33, No. 146, April 1979, pp. 680-687.

19. Parlet, B. N.: The Symmetric Eigenvalue Problem, Prentice-Hall, 1980.

20. Underwood, R.: An Iterative Block Lanczos Method for the Solution of Large Scale Symmetric Eigenproblems. Report STAN-CS-75-496, Stanford Univerisity, 1975.

21. Mera, A.: MSC/NASTRAN Normal Mode Analysis with GDR: An Evaluation of Limitations. MSC/NASTRAN User's Conference, Mar. 1985.

22. Grimes, R. G.; Lewis, J. G.; Simon, H. D.; and Komzsik, L.: Shifted Block Lanczos Algorithm in MSC/NASTRAN. MSC/NASTRAN User's Conference, Mar. 1985.

23. Wilson, E. L.; Yuan, M.; and Dickens, J. M.: Dynamic Analysis by Direct Superposition of Ritz Vectors. Mathematics of Computation, Vol. 33, No. 146, April 1979, pp. 680-687.

24. Bathe, K-J: Finite Element Procedures in Engineering Analysis, Prentice-Hall, 1982.

25. Dong, S. B.: A Block-Stodola Eigensolution Technique for Large Algebraic Systems With Non-Symmetrical Matrices. International Journal for Numerical Methods in Engineering, Vol. 11, pp. 247-267, 1977.

26. Ojalvo, I. U.: Proper Use of Lanczos Vectors for Large Eigenvalue Problems. Computers & Structures Journal, Vol. 20, No. 1-3, 1985, pp. 115-120.

27. Weingarten, E. I.; Ramanathan, R. K.; and Chen, C. N.: Lanczos Eigenvalue Algorithm for Large Structures on a Mini-Computer. Advances and Trends in Structural Solid

Mechanics, A.K. Noor and J.M. Housner, eds., Pergamon Press, 1983, pp. 253-258.

28. The NASTRAN Prpogrammer's Manual (Level 17.5), National Aeronautics and Space Administration (NASA), Washington, D.C., NASA SP-223(05), Dec. 1978.

29. Gupta, K. K.: Eigenproblem Solution by a combined Sturm Sequence and Inverse Iteration. International Journal for Numerical Methods in Engineering, Vol. 1, 1973, pp.17-42, 509-518.

30. Wilkinson, J. H.: The Algebraic Eigenvalue Problem, Clarendon Press, Oxford, 1965.

31. Golub, G.H.; Underwood, R.; and Wilkinson, J. H.: The Lanczos Algorithm for the Symmetric Eigenvalue Problem, Report Stan-CS-72-270, Stanford University, Palo Alto, Calif., 1972.

32. Natvig, J.; Nour-Omid, B.; and Parlett, B. N.: Effect of the Cyber 205 on Methods for Computing Natural Frequencies of Structures. Report PAM-218, University of California, Berkeley, March 1984.

33. Daniel, J. W.; Gragg, W. B.; Kaufman, L.; and Stewart, G. W.: Reorthogonalization and Stable Algorithms for Updating the Gram-Schmidt QR Factorization. Mathematics of Computation, Vol. 30, 1976, pp. 772-795.

34. Parlett, B.; and Scott, D. S.: The Lanczos Algorithm with Implicit Deflation. Report ERL M77/70, Univerisity of California, Berkeley, 1977.

TABLE 1 Time Comparison (CPU seconds)

Problem 1: 2380 Degrees of freedom, 2-D plate model			
Method:	Cosmic FEER	Rockwell Band LANCZOS	
Guyan Reduction:	NO	NO	YES
IBM 3081	307	203(211)	176(550)
IBM 3090	144	95(99)	79(216)
CRAY X-MP	90	48(52)	74(154)
Problem 2: 6006 Degrees of freedom, 8-node brick model			
CRAY X-MP	680	596(971)	--

FLUTTER ANALYSIS OF LOW ASPECT RATIO WINGS

L. A. Parnell
Naval Ocean Systems Center, San Diego, CA

SUMMARY

Several very low aspect ratio flat-plate wing configurations are analyzed for their aerodynamic instability (flutter) characteristics. All of the wings investigated are delta planforms with clipped tips, made of aluminum alloy plate and cantilevered from the supporting vehicle body. Results of both subsonic and supersonic NASTRAN aeroelastic analyses as well as those from another version of the program implementing the supersonic linearized aerodynamic theory are presented. Results are selectively compared with published experimental data. Subsonic predictions are found to be reasonably consistent with the experimental data; however, supersonic predictions of the Mach Box method in NASTRAN are found to be erratic and erroneous, requiring the use of a separate program.

INTRODUCTION

Very low aspect-ratio wings are commonly used to control high speed missiles and new configurations of the wings are considered as missile designs are developed having different flight characteristics and design constraints than their predecessors. An analysis of the aeroelastic behavior of these wings is required to assure stable operation of the new configuration throughout the flight of the missile. This paper reports an evaluation of the aeroelasticity capabilities of NASTRAN in the performance of such an analysis. A thorough investigation is made of the flutter characteristics of two wing configurations, with results compared to published experimental data.

MODEL DESCRIPTION

The wings evaluated in this paper are of a flat-plate configuration with a clipped-tip delta planform and a large leading edge sweep angle. Two wing root chords were examined, having aspect ratios of 1.17 and 1.91, respectively. Aeroelastic instability was calculated throughout a wide Mach number range, both subsonic and supersonic. Both of the wings are assumed to be made of 6061 aluminum alloy plate with leading edges beveled as shown in figure 1. The presence of beveling was not included in the structural or aerodynamic models, however, as including such small details would have substantially increased the complexity of the finite element models with only modest improvement in the accuracy of the results.

Each wing evaluated in the investigation was modeled as a structure rigidly fixed at its line of intersection with the missile. Although such a model ignores the attachment flexibility which may be present at the root of the wing and neglects the strains which occur locally in the support shell, it can be shown that disregarding the additional flexibility provided by typical attachment methods has little effect on the predictions of the natural vibration (and, thus, flutter) characteristics of the wings. Similarly, the models idealize with little adverse effect the forward end of the leading edge of each wing as extending

to a point, rather than being truncated as is necessitated by typical wing attachment methods. Figure 2 shows the finite element mesh, Doublet-Lattice panel boxes (for the subsonic regime) and a typical Mach Box surface (for the supersonic regime) used in the analysis of one of the wings. The number and distribution of finite elements and panels changed with wing configuration and the Mach Box surfaces were different for each Mach number as well. Nevertheless, the diagrams in the figure are representative of all of the models generated in the investigation.

ANALYSIS PROCEDURE

Flutter analysis using the aeroelastic capabilities of the NASA Structural Analysis program, NASTRAN (ref. 1-3), begins with development and verification of a finite element structural model which will provide accurate normal vibration mode predictions. After giving consideration to the modeling limitations described in the previous section, the idealized structural finite element models were generated using undamped triangular and quadrilateral plate elements which have both bending and inplane stiffness and coupled mass matrices; the number and distribution of elements were selected to approximate equilateral triangles and unit-aspect-ratio quadrilaterals, as nearly as could be done practically. A fixed boundary at the wing roots and constraints on the remaining elements were employed to eliminate unimportant (inplane) vibration modes. Mode shapes and eigenvalues (natural frequencies) were determined by Givens' tridiagonal method (ref. 1,4). The validity of the resulting model's representation of the vibration modes and frequencies of actual delta wing structures was ascertained by comparing representative results with published experimental data. Appendix A presents such a comparison between predictions for the two wings considered in this paper and data from reference 5.

Having confirmation that the normal modes representation of the wings is accurate, the aerodynamic analysis proceeds by utilizing the eigenvectors as the generalized coordinates for the flutter solution; with NASTRAN, the analyst has a choice of the aerodynamic theory and the flutter method to be used. In this paper flutter in subsonic flow was predicted using the Doublet-Lattice aerodynamic theory and the usual American K-method of solving the dynamic aeroelastic stability problem. The supersonic problem was solved by means of the Mach Box program developed by Donato and Huhn (ref. 6), both as implemented in NASTRAN (ref. 3) and with another version of the program (ref. 7).

The definition of the Doublet-Lattice panel boxes is at the complete discretion of the analyst. Those shown in figure 2(b) typify the number and distribution used throughout this paper and follow recommended practice† that all aerodynamic boxes have an aspect ratio between one and two (and as close to unity as is practical). The Mach boxes, cf. figure 2(c), are determined by the analyst's choice of their spanwise number and by the requirement that each box have a diagonal parallel to the Mach line. Details of the aerodynamic computation are done internally by the computer codes, including actual generation of the aerodynamic grid points, computation of the steady and oscillatory air loads, transformation of the aerodynamic influence coefficients into modal coordinates and providing the interconnections between the aerodynamic and structural degrees of freedom through surface splines. The codes then generate numerical solutions to the linearized, three- dimensional unsteady perturbation potential flow equation, transform the results into physical coordinates and provide the pertinent output, viz. summaries providing flutter velocity (V_f) and frequency (F_f), artificial structural damping (g) and reduced frequency (k) for all modes, Mach numbers and air density ratios selected by the analyst. Plots showing velocity-damping and velocity-frequency curves are provided to assist in evaluation of the

† Aeroelasticity analysis conventions and recommendations were kindly provided by R. Ricketts and R. Doggett, Configuration Aeroelasticity Branch, NASA Langley Research Center.

results of the computations.

As the solution to the equation for modal flutter analysis is valid only when the artifical damping is zero (cf. ref. 1), tabular results must be interpolated for a given mode to determine values of k, V_f and F_f at the flutter point. Computations to determine the flutter velocity were repeated several times with different air density ratios (altitudes), and plotted against missile flight speeds in order to interpolate to the Match Point at a given Mach number, i.e., that air density ratio where the speed at which flutter occurs corresponds to the missile speed. The collection of these Match Points forms the flutter curve in which the subsonic and supersonic results may be joined by assuming a transonic dip in the flutter dynamic pressure, q_f , of 30% of the Mach 0.5 value to estimate q_f at the speed of sound. This curve is then compared with the missile flight envelope on a dynamic pressure vs. Mach number plot to determine the aerodynamic stability of a wing design when used on a given missile.

The theoretical predictions in this paper were evaluated in several ways to establish their validity. As the dynamic aeroelastic analysis approach implemented in NASTRAN for both subsonic and supersonic flow is the modal method, all results depend on accurate determination of the natural vibration modes of the structure and this was verified as mentioned previously. A check of the aerodynamic analysis procedures and computational results used for evaluation of the wings considered was made at the outset of the study by comparing NASTRAN flutter predictions with published experimental and theoretical results for a delta planform wing (ref. 8). Appendix B presents results of this comparison. Erratic behavior of the NASTRAN supersonic Mach Box predictions was subsequently noted, so the separate program of ref. 7 was used to repeat the analysis of the wings.

RESULTS AND DISCUSSION

The predicted behavior of the wings evaluated are summarized in tables I and II. The first five modal frequencies of each wing and the range of selected flutter parameters are listed in table I. A detailed summary of all the predicted flutter characteristics is listed in table II for each Mach number investigated. A plot of the dynamic pressure, q, as a function of Mach number for the theoretical flutter condition of both wing configurations is shown in figure 3. In this figure, all points plotted represent an instability condition. Flutter will occur at those Mach numbers where a flight envelope (plus a margin) drawn on the figure falls above the instability curve. As the nearly horizontal subsonic curves in figure 3 should have a positive slope, reflecting less dynamic pressure at the lower Mach numbers (cf. Appendix B), substantial unconservative errors in the Doublet-Lattice predictions are indicated there. Predictions of both the NASTRAN and ref. 7 implementations of the Mach Box program are shown in the figure and listed in table II. Although the NASTRAN Mach Box predictions are more conservative than those of ref. 7, the substantial differences (e.g., averaging 24.8% in q) and clearly erroneous results which were encountered at times in the analyses preclude the use of that NASTRAN procedure with any confidence until improvements are made in those computer routines.

It is instructive to note that flutter characteristics for wings having planforms similar to that considered in this paper can be inferred from presented results through the scaling law,

$$\frac{q}{q_o}\left(\frac{l}{l_o}\right)^4 = \frac{EI}{(EI)_o}.$$

This scaling law permits estimates of the flutter characteristics of wings having similar planforms to one of the configurations examined but having different materials, thicknesses or characteristic lengths. For

example, if a wing is made of a different gage material but is otherwise identical to a wing whose aerodynamic characteristics are known, the ratio of flutter dynamic pressures of the two wings would be proportional to the third power of their thickness ratio.

CONCLUDING REMARKS

The flutter analyses reported in this paper have demonstrated that the aeroelasticity capability is a powerful extension to the NASTRAN program's widely used structural and dynamics analysis procedures. Comparison of predictions with experimental data has verified that conventional modeling methods, analysis procedures and the NASTRAN computational routines have, in general, produced accurate predictions. The ease with which both structural and aeroelasticity analyses may proceed in conjunction with one another in the development of new aircraft or missile designs make the aeroelastic capability in NASTRAN a very convenient as well as useful feature of the program. However, the Mach Box program implementation in NASTRAN apparently has either errors or limitations in the algorithms which currently preclude recommending its use, at least for the low aspect ratio wing configurations examined in this paper.

SYMBOLS

A	aspect ratio of wing
b	root chord, cm
c	velocity of sound, m/s
D	flexural rigidity, Nm
E	modulus of elasticity, kPa
f	frequency, Hz
g	artificial damping
I	moment of inertia, cm^4
k	reduced frequency ($\omega b/2V$)
l	semi-span of wing, cm
M	Mach number
q	dynamic pressure, Pa
t	wing thickness, cm
V	velocity, m/s
γ	density of wing material, Kg/m^3
Δ	relative difference
Δl	length of wing clipped, cm
μ	Poisson's ratio
ρ	air density, Kg/m^3
ω	wing circular frequency, 1/s

Subscripts

f	flutter
n	mode number
o	reference value

REFERENCES

1. "The NASTRAN Theoretical Manual," SP-221(05), NASA Scientific and Technical Information Office, Washington, D.C., June 1985.

2. "The NASTRAN User's Manual," SP-222(05), NASA Scientific and Technical Information Office, Washington, D.C., January 1981.

3. Rodden, W.P., R.L. Harder and E.D. Bellinger, "Aeroelastic Addition to NASTRAN," NASA CR-3094, March 1979.

4. Givens, W. "Numerical Computation of the Characteristic Values of a Real Symmetric Matrix," Oak Ridge National Lab., ORNL-1574, 1954.

5. Gustafson, P.N., W.F. Stokey and C.F. Zorowski, "The Effect of Tip Removal on the Natural Vibrations of Uniform Cantilevered Triangular Plates", J. Aeronaut. Sci, 21:621 (1954).

6. Donato, V.W. and C.R. Huhn, Jr., "Supersonic Unsteady Aerodynamics for Wings with Trailing Edge Control Surfaces and Folded Tips," Air Force Flight Dynamics Lab., AFFDL-TR-68-30, August 1968.

7. "MBOXTI", the AFFDL MBOX computer code with revisions and updates by Texas Instruments, Inc. and E.L. Jeter, Naval Weapons Center, China Lake, CA, 1984.

8. Hanson, P.W. and G.M. Levey, "Experimental and Calculated Results of a Flutter Investigation of Some Very Low Aspect-Ratio Flat-Plate Surfaces at Mach Numbers from 0.62 to 3.00," NASA TN D-2038, 1963.

APPENDIX A. NORMAL MODES OF WINGS A AND B

In order to determine the accuracy of normal mode calculations for the wings evaluated in this paper, predictions are compared with known characteristics of built-in, clipped triangular plates. Using the procedures described in reference 5, the unknown modal frequencies of a plate with planform similar to that of one whose vibration characteristics have been experimentally determined are given by

$$\omega' = \omega_D \sqrt{D' / (\gamma' t' l_o'^4)} \qquad \text{(A-1)}$$

where primed quantities refer to the plate in question and unprimed to the known reference plate. In equation (A-1) $\omega_D = \omega \sqrt{\gamma t l_o^4 / D}$ is the dimensionless angular frequency of the plate based on its semi-span and flexural rigidity, $D = Et^3/[12(1-\mu^2)]$. Frequency data and mode shapes are presented in reference 5 for plates with aspect ratios of 2 and 4 having clipping fractions, $\Delta l/l_o$, between zero (full triangle) and 0.4. As that work reports linear variation in natural frequency with aspect ratio and good results when interpolating between clipping fractions, characteristics of both wings examined in this paper may be inferred from the published data. The procedure consists of utilizing curves of frequency shift, $\Delta\omega/\omega$, as a function of clipping fraction to interpolate the experimental data to the amount of clipping for the wings evaluated, followed by interpolation between unclipped aspect ratios to the actual

wing configuration. For wing B the clipping fraction is $\Delta l/l_o = 0.270$ and the unclipped aspect ratio is $A_o = 2.038$. Table A-I shows interpolation of the experimental data to these characteristics.

Comparing the interpolated data from reference 5 with the results of the finite element model shows less than 5% error in the NASTRAN frequency predictions for the five modes used in the flutter analysis, as listed in table A-II(b). The mode shapes (eigenvectors) determined by the NASTRAN analysis are presented in figure A in the form of contour plots. Comparing these predictions with the mode line photographs of reference 5 shows excellent agreement and completes validation of the finite element model used for modal formulation of the aerodynamic instability analysis.

A similar interpolation of experimental data of reference 5 to the configuration of wing A is given in tables A-III and A-II(a). The NASTRAN predictions are not as good as in the wing B configuration, showing up to 9% deviation from experimental results. This larger error is due to the use of a coarser grid of elements for the wing A model (21 total elements) than for the wing B model (45 total elements). These errors are, however, small enough to validate use of the finite element model used in the flutter analysis of wing B.

APPENDIX B. COMPARISON OF NASTRAN PREDICTIONS WITH EXPERIMENTAL FLUTTER CHARACTERISTICS OF A NASA WING.

As a means of verifying the validity of the procedures used in this paper, a flutter analysis was performed on a delta wing whose measured characteristics were reported in reference 8. Model 1A of that reference was evaluated for both subsonic and supersonic flutter conditions using the NASTRAN Doublet-Lattice and Mach Box methods, respectively. Figure B-1 shows the model geometry and reported node lines for the model. Modal results for the triangular plate were obtained using an 18-element matrix composed of 15 quadrilateral and 3 triangular elements. Table B-I presents a comparison of experimental and predicted modal frequencies for the model.

The aeroelastic instability analyses used 48 Doublet-Lattice panel boxes for subsonic flow and 20 chordwise Mach boxes for supersonic flow (the number of spanwise boxes being determined by Mach number). Numerical results were obtained using the same methodology as was employed in the remainder of this paper. They are compared with the experimental data of reference 8 in table B-II and plotted in figure B-2. Although these comparisons show substantial predictive errors, those in the important parameter of flutter dynamic pressure, q, are acceptable. The error is large only at the lowest Mach number examined. For the highest (and most critical) Mach number compared, excellent agreement occurs in this parameter, especially when the rather poor modal results (shown in table B-I) are considered.

As the modal comparisons used in the body of this paper are substantially better than those shown in this appendix, the aeroelasticity predictions may be expected to be correspondingly improved. In addition, even though the errors in the dynamic pressure predictions in this appendix are large at times, they are, with the exceptions of the lowest speed condition, well within the flutter margin normally imposed on vehicle flight envelopes. The large low-speed error is an unconservative instability prediction in this regime and indicates that the nearly horizontal theoretical curves shown in figure 3 should show a reduction at the lower Mach numbers.

TABLE I. MODAL FREQUENCIES AND FLUTTER ANALYSIS CONDITIONS

Wing	Modal Frequencies (Hz)					Range of Flutter Conditions		
	f_1	f_2	f_3	f_4	f_5	M	ρ/ρ_o	F_f(Hz)
A	203.5	560.7	1118	1167	1887	.50 - 1.75	9.47 - 14.1	362.8 - 824.5
B	140.1	310.3	590.7	815.5	996.1	.50 - 2.00	3.09 - 9.55	202.3 - 243.3

TABLE II. THEORETICAL FLUTTER PREDICTIONS

Wing	M	Flutter Conditions †					
		ρ/ρ_o	k	V (m/s)	q (MPa)	c (m/s)	f_f (Hz)
A	0.50	14.1	1.082	456	1.794	911	442.1
	0.60	12.2	0.967	497	1.843	828	430.0
	0.70	10.9	0.858	538	1.926	768	412.7
	0.80	9.80	0.754	579	2.040	724	390.3
	0.90	9.07	0.653	622	2.149	691	362.8
	1.20	6.92	0.929	716	2.176	597	600.4
	1.50	8.32	0.825	991	5.003	660	730.1
	1.75	9.47	0.744	1240	8.931	709	824.5
B	0.50	9.55	0.956	357	0.744	713	237.7
	0.60	8.05	0.864	388	0.743	647	233.2
	0.70	6.93	0.776	419	0.746	599	226.5
	0.80	6.14	0.693	451	0.766	564	216.7
	0.90	5.50	0.604	482	0.782	535	202.3
	1.50	3.76	0.978	691	1.099	461	235.5
	1.75	3.40	0.886	779	1.267	445	240.5
	2.00	3.09	0.811	864	1.411	431	243.3
B (NASTRAN)	1.50	3.26	0.36	658	0.866	439	
	1.75	2.76	0.32	728	0.898	416	
	2.00	2.63	0.28	815	1.072	408	

† Subsonic predictions obtained from NASTRAN (ref. 1-3), supersonic from ref. 7 except as noted.

TABLE A-I. NORMAL MODES OF WING B

(a) Determination of Frequency Shifts for the Specific Clipping Fraction.

Mode	ω''_D ($\frac{\Delta l}{l} = 0$) †		$\frac{\Delta\omega}{\omega_o}$ ($\frac{\Delta l}{l} = 0.270$) ††		ω''_D ($\frac{\Delta l}{l} = 0.270$)	
	Series I	Series II	Series I	Series II	Series I	Series II
1	5.50	5.87	.339	.379	7.365	8.095
2	14.7	23.8	.186	.172	17.43	27.89
3	27.5	32.4	.539	.331	42.32	43.12
4	29.8	56.1	.036	.166	30.87	65.41
5	46.5	76.0	.090	.366	50.68	103.82
6	57.0	99.7	.068	.103	60.88	109.97

Aspect ratio of unclipped plates: A_o = 2 (Series I), 4 (Series II).

† Data from Tables 1 and 3, reference 5.
†† Taken from Figures 8 and 9, reference 5.

(b) Interpolation Between (Unclipped) Aspect Ratios.

Mode	ω''_D *	Wing B **	
		ω''_B	f_B
1	7.38	852	136
2	17.6	2036	324
3	42.3	4888	778
4	31.5	3640	579
5	51.7	5969	950
6	61.8	7137	1136

* $\omega''_{D_n} = \omega''_{D_{I_n}} + \frac{0.038}{2.0}(\omega''_{D_{II_n}} - \omega''_{D_{I_n}})$

** $\omega''_B = \omega''_D \sqrt{D / \gamma h l_o^4} = 115.5\omega''_D$, $f_B = \frac{\omega''}{2\pi} = 18.38\omega''_D$

TABLE A-II. COMPARISON OF NATURAL MODES OF LOW ASPECT RATIO WINGS

(a) Wing A.

Mode	Frequency (Hz)		
	Experimental †	NASTRAN *	Δ (%)
1	202	203.5	-0.74
2	543	560.7	-3.2
3	1040	1118.0	-7.0
4	1094	1167.4	-6.3
5	1719	1886.7	-8.9
6	2096	2323.7	-9.8

(b) Wing B.

Mode	Frequency (Hz)		
	Experimental †	NASTRAN *	Δ (%)
1	136	140.1	-2.9
2	324	310.3	4.4
3	579	590.7	-2.0
4	778	815.5	-4.6
5	950	996.1	-4.6
6	1136	1213.	-6.3

† As interpolated from data of reference 5 to the configuration (aspect ratio and clipping fraction), dimensions and materials of the wings examined.

* Using Givens method with coupled mass matrices. A total of 21 elements were used for wing A, 45 for wing B.

TABLE A-III. NORMAL MODES OF WING A

(a) Determination of Frequency Shifts for the Specific Clipping Fraction.

Mode	$\omega^{\sim}_D$ ($\frac{\Delta l}{l} = 0$) †		$\frac{\Delta\omega}{\omega}$ ($\frac{\Delta l}{l} = 0.061$) ††		$\omega^{\sim}_D$ ($\frac{\Delta l}{l} = 0.061$)	
	Series I	Series II	Series I	Series II	Series I	Series II
1	5.50	5.87	.017	.042	5.59	6.116
2	14.7	23.8	.011	.022	14.86	24.32
3	27.5	32.4	.045	.022	28.74	33.11
4	29.8	56.1	0.0	.011	29.8	56.72
5	46.5	76.0	.011	.056	47.01	80.26
6	57.0	99.7	.005	0.0	57.28	99.7

Aspect ratio of unclipped plates: A_o = 2 (Series I), 4 (Series II).

† Data from Tables 1 and 3, reference 5.
†† Taken from Figures 8 and 9, reference 5.

(b) Interpolation Between (Unclipped) Aspect Ratios.

Mode	$\omega^{\sim}_D$ *	Wing A **	
		$\omega^{\sim}_A$	f_A
1	5.60	1270.	202.
2	15.0	3410.	543.
3	28.8	6534.	1040.
4	30.3	6872.	1094.
5	47.6	10801.	1719.
6	58.1	13169.	2096.

* $\omega^{\sim}_{D_n} = \omega^{\sim}_{D_{I_n}} + \frac{0.038}{2.0} (\omega^{\sim}_{D_{II_n}} - \omega^{\sim}_{D_{I_n}})$

** $\omega^{\sim}_A = \omega^{\sim}_D \sqrt{D / \gamma h l_o^4} = 226.7 \omega^{\sim}_D$, $\quad f_A = \frac{\omega^{\sim}_A}{2\pi} = 36.07\, \omega^{\sim}_D$

TABLE B-I. FREQUENCY COMPARISONS WITH A NASA DELTA-WING MODEL

(a) Selected Experimental Frequencies (from Ref. 8, Table I, Model 1A).

M	Frequency (Hz)			
	F_1	F_2	F_3	F_4
0.64	72	171	320	367
0.79	79	193	350	396
1.30	75	120	305	367
2.00	75	173	320	379

(b) Natural Frequency Comparison.

Mode	Frequency (Hz)		
	Experimental †	NASTSRAN ††	Δ(%)
1	75.2	85.9	14.2
2	176.8	209.2	18.4
3	323.8	389.2	20.2
4	377.2	475.4	26.0

† Average of data in table (a). †† Using 18 elements.

TABLE B-II. FLUTTER CHARACTERISTICS OF A NASA DELTA WING MODEL

M	Experimental Results †			NASTRAN Predictions ††			Δ(%)		
	ρ/ρ_o	q (kPa)	f_f	ρ/ρ_o	q (kPa)	f_f	ρ/ρ_o	q	f_f
0.64	0.6064	16.9	150	0.8621	24.3	165	42.2	43.2	9.9
0.79	0.6186	25.5	150	0.6350	25.6	154	2.7	0.6	2.5
1.30	0.3305	30.8	150	0.2801	25.5	104	-15.2	-17.3	-30.5
2.00	0.2489	40.5	153	0.2061	44.3	110	-17.2	9.3	-27.8

† From Table I Model 1A of ref. 8.

†† Using modal results shown in Table B-I, 48 Doublet-Lattice panel boxes (for subsonic predictions) and 20 chord-wise Mach boxes (for supersonic predictions).

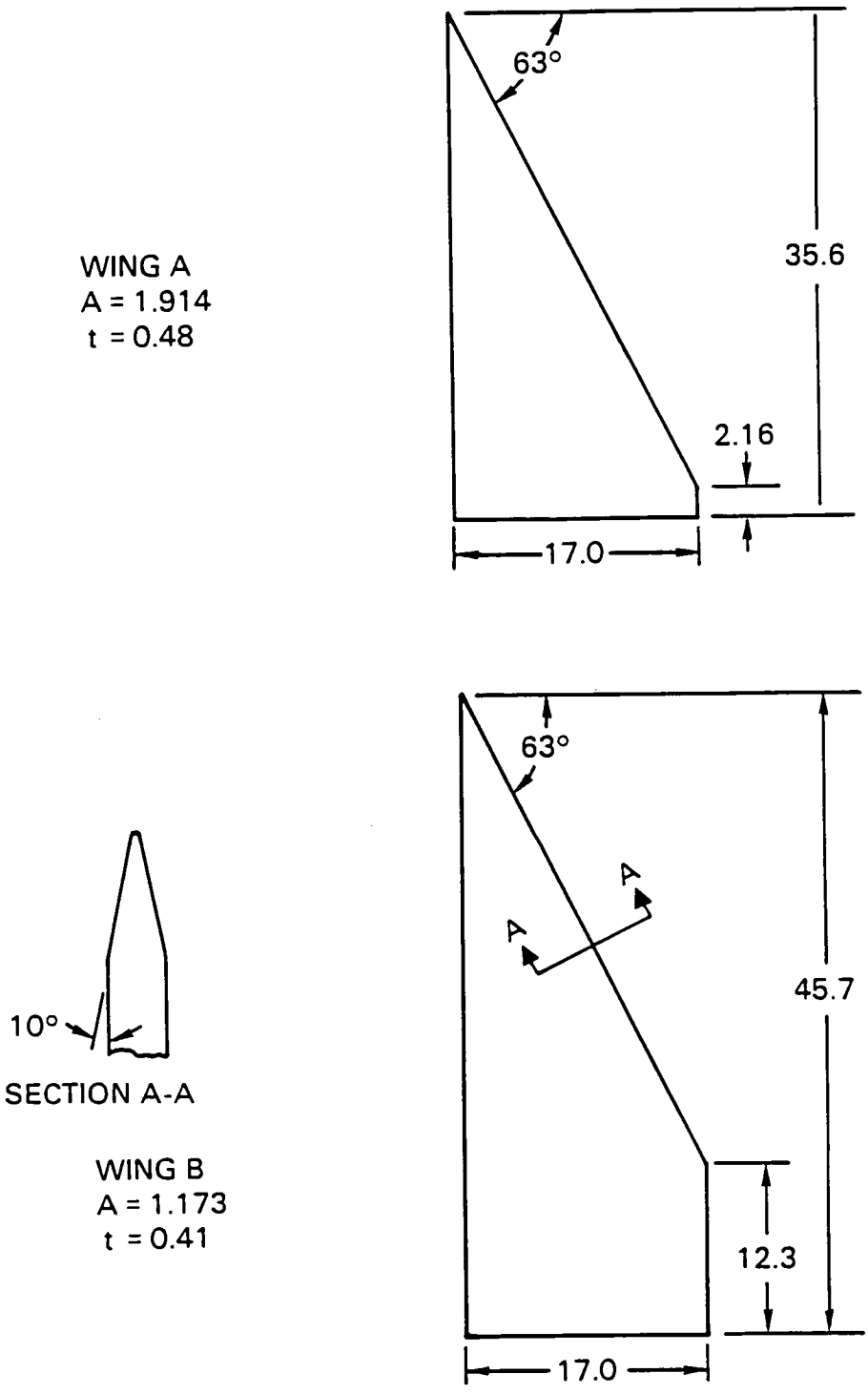

Figure 1. Wing geometries.

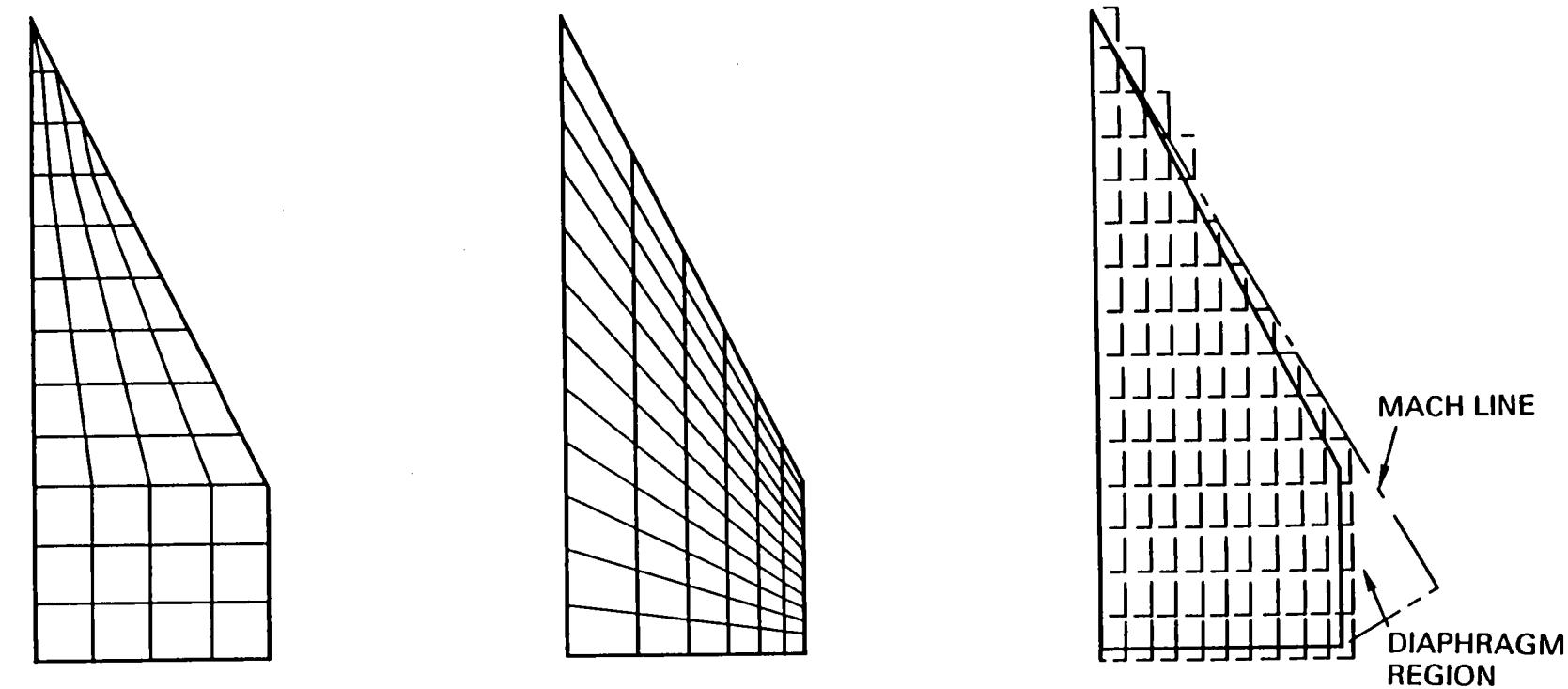

(a) FINITE ELEMENTS

(b) DOUBLET-LATTICE PANEL BOXES

(c) MACH BOXES (M = 2.0)

Figure 2. Wing B model characteristics.

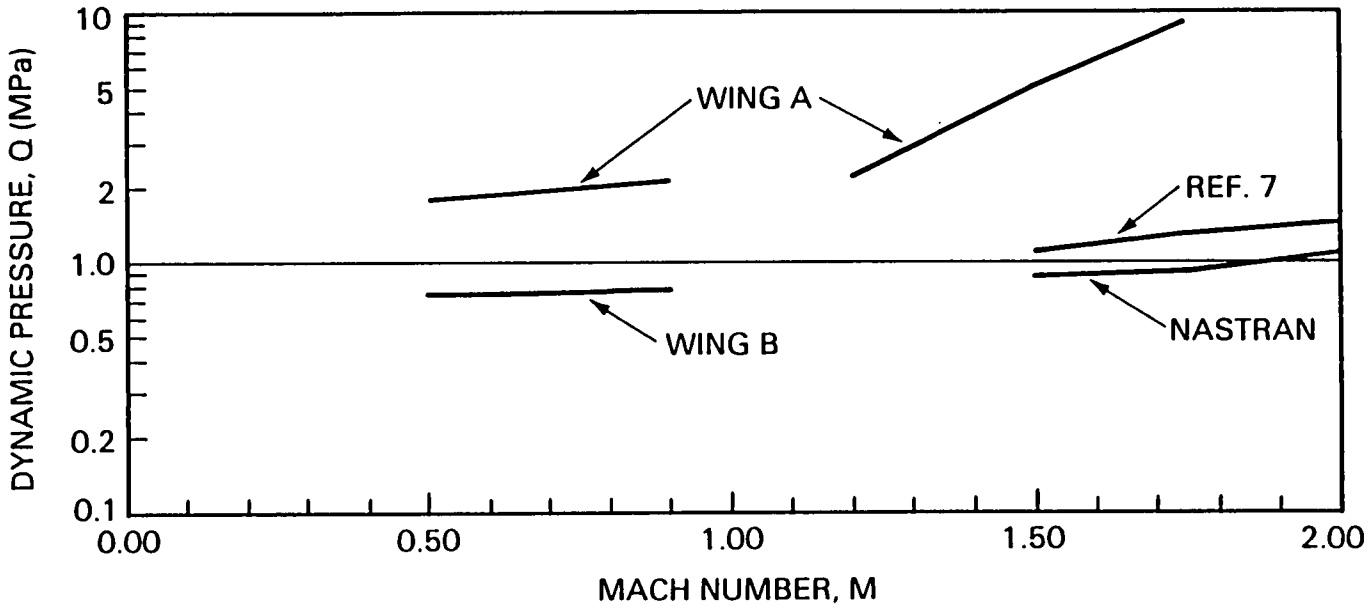

Figure 3. Flutter characteristics of wings A, B.

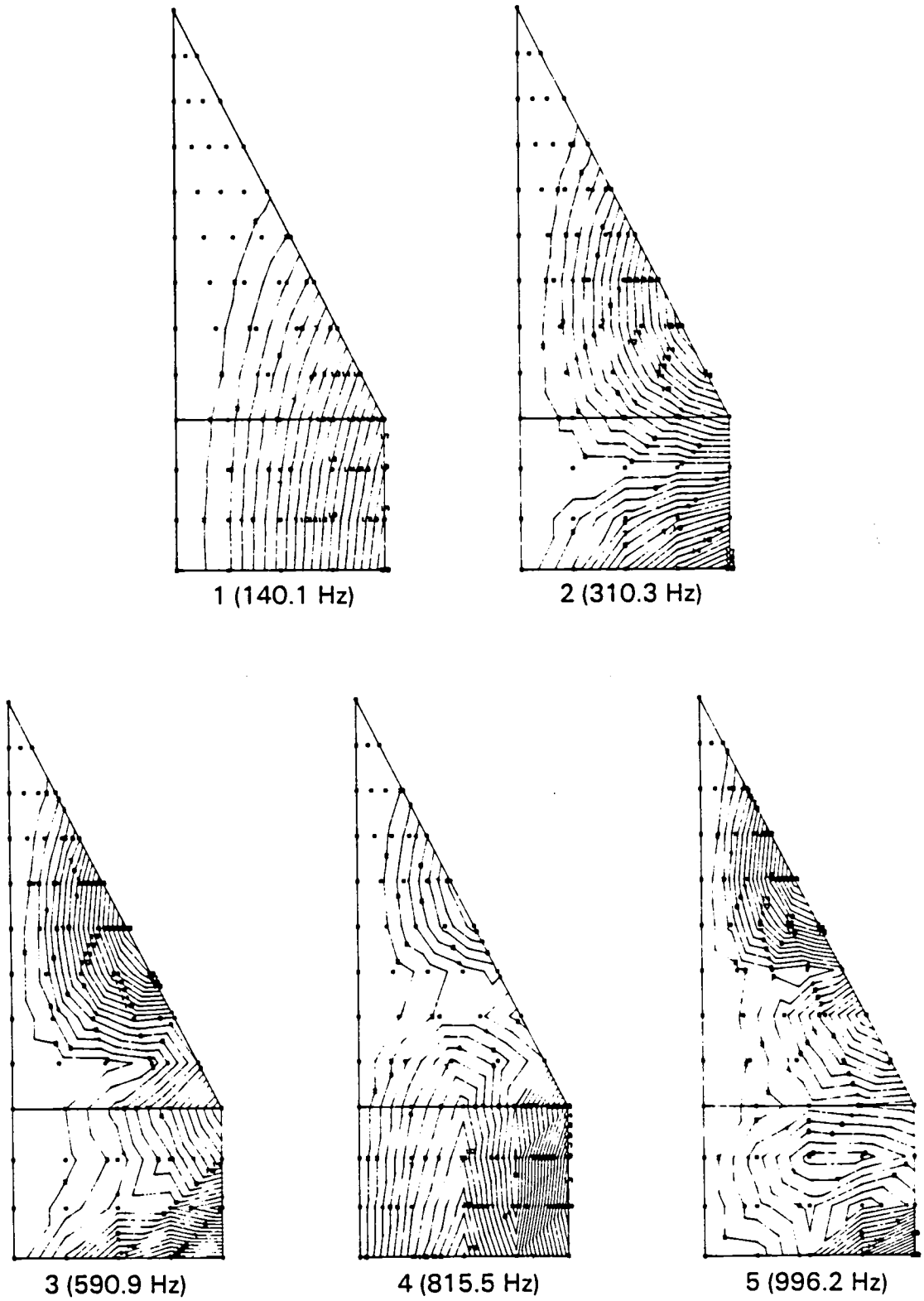

Figure A. Mode shapes and frequencies of Wing B as predicted by NASTRAN.

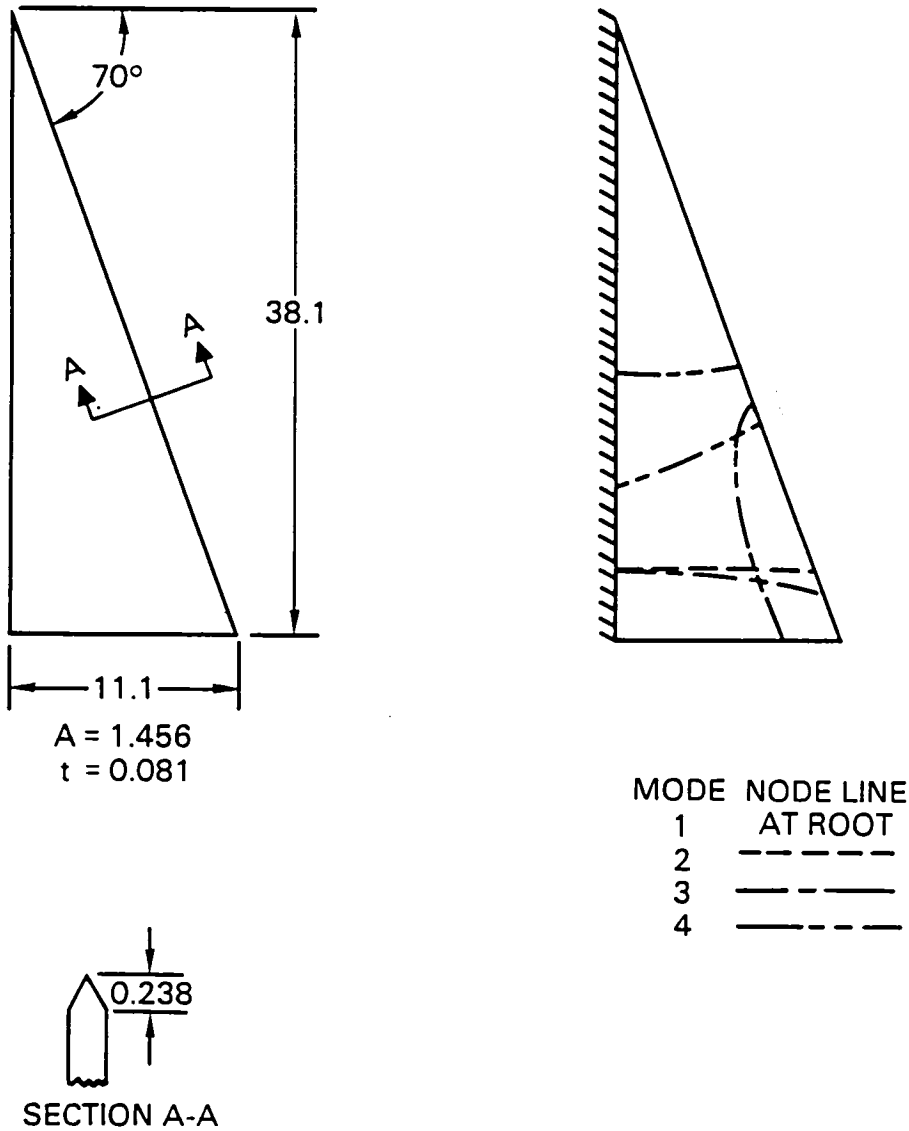

Figure B-1. Geometry and node lines for model 1A of reference 8.

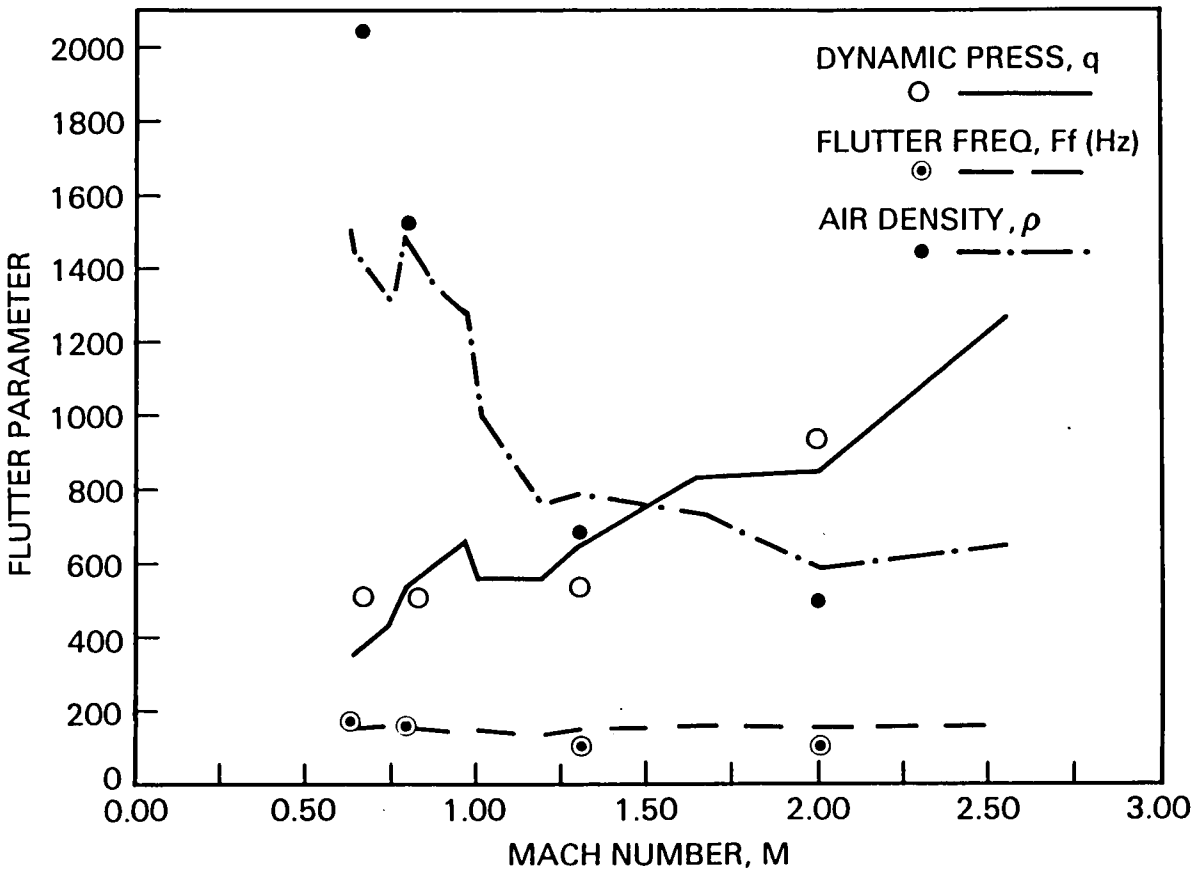

Figure B-2. Flutter characteristics of a NASA delta-wing model. Lines are experimental data of reference 8. Symbols are NASTRAN predictions.

FINITE ELEMENT MODELLING OF NON-LINEAR MAGNETIC CIRCUITS USING COSMIC NASTRAN

T. J. SHEERER

TEXAS INSTRUMENTS
DATA SYSTEMS GROUP

ABSTRACT

The general purpose Finite Element program COSMIC NASTRAN currently has the ability to model magnetic circuits with constant permeablilities. An approach has been developed which, through small modifications to the program, allows modelling of non-linear magnetic devices including soft magnetic materials, permanent magnets and coils. Use of the NASTRAN code results in output which can be used for subsequent mechanical analysis using a variation of thesame computer model. Test problems have been found to produce theoretically verifiable results.

INTRODUCTION

Several computer programs exist for the modelling of Magnetic Scalar or Vector Potential by the Finite Element Method [1,2,3], although most are not well-suited for applications to magneto-mechanical design. The close analogy between the equations of Steady-State Heat Transfer and Magnetostatics has been noted [4,5] and for the linear (constant permeability) case it has been shown that NASTRAN's Heat Transfer capabilities produce theoretically verifiable solutions to Magnetostatic problems. Several features have already been added to NASTRAN to take advantage of this [6]. The analogy between the equations of Heat Transfer and Magnetostatics are not exact, however, in the non-linear case, and existing Rigid Formats cannot be used. In this paper a method is described wherein, using DMAP ALTER statements and new NASTRAN modules, non-linear Magnetostatic problems are solved iteratively.

THEORY

There are several formulations of Magnetostatic equations. The most appropriate for this analysis is also the most familiar:

$$B = \mu.H \qquad (1)$$

where B is the Magnetic Flux Density, H is the Magnetic Field Strength and μ the permeability. H is the Magnetic Scalar Potential Gradient where V is the Magnetic Potential

$$H = - \text{ grad}(V) \qquad (2)$$

With this formulation the analogy with Static Heat Transfer is

apparent

$$B = -\mu . \text{ grad}(V) \quad (3)$$

$$\dot{q} = -k . \text{ grad}(T) \quad (4)$$

(where $\dot{q}$ is the normalized heat flow, k the Thermal Conductivity and T the Temperature).

By use of the Thermal analogues of the terms in (3) linear Magnetostatic problems can be solved for V, and the derived quantities B and H obtained by differentiation using the NASTRAN DMAP sequence for Static Heat Transfer Analysis. Table (1) shows the analogies and differences between the two cases. In the non-linear case the permeability, μ, is not constant and varies not as a function of potential, but of potential gradient

$$B = = -\mu \text{ (grad(V))} .\text{grad(V)} \quad (5)$$

Problems of this type are solved iteratively; initial values are assigned to μ and a solution obtained in V. The derived quantity H is used to assign new permeability values to each element of the model from a reference table of B vs. H and the process is repeated until the desired degree of convergence is obtained. This has been done by a modification to the Static Heat Transfer Analysis DMAP sequence of NASTRAN and use of two new modules. It is noted that the Nonlinear Static Heat Transfer Analysis DMAP is less suitable as the iteration is carried out in the modules rather than the DMAP listing, and the non-linear cases are not analogous since k depends on T rather than grad(T)

$$\dot{q} = - k (T) . \text{ grad}(T) \quad (6)$$

IMPLEMENTATION

The Static Heat Transfer Analysis DMAP sequence [7] can be considered to have three segments: (1) Matrix Formulation , (2) Matrix Solution, (3) Result Interpretation. In order to minimize execution time in an iterative modification of the Rigid Format it is required to repeat as little of segment (1) as possible. The iterative process requires that, as new permeability values are obtained for each element, the Global Stiffness Matrix (HKGG) be updated. HKGG is not ordered by element but is generated from the element-ordered Element Stiffness Matrix (HKELM). HKELM is generated immediately prior to HKGG in the DMAP sequence. The effect of changes in permeability can be applied to HKELM by multipling all element records in HKELM by the ratio of old and new permeabilities, after which HKGG is reformulated by a linear combination of terms from HKELM. The bulk of the Matrix Formulation operation are eliminated. This reduces execution times by approximately 40%. In practice it is convenient to give unit permeability (conductivity) values to all material in the Bulk Data File and this create a reference HKELM with unit properties. This file is used by the dummy module MODA to generate an initial

HKELM using data from an external file. After a solution is obtained the module MODC obtains new permeablilty values and creates a new HKELM. The program then loops to the statement forming the HKELM block. Fig(1) shows the sequence and Fig.(2) is a listing of the required DMAP alter statements.

ITERATION METHOD

Successive iterations are performed with new permeability values obtained from linear interpolation of a table of B vs. H for each material type. After a solution is found and H calculated the corresponding value of B is obtained and μ calculated for the next iteration. To avoid instability a damping coefficient of 0.05 to 0.10 is applied in the case of soft materials and of 0.75 to 0.90 for permanent magnets. The large factor is necessary in permanent magnets as, in certain conditions, μ tends to infinity. This condition is unlikely to be a valid physical solution but the large damping factor is required to prevent the iterative process from overshooting the correct solution and approaching the condition. Fig.(3) shows a generalized Magnetic Hysteresis curve. The broken line is an initial magnetization curve while the solid line is the Hysteresis loop. The permeability anywhere on the line is the value of B/H. In the second and fourth quadrants where $B/H < 0$ the value is refered to as B/H rather than μ. In a soft material such as iron values of μ are very large and the coercive force Hc as shown in Fig.(3) is very small. In this case a curve such as Fig.(4) adequately models the material. Fig. (5) shows the second quadrant of a permanent magnet hysteresis curve. This is refered to as a "demagnetization curve" as the magnet is being demagnetized by a negative value of H, and B/H is negative. It is possible to operate a permanent magnet in the first quadrant, but for it to fulfill the purpose of a magnet (ie to produce flux) it must operate in the second or fourth quadrant. The second and fourth quadrants are physically indistinguishable, and the algorithms used for soft materials are also usable for the fourth quadrant of the Magnetization curve, so data on permanent magnets are entered as positive H values and negative B values as in Fig.(6). Materials enclosed by coils may be considered to be subject to an additional magnetizing force which shifts the axis of the Magnetization curve in one direction or other as in Fig.(7). In either case the result is that the Magnetization curve looks like that of a permanent magnet, and the coil may be modelled as such.

VERIFICATION

For verification purposes a simple model on a plate of material in air subect to an external field or potential difference was used. More complex models are not verifiable analytically for realistic material properties in the non-linear case. It has already been shown [4,5] that NASTRAN produces verifiable results for more complex geometries in the linear case, and the non-linear solution method is simply an iteration of linear solutions. In each case tested the solution has been checked for agreement with the equations of Magnetostatics. The

first model discussed here consists of two dissimilar soft magnetic materials in air, subject to an externally applied flux level of 1490 Gauss as in Fig. (8). The magnetic properties are listed in table (2). Convergence to the correct values of B in both materials occurs in about ten iterations with a 10 % damping coefficient as shown in Fig(9). In the absence of damping the iterations oscillate about the correct solution. The second model (Fig(10)) is of a permanent magnet in air subject to a fixed potential difference. Table (3) lists the demagnetization curve. In this case convergence occurs in six iterations with 90 % damping as shown in Fig. (11).

CONCLUSIONS

An iterative method has been demonstrated for the application of NASTRAN to non-linear magnetostatic problems. The method is shown to work for simple cases. Refinement is required in the modelling of anisotropic materials, and in the modelling of hysteresis effects by means of restarts with varying loads. The method as developed thus far is comparable with some specialized programs and has the advantage of commonality with the NASTRAN program and the inherent flexibility thereof.

REFERENCES

[1]: J. Simpkin and C. W. Trowbridge, IEE Proc., Vol. 127, 368-374 (1980)
[2]: J. L. Brauer, Research and Development, 71-73 (Dec. 1984)
[3]: M.V.K. Chari, A. Konrad, M.A. Palmo and J. D'Angelo, ,IEEE Trans. Magn., Vol MAG-18, 436-446, (1982)
[4]: F.E. Baker, S.H. Brown, J.L. Brauer and T.R. Gerhardt, Int. J. Num. Meth. Eng., Vol.19, 271-280 (1983)
[5]: T.W. McDaniel, R.B. Fernandez, R.R. Root and R.B. Anderson, Ibid, Vol.19, 725-737 (1983)
[6]: M. Hurwitz, NASTRAN users' manual, 1.15-1 - 1.15-9
[7]: NASTRAN users' manual, 3.17-1 - 3.17-10

TABLE 1: ANALOGIES AND DIFFERENCES BETWEEN HEAT TRANSFER AND MAGNETOSTATICS

HEAT TRANSFER QUANTITY	MAGNETOSTATIC QUANTITY
k Thermal conductivity	μ Magnetic Permeability
$k = f(T)$	$\mu = f(H)$
$\dot{q}$ Heat Flux per unit area	B Magnetic Flux Density
grad (T) Temperature Gradient	H Magnetic Field Strength or Potential Gradient
T Temperature	V Magnetic Potential

TABLE (2): MAGNETIC PROPERTIES OF SOFT MATERIALS MODELLED

MATERIAL 1 = AIR : B = H

MATERIAL 2 = SILICON STEEL

H (OERSTEDS)	B (GAUSS)
0.0	0.0
0.1	1750.0
0.2	6600.0
0.3	12000.0
0.4	13000.0
0.5	13700.0
1.0	15400.0
10.0	17750.0
100.0	19250.0
1000.0	19500.0
2000.0	20500.0

MATERIAL 3 = SUPERMENDURE

H(OERSTEDS)	B (GAUSS)
0.00	0.0
0.01	4500.0
0.10	7200.0
0.50	7750.0
1.00	7800.0
10.00	7900.0
100.00	8000.0
200.00	8200.0
2000.00	10000.0

TABLE 3: MAGNETIC PROPERTIES OF PERMANENT MAGNET MODELLED

H (OERSTEDS)	B (GAUSS)
0.0	-800.0
200.0	-600.0
400.0	-300.0
500.0	0.0

FIG (1)

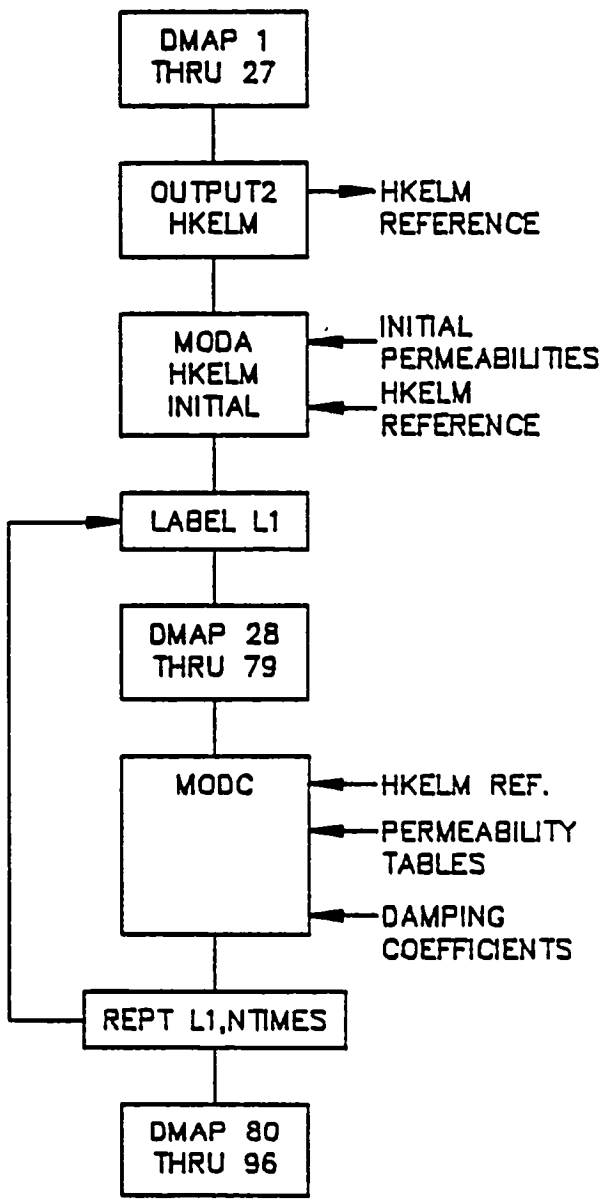
DMAP 1
THRU 27
OUTPUT2
HKELM
HKELM
REFERENCE
MODA
HKELM
INITIAL
INITIAL
PERMEABILITIES
HKELM
REFERENCE
LABEL L1
DMAP 28
THRU 79
MODC
HKELM REF.
PERMEABILITY
TABLES
DAMPING
COEFFICIENTS
REPT L1,NTIMES
DMAP 80
THRU 96

Fig.(2): NASTRAN DMAP ALTERS

```
NASTRAN TITLEOPT=-1
ID MAG1A,NASTRAN
APP HEAT
TIME 10000
SOL,1,1
ALTER 27
OUTPUT2 HEST,,,, // 0 / 18 $
OUTPUT2 HKELM,,,, // 0 / 15 $
MODA // -1 $
LABEL L1 $
INPUTT2 / HKELM,,,, / 0 / 19 $
ALTER 79
OUTPUT2 HOEF1,,,,// 0 / 14 $
MODC // -1 $
PURGE HKGG,GPST/HNOKGG $
EMA HGPECT,HKDICT,HKELM/HKGG,GPST $
REPT L1,2 $
ENDALTER
CEND
```

Fig.(3): MAGNETIC HYSTERESIS CURVE

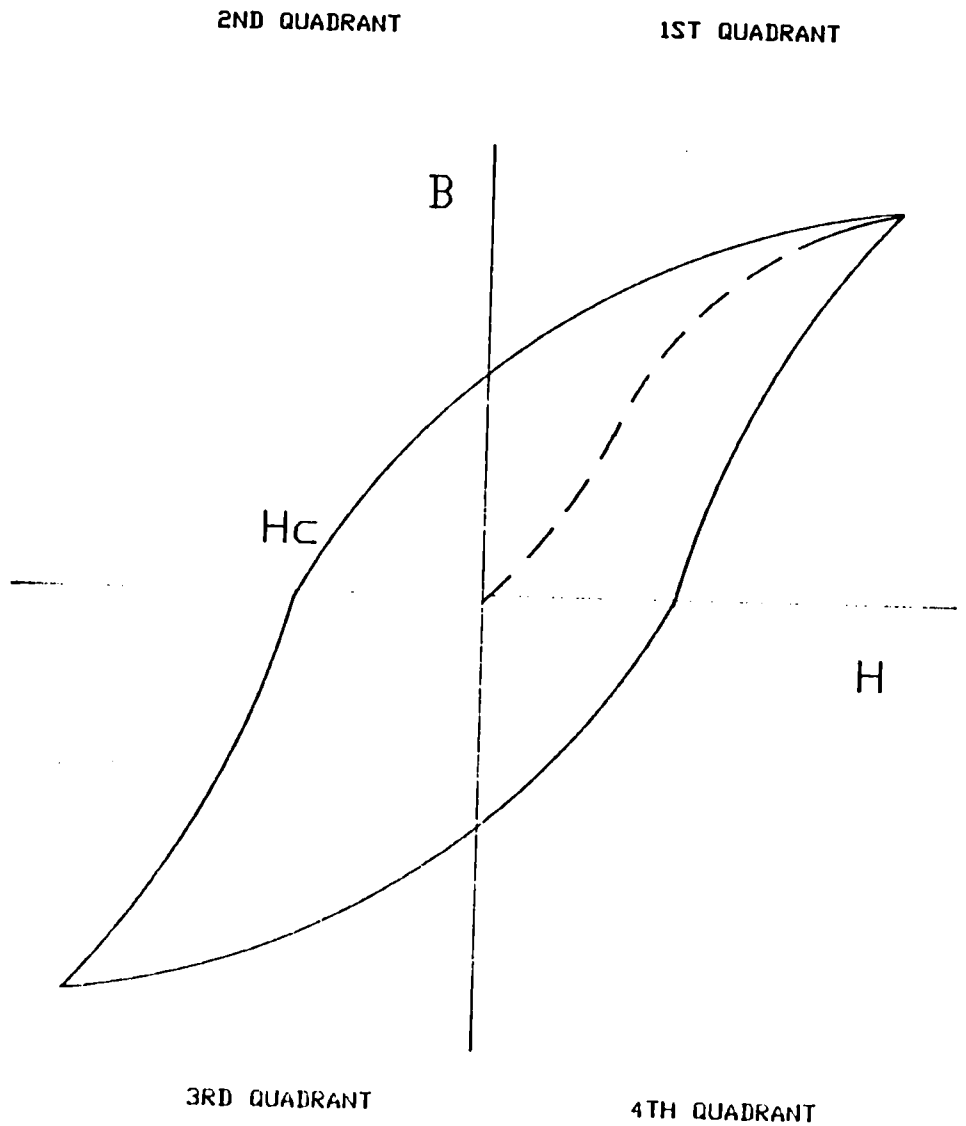

Fig.(4): SOFT MATERIAL MAGNETIZATION CURVE

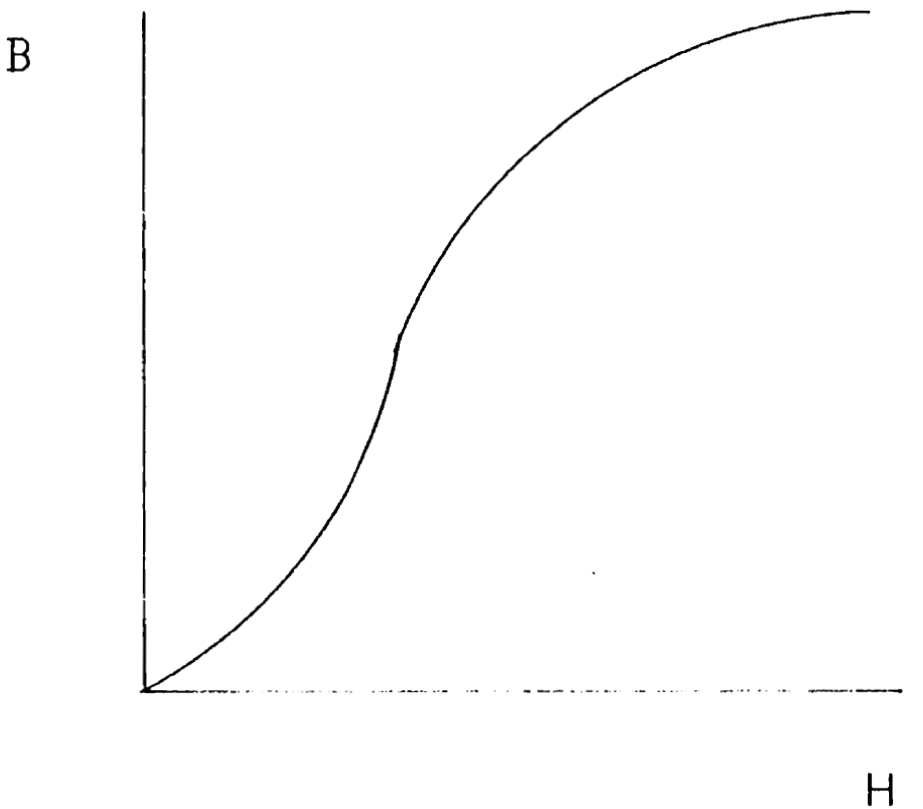

Fig.(5): PERMANENT MAGNET DEMAG. CURVE

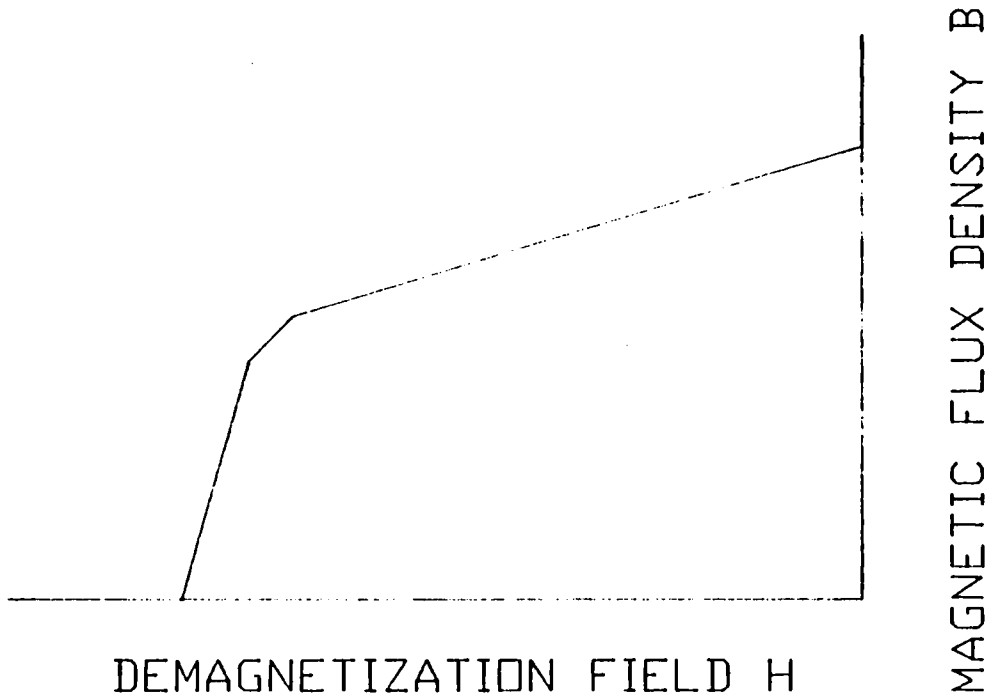

Fig.(6): FOURTH QUADRANT DEMAG. CURVE

Fig.(7): EFFECTS OF COIL ON MAGNETIZATION

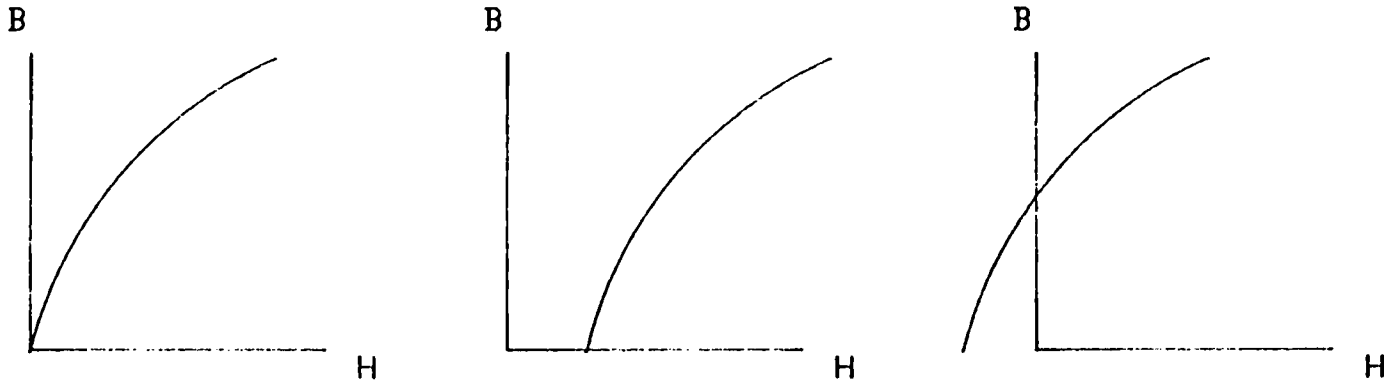

NATIVE CURVE

REVERSE BIAS

H = Hext - Hcoil

FORWARD BIAS

H = Hext + Hcoil

Fig.(8): MODEL OF DISSIMILAR STEELS IN AIR

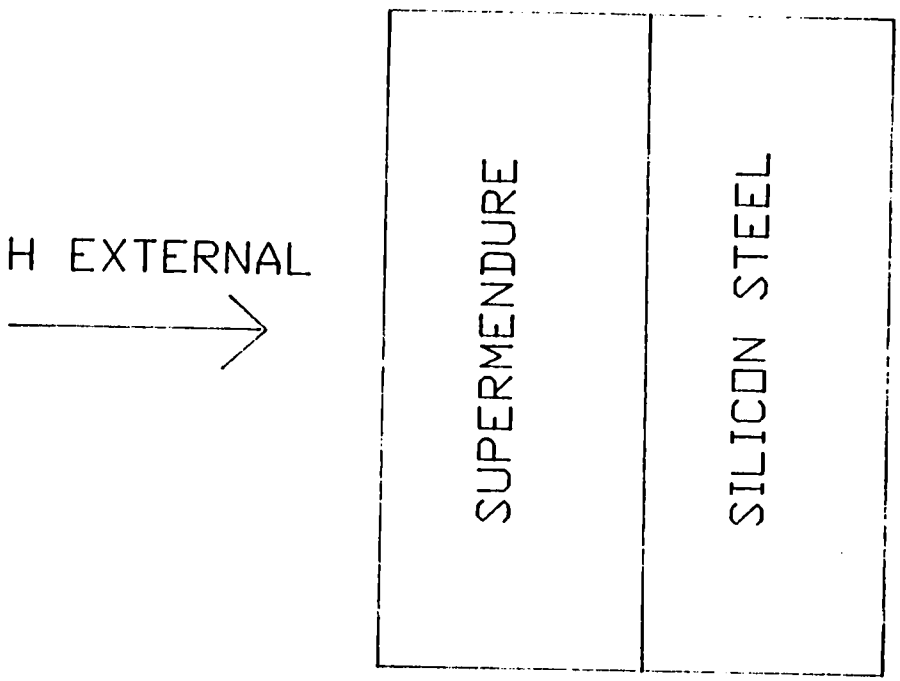

Fig.(9): Iteration of Soft Material

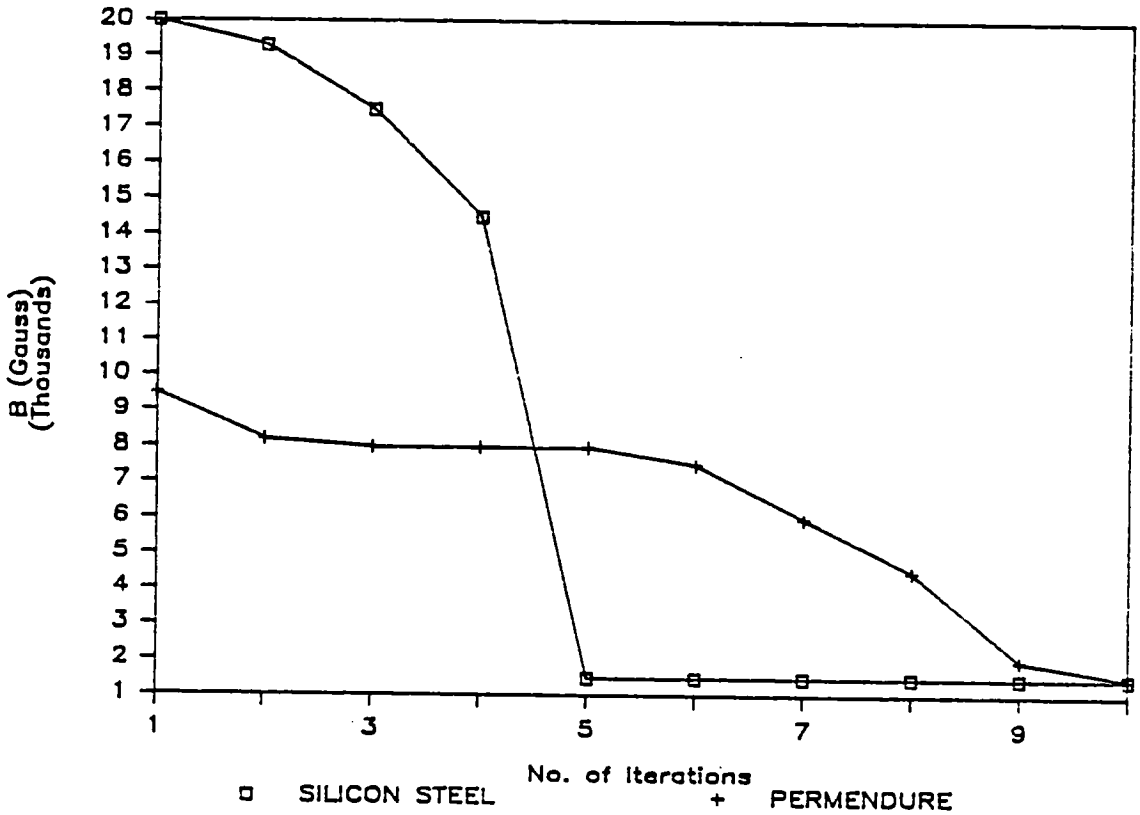

Fig.(10): MODEL OF PERMANENT MAGNET IN AIR

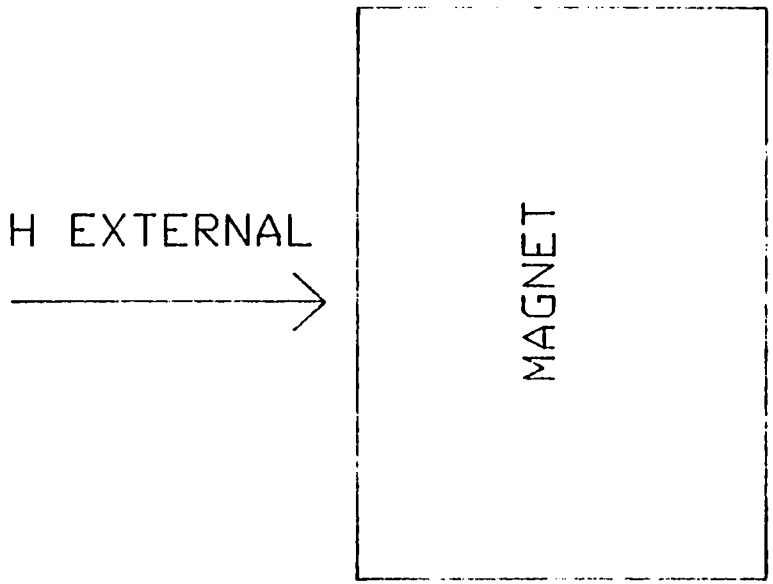

Fig.(11): Iteration of Magnet in Air

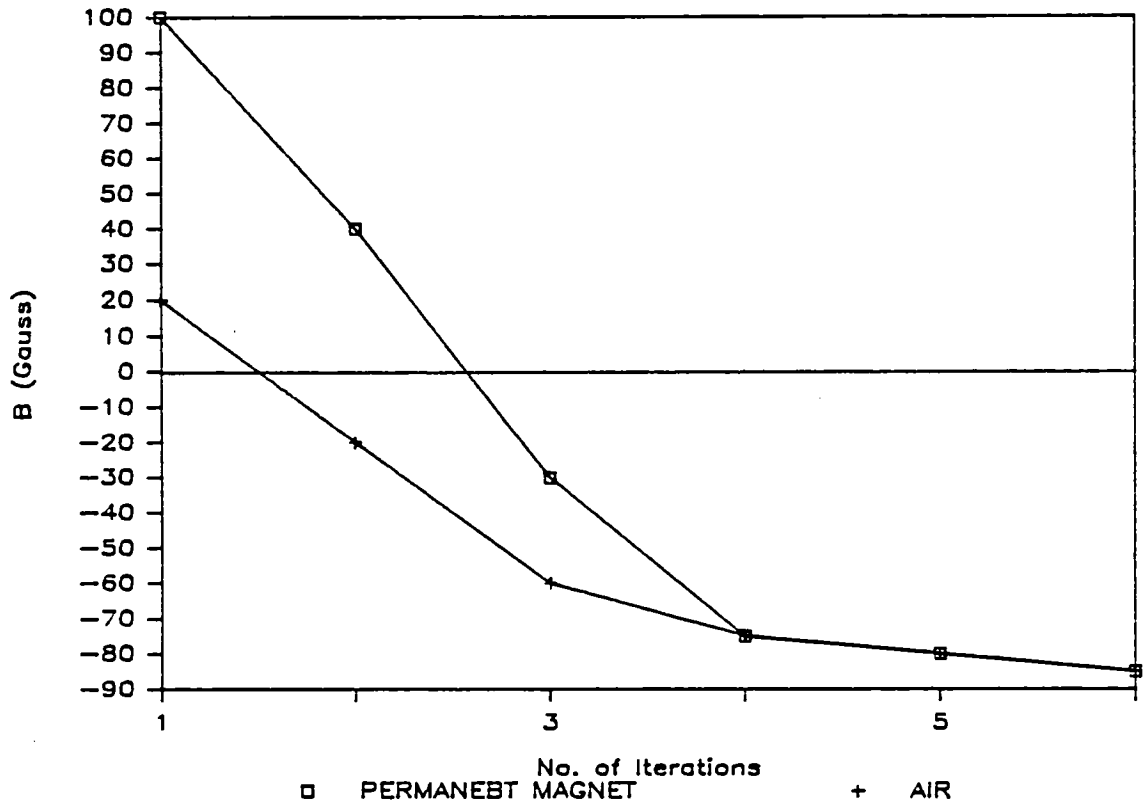

CALCULATING FAR-FIELD RADIATED SOUND PRESSURE LEVELS FROM NASTRAN OUTPUT

Robert R. Lipman

David W. Taylor Naval Ship Research and Development Center
Numerical Structural Mechanics Branch
Bethesda, Maryland 20084-5000

SUMMARY

FAFRAP is a computer program which calculates far-field radiated sound pressure levels from quantities computed by a NASTRAN direct frequency response analysis of an arbitrarily shaped structure. Fluid loading on the structure can be computed directly by NASTRAN or an added-mass approximation to fluid loading on the structure can be used. Output from FAFRAP includes tables of radiated sound pressure levels and several types of graphic output. FAFRAP results for monopole and dipole sources compare closely with an explicit calculation of the radiated sound pressure level for those sources.

INTRODUCTION

FAFRAP computes far-field radiated sound pressure levels using the Helmholtz exterior integral equation by numerically integrating fluid pressures and normal velocities over the fluid-structure interface of a finite element model. The numerical integration requires the XYZ coordinates, unit normal vector, tributary area, fluid pressure, and outward normal velocity for every grid point on the fluid-structure interface. ALTER statements in a NASTRAN direct frequency response analysis are used to obtain these quantities. Fluid pressures at the fluid-structure interface are computed directly by NASTRAN if an explicit fluid finite element mesh is used. Alternatively, FAFRAP will calculate fluid pressures if an added-mass approximation to fluid loading is used.

THEORY

Consider the arbitrarily shaped body in figure 1. Let $\underline{z}$ be the position vector to an exterior fluid point P, and $z = |\underline{z}|$. Let $\underline{x}$ be the position vector to a point on the fluid-structure interface (with $x = |\underline{x}|$), let $\underline{r} = \underline{z} - \underline{x}$ (with $r = |\underline{r}|$), and let $\underline{n}$ be the unit outward normal at the location $\underline{x}$. The time-harmonic ($e^{i\omega t}$) pressure at $\underline{z}$ is given by the Helmholtz integral (ref. 1)

$$p(\underline{z}) = \int_S [i\omega\rho v_n(\underline{x}) + (ik + 1/r)p(\underline{x})\cos\beta\ ](e^{-ikr}/4\pi r)\ dS \qquad (1)$$

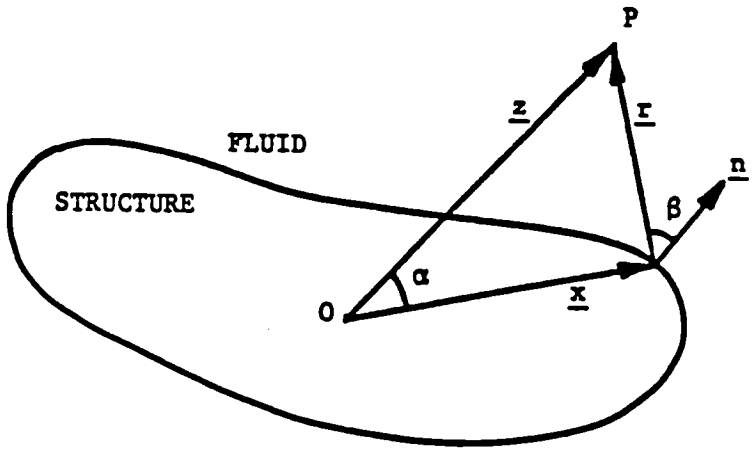

Figure 1. Geometry for Far-Field Radiated Sound Pressure Level Computations

where $v_n(\underline{x})$ and $p(\underline{x})$ are the complex normal surface velocity and complex surface pressure, respectively, and $k = \omega/c$, where ω = circular frequency, and c = speed of sound in the fluid.

Equation (1) can be simplified if only far-field locations are of interest. As $|\underline{z}| \to \infty$, $ik + 1/r \to ik$, and from the law of cosines, $r \to z - x\cos\alpha$. Therefore, at far-field locations

$$p(\underline{z}) \doteq (ik\, e^{-ikz}/4\pi z) \int_S [\rho c v_n(\underline{x}) + p(\underline{x}) \cos\beta\,] e^{ikx\cos\alpha}\, dS \qquad (2)$$

where $\cos\beta \doteq (\underline{z}/|\underline{z}|)\cdot \underline{n}$.

One convention for presenting far-field pressures is as "sound pressure level (RMS) in dB relative to 1 μPa at 1 yard." Sound pressure levels (SPL) due to an excitation force applied as amplitude rather than RMS is obtained from eq. (2) by substituting z = 36 inches and by multiplying by the conversion factor 1 psi = 6.895×10^9 μPa to convert pressure $p(\underline{z})$ from pounds per square inch (psi) to micropascals (μPa). Therefore, for $|\underline{z}|$ = 36 inches

$$SPL = 20 \log ((6.895\times10^9\, p(\underline{z}))/\sqrt{2}) \qquad (3)$$

FLUID LOADING

Fluid pressures on the fluid-structure interface can be computed by NASTRAN if an explicit fluid finite element mesh is used. The finite element method that models the exterior surrounding fluid out to a predetermined distance is described by Everstine (refs. 2,3). This method uses, as the fundemental unknowns, the structural displacements and a velocity potential in the fluid. The outer boundary is terminated with nonreflective (wave-absorbing) boundary conditions, which assume that the outgoing waves are locally planar.

This approach to fluid loading results in an accurate model of the fluid mass at the expense of a much larger model due to the increased number of degrees of freedom introduced in modeling the fluid region.

An alternative to using an explicit fluid finite element mesh is to use an appropriate added-mass approximation to fluid loading. The added-mass is applied to the grid points on the fluid-structure interface. For example, at low frequencies for a conical section, the effect of the fluid pressure is that of a mass-like impedance. Junger and Feit (ref. 4) show this impedance to be

$$z = -i\omega m_a \tag{4}$$

where the effective added mass per unit area is

$$m_a = \rho_f R(n/(n^2+1)) \tag{5}$$

where ρ_f = fluid mass density, R = radius of conical section, and n = circumferential harmonic number.

IMPLEMENTATION

The numerical integration of eq. (2) requires, for each grid point on the fluid-structure interface, the XYZ coordinates, unit normal vector, tributary area, fluid pressure, and outward normal velocity. All of these quantities can be obtained directly from NASTRAN using the OUTPUT2 utility module. The following ALTER statements will output the required data blocks on to the NASTRAN UT1 file.

```
$ FAFRAP ALTER STATEMENTS, RIGID FORMAT 8, APR 84 VERSION
ALTER 21,21 $
GP3 GEOM3,EQEXIN,GEOM2/SLT,GPTT/S,N,NOGRAV/NEVER=1 $
ALTER 55 $
SSG1 SLT,BGPDT,CSTM,SIL,EST,MPT,GPTT,EDT,,CASECC,DIT/
     PG/LUSET/NSKIP
SDR2 CASECC,CSTM,MPT,DIT,EQEXIN,SIL,GPTT,EDT,BGPDT,,,,
     EST,XYCDB,PG/OPG1,,,,,/*STATICS*/S,N,NOSORT2/-1/
     S,N,STRNFLG $
ALTER 137 $
OUTPUT2 PG,BGPDT,EQEXIN,FRL,UPVC $
ENDALTER $
```

These ALTER statements allow a static unit pressure load to be applied to the structure during the dynamic frequency response analysis. The unit pressure load is applied to the fluid-structure interface of the finite element model. The components of the load vector created by the static pressure load are used by FAFRAP to compute the unit normal vector and tributary area of the grid points on the fluid-structure interface. The following is a list of the

quantities in the data blocks written with the OUTPUT2 statement.

PG - load vector components
BGPDT - XYZ coordinates
EQEXIN - internal to external grid point numbering equivalencing
FRL - frequency response list
UPVC - grid point displacements

The displacements are converted to velocities by the relationship $v = i\omega u$, where u is displacement and v is velocity. If an explicit fluid finite element mesh has been used, then the pressure at a fluid grid point on the fluid-structure interface is evaluated as the time derivative of the velocity potential (ref. 2). If an added-mass approach to fluid loading is used, FAFRAP calculates pressure from the displacement.

Several user-defined input parameters to FAFRAP control the number of far-field locations at which to calculate an SPL and the different types of output.

OUTPUT

Several types of output are available from FAFRAP. There are tables of computed values and three types of graphics output. Table 1 lists the SPL at far-field locations. The headings COLAT and LON refer to colatitudinal and longitudinal far-field locations, respectively. These tables are printed for each subcase and frequency. Table 2 lists phasor sum, RMS velocity, maximum SPL and where it occurs, maximum SPL in a horizontal plane and where it occurs, and radiated power for each subcase. Equations 6 and 7 define the phasor sum and RMS velocity, respectively,

$$\text{phasor sum} = \sum_i (v_{n,i} A_i) \; / \; A \tag{6}$$

$$\text{RMS velocity} = \sum_i \sqrt{(|v_{n,i}|^2 A_i)} \; / \; A \tag{7}$$

where the summation is for all i grid points on the fluid-structure interface. Radiated power represents a summation of all pressure intensities in the far-field.

A separate plotting program, FAFPLOT, was written to display SPL's in any of the three principal planes for any subcase or frequency. Figure 2 is an example of a polar plot of SPL generated by FAFPLOT. The two numbers in the lower left-hand corner refer to the subcase and frequency defined for that plot. The polar plot is useful in evaluating the sound pressure pattern generated by the structure.

Log-log plots can be generated for plots of pressure, velocity, or impedance at a grid point on the fluid-structure interface versus frequency. An example of this type of plot is shown in figure 3. The log-log plots are useful in evaluating the response of specific points on the fluid-structure interface for different load cases.

PATRAN (ref. 5) can also be used to display all of the SPL's in the far-field for one subcase and frequency as a color contour plot (fig. 4). This type of plot gives a good view of the overall radiated sound pressure pattern.

COMPARISON TO ANALYTICAL SOLUTION

Analytical solutions exist for the pressure fields produced by two simple radiators, the monopole and dipole sources. The equations defining the pressure fields generated by these sources were used to validate the results of FAFRAP. A NASTRAN analysis was performed for each of the sources to provide the necessary input for FAFRAP. The equations defining the pressure fields for a monopole and dipole source can be found in equations 4.15 and 4.75 respectively, of Ross (ref. 6). After converting the equations to provide results in the correct units, the difference between the far-field radiated SPL calculated by FAFRAP and the values obtained from the equations was less than one percent.

REFERENCES

1. Lamb H., Hydrodynamics, sixth edition, Dover Publications, New York, 1945, p. 498.

2. Everstine, G.C., "A Symmetric Potential Formulation for Fluid-Structure Interaction," Journal of Sound and Vibration, Vol. 79, pp. 157-160, November 1981.

3. Everstine, G.C., F.M. Henderson, and R.R. Lipman, "Finite Element Prediction of Acoustic Scattering and Radiation From Submerged Elastic Structures," Twelfth NASTRAN User's Colloquium, NASA CP-2328, National Aeronautics and Space Administration, Washington, D.C., pp. 192-209, May 1984.

4. Junger, M.C. and D. Feit, Sound, Structures, and Their Interaction, The MIT Press, Cambridge, Massachussets, 1972, pp. 208,266.

5. PATRAN User's Guide, PDA Engineering Software Products Division, Santa Ana, California, 1984.

6. Ross, D., Mechanics of Underwater Noise, Pergamon Press, New York, 1976, pp. 61,77.

EXAMPLE OF FAFRAP OUTPUT
01/16/86 12.24.57.

SUBCASE 1, FREQUENCY = 55.5

COLAT	LON	SPL (DB)	PHASE
.0	.0	92.651	42.3
18.0	.0	103.330	84.1
18.0	18.0	103.633	88.1
18.0	36.0	103.340	92.5
18.0	54.0	102.431	97.7
18.0	72.0	100.827	104.0
18.0	90.0	98.385	113.1
18.0	108.0	94.974	126.9
18.0	126.0	91.329	140.8
18.0	144.0	91.027	205.0
18.0	162.0	93.156	231.3
18.0	180.0	94.582	243.7
18.0	198.0	94.843	250.4
18.0	216.0	93.916	255.4
18.0	234.0	90.897	261.3
18.0	252.0	83.256	281.7
18.0	270.0	64.366	46.2
18.0	288.0	93.425	66.8
18.0	306.0	97.934	72.8
18.0	324.0	100.682	76.6
18.0	342.0	102.387	80.3
36.0	.0	105.197	43.9
36.0	18.0	105.413	49.1
36.0	36.0	104.992	55.5
36.0	54.0	103.894	63.9
36.0	72.0	102.072	76.2
36.0	90.0	99.767	96.1
36.0	108.0	98.232	126.2
36.0	126.0	98.649	154.9
36.0	144.0	99.703	172.3
36.0	162.0	100.232	181.4
36.0	180.0	100.032	186.3
36.0	198.0	99.111	189.1
36.0	216.0	97.342	190.7
36.0	234.0	94.142	191.2
36.0	252.0	86.908	193.1
36.0	270.0	83.829	45.9
36.0	288.0	94.859	32.7
36.0	306.0	99.726	33.3
36.0	324.0	102.592	35.9
36.0	342.0	104.306	39.5

Table 1. Sound Pressure Levels in the Far-Field

EXAMPLE OF FAFRAP OUTPUT
'1/16/86 12.24.37.

SC	FREQ	PHASOR SM	RMS VEL	MAX SPL	COLAT	LON	HF7 SPL	COLAT	LON	ERROR
1	50.0	1.120E-08	4.685E-06	95.595	144.	198.	91.41.	36.	9[illegible]	3.3[illegible]E- 3
1	51.0	1.282E-08	5.23[illegible]E-06	97.6[illegible]	144.	1[illegible]8.	92.14	36.	9[illegible]	4.6[illegible]E-03
1	52.0	1.491E-08	5.92[illegible]E- 6	99.446	144.	198.	94.373	36.	9[illegible]	6.577E-03
1	53.0	1.770E-08	6.781E-06	1[illegible].3[illegible]7	144.	198.	96.[illegible]	36.	9[illegible]	9.[illegible]E-03
1	54.0	2.159E-08	7.9[illegible]4E- 6	1[illegible].3[illegible]1	144.	198.	97.792	36.	9[illegible]	1.[illegible]E-02
1	55.0	2.731E-08	9.425E-06	105.484	144.	198.	99.707	36.	9[illegible]	2.[illegible]E- 2
1	56.0	3.639E-08	1.159E-05	107.539	144.	198.	1[illegible]2.[illegible]7	36.	9[illegible]	3.[illegible]E- 2
1	57.0	5.231E-08	1.491E-05	11[illegible].6[illegible]4	144.	198.	1[illegible]4.626	36.	9[illegible]	7.[illegible]E-02
1	58.0	8.340E-08	2.043E-05	114.294	144.	198.	[illegible]7.[illegible]4	144.	[illegible]7[illegible]	[illegible]
1	59.0	1.4[illegible]5E-07	3.[illegible]36E-05	11[illegible].5[illegible]7	144.	198.	111.[illegible]5[illegible]	36.	9[illegible]	3.[illegible]E-01
1	60.0	1.621E-07	4.266E-05	121.721	144.	198.	11[illegible].[illegible]4[illegible]	36.	9[illegible]	7.[illegible]E-01
1	61.0	8.572E-08	3.[illegible]51E-05	120.121	144.	198.	114.453	36.	9[illegible]	3.[illegible]E- 1
1	62.0	2.[illegible]19E-08	2.[illegible]44E- [illegible]	11[illegible].[illegible]41	144.	198.	11 .453	36.	9[illegible]	2.[illegible]E-01
1	63.0	1.377E-08	1.[illegible]72E-05	[illegible]4.[illegible]58	144.	198.	[illegible] 7.[illegible]5[illegible]	36.	9[illegible]	1.[illegible]E- 1
1	64.0	1.367E-08	1.428E-05	112.[illegible]59	144.	198.	[illegible]5.[illegible]	36.	9[illegible]	9.[illegible]E-02
1	65.0	1.105E-08	1.151E-05	111.292	144.	198.	1[illegible]4.[illegible]7	36.	9[illegible]	7.[illegible]E- 2
1	66.0	1.[illegible]44E-08	9.644E-06	110.210	144.	198.	1[illegible]3.[illegible]5	36.	9[illegible]	5.[illegible]E- 2
1	67.0	9.[illegible]3[illegible]E-09	8.[illegible]6[illegible]E-06	1[illegible]9.331	144.	198.	1[illegible]2.[illegible]29	36.	9[illegible]	4.[illegible]E-02
1	68.0	9.183E-09	7.[illegible]1[illegible]E-06	[illegible] 8.[illegible]1	144.	198.	[illegible]...[illegible]7	36.	9[illegible]	[illegible]E- 2
1	69.0	[illegible].[illegible]7[illegible]E-09	[illegible].[illegible]21E-06	[illegible]7.484	144.	198.	[illegible]1.[illegible]	36.	9[illegible]	[illegible]E-02
1	70.0	[illegible].[illegible]4[illegible]E-09	[illegible].[illegible]97E-07	[illegible]7.434	144.	198.	[illegible]...[illegible]4[illegible]	36.	9[illegible]	[illegible]E- 2

Table 2. Summary of FAFRAP Results

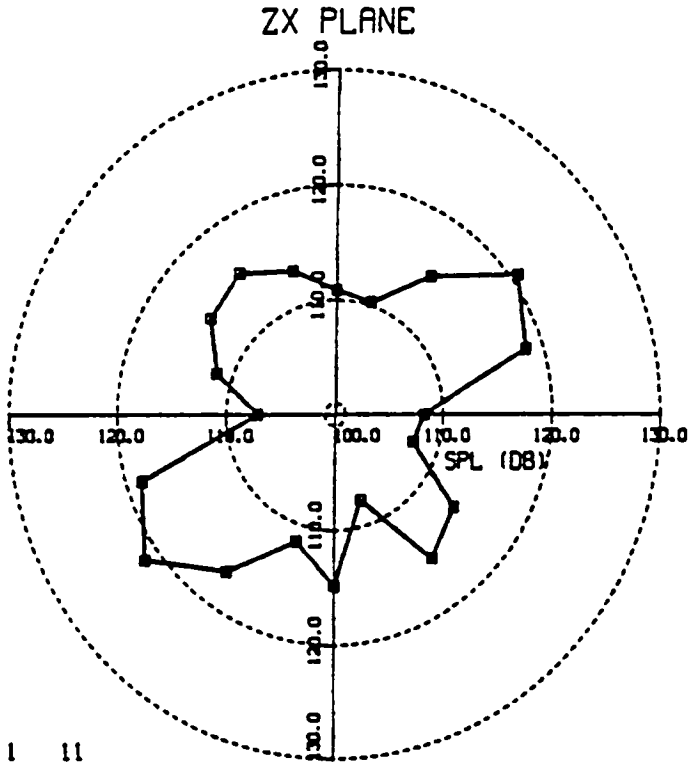

Figure 2. Polar Plot of Sound Pressure Levels in the Far-Field

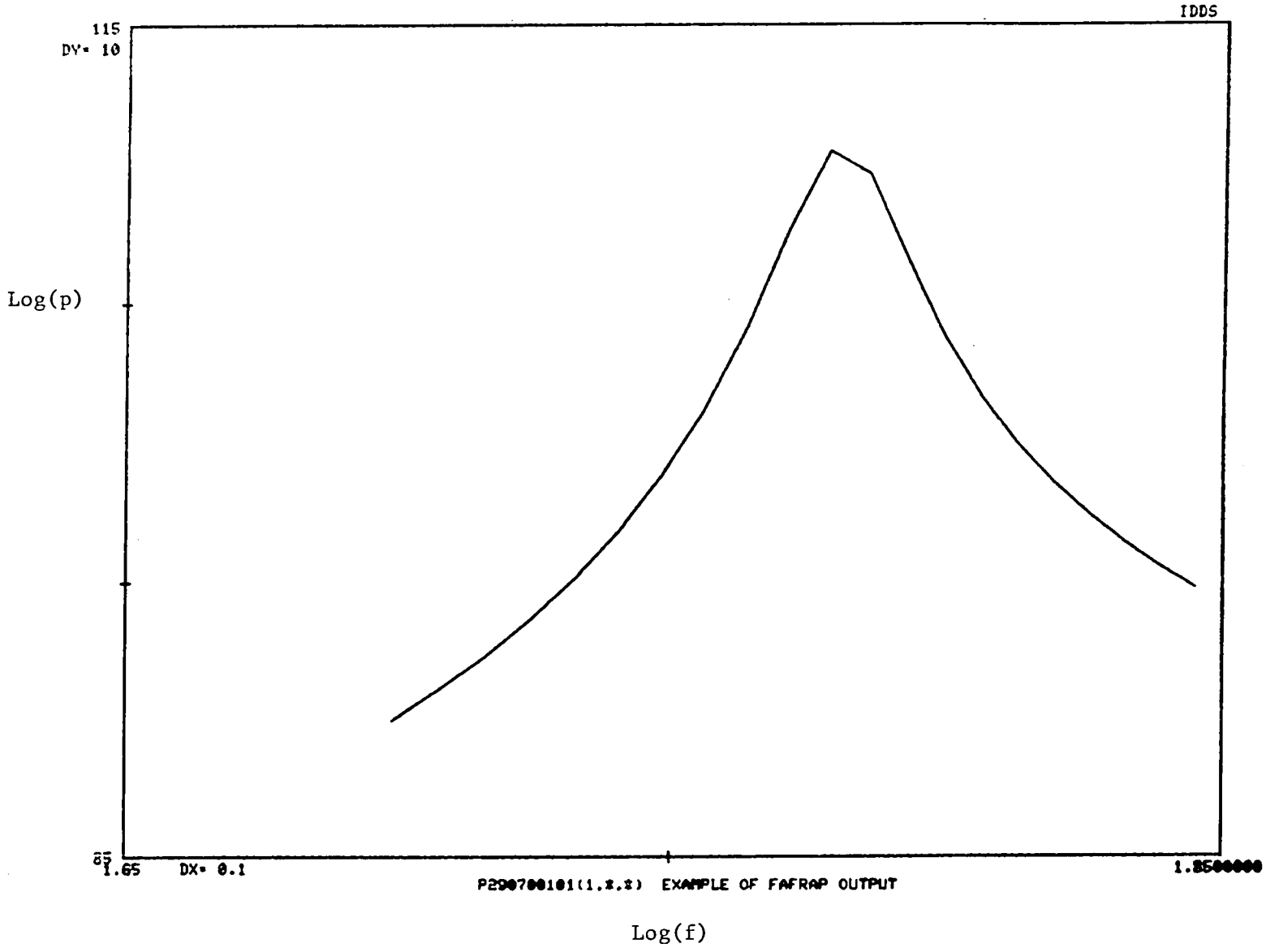

Figure 3. Log-log Plot of Pressure Versus Frequency at a Grid Point

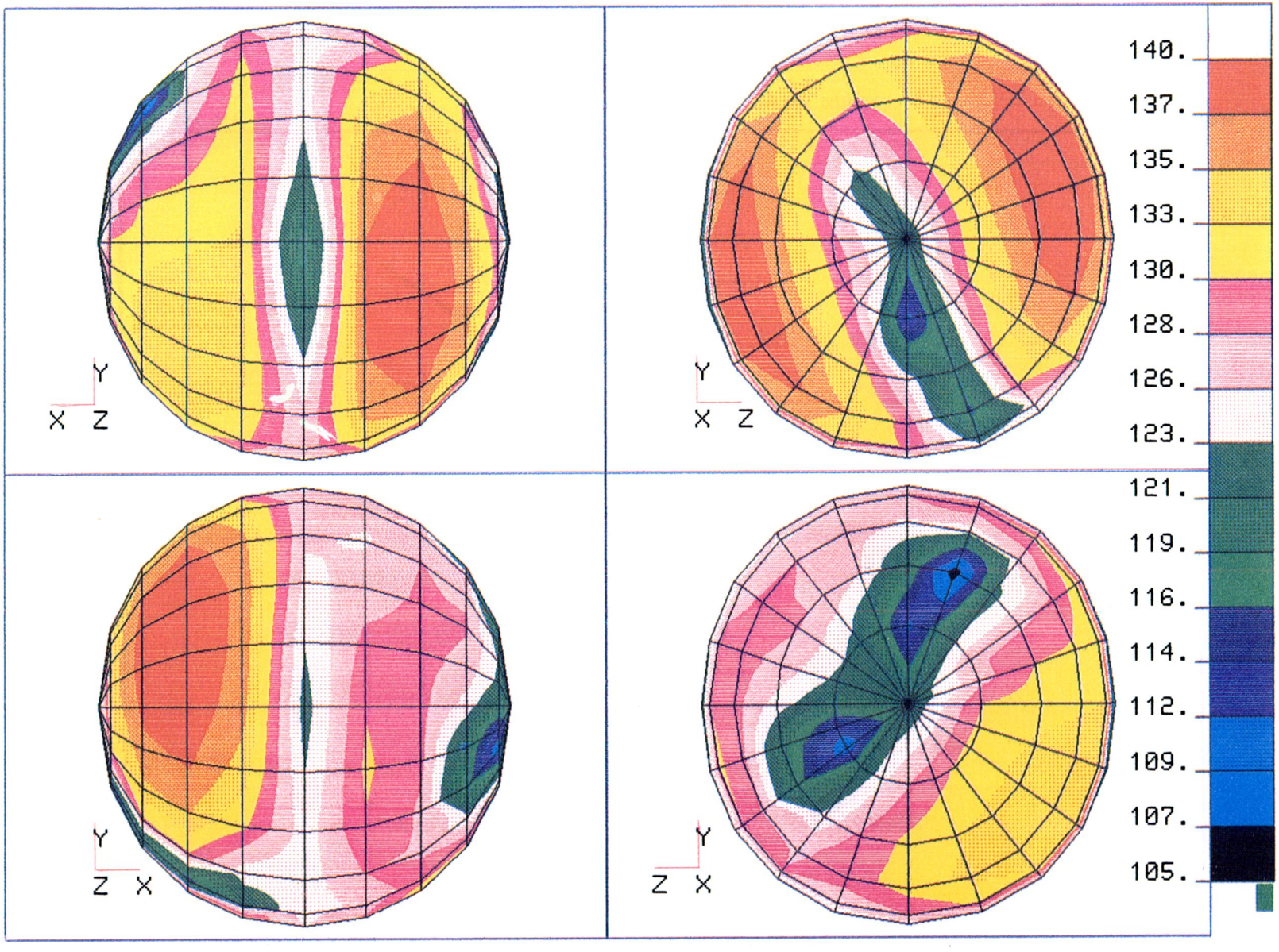

Figure 4. Contour Plot of Sound Pressure Levels in the Far-Field

A GENERAL LOW FREQUENCY ACOUSTIC RADIATION CAPABILITY FOR NASTRAN

by

G.C. Everstine, F.M. Henderson, E.A. Schroeder, and R.R. Lipman

Numerical Mechanics Division
David W. Taylor Naval Ship Research and Development Center
Bethesda, Maryland 20084-5000

ABSTRACT

A new capability called NASHUA is described for calculating the radiated acoustic sound pressure field exterior to a harmonically-excited arbitrary submerged 3-D elastic structure. The surface fluid pressures and velocities are first calculated by coupling a NASTRAN finite element model of the structure with a discretized form of the Helmholtz surface integral equation for the exterior fluid. After the fluid impedance is calculated, most of the required matrix operations are performed using the general matrix manipulation package (DMAP) available in NASTRAN. Far-field radiated pressures are then calculated from the surface solution using the Helmholtz exterior integral equation. Other output quantities include the maximum sound pressure levels in each of the three coordinate planes, the rms and average surface pressures and normal velocities, the total radiated power, and the radiation efficiency. The overall approach is illustrated and validated using known analytic solutions for submerged spherical shells subjected to both uniform and non-uniform applied loads.

INTRODUCTION

A fundamental problem of interest in acoustics is the calculation of the far-field acoustic pressure field radiated by a general submerged three-dimensional elastic structure subjected to internal time-harmonic loads. This problem is usually solved by combining a finite element model of the structure with a fluid loading computed using either finite element [1-3] or boundary integral equation [4-10] techniques.

Although both approaches are computationally expensive for large structural models, the fluid finite element approach is burdened with the additional complications caused by the approximate radiation boundary condition at the outer fluid boundary, the requirements on mesh size and extent, and the difficulty of generating the fluid mesh [1,3].

In contrast, the boundary integral equation (BIE) approach for generating the fluid loading is mathematically exact (except for surface discretization error) and requires no additional modeling effort to convert an existing model of a dry structure for use in submerged analyses. The savings in engineering time, however, is partially offset by the somewhat greater computing costs associated with the BIE approach.

Although several general BIE acoustic radiation capabilities have been developed previously, none was developed for the widely-used, nonproprietary structural analysis code NASTRAN. Here we present a new capability known as

NASHUA which couples a NASTRAN finite element model of a dry structure with a fluid loading calculated by a discretized form of the Helmholtz surface integral equation.

The primary purposes of this paper are to describe in detail the theoretical basis for NASHUA and to demonstrate its validity by showing results of radiation calculations for the elementary problems of uniformly-driven and sector-driven spherical shells. Detailed user's information will not be presented here since a user's guide for NASHUA was published previously [11].

THEORETICAL APPROACH

We wish to calculate the far-field acoustic pressure field radiated by a general submerged three-dimensional elastic structure subjected to internal time-harmonic loads. In general, our approach combines in a highly automated fashion a finite element model of the strucure with a Helmholtz boundary integral equation model of the fluid.

The Structure

The dry structure, when modeled with finite elements in a conventional way, results in the equation of motion in the frequency domain

$$(-\omega^2 M + i\omega B + K)u = F \tag{1}$$

where M, B, and K are the structural mass, viscous damping, and stiffness matrices, respectively, ω is the circular frequency of excitation, F is the complex amplitude of the applied force, and u is the complex amplitude of the displacement vector. The time dependence $\exp(i\omega t)$ has been suppressed. For structures with material damping or a nonzero loss factor, K is complex. We note from Equation (1) that the structural impedance matrix (the ratio of force to velocity) is

$$Z_S = i\omega M + B - iK/\omega \tag{2}$$

The Exterior Fluid

For the fluid, the pressure p satisfies the reduced wave equation

$$\nabla^2 p + k^2 p = 0 \tag{3}$$

where $k = \omega/c$ is the acoustic wave number, and c is the speed of sound in the fluid. Equivalently, p is the solution of the Helmholtz integral equation [12]

$$\int_S p(\underline{x})(\partial D(r)/\partial n)dS - \int_S q(\underline{x})D(r)dS = \begin{cases} p(\underline{x}')/2, & \underline{x}' \text{ on } S \\ p(\underline{x}'), & \underline{x}' \text{ in } E \end{cases} \tag{4}$$

where S and E denote surface and exterior fluid points, respectively, r is the distance from $\underline{x}$ to $\underline{x}'$ (Figure 1), D is the Green's function

$$D(r) = e^{-ikr}/4\pi r \tag{5}$$

and

$$q = \partial p/\partial n = -i\omega\rho v \tag{6}$$

where ρ is the density of the fluid, and v is the outward normal component of velocity on S. As shown in Figure 1, $\underline{x}$ in Equation (4) is the position vector for a typical point P_j on the surface S, $\underline{x}'$ is the position vector for the point P_i which may be either on the surface or in the exterior field E, the vector $\underline{r} = \underline{x}' - \underline{x}$, and $\underline{n}$ is the unit outward normal at P_j. We denote the lengths of the vectors $\underline{x}$, $\underline{x}'$, and $\underline{r}$ by x, x', and r, respectively. The normal derivative of the Green's function D appearing in Equation (4) can be evaluated as

$$\partial D(r)/\partial n = (e^{-ikr}/4\pi r)\ (ik + 1/r)\ \cos\beta \tag{7}$$

where β is defined in Figure 1.

The substitution of Equations (6) and (7) into the surface equation (4) yields

$$p(\underline{x}')/2 - \int_S p(\underline{x})\ (e^{-ikr}/4\pi r)\ (ik + 1/r)\ \cos\beta\ dS$$

$$= i\omega\rho \int_S v(\underline{x})\ (e^{-ikr}/4\pi r) dS \tag{8}$$

where $\underline{x}'$ is on S. This equation can be interpreted as an integral equation relating the pressure p and normal velocity v on S. If Equation (8) is discretized for numerical computation, we obtain the matrix equation

$$Ep = Cv \tag{9}$$

on S. With low-order approximations to the integrals, E can be evaluated simply as

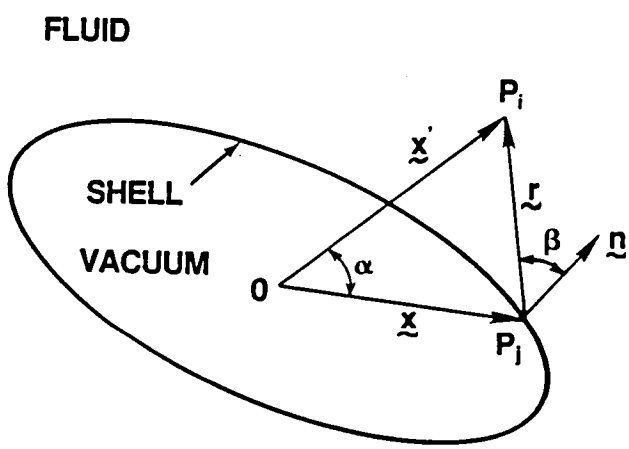

Figure 1 - Notation for Helmholtz Integral Equations

$$E_{ij} = -(e^{-ikr}/4\pi r)\ (ik + 1/r)\ (\cos \beta_{ij})A_j, \quad i \neq j \tag{10}$$

where A_j is the area assigned to the point $\underline{x}_j$, and $r = r_{ij} = |\underline{x}_i - \underline{x}_j|$. Similarly,

$$C_{ij} = (i\omega\rho\ e^{-ikr}/4\pi r)A_j, \quad i \neq j \tag{11}$$

In general, surface areas in NASHUA are obtained from the NASTRAN calculation of the load vector resulting from an outwardly directed static unit pressure load on the structure's wet surface.

The use of low-order integration in Equations (10) and (11) yields roughly the same accuracy as would be obtained if linear shape functions were used for the variation of p and v over the element [7]. (This property is analogous to the situation in one-dimensional Newton-Cotes integration in which odd-point formulas are preferred to the next higher-order even-point formulas, since both have the same order of accuracy [13].) Moreover, the integration scheme selected is particularly easy to implement since it requires a knowledge only of the area assigned to each point rather than any information about the elements on the wet surface.

The above two formulas for E_{ij} and C_{ij} are applicable only for the off-diagonal terms ($i \neq j$), because r vanishes for $i = j$. For this singular case, the integrals in Equation (8), which are in fact well-defined, must be evaluated by a different approach. Consider first the velocity integral in Equation (8). Following Chertock [14], if we assume that v is constant over a small circular patch of radius b_i centered at $\underline{x}$, then, from Equation (8),

$$C_{ii} = i\omega\rho \int_0^{2\pi} \int_0^{b_i} (e^{-ikr}/4\pi r)\ r\,dr\,d\theta \tag{12}$$

where b_i is selected so that $\pi b_i^2 = A_i$, the total area assigned to the point. The evaluation of this integral yields

$$C_{ii} = i\omega\rho A_i/2\pi b_i \tag{13}$$

where

$$b_i = (A_i/\pi)^{1/2} \tag{14}$$

The evaluation of the "self term" E_{ii} is similar except that the curvature of the radiating surface must be taken into account because the singularity in the pressure term of Equation (8) is one order higher than that of the velocity term. Here we assume that p is constant over a small spherical cap located at $\underline{x}_i$ and having curvature c_i and area A_i. Then, from Equation (1),

$$E_{ii} = 1/2 - \int_0^{2\pi} \int_0^{b_i} (e^{-ikr}/4\pi r)\ (ik + 1/r)\ (-rc_i/2)\ r\,dr\,d\theta \tag{15}$$

where we have used the approximation

$$\cos \beta = -rc_i/2 \tag{16}$$

The evaluation of this integral yields

$$E_{ii} = 1/2 + (1 + ikb_i)\ (c_iA_i)/(4\pi b_i) \tag{17}$$

where we interpret c_i as the mean curvature at $\underline{x}_i$.

The use of b_i in Equation (13) and (17) facilitates the calculation of the self terms at points lying in planes of symmetry, since A_i is halved or quartered at such points, but b_i is computed from Equation (14) as if the full area at the point were applicable.

The need to know the mean curvatures at each wet point is the major impediment to full generality for the NASHUA procedure, since there is no mechanism built into NASTRAN that enables the user to extract the curvature of a surface at a point. NASHUA handles this problem by placing some minor restrictions on the analyst so that the curvatures can be computed for the commonly-occurring geometries of spheres, cylinders, conical sections, and flat sections. For other shapes, the user must insert a few lines of code into the NASHUA processor SURF to compute the curvature at each point, given its location.

In contrast to the situation for curvatures, the NASHUA requirement for surface areas and normals is handled with full generality, since the user defines the wet surface by applying a static, outwardly-directed, unit pressure load to that surface.

We note from Equation (9) that, if E^{-1} exists, the impedance matrix Z_f for the exterior fluid is

$$Z_f = A\ E^{-1}C \tag{18}$$

where A is the diagonal area matrix for the wet surface.

The Coupled System

The structural and fluid impedance matrices given by Equations (2) and (18) cannot be added to yield the impedance matrix for the submerged structure since Z_s and Z_f are not conformable. The matrix Z_s has dimension s x s, and Z_f has dimension f x f, where s is the number of structural degrees of freedom (wet and dry, including interior points), and f is the number of fluid degrees of freedom (DOF) on the fluid-structure interface. That is, f is equal to the number of wet points.

However, in terms of the wet DOF of the problem, the applied forces and the resulting velocities are related by

$$(z_s + Z_f)\ v = F^{(n)} \tag{19}$$

where v = complex amplitude of the velocity vector for the wet DOF (the surface normals)

$F^{(n)}$ = complex amplitude of the force vector applied to the wet DOF

z_s = impedance matrix for the structure in terms of the wet DOF

Z_f = impedance matrix for the exterior fluid

The structural impedance matrix Z_s and applied load vector F expressed in terms of all structural DOF can be related to the smaller matrices z_s and $F^{(n)}$ using

the transformation matrix G defined by the equation

$$F = G\, F^{(n)} \tag{20}$$

where F is a vector of dimension s (the total number of structural DOF), $F^{(n)}$ is a vector of dimension f (the number of fluid (wet) DOF on the surface), and G is the s x f matrix of direction cosines which converts $F^{(n)}$ to F. Thus,

$$z_s^{-1} = G^T Z_s^{-1} G \tag{21}$$

$$z_s^{-1} F^{(n)} = G^T Z_s^{-1} F \tag{22}$$

where the latter equation indicates the transformation of the velocity vector.

Algebraic manipulation of the preceding four equations yields [6,7]

$$H p = Q \tag{23}$$

where

$$H = E + C\, G^T Z_s^{-1} G A \tag{24}$$

$$Q = C\, G^T Z_s^{-1} F \tag{25}$$

Matrices E, C, and A have dimension f x f, Z_s is s x s, G is s x f, and F is s x r, where s is the number of structural DOF, f is the number of fluid DOF (on the wet surface), and r is the number of load cases. Since H and Q depend on geometry, material properties, and frequency, Equation (23) may be solved to yield the surface pressures p. Surface normal velocities 'v' may then be recovered using

$$v = G^T Z_s^{-1} F - G^T Z_s^{-1} G A p \tag{26}$$

To summarize, the NASHUA solution procedure uses NASTRAN to generate K, M, B, and F and to generate sufficient geometry information so that E, C, G, and A can be computed by a separate program (SURF). Then, given all matrices on the right-hand sides of Equations (24) and (25), a NASTRAN DMAP analysis is used to compute H and Q. Equation (23) is then solved for the pressures 'p' using a new block solver (OCSOLVE) written especially for this problem. Next, NASTRAN DMAP is used to recover the surface velocities 'v' according to Equation (26). This completes the surface solution.

The Far-Field Solution

Given the solution for the pressures and velocities on the surface, the exterior Helmholtz integral equation, Equation (4), can be integrated to obtain the radiated pressure at any desired location $\underline{x}'$ in the field. We first substitute Equations (6) and (7) into Equation (4) to obtain a form suitable for numerical integration:

$$p(\underline{x}') = \int_S [i\omega\rho v(\underline{x}) + (ik + 1/r)p(\underline{x}) \cos\beta]\, (e^{-ikr}/4\pi r)dS \tag{27}$$

where all symbols have the same definitions as were used previously, and $\underline{x}'$ is in the exterior field. Thus, given the pressure p and normal velocity v on the surface S, the pressure at $\underline{x}'$ can be determined by numerical quadrature using Equation (27).

In applications, however, the field pressures generally of interest are in the far-field, so we develop an asymptotic form of Equation (27) for use instead of Equation (27). In the far-field, $x' \to \infty$ implies

$$ik + 1/r \to ik \tag{28}$$

$$\cos \beta \to \underline{n} \cdot \underline{x}'/x' \tag{29}$$

and, from the application of the law of cosines,

$$r \to x' - x \cos \alpha \tag{30}$$

where α is defined in Figure 1. Hence, in the far-field [6],

$$p(\underline{x}') = (ike^{-ikx'}/4\pi x') \int_S [\rho c v(\underline{x}) + p(\underline{x}) \cos \beta] e^{ikx \cos \alpha} \, dS \tag{31}$$

where the asymptotic form, Equation (29), is used for cos β. We note that, since Equation (31) is a far-field formula, the pressure varies inversely with distance x' everywhere so that any range x' may be used in its evaluation, e.g., 36 inches (one yard). Numerically, the integral in Equation (31) is evaluated as

$$p(x') = (ike^{-ikx'}/4\pi x' \sum_j (\rho c v_j + p_j \cos \beta_{ij}) e^{ikx \cos \alpha} A_j \tag{32}$$

Other Output Quantities

Given both the surface and far-field solutions, a variety of other quantities of interest in applications can be computed. The average and root-mean-square normal velocities on the surface are defined as

$$v_{avg} = \int_S v dS/A \simeq \sum_i v_i A_i/A \tag{33}$$

$$v_{rms} = \left(\int_S |v|^2 \, dS/A\right)^{1/2} \simeq \left(\sum_i |v_i|^2 \, A_i/A\right)^{1/2} \tag{34}$$

where A is the total area of the radiating surface. The volume velocity, a measure of source strength, is Av_{avg}. Average and rms surface pressures can also be computed using Equations similar to (33) and (34) if 'v' is replaced by 'p.'

The acoustic intensity at a point on the surface is the product of the pressure there with the component of normal velocity which is in phase with the pressure:

$$I = \mathrm{Re}(pv^*) \tag{35}$$

where the asterisk denotes the complex conjugate. (There is no factor 1/2 in Equation (35) if we assume that pressures and velocities are already "effective" values rather than amplitudes.)

The power radiated can be obtained by integrating the acoustic intensity over the surface

$$W_{rad} = \int_S Re(pv^*)\, dS \approx \sum_i Re(p_i v_i^*) A_i \tag{36}$$

Since for low frequencies, p and v are nearly orthogonal (i.e., the fluid behaves like an added mass), this integral can be sensitive to small errors in p and v on the surface. To circumvent this problem, the radiated power is also computed by integrating the acoustic intensity over the far-field sphere, where $p = \rho c v$:

$$W_{rad} = \int_{S_o} (|p|^2/\rho c) dS_o \approx \sum_i |p_i|^2 A_{oi}/\rho c \tag{37}$$

where S_o is the surface of the far-field sphere, and the numerical approximation is summed over all far-field points where pressure is evaluated. For a non-dissipative medium, the last two equations are theoretically equivalent. Numerically, the second form, Equation (37), is better behaved, but it has the slight disadvantage of requiring the computation of the far-field solution at a large enough number of points so that the integration can be accurately performed.

Given the power radiated and the rms surface velocity, the radiation efficiency σ can be computed:

$$\sigma = W_{rad}/(\rho c A v_{rms}^2) \tag{38}$$

where v_{rms}^2 is the mean-square velocity on the surface, and A is the area of the surface [15].

OVERVIEW OF NASHUA SOLUTION PROCEDURE

The overall organization and setup of the solution procedure is summarized in Figure 2. NASTRAN appears three times in the procedure; to distinguish one NASTRAN execution from another, the integers 1, 2, or 3 are appended to "NASTRAN" in the figure.

A separate NASTRAN model is prepared and run (Step 1 in Figure 2) for each unique set of symmetry constraints. Since up to three planes of reflective symmetry are allowed, there would be one, two, four, or eight such runs. Step 1 generates files containing geometry information and the structure's stiffness (K), mass (M), and damping (B) matrices.

For each symmetry case and drive frequency, the Step 2 sequence is run in a single job. The SURF program reads the geometry file generated by NASTRAN in Step 1 and, using the Helmholtz surface integral equation, generates the fluid matrices E and C for the exterior fluid, the area matrix A, the structure-fluid transformation matrix G, and a condensed geometry file to be used later by FAROUT (Step 4) for the field calculation. SURF is followed by a NASTRAN DMAP job which takes the matrices K, M, B, and F from Step 1 and the matrices E, C, A, and G from SURF and calculates H and Q according to Equations (24) and (25). Equation (23) is then solved for the surface pressure vector 'p' by program OCSOLVE. OCSOLVE is a general block solver for full, complex, nonsymmetric systems of linear, algebraic equations. The program was designed to be particularly effective on such systems and executes about 20 times faster than NASTRAN's equation solver,

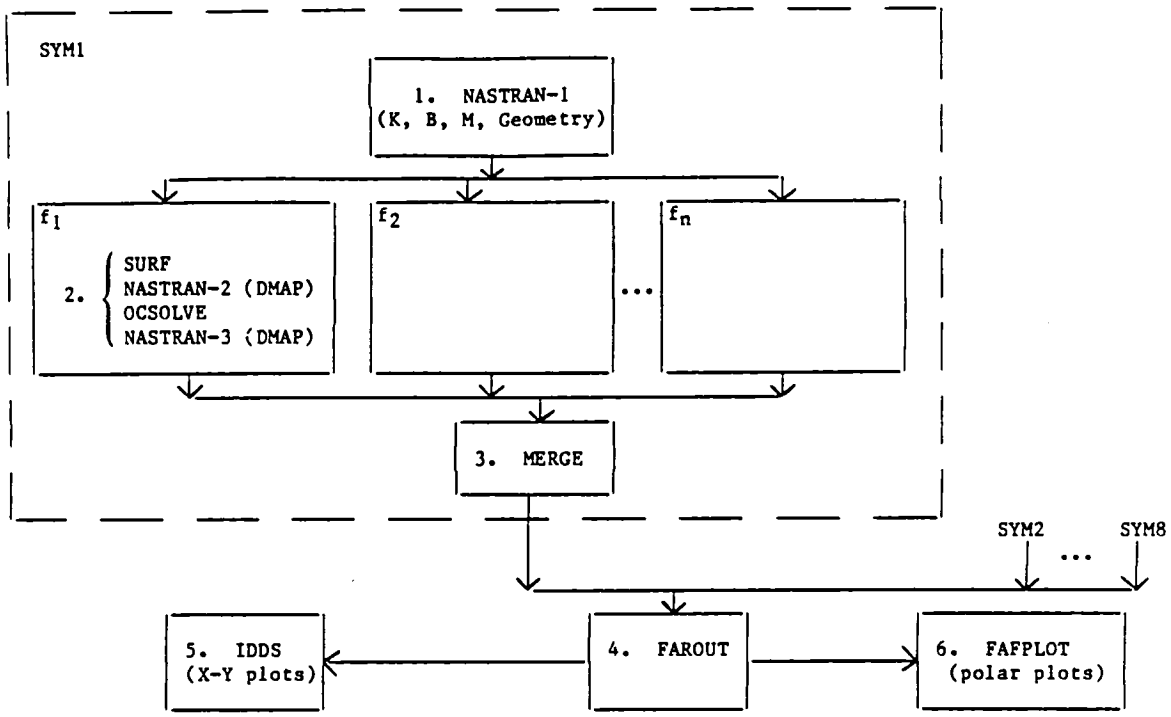

Figure 2 - Summary of NASHUA Solution Procedure

which was not designed for efficient solution of such systems of equations. NASTRAN is then re-entered in Step 2 with 'p' so that the outward normal surface velocity vector 'v' can be recovered using DMAP operations according to Equation (26). A file containing the surface pressures and velocities for each unique symmetry case and frequency is saved at the conclusion of Step 2.

After all frequencies have been run for a given symmetry case, the surface pressure and velocity results are reformatted and merged into a single file using program MERGE (Step 3). This program is run separately for each symmetry case. Recall that there are one, two, four, or eight possible symmetry cases.

Steps 1 to 3 are repeated for each symmetry case. After all symmetry cases are completed (with Step 3 completed for each), program FAROUT (Step 4) is run to combine the symmetry cases and to integrate over the surface. FAROUT uses as input the geometry file generated by SURF (Step 2) and the surface solutions from the one, two, four, or eight files generated by MERGE (Step 3). The far-field pressure solution is obtained by integrating the surface pressures and velocities using the far-field form of the exterior Helmholtz integral equation, Equation (31). Output from FAROUT consists of both tables and files suitable for plotting by IDDS (Step 5) and FAFPLOT (Step 6).

IDDS (Step 5) is a general purpose interactive X-Y plotting program which is used here for plotting surface velocities and impedances versus frequency [16]. FAFPLOT (Step 6) is an interactive graphics program for making polar plots of the

far-field sound pressure levels in each of the three principal coordinate planes [17].

Complete details on the requirements and deck setups for the entire solution procedure are given in the NASHUA user's guide [11].

FREQUENCY LIMITATIONS

It is known that the fluid matrices E and C in the surface Helmholtz integral equation formulation are singular at the frequencies of the resonances of the corresponding interior acoustic cavity with Dirichlet (zero pressure) boundary conditions [5]. Although the NASHUA formulation described in the previous section was designed to avoid having to invert either E or C in Equations (23) to (25), the coefficient matrix H is also poorly conditioned at these frequencies (referred to as the "critical" or "forbidden" frequencies of the problem). Therefore, to be safe, the user should avoid excitation frequencies which exceed the lowest critical frequency for the geometry in question.

For spheres, for example, the lowest critical frequency occurs at $ka = \pi$. For long cylinders with flat ends, the lowest critical frequency occurs at $ka \approx 2.4$, where k is the acoustic wave number, and 'a' is the radius of the sphere or cylinder. For short cylinders with flat ends, the lowest critical frequency is slightly higher than for long cylinders.

RESTRICTIONS ON MODEL

Although the NASHUA solution procedure was designed to be general enough so that arbitrary three-dimensional structures could be analyzed, a few restrictions remain. In our view, however, none is a burden, since a NASTRAN deck for a dry structure modeled with low-order finite elements can be adapted for use with NASHUA in a few hours. The following general restrictions apply:

1. All translational DOF for wet points must be in NASTRAN's "analysis set" (a-set), since (a) all symmetry cases must have the same wet DOF, and (b) the fluid matrices E and C involve all wet points. This restriction also affects constraints. Thus, constraints on translational DOF of wet points may not be imposed with single point constraint (SPC) cards, but must instead be imposed using large springs connected between ground and the DOF to be constrained. Generally, this restriction affects only those DOF which are constrained due to symmetry conditions.

2. The wet face of each finite element in contact with the exterior fluid must be defined by either three or four grid points, since the numerical discretization of the Helmholtz surface integral equation assumes the use of low order elements. In particular, NASTRAN elements with midside nodes (e.g., TRIM6, IS2D8, or IHEX2) may not be in contact with the exterior fluid.

3. Symmetry planes must be coordinate planes of the basic Cartesian coordinate system.

4. No scalar points or extra points are allowed, since program SURF assumes that each point is a grid point.

5. For cylindrical shells, the axis of the cylinder should coincide with one of the three basic Cartesian axes; for spherical shells, the center of the sphere should coincide with the basic origin. These restrictions facilitate the treatment of symmetry planes and the calculation of curvatures in program SURF.

6. At least one degree of freedom in the model should be constrained with an SPC, MPC, or OMIT so that the NASTRAN data block PL is generated.

7. Thin structures with fluid on both sides should be avoided, since the formulations for the fluid matrices are singular if two wet points are coincident. A precise restriction is not known.

TIME ESTIMATION

Most of the computer time required to execute the entire NASHUA procedure is associated with the back solve operation (FBS) in Step 2, Equation (24), in which the matrix $Z_s^{-1}GA$ is computed given the triangular factors of Z_s and the matrix GA. Z_s is a complex, symmetric, banded matrix of dimension s x s, where s is the number of structural DOF in the problem, and GA is a real, sparsely-populated, rectangular matrix of dimension s x f, where f is the number of fluid DOF (the number of wet points on the surface). This FBS time is proportional to f and typically accounts for about two-thirds of the total time to make a single pass through the NASHUA procedure.

For example, consider a problem with the following characteristics:

$s = 2973$ (number of structural DOF)
$f = 496$ (number of fluid DOF)
$W_{avg} = 129$ (average wavefront of stiffness matrix)

On the CDC Cyber 176 computer at DTNSRDC, the computer time ("wall-clock" time) required to solve this problem in a dedicated computer environment for a single symmetry case and one drive frequency was about 30 minutes, of which 19 minutes were spent in the FBS operation.

EXAMPLE 1: UNIFORMLY-DRIVEN SPHERICAL SHELL

We first demonstrate NASHUA's ability to solve radiation problems by solving the problem of the uniformly-driven submerged spherical shell, a problem with a closed-form solution. In this problem, a thin-walled spherical shell is submerged in a liquid and driven internally with a spherically-symmetric time-harmonic pressure load. Since the solution is also spherically-symmetric, the field solution depends only on radial distance from the origin.

Analytic Solution

The shell stiffness (the total static force required to increase the radius a unit amount) is

$$k_s = 8\pi Eh/(1-\nu) \tag{39}$$

where E and ν are the Young's modulus and Poisson's ratio for the shell material, and h is the thickness of the shell. The shell mass is

$$m_s = 4\pi a^2 h \rho_s \tag{40}$$

where 'a' is the mean shell radius, and ρ_s is the density of the shell material. Hence, for a uniform time-harmonic pressure drive, the structural impedance is

$$Z_s = (\omega^2 m_s - k_s) i/\omega \tag{41}$$

where ω is the circular frequency of the excitation.

For the surrounding fluid, the ratio of surface pressure to surface velocity is [5]

$$p/v = i\omega\rho a/(1 + ika) \tag{42}$$

where ρ is the density of the fluid and $k = \omega/c$. Hence, the fluid impedance (ratio of total force to velocity) is

$$Z_f = i\omega\rho 4\pi a^3/(1+ika) \tag{43}$$

For the harmonically-driven submerged shell, the surface velocity is therefore

$$v = 4\pi a^2 p_o/(Z_s + Z_f) \tag{44}$$

where p_o is the amplitude of the internal pressure drive. The surface pressure can be recovered from Equation (42). The fluid pressure in the exterior field decays inversely with distance [18]; hence

$$p_r = p(a/r)e^{-ik(r-a)} \tag{45}$$

where p_r is the pressure at distance r from the origin, and p is the pressure on the surface. Note that if the expression for surface velocity v obtained from Equation (42) is substituted into the far-field radiated pressure formula, Equation (31), Equation (45) is obtained.

The radiation efficiency for this problem is obtained by substituting the surface solution, Equation (42), into Equations (36) and (38):

$$\sigma = (ka)^2/(1 + (ka)^2) \tag{46}$$

NASHUA Solution

We solve with NASHUA the problem with the following characteristics [19]:

a	= 5 m	(shell radius)
h	= 0.15 m	(shell thickness)
E	= 2.07×10^{11} Pa	(Young's modulus)
ν	= 0.3	(Poisson's ratio)
ρ_s	= 7669 kg/m^3	(shell density)
ρ	= 1000 kg/m^3	(fluid density)
c	= 1524 m/s	(fluid speed of sound)
p_o	= 1 Pa	(internal pressure)

One octant of the shell was modeled with NASTRAN's CTRIA2 membrane/bending elements as shown in Figure 3. With 20 elements along each edge of the domain, the model has 231 wet points and 1263 structural DOF. Three planes of symmetry were imposed.

The NASHUA model was run for 15 drive frequencies in the nondimensional frequency range ka = 0.5 to ka = 8.0, where 'a' is the shell radius. Table 1 shows a comparison between the NASHUA calculations and the closed-form solution for surface pressures, surface velocities, and far-field radiated pressures. Clearly, the NASHUA calculations agree very closely with the closed-form solution for all ka's except those near ka = π and ka = 8.18, where the Helmholtz integral equation is singular [19], as discussed in a previous section.

EXAMPLE 2: SECTOR-DRIVEN SPHERICAL SHELL

The uniformly-driven spherical shell problem described in the preceding section is necessary but probably not sufficient to validate NASHUA. A more challenging problem, both analytically and numerically, is the spherical shell with a uniform pressure drive over a sector, as shown in Figure 4. (Here we use the term "analytic" to refer to a series solution which converges to the exact solution.) The particular problem solved has the internal pressure load applied over the polar angle γ = 36 degrees.

This problem was solved with the same finite element model used in Example 1. Thus, with two load cases (subcases), both problems can be solved together. However, with a one-octant model of the sphere (Figure 3), the NASHUA solution of this problem requires running both symmetric and anti-symmetric parts of the

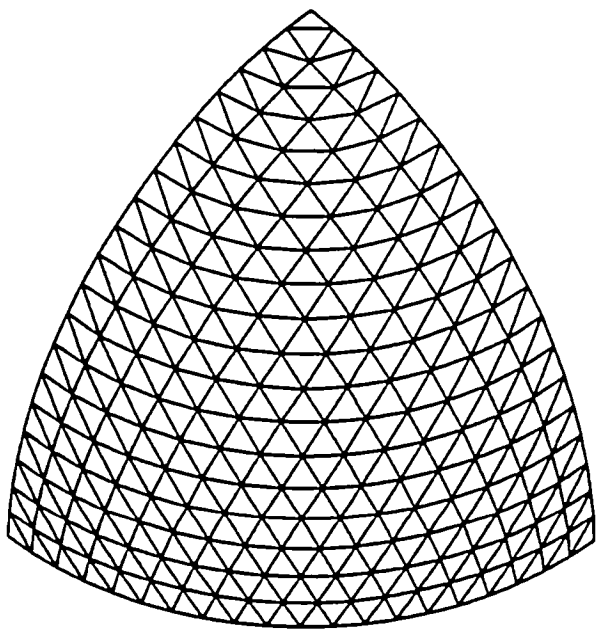

Figure 3 - Finite Element Model of One Octant of Spherical Shell

Table 1 - Comparison of NASHUA Solution with Closed-Form Solution for Uniformly-Driven Spherical Shell

	Average Surface Pressure			Average Surface Velocity			Far-Field Pressure		
ka	NASHUA	Exact	% Error	NASHUA	Exact	% Error	NASHUA*	Exact	% Error
	($\times 10^{-1}$)	($\times 10^{-1}$)		($\times 10^{-7}$)	($\times 10^{-7}$)		($\times 10^{-2}$)	($\times 10^{-2}$)	
0.5	0.302	0.303	0.3	0.445	0.444	0.2	0.151	0.151	0.0
1.0	1.02	1.02	0.0	0.948	0.947	0.1	0.508	0.510	0.4
1.5	1.91	1.92	0.5	1.51	1.51	0.0	0.944	0.958	1.5
2.0	2.92	2.92	0.0	2.14	2.14	0.0	1.48	1.46	1.4
2.5	4.04	4.03	0.2	2.84	2.85	0.4	2.04	2.02	1.0
2.8	4.80	4.76	0.8	3.28	3.32	1.2	2.42	2.38	1.7
3.0	5.41	5.28	2.5	3.54	3.65	3.0	2.73	2.64	3.4
3.1	6.10	5.54	10.1	3.41	3.82	10.7	3.07	2.77	10.8
3.14	10.1	5.65	78.8	0.231	3.89	94.1	5.05	2.82	79.1
3.2	5.35	5.81	7.9	4.35	4.00	8.8	2.69	2.91	7.6
3.3	5.89	6.09	3.3	4.32	4.17	3.6	2.96	3.04	2.6
3.5	6.53	6.64	1.7	4.61	4.53	1.8	3.29	3.32	0.9
4.0	7.97	8.04	0.9	5.50	5.44	1.1	4.01	4.02	0.2
5.0	9.97	10.0	0.3	6.75	6.70	0.7	5.10	5.01	1.8
8.0	7.02	7.04	0.3	4.82	4.65	3.7	3.73	3.52	6.0

* worst case

Notes:
1. The average surface velocity is defined in Equation (33); the average surface pressure is similarly defined.
2. The "% Error" is defined as 100*|NASHUA - Exact|/Exact
3. SI units are used (Pa for pressure and m/s for velocity). Far-field pressures are calculated at a range of 100m.
4. The NASHUA far-field pressure used is the one on the far-field sphere which deviates the most in absolute value from the exact result.
5. The critical frequencies which affect these calculations are located at ka = π and ka = 8.18.

problem, thus providing a good check on NASHUA's ability to combine symmetry cases.

The benchmark solution to which the NASHUA results are compared is a series solution which we developed based on equations in the Junger and Feit book [20]. The results of this comparison are shown in Table 2 for four different non-dimensional drive frequencies ka, where 'a' is the radius of the sphere. None of the drive frequencies is near a critical frequency. For each drive frequency ka, the normalized far-field pressure $|p_r r/p_o a|$ is listed for each colatitude angle θ,

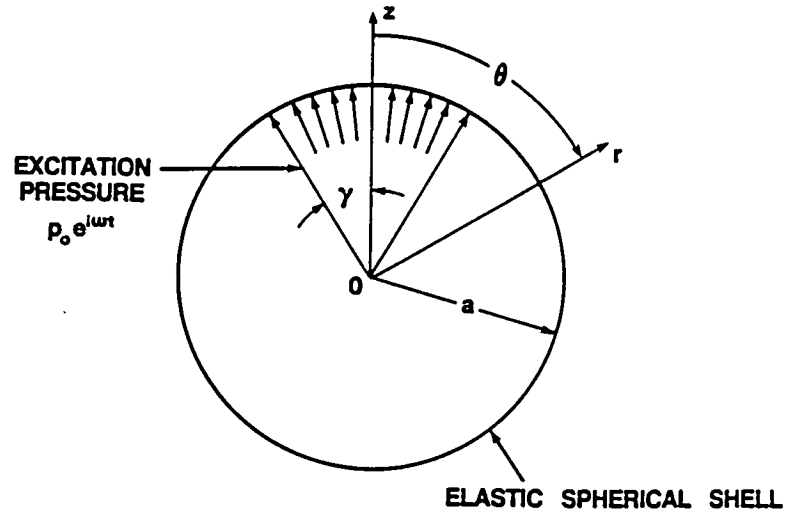

Figure 4 - Submerged Elastic Spherical Shell Driven over Sector

where p_r is the far-field pressure at distance r from the origin, and p_o is the internally-applied pressure. Clearly, the NASHUA solution again agrees very well with the exact solution.

DISCUSSION

A very general capability has been described for predicting the acoustic sound pressure field radiated by arbitrary three-dimensional elastic structures subjected to time-harmonic loads. Sufficient automation is provided so that, for many structures of practical interest, an existing NASTRAN structural model can be adapted for NASHUA acoustic analysis within a few hours.

One of the major benefits of having NASHUA linked with NASTRAN is the ability to integrate the acoustic analysis of a structure with other dynamic analyses. Thus the same finite element model can be used for modal analysis, frequency response analysis, linear shock analysis, and underwater acoustic analysis. In addition, many of the pre- and postprocessors developed for use with NASTRAN become available for NASHUA as well.

There are two areas in which improvements to NASHUA would be desirable. The first is to remove the frequency limitation caused by the presence of the critical frequencies inherent in the Helmholtz integral equation formulation. As a result, cylindrical shells, for example, can be safely analyzed by NASHUA only for $ka < 2.4$, where 'a' is the radius. Since for some problems, it would be of interest to treat higher frequencies, the limitation should be removed. A conversion to a different formulation (e.g., Burton and Miller [8] or Mathews [10] is being considered.

The second area in which NASHUA could be improved would be to extend the program's capabilities to include acoustic scattering as well as radiation. Generally, this improvement requires replacing the mechanical drive force with an incident loading, a relatively modest change [2].

Table 2 - Comparison of NASHUA Solution with Converged Series Solution for Sector-Driven Spherical Shell

ka	Colatitude θ (degrees)	Normalized Far-Field Pressure, $p_r r/p_o a$		
		NASHUA	Exact	% Error
0.5	0	0.0514	0.0514	0.0
	30	0.0445	0.0445	0.0
	60	0.0257	0.0258	0.4
	90	0.0035	0.0035	0.0
	120	0.0258	0.0259	0.4
	150	0.0446	0.0446	0.0
	180	0.0515	0.0515	0.0
1.0	0	0.0887	0.0889	0.2
	30	0.0744	0.0745	0.1
	60	0.0434	0.0434	0.0
	90	0.0235	0.0237	0.8
	120	0.0448	0.0448	0.0
	150	0.0784	0.0786	0.3
	180	0.0939	0.0942	0.3
2.0	0	1.183	1.163	1.7
	30	0.278	0.276	0.7
	60	0.667	0.666	0.2
	90	0.131	0.128	2.3
	120	0.721	0.716	0.7
	150	0.757	0.695	8.9
	180	1.977	1.860	6.3
5.0	0	0.510	0.512	0.4
	30	0.292	0.292	0.0
	60	0.020	0.017	17.6
	90	0.100	0.097	3.1
	120	0.161	0.160	0.6
	150	0.169	0.163	3.7
	180	0.177	0.170	4.1

REFERENCES

1. Everstine, G.C., "A Symmetric Potential Formulation for Fluid-Structure Interaction," J. Sound and Vibration, vol. 79, no. 1, pp. 157-160 (1981).

2. Everstine, G.C., "Structural-Acoustic Finite Element Analysis, with Application to Scattering," Proc. 6th Invitational Symposium on the Unification of Finite Elements, Finite Differences, and Calculus of Variations, ed. by H. Kardestuncer, Univ. of Connecticut, pp. 101-122 (1982).

3. Kalinowski, A.J., and C.W. Nebelung, "Media-Structure Interaction Computations Employing Frequency-Dependent Mesh Sizes with the Finite Element Method," The Shock and Vibration Bulletin, vol. 51, part 1, pp. 173-193 (1981).

4. Chen, L.H., and D.G. Schweikert, "Sound Radiation from an Arbitrary Body," J. Acoust. Soc. Amer., vol. 35, no. 10, pp. 1626-1632 (1963).

5. Schenck, H.A., "Improved Integral Formulation for Acoustic Radiation Problems," J. Acoust. Soc. Amer., vol. 44, no. 1, pp. 41-58 (1968).

6. Henderson, F.M., "A Structure-Fluid Interaction Capability for the NASA Structural Analysis (NASTRAN) Computer Program," Report 3962, David Taylor Naval Ship R&D Center, Bethesda, Maryland (1972).

7. Wilton, D.T., "Acoustic Radiation and Scattering From Elastic Structures," Int. J. Num. Meth. in Engrg., vol. 13, pp. 123-138 (1978).

8. Burton, A.J., and G.F. Miller, "The Application of Integral Equation Methods to the Numerical Solution of Some Exterior Boundary-Value Problems," Proc. Roy. Soc. Lond. A, vol. 323, pp. 201-210 (1971).

9. Baron, M.L., and J.M. McCormick, "Sound Radiation from Submerged Cylindrical Shells of Finite Length," ASME Trans. Ser. B, vol. 87, pp. 393-405 (1965).

10. Mathews, I.C., "A Symmetric Boundary Integral-Finite Element Approach for 3-D Fluid Structure Interaction," in Advances in Fluid-Structure Interaction - 1984, PVP-Vol. 78 and AMD-Vol. 64, ed. by G.C. Everstine and M.K. Au-Yang, American Society of Mechanical Engineers, New York, pp. 39-48 (1984).

11. Everstine, G.C., "User's Guide to the Coupled NASTRAN/Helmholtz Equation Acoustic Radiation Capability (NASHUA)," Report CMLD-86/03, David Taylor Naval Ship R&D Center, Bethesda, Maryland (1986).

12. Lamb, H., Hydrodynamics, sixth ed., Dover Publications, New York (1945).

13. Vandergraft, J.S., Introduction to Numerical Computations, second ed., Academic Press, New York (1983).

14. Chertock, G., "Integral Equation Methods in Sound Radiation and Scattering from Arbitrary Surfaces," Report 3538, David Taylor Naval Ship R&D Center, Bethesda, Maryland (1971).

15. Ghering, W.C., Reference Data for Acoustic Noise Control, Ann Arbor Science Publishers, Inc., Ann Arbor, Michigan (1978).

16. Marquardt, M.B., "DIGIT: The Curve Digitizing Subsystem of the Interactive Data Display System," Report DTNSRDC-80/038, David Taylor Naval Ship R&D Center, Bethesda, Maryland (1980).

17. Lipman, R.R., "Calculating Far-Field Radiated Sound Pressure Levels from NASTRAN Output," 14th NASTRAN Users' Colloquium, National Aeronautics and Space Administration, Washington, DC (1986) (this volume).

18. Kinsler, L.E., A.R. Frey, A.B. Coppens, and J.V. Sanders, Fundamentals of Acoustics, third ed., John Wiley and Sons, New York (1982).

19. Huang, H., and Y.F. Wang, "Asymptotic Fluid-Structure Interaction Theories for Acoustic Radiation Prediction," J. Acoust. Soc. Amer., vol. 77, no. 4, pp. 1389-1394 (1985).

20. Junger, M.C., and D. Feit, Sound, Structures, and Their Interaction, The MIT Press, Cambridge, Massachusetts (1972).

A FINITE ELEMENT SURFACE IMPEDANCE REPRESENTATION FOR STEADY-STATE PROBLEMS

A. J. KALINOWSKI

NAVAL UNDERWATER SYSTEMS CENTER
NEW LONDON, CONNECTICUT 06320

SUMMARY

A procedure for determining the scattered pressure field resulting from a monochromatic harmonic wave that is incident upon a layered energy absorbing structure is treated. The situation where the structure is modeled with finite elements and the surrounding acoustic medium (water or air) is represented with either acoustic finite elements--or--some type of boundary integral formulation, is considered. Finite element modeling problems arise when the construction of the structure, at the fluid-structure interface, are nonhomogeneous and in particular when the inhomogeneities are small relative to the acoustic wave length. An approximate procedure is presented for replacing the detailed microscopic representation of the layered surface configuration with an equivalent simple surface impedance finite element, which is especially designed to work only at limited frequencies. An example problem is presented using NASTRAN, however the procedure is general enough to adapt to practically any finite element code having a steady state option.

INTRODUCTION

This paper addresses the topic of solving acoustic-structure interaction problems involving a configuration having some sort of soft layered viscoelastic material, applied to a stiffer main body. Typically, acoustic sound energy impinges upon the treated structure (e.g. Figure 1a) and it is of interest to determine the reflected acoustic pressure. Specifically, the finite element method of solution is considered for the representation of the acoustically surface treated structure, and either acoustic finite elements (ref. 6,7)--or--some type of boundary integral method (ref. 8) that does not directly involve modeling the fluid is considered for the fluid. For either type of fluid representation there still remains the difficult problem of representing the energy absorbing properties of the viscoelastic outer layer in cases where the microscopic details are too complicated to represent with finite elements in the practical case where a large region of the structure is to be analyzed. On the other hand if only a small patch of the structure were

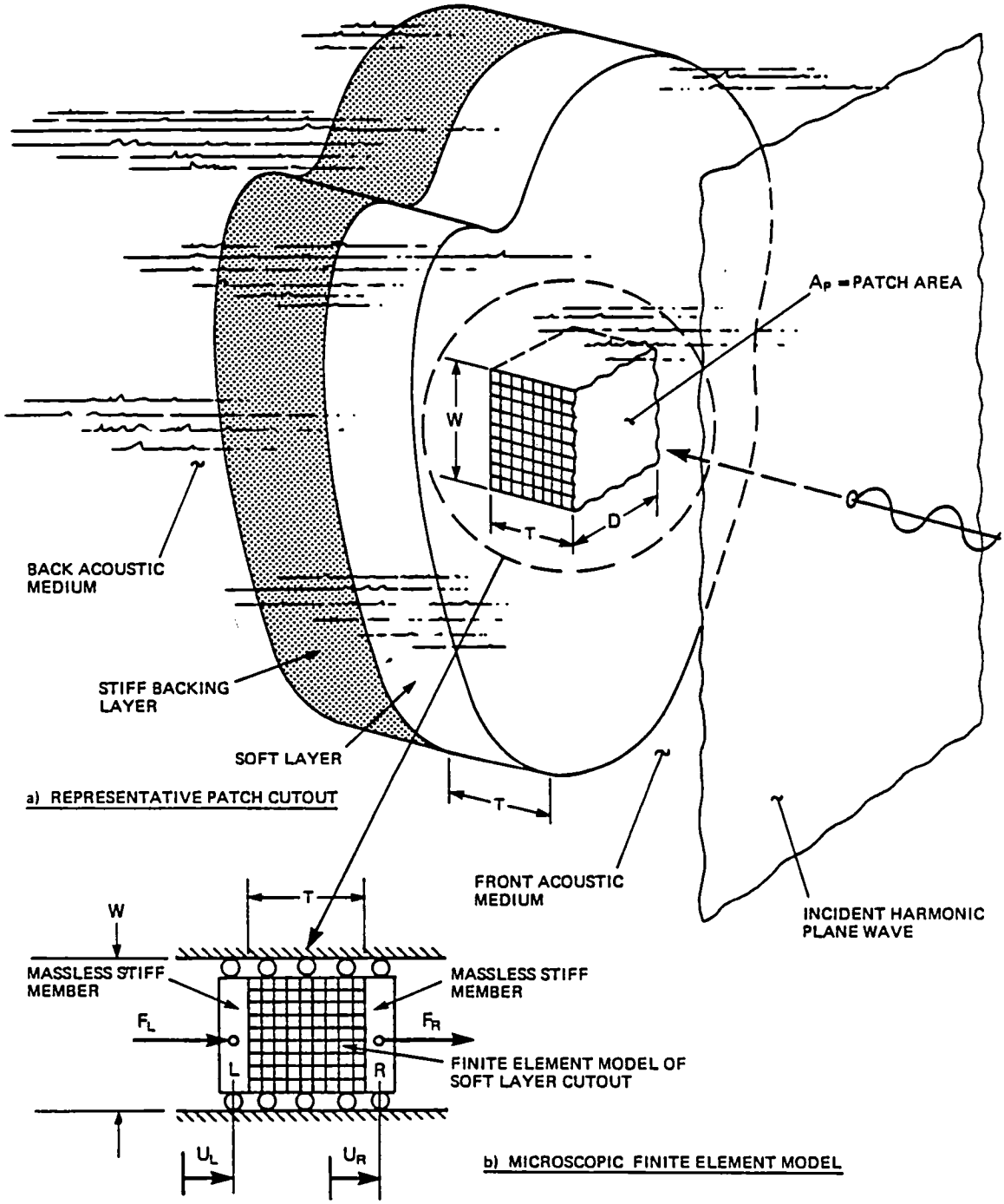

FIGURE - 1 GENERATION OF MACRO DYNAMIC STIFFNESS ($\bar{K}$)

considered of, say, area A_p (see Figure 1a), it would be well within the range of practical finite element analysis.

The idea pursued here is to use this microscopic patch, in some sense, to generate a super finite element with many less degrees-of-freedom as the detailed microscopic patch, yet produces nearly the same reflected pressure field had the main body been entirely been modeled with the detailed finite element representation. Essentially the finer details of the soft nonhomogeneous layer are smeared out and represented by a sequence of simplier macroscopic elements. Conceptionally, the Figure 1a configuration is replaced by the simplier finite element model shown in Figure 2, where the concept is generalized to apply to a curved surface. In Figure 2, the details of the stiff backing layer are not shown and are left as a choice to the model maker whether to represent the backing structure with say plate elements or solid brick elements. A choice of which acoustic fluid representation (i.e. finite element or boundary integral method) must also be made. The remainder of this paper focuses on the problem of defining the properties of the microscopic viscoelastic nonhomogeneous layer by specifically prescribing an equivalent macroscopic lumped parameter element of the type shown in Figures 3 and 4.

Obtaining an approximate simplier model to represent a more complex nonhomogeneous viscoelastic layer has been considered by others, refs. (1-5). However in these earlier works, particularly ref. (1 and 5), the emphasis was concerned with obtaining a simple lumped parameter representation of the layer directly in terms of the identifiable physical parameters of the layer (e.g. modulus of elasticity and thickness) so that the physics of the layer's acoustical performance could be explained. In contrast, for the work presented here, we use the lumped parameter only as a means towards fitting the actual microscopic surface impedance, and the meaning of the lumped parameters need not be related to any specific physical properties of the nonhomogeneous layer. Further, in none of the referenced works (1-5), has an attempt been made to apply the results of the work to some sort of finite element scheme such as in Figure 2.

OUTLINE OF THE METHOD

Before proceeding to the detailed development, a brief outline of the procedure is helpful. The first step is to cut out a representative patch, of surface area, A_p, from the overall configuration, such as the one shown in Figure 1a. Next a detailed finite element model of the patch is constructed, like shown in Figure 1b, where from this finite element model of the soft nonhomogeneous layer alone, we can obtain the smeared out macroscopic dynamic stiffness. Next, through a curve fitting process, an equivalent simple lumped parameter finite element model is designed that has the same surface impedance as the finite element patch at only one frequency (for the Figure 3 model) or at only two frequencies (for the Figure 4 model). Next the simple lumped parameter elements are distributed over the whole surface of the structure (e.g. Figure 2), where the same lumped parameters are used for all surface nodes, except for an alteration accounting for the fact that the surface area, A_n, around each node might be different if a variable mesh is used. The fact

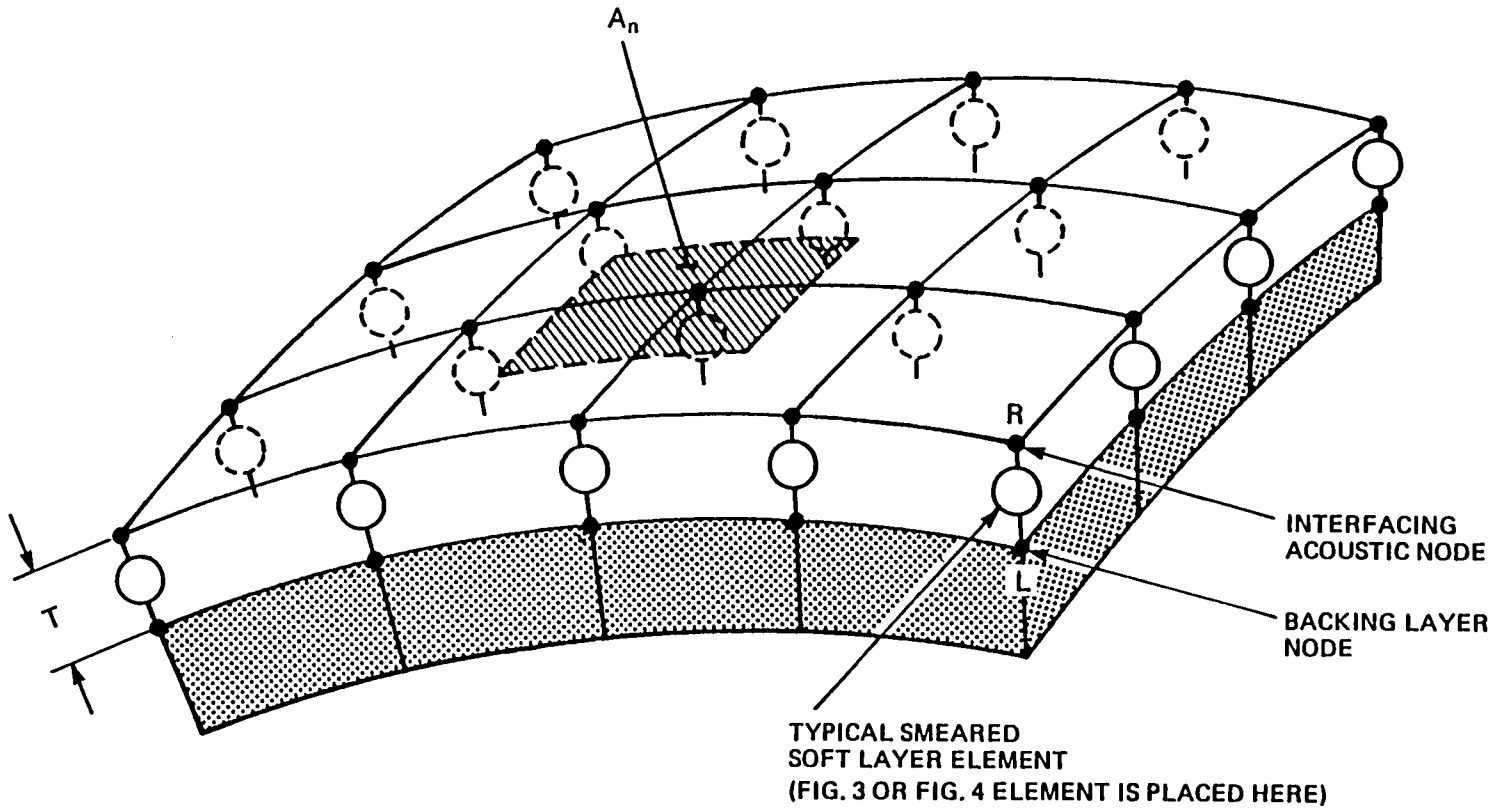

FIGURE - 2 SINGLE ELEMENT SMEARED MACROSCOPIC REPRESENTATION OF SOFT LAYER

that the direction of the normal to the surface changes on a curved surface is treated automatically when the bar version (NASTRAN CONROD) of the lumped parameter model (Figure 3C or Figure 4C) is used. Finally, the fluid is connected to the fluid side terminals of the lumped parameter elements (either acoustic finite elements--or--the boundary integral interaction matrix), and the scattering problem is solved in the usual manner for scattering from a homogeneous elastic body (e.g. using NASTRAN rigid format 8 with the acoustic elements of ref. 6 or 7 as appropriate and absorbing radiation boundary of ref. 9).

MACROSCOPIC IMPEDANCE DETERMINATION

The first step is to obtain the macroscopic surface impedance of a small patch of the actual nonhomogeneous viscoelastic layer. The methodology given here is general enough to treat a variety of inhomogeneities ranging from the tubes of ref. (3) to the imbedded voids used in refs. (2) and (5). Therefore in what follows, we are not specific about the layer, wherein the only requirement is that the patch size, A_p, is just large enough to pick up a typical repeated pattern. The Figure 1a, shows the sample patch as a WxD rectangular one, however, the shape should be whatever is convenient to represent the repeated pattern. Figure 1b shows a generic finite element representation. It is important to point out that the details of the finite element model must be fine enough to properly represent the complex spatial response existing within the layer. It is further assumed that the Figure 1a viscoelastic layer is infinite in extent and that plane of symmetry type boundary conditions can be applied to all four lateral faces (of areas WxT and DxT). This boundary condition is represented by the zero lateral constraint indicated by the rollers shown in Figure 1b.

The Figure 1b model is designed to respond to normal pressure that is approximately uniform over the patch surface. To obtain the smeared effects of the inhomogeneities, a weightless rigid "piston like" member is attached to the left and right surfaces of the layer (hence the designation L and R to denote the left and right surface nodes and all other pertinent surface related items). The attachment of the pistons to the layer is a rigid connection in the normal direction of motion, however the lateral direction attachment depends on the specifics of the application. The usual case is also a rigid attachment in a direction transverse to the motion direction on the left side (attachment to stiff backing structure), where as the attachment can allow transverse slip on the right side (attachment to the fluid). Double nodes are required when such slip is allowed.

The relationship relating the left and right piston faces and displacements are given by

$$\underset{\{F\}_B}{\begin{Bmatrix} F_L \\ F_R \end{Bmatrix}} = \underset{[\bar{K}]_{2x2}}{\begin{bmatrix} \bar{K}_{LL} & \bar{K}_{LR} \\ \bar{K}_{RL} & \bar{K}_{RR} \end{bmatrix}} \underset{\{U\}_B}{\begin{Bmatrix} U_L \\ U_R \end{Bmatrix}} \qquad (1)$$

where the forces, F_L and F_R, on the left and right piston vary harmonically according to

$$F_L = \bar{F}_L \exp(i\omega t), \quad F_R = \bar{F}_R \exp(i\omega t) \tag{2}$$

and the piston displacements U_L, U_R according to

$$U_L = \bar{U}_L \exp(i\omega t) \quad U_R = \bar{U}_R \exp(i\omega t) \tag{3}$$

The 2x2 dynamic stiffness, $[\bar{K}]$, which is the coefficient of $\{U\}_B$ in equation (1), can be computed from the fundamental matrices $[K]$, $[M]$, and $[C]$ of the figure (1b) microscopic finite element model by decomposing the response into boundary nodes (B subscripts) and interior nodes (I subscripts). Thus

$$\begin{Bmatrix} F_B \\ \hline F_I \end{Bmatrix} = \underbrace{\left[\begin{array}{c|c} K_{BB} & K_{BI} \\ \hline K_{IB} & K_{II} \end{array}\right]}_{[\bar{K}]_T} \begin{Bmatrix} U_B \\ \hline U_I \end{Bmatrix} \tag{4}$$

can be used to solve for $\{F\}_B$ in terms of $\{U\}_B$, (note that $\{F\}_I = \{0\}$ since there are no forces on the internal nodes), where the elements of $[\bar{K}]$ are of the form

$$[\bar{K}]_T = (-[M]\omega^2 + [K] + i\omega [C])$$

It follows that after eliminating $\{U\}_I$ from (4), we obtain

$$\{F\}_B = [\bar{K}_{BB} - \bar{K}_{BI} \bar{K}_{II}^{-1} \bar{K}_{IB}]\{U\}_B \tag{5}$$

and comparing equations (1) and (5), it is evident that $[\bar{K}]$ can be computed from

$$[\bar{K}] = [\bar{K}_{BB} - \bar{K}_{BI} \bar{K}_{II}^{-1} \bar{K}_{IB}] \tag{6}$$

Therefore, one approach to obtaining the $[\bar{K}]$ representation of the microscopic layer at some desired frequency, say ω_1, would be to evaluate $[\bar{K}]$ by constructing the right hand side of equation (6) with a DMAP sequence of instructions. This however is an unwieldly process which involves both partitioning the microscopic $[\bar{K}]_T$ matrix (e.g. ref. 10) and forming the inverse of $[\bar{K}]_{II}$, which could be a costly process.

An alternate process for generating $[\bar{K}]$ is to compute it directly from two finite element runs, involving the Figure 1b patch model. For a single frequency ω_1, we need to solve for the four complex constants comprising $[\bar{K}]$ in equation (1). These four constants are generated from the following two finite elements runs which are referred to as computer "run-a" and "run-b"

- "run-a"; set $\bar{F}_L^a = 1.0$, $\bar{U}_L^a = 0.0$, compute $\bar{U}_L^a$, $\bar{F}_R^a$ from NASTRAN "run-a"

NOTE: Superscripts a and b refer to "run-a" and "run-b"

"run-b"; set $\bar{F}^b_R = 1.0$, $\bar{U}^b_L = 0.0$, compute

$\bar{U}^b_R$, $\bar{F}^b_L$ from NASTRAN "run-b"

Where the complex forces, $\bar{F}^a_R$ and $\bar{F}^b_L$ are read from the forces of constraint printout as activated by the presence of SPCFORCES = ALL card in the case control in the case of NASTRAN. The $\bar{U}^a_L$ and $\bar{U}^b_R$ complex displacement amplitudes are part of the normal finite element output as activated by the DISPLACEMENT = ALL card. Inserting the results of these two runs directly into equation (1) gives four equations and four unknowns to determine the four complex stiffness entries of the 2x2 $[\bar{K}]$ matrix, namely

$$[\bar{K}(\omega)] = \begin{bmatrix} \frac{1}{\bar{U}^a_L} & \frac{\bar{F}^b_L}{\bar{U}^b_R} \\ \frac{\bar{F}^a_R}{\bar{U}^a_L} & \frac{1}{\bar{U}^b_R} \end{bmatrix} \equiv \begin{bmatrix} \left(\bar{K}^r_{LL} + \bar{K}^i_{LL}\right) & \left(\bar{K}^r_{LR} + i\bar{K}^i_{LR}\right) \\ \text{SYMM} & \left(\bar{K}^r_{RR} + i\bar{K}^i_{RR}\right) \end{bmatrix} \quad (7)$$

where the matrix $[\bar{K}]$ is symmetric. The response and constraint forces will in general be complex when the microscopic finite element model of Figure 1b consist of materials having viscoelastic dissipation (this effect is activated by the GE parameter on a NASTRAN MAT1 card). For each frequency, ω, there are six numbers $\bar{K}^r_{LL}$, $\bar{K}^i_{LL}$, ... $\bar{K}^i_{RR}$ that define the smeared macroscopic stiffness. Upon repeating the process described to generate equation (7) over a sweep of frequencies, a frequency description of the smeared macroscopic stiffness can be obtained like the one illustrates in Figure 6. Using the frequency sweep option in NASTRAN, the data used to generate the Figure 6 example was generated with just two computer runs, by frequency sweeping the two "run-a", "run-b" cases described earlier.

LUMPED PARAMETER ELEMENTS

The three complex terms in equation (7) define the equivalent dynamic stiffness for a patch of area A_p normal to the surface, in a global coordinate system with one coordinate axis also in line with the normal to the surface. There now remains the task of implementing equation (7) as an element in the finite element code, so that the as yet undefined layer elements shown in Figure 2 can be implemented. Two basic lumped parameter models are developed herein. The first one is a single frequency model, that is designed to represent equation (7) only at one selected frequency. The second model is similar, except it is designed to represent equation (7) at two selected frequencies. Further, the second model automatically interpolates between the two selected frequency and therefore attempts to represent the nonhomogeneous layer response over a limited hand of frequencies. The area of the patch, A_p, used to generate the macroscopic stiffness of equation (7) is in general, different from the area factor, A_n, used to convert distributed loads into concentrated nodal forces (see Figures 2 for A_n). Consequently, the generalized stiffness per unit patch area $(1/A_p)[\bar{K}]$ is a more fundamental quantity to work with. The dynamic stiffness to use at a typical node

connection shown in Figure 2 then would be

$$[\tilde{K}] = (A_n/A_p)[\bar{K}] \tag{8}$$

Implementation of $[\tilde{K}]$ in the finite element code is awkward, although straight forward, when the element is not in alignment with one of the axis of the global coordinate system. In this case, equation (8) is further modified with a coordinate transformation

$$[\tilde{K}]' = [T]^T[\tilde{K}][T] \tag{9}$$

where $[T]$ is the usual local to global coordinate transformation used in rod finite elements (ref. 11).

The implementation of equation (9) directly might require some sort of preprocessor, to generate the $[\tilde{K}]'$ matrix in conjunction with the coordinate transformations. A simplier alternate procedure is also given, that redefines the local $[\bar{K}]$ matrix in terms of rods (tension members such as CONROD and CVISC elements in NASTRAN), and the existing machinery in the finite element code will automatically take care of any transformations. Still another way to treat the coordinate transformation is to let each node have its own coordinate system, where one of the axis is aligned along the normal to the surface. This can be invoked in NASTRAN via a CORD1R card. In this manner, NASTRAN would automatically take care of the transformations, however it would require every node to have its own coordinate system.

Single Frequency Lumped Parameter Element

Here we are concerned with implementing equation (7), to each surface node (e.g. as in Figure 2), but we only require that the analysis be done at one frequency, ω_1. We give three alternate methods of installing the appropriate nodal dynamic stiffness.

a) Direct Matrix Entry Version

For programs such as NASTRAN that accept direct entries to the assembled global dynamic stiffness matrix ($[K_{dd}]$, in NASTRAN) the components of equation (9) can be entered directly with DMIG cards. Since NASTRAN accepts complex entries, there is no problem with inserting both the real and imaginary parts of the $[\tilde{K}]'$ matrix into NASTRAN.

For finite element codes other than NASTRAN that do not accept a complex stiffness entry directly,it can be done indirectly by inserting the real part of $[\tilde{K}]'$ through the usual structural stiffness entry, $[K]$, and the imaginary part of $[\tilde{K}]'$ through the damping matrix, $[C]$, after dividing img.pt($[\tilde{K}]'$) by ω_1.

b) Spring-Damper Entry Version

The matrix $[\tilde{K}]$, (before coordinate transformation) can be built from simple

lumped parameter springs and damper as illustrated in Figure 3b. The idea is to assign values to the springs and dampers, so that the assembled [K] matrix is formed. By inspection of Figure 3b, the local element dynamic stiffness is

$$[\tilde{K}] = \begin{bmatrix} (K_\ell + K_m) + i\omega (C_m + C_\ell) & -K_m - i\omega C_m \\ \text{SYMM} & (K_r + K_m) + i\omega (C_m + C_r) \end{bmatrix} \quad (10)$$

Upon equating equations (8) and (10) in conjunction with equation (7), we arrive at the following constants for the single frequency lumped parameter model:

$$\begin{aligned} K_m &= -\bar{K}^r_{LR}\bar{A} & C_\ell &= (\bar{K}^i_{LL} + \bar{K}^i_{LR})\bar{A}/\omega \\ C_m &= -\bar{K}^i_{LR}\bar{A}/\omega & K_r &= (\bar{K}^r_{RR} + \bar{K}^r_{LR})\bar{A} \\ K_\ell &= (\bar{K}^r_{LL} + \bar{K}^r_{LR})\bar{A} & C_r &= (\bar{K}^i_{RR} + \bar{K}^i_{LR})\bar{A}/\omega \end{aligned} \quad (11)$$

where $\bar{A} = A_n/A_p$, is the nodal area to patch area ratio.

In the NASTRAN program, these lumped parameters are entered via CELAS2 and CDAMP2 cards. When the elements are not in line with the global axis, coordinate transformations are involved, i.e. involving equation (9)--or--employing different reference frames for each element using CORD1R cards.

c.) Three Rod Version

The three rod element (made from CONROD elements in NASTRAN) shown in Figure 3b is an alternate procedure to install the desired equation (9) dynamic stiffness. The rods, properly sized, will generate the same dynamic stiffness matrices as either of the two mentioned ones, but has the advantage that the coordinate transformations, should they be needed, are taken into account automatically in the finite element program. The same dynamic stiffness realized by the Figure 3b model can be achieved with the Figure 3c three massless rod model by using the following rod properties shown in Table 1.

TABLE 1 Single Frequency Rod Properties

	Mass Density ρ	Young's Modulus E	Poisson's Ratio ν	Loss Factor η	Cross Sec Area A	Rod Length L
Left rod	0	K_ℓ	0	$\omega C_\ell/K_\ell$	T	T
Middle rod	0	K_m	0	$\omega C_m/K_m$	T	T
Right rod	0	K_r	0	$\omega C_r/K_r$	T	T

The stiffness of a rod is AE/L, and the damping matrix is η AE/L, thus it can be seen how the Figure 3b and 3c models result in equivalent dynamic stiffness matrices. The 6 Constants K_ℓ,. . .C_r are still computed using Equation 11. The material properties ρ, E, ν, η, A appear on the CONROD and MAT1 cards in

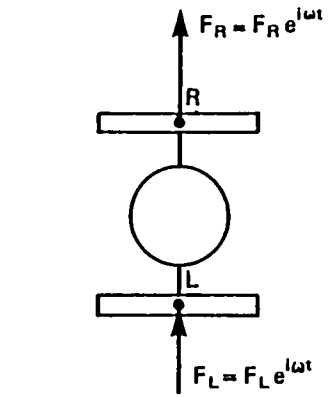

$$\begin{Bmatrix} \bar{F}_L \\ \hline \bar{F}_R \end{Bmatrix} = \left[\begin{array}{c|c} \bar{K}_{LL} & \bar{K}_{LR} \\ \hline \bar{K}_{RL} & \bar{K}_{RR} \end{array}\right] \begin{Bmatrix} \bar{U}_L \\ \hline \bar{U}_R \end{Bmatrix}$$

a) DIRECT MATRIX ENTRY VERSION

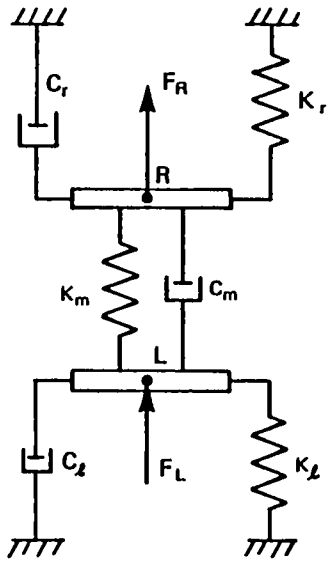

b) SPRING - DAMPER VERSION

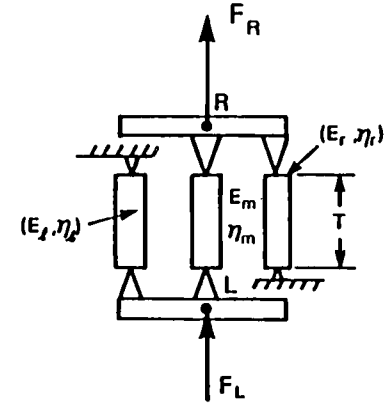

$\rho_\ell = \rho_m = \rho_r = 0$

c) THREE MASSLESS RODS VERSION

FIGURE - 3 SINGLE FREQUENCY IMPEDENCE ELEMENT

NASTRAN, however length T is computed by the program as the distance between terminal nodes R, and L in Figure 2. The user must be sure to enter a T in the area slot that is consistent with this length! Also care must be taken to ground out one end of the left and right rod as shown schematically in Figure 3c. See Table 2 comments for entering a negative modulus, E.

Two-Frequency Lumped Parameter Element

The object of this macroscopic element is to have a single element represent the dynamic stiffness of the patch over a limited range of frequencies, without having to change the parameter constants. This would have use as a convenience feature when performing a frequency sweep analysis--or--may be of use in a transient type solution, where the model is expected to be accurate over a narrow band of frequencies.

a.) Mass-Spring-Damper Version

The element local dynamic stiffness matrix for the model shown in Figure 4b is given by the relation

$$[\tilde{K}] = \begin{bmatrix} (K_\ell + K_m) - \omega^2(M_\ell + M_m\beta_1) + i\left(\omega(C_m + C_\ell) + K_\ell^c + K_m^c\right) & -(K_m + M\beta\omega^2) - i\left(C_m\omega + K_m^c\right) \\ \text{SYMM} & (K_r + K_m) - \omega^2(M_r + M\beta_1) + i\left(\omega(C_m + C_r) + K_r^c + K_m^c\right) \end{bmatrix} \quad (12)$$

The structure of equation (12) permits one to vary both the real and imaginary parts of the three main entries of the $[\tilde{K}]$ matrix by changing the frequency ω. Note that had a lumped mass been used for the center mass element, the real part of the K_{LR} entry would not depend on frequency. A set of twelve equations and twelve unknowns can be set up to solve for twelve unknown lumped parameters K_ℓ, ...M_m appearing in equation (12). The system of equations is obtained by equating corresponding real and imaginary parts of equation (12) and (8) at the first desired frequency, ω_1 and again equating equations (12) and (8) evaluated at the second desired frequency, ω_2. Let the entries of equation (7) with a subscript 1 refer to the "run-a", "run-b" pair of stiffness generating runs described earlier at frequency (i.e. $\bar{K}_{LL1}$,...$\bar{K}_{RR1}$) and similarly let entries of equation (7) with subscripts 2 refer to the "run-a", "run-b" pair run at frequency ω_2 (i.e. $\bar{K}_{LL2}$,...$\bar{K}_{RR2}$. Solving these twelve weakly coupled equations, the following twelve results are obtained for the unknown lumped parameters, K_m ...K_r^c

$$K_m = (\omega_2^2 \bar{K}^r_{LR1} - \omega_1^2 \bar{K}^r_{LR2})/\Delta_2$$

$$M_m = -(\bar{K}^r_{LR1} - \bar{K}^r_{LR2})/(\beta_2 \Delta_2)$$

$$C_m = (\bar{K}^i_{LR2} - \bar{K}^i_{LR1})/\Delta_1$$

$$K^c_m = (\omega_2 \bar{K}^i_{LR1} - \omega_1 \bar{K}^i_{LR2})/\Delta_1$$

$$K_\ell = (\omega_1^2 B_2 - \omega_2^2 B_1)/\Delta_2$$

$$M_\ell = (B_2 - B_1)/\Delta_2$$

$$C_\ell = (D_1 - D_2)/\Delta_1$$

$$K^c_\ell = (\omega_1 D_2 - \omega_2 D_1)/\Delta_1$$

$$K_r = (\omega_1^2 F_2 - \omega_2^2 F_1)/\Delta_2$$

$$M_r = (F_2 - F_1)/\Delta_2$$

$$C_r = (G_1 - G_2)/\Delta_1$$

$$K^c_r = (\omega_1 G_2 - \omega_2 G_1)/\Delta_1$$

where $\Delta_1 = (\omega_1 - \omega_2)/\bar{A}$ $\quad \Delta_2 = (\omega_1^2 - \omega_2^2)/\bar{A}$ $\quad \bar{A} = A_n/A_p$ (13)

$$B_1 = \bar{K}^r_{LL1} - K_m + M_m \omega_1^2 \beta_1$$

$$B_2 = \bar{K}^r_{LL2} - K_m + M_m \omega_2^2 \beta_1$$

$$D_1 = \bar{K}^i_{LL1} - \omega_1 C_m - K^c_m$$

$$D_2 = \bar{K}^i_{LL2} - \omega_2 C_m - K^c_m$$

$$F_1 = \bar{K}^r_{RR1} - K_m + M_m \omega_1^2 \beta_1$$

$$F_2 = \bar{K}^r_{RR2} - K_m + M_m \omega_2^2 \beta_1$$

$$G_1 = \bar{K}^i_{RR1} - \omega_1 C_m - K^c_m$$

$$G_2 = \bar{K}^i_{RR2} - \omega_2 C_m - K^c_m$$

It is noted that β_1 and β_2 are not unknowns, but rather free parameters that can be selected by the user. However, when using the six rod version discussed later, one must use the β_1, β_2 factors corresponding to the consistent mass matrix being employed by the finite element program being used. The implementation of the model shown in Figure (4b) cannot be achieved, due to the fact we need a complex spring, iK_r^c, which is not possible to enter with say an CELAS2 card in NASTRAN. Instead, it can be realized either with the direct matrix entry option or with a six rod element shown in Figure 4c as explained next.

b) Direct Matrix Entry Version

Once the basic lumped parameters have been computed, via equation (13), the element matrix in equation (12) can be entered directly with DMIG cards for the assembled global NASTRAN $[K_{dd}]$ matrix, $[B_{dd}]$ and $[M_{dd}]$ matrices. Again letting the notation L, R denote the left right terminal node notation, we have

$$\left.\begin{aligned} [K_{dd}]_{LL} &= (K_\ell + K_m),\ i(K_\ell^c + K_m^c) \\ [K_{dd}]_{LR} &= -K_m,\ -iK_m^c \\ [K_{dd}]_{RR} &= (K_r + K_m),\ i(K_r^c + K_m^c) \end{aligned}\right\} \text{(enter as complex on DMIG card)}$$

$$[B_{dd}]_{LL} = C_m + C_\ell \qquad (14)$$

$$[B_{dd}]_{LR} = -C_m \qquad [B_{dd}]_{RR} = C_m + C_r$$

$$[M_{dd}]_{LL} = M_\ell + M_m\beta_1$$

$$[M_{dd}]_{LR} = M_m\beta_2$$

$$[M_{dd}]_{RR} = M_r + M_m\beta_1$$

As in the previous single frequency model, step to account for the coordinate transformation must be taken where applicable. The next 6-rod model will handle the coordinate transformations automatically.

c) Six Rod Element Version

A constant mass viscoelastic rod element with viscoelastic damping, η, has a dynamic stiffness matrix of the form:

$$[\bar{K}]_{rod} = \begin{bmatrix} (AE/\ell - m\omega^2\beta_1) + i\eta AE/\ell & -(AE/\ell + m\omega^2\beta_2) - i\eta AE/\ell \\ \text{SYMM} & (\frac{AE}{\ell} - m\omega^2\beta_1) + i\eta AE/\ell \end{bmatrix} \qquad (15)$$

where A is the rod cross section area; $m = A\rho\ell$ the total rod mass; ℓ is the rod

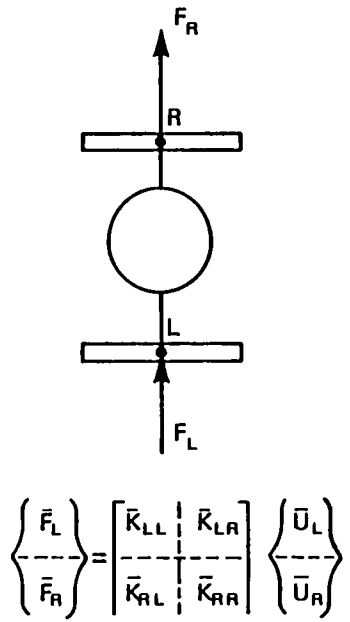
F_R
R
L
F_L
$\begin{Bmatrix} \bar{F}_L \\ \bar{F}_R \end{Bmatrix} = \begin{bmatrix} \bar{K}_{LL} & \bar{K}_{LR} \\ \bar{K}_{RL} & \bar{K}_{RR} \end{bmatrix} \begin{Bmatrix} \bar{U}_L \\ \bar{U}_R \end{Bmatrix}$

a) DIRECT MATRIX ENTRY VERSION

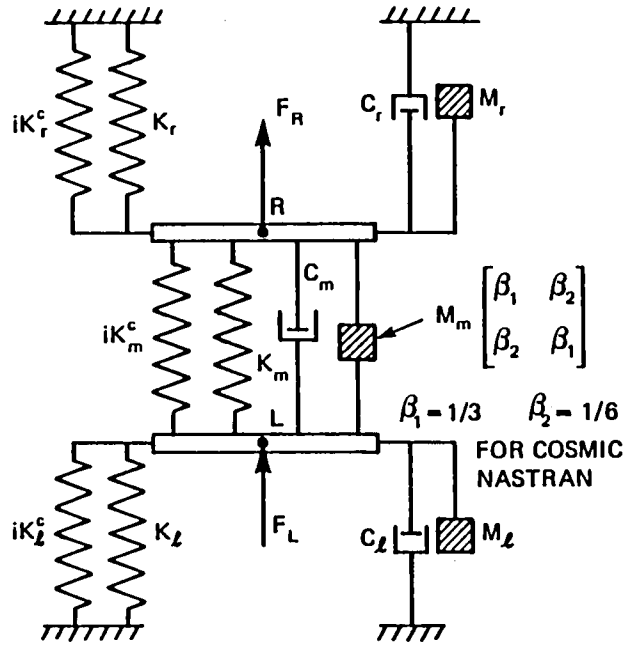

b) MASS - SPRING - DAMPER VERSION

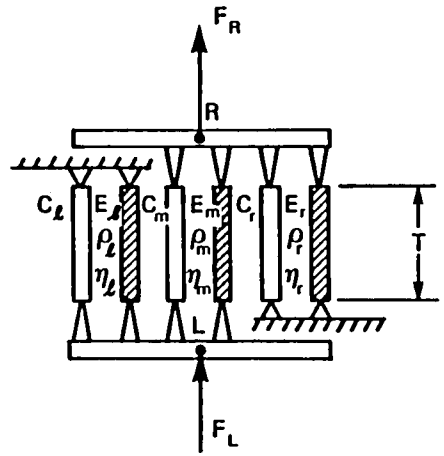

c) SIX - RODS VERSION

SHADED — CONSISTANT MASS VISCOELASTIC ROD
UNSHADED — VISCOUS DAMPER ROD

FIGURE - 4 TWO-FREQUENCY IMPEDENCE ELEMENT

length, E the modulus of elasticity and β_1 , β_2 are the mass distribution factors. It should be noted that the β factors may be different versions of NASTRAN (see note below Table 2).

Upon comparing equation (14) to equation (15), a set of equivalent rods can be defined to correspond exactly to the Figure 4b configuration. Table 2 below give the equivalent constants

TABLE 2 Two Frequency Rod Properties

	Mass density ρ	Young's Modulus E	Poisson's Ratio ν	Loss Factor η	Lumped Damping Constant C	Cross Sectional Area A	Rod Length (Indirect input) L
left viscoelastic rod	$M_\ell/(\beta_1 T^2)$	K_ℓ	0	K_ℓ^c/K_ℓ	—	T	T
left damper rod	--	--	—	--	C_ℓ	--	T
mid viscoelastic rod	M_m/T^2	K_m	0	K_m^c/K_m	—	T	T
mid damper rod	--	--	--	--	C_m	--	T
right viscoelastic rod	$M_r/(\beta_1 T^2)$	K_r	0	K_r^c/K_r	--	T	T
right damper rod	--	--	--	—	C_r	--	T

NOTE:
- For COSMIC NATRAN $\beta_1 = 1/3$ $\beta_2 = 1/6$
- For MSC NASTRAN $\beta_1 = 5/12$ $\beta_2 = 1/12$

In both COSMIC or MSC NASTRAN, the viscoelastic rods are implemented with CONROD elements (with GE as the loss factor on a MAT1 card) and the damper rods are implemented with CVISC elements where the lumped parameter damping constant is directly entered on the corresponding PVISC property card. The twelve basic constants K_m ...M_r given by equation (13) are the raw data that make up the 6 rod model. The rod length is not direct input to the 6 rods, but is rather computed automatically by the finite element program based on the length between "L" node and "R" node. It is important that the, T, length factor used for the dummy rod density and dummy rod area in Table 2 must be totally consistent with the distance between nodes L and R. Also care must be taken to ground out one end of the left CONROD and CVISC elements and also one end of the right CONROD and CVISC elements. Should E be negative, leave it blank and instead use a dummy positive shear modulus, G, and corresponding negative Poisson's ratio that corresponds to the desired negative E. For example, set G = |E| and set ν = -1.5.

DEMONSTRATION EXAMPLE PROBLEM

A soft inhomogeneous viscoelastic layer is attached to a stiff backing plate as shown in Figure 5a. The submerged sheet is a generic configuration that does not correspond to any particular real application, and is included here only to give some idea of the accuracy of the solution methodology in a simple application. Further, the details of the model are too lengthy to give here, and are beyond the intent of this demonstration problem. The example problem is kept simple by assuming the inhomogeneities are planar, thus permitting us to use two dimensional elements having a unit depth for the D variable of Figure 1a. The inhomogeneities were simulated by simply assigning different material constants (Young's modulus, mass density and dissipation loss factor) to soft layer finite elements in Figure 5b in the region marked soft layer. The inhomogeneities were distributed mainly in nonlayered patterns.

In the sample problem, the two frequency element of Figure 4 was used. The TxW region in Figure 5b, was used to generate the macroscopic dynamic stiffness versus frequencies using the "run-a", "run-b" procedure described earlier in the paper, in conjunction with the stiffness generator procedure illustrated in Figure 1b. The results of these 5x2 runs are shown in Figure 6, where the frequencies, ω, are normalized (divided) by (C_a/W) where C_a is the incident side acoustic medium wave speed. Further, the dynamic stiffnesses are normalized (divided) by the patch area, $A_p = WD$.

We arbitrarily selected the Figure 4 two frequency model to work at normalized frequencies of .733 and .837, as shown by the triangle markers in Figure 6. We purposely did not make the spread greater, so that some idea of how well the model would work in between the forced points could be examined. For example, the dashed line shown connecting the two forced points in Figure 6 ($\bar{K}_{RR}$ plot) represents the dynamic stiffness of the $\bar{K}_{RR}$ component of the Figure 4 two-frequency model. Since we have not forced the dynamic stiffness to be exactly equal to the patch model, some error can be expected in the response results if the two frequency model is used at the in between non forced frequency points.

The direct stiffness, mass, and damping via DMIG cards option (i.e. with equations 14) was used to implement the Figure 4 two-frequency model. The 6-bars model was not tried, because the CVISC viscous damping elements do not always assemble properly on the DEC VAX SERIES MODEL 11/780, April, 1984 release of NASTRAN. Hopefully these elements will be fixed in future releases.

The Figure 5b finite model was subject to an incident harmonic wave of strength P_o at the two normalized frequencies of .733 and .837 corresponding to the forced frequencies of the Figure 4 two-frequency model. The finite element model was first run with the full microscopic finite element representation for the soft layer (e.g. the soft inhomogeneous layer is represented with 398 quadrilateral and triangular elements)--and--secondly was rerun with one single Figure 4 type element replacing the original 398 finite elements. The reflected pressure at the far end of the finite element model was used to compare results. The results are shown in Table 3.

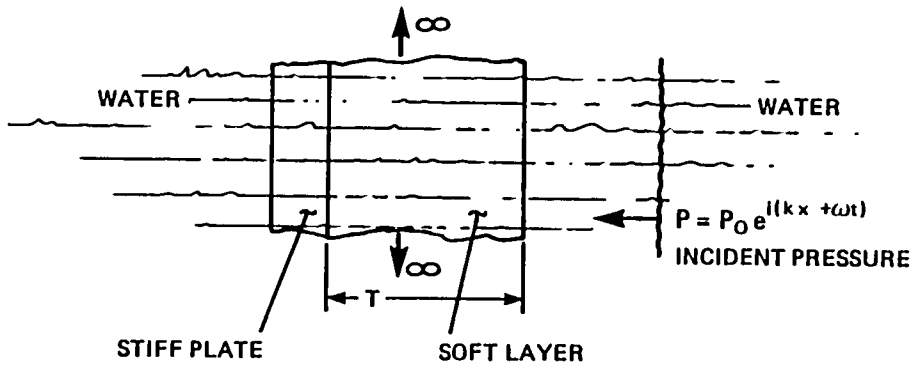

a) SUBMERGED FLAT PLATE

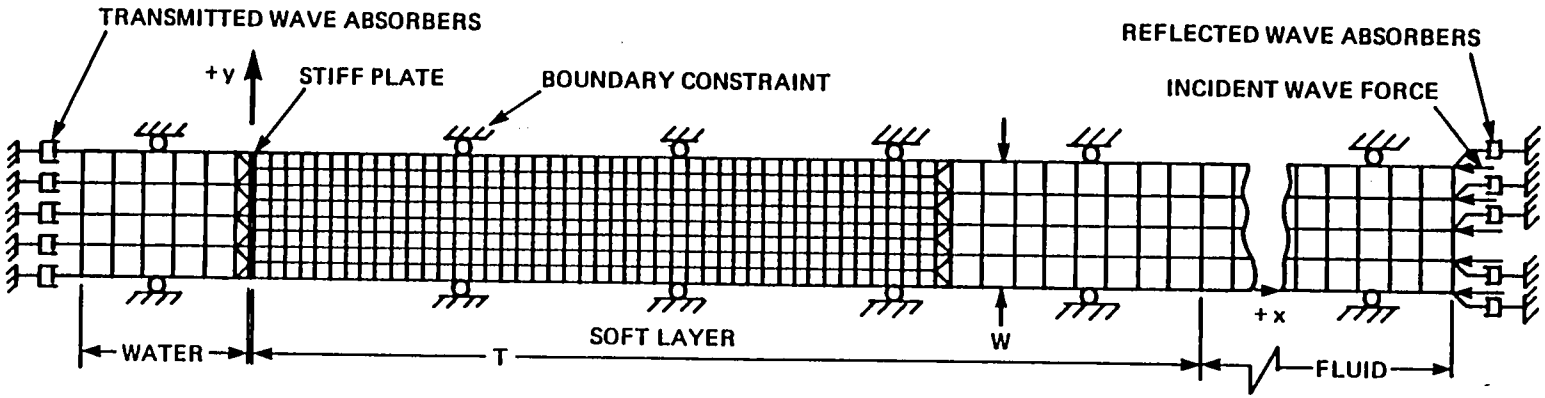

- 398 ELEMENTS FOR SOFT LAYER ALONE
- 856 ELEMENTS (CQDMEM, (TRMEM, CBAR)) (ENTIRE MODEL)
- 588 GRID POINTS

W = WIDTH OF REPRESENTATIVE MICROSCOPIC PATCH OF SOFT LAYER

b) FINITE ELEMENT MODEL

FIGURE - 5 SAMPLE NON-HOMOGENOUS MICROSCOPIC FINITE ELEMENT MODEL

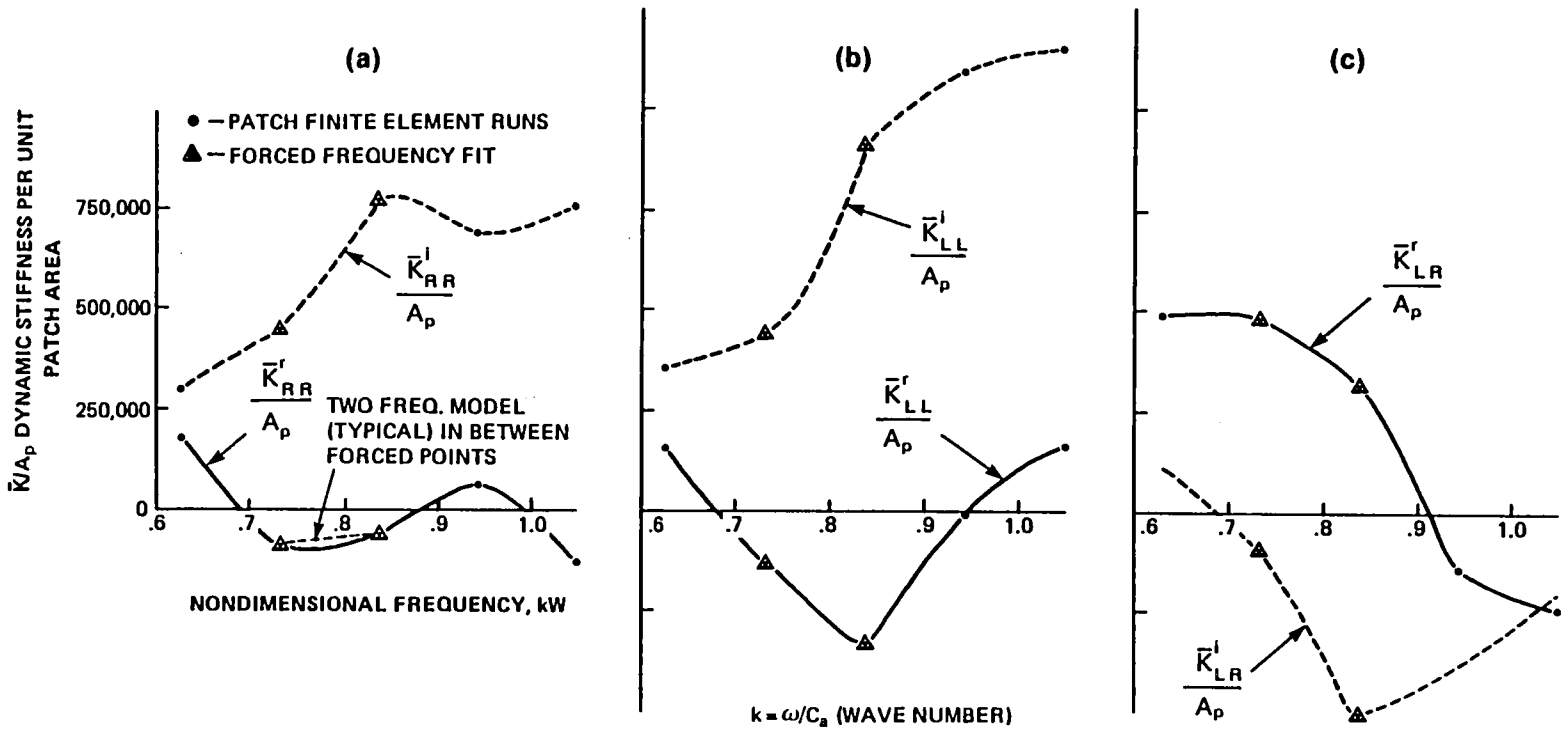

FIGURE - 6 MACROSCOPIC DYNAMIC STIFFNESS VS. NONDIMENSIONAL FREQUENCY

TABLE 3 Comparison of Results (REFLECTED PRESSURE/ P_o)

$\omega W/C_a$	398 Finite Element Model	1-Macroscopic element
.733	.1782	.1784 ← Two freq model
.785	.1357	.1032 designed to work
.837	.05476	.05476 ← at these two values

CONCLUDING REMARKS

The method presented provides a simple means for representing complicated finite element models of inhomogeneous viscoelastic layers with simplier elements, that are designed to work at specific frequencies. Preliminary results for the two-frequency macroscopic element on the simple flat sheet showed good results for the reflected pressure when compared to the same analysis using a full blown microscopic finite element implementation. The results were not quite as good, 23.9% error, for the comparison involving the "in between frequency run". However, the macroscopic elements are not specifically designed to work at the intermediate frequencies, and therefore it would be a windfall situation had they worked there as well. For example if the spread between the two frequencies were made larger, where the second forced frequency point in Figure 6 had been say, 1.0 instead of the .837, a substantial misfit in the dynamic stiffness would be expected due to the curved shape of $\bar{K}'_{LL}$, particularly in the range $0.8<kW<0.9$. If results are desired in this range, new lumped parameters should be recomputed and a new 2-frequency model be used that is valid for the desired frequencies.

The next future checkout application of the macroscopic elements should be for a curved surface of the type shown in Figure 2. It must be remembered that the macroscopic elements are not intended to represent the physics of the actual dynamic system existing between the L, R terminal nodes but rather simply represent the impedance of the actual inhomogeneous soft layer at those two frequencies.

REFERENCES

1. Pritz, T., "Transfer Function Method for Investigating the Complex Modulus of Acoustic Materials: Spring-Like Specimen", Journal of Sound and Vibrations, 72(3), 1980.

2. Khaikovich, I. M. and Khalfin, L. A., "The Effective Dynamic Parameters for Sound Propagation In Inhomogeneous Media", Soviet Physics (Acoustics), 4(3), July 1958.

3. Toulis, W. J., "Acoustic Refraction and Scattering with Compliant Elements .II. Analysis:, J. Acoustic Soc. Am. 29 (9) Sept. 1957.

4. George, J. and Uberall, H., "Approximate Methods to Describe the Reflections From Cylinders and Spheres With Complex Impedance, J. Acoustic Soc. Am. GS (1), Jan. 1979.

5. Stephens, R. W. B., Physics of Plastic, ed. P. Ritchie, D. VanNostrand Co., Princeton, 1965 (Chapter 9).

6. Kalinowski, A. J., and Nebelung, "Solution of Axisymmetric Fluid Structure Interaction Problem with NASTRAN", 10th NASTRAN Users' Colloquium (NASA Cof. Pub. 2249), May 1982.

7. Everstine, G. C., Schroeder, E. A. and Marcus, M. S., "The Dynamic Analysis of Submerged Structures", 4th NASTRAN Users' Colloquium, (NASA Conf. Pub. TMX-3278), 1975.

8. Kalinowski, A. J., "A Survey of Finite Element-Related Techniques As Applied to Acoustic Propagation In the Ocean" Parts I & II, The Shock and Vibration Digest, Vol II (3,4), March, April 1979.

9. Kalinowski, A. J., "Geometrically Corrected Viscous Boundaries For Steady State Acoustic Scattering and Radiation Problems", Proceedings of ASME Winter Annual Meeting, Nov. 1981, ASME Publication AMD-Vol. 46.

10. Kalinowski, A. J., "Steady State Solutions to Dynamically Loaded Periodic Structures," 8th NASTRAN Users' Colloquium, Oct. 1979.

11. Przemieniecki, J. S., Theory of Matrix Structural Analysis, McGraw Hill, 1968.

1. Report No.	2. Government Accession No.	3. Recipient's Catalog No.
NASA CP-2419		

4. Title and Subtitle	5. Report Date
Fourteenth NASTRAN® Users' Colloquium	May 1986
	6. Performing Organization Code
7. Author(s)	8. Performing Organization Report No.
	10. Work Unit No.
9. Performing Organization Name and Address COSMIC, NASA's Computer Software Management and Information Center The University of Georgia Athens, GA 30602	11. Contract or Grant No.
	13. Type of Report and Period Covered Conference Publication
12. Sponsoring Agency Name and Address National Aeronautics and Space Administration Washington, DC 20546	14. Sponsoring Agency Code

15. Supplementary Notes

Also available from COSMIC, Athens, GA 30602

16. Abstract

This publication is the proceedings of a colloquium, and it contains technical papers contributed during the Thirteenth NASTRAN® Users' Colloquium held in San Diego, California, on May 5-9, 1986. The authors review general application of finite element methodology and the specific application of the NASA Structural Analysis System, NASTRAN, to a variety of static and dynamic structural problems.

17. Key Words (Suggested by Author(s))	18. Distribution Statement
NASTRAN structural analysis structures finite element analysis colloquium	Unclassified - Unlimited Subject Category 39

19. Security Classif. (of this report)	20. Security Classif. (of this page)	21. No. of Pages	22. Price
Unclassified	Unclassified	338	A15

For sale by the National Technical Information Service, Springfield, Virginia 22161

National Aeronautics and
Space Administration
Code NIT-4

Washington, D.C.
20546-0001

Official Business
Penalty for Private Use, $300

SPECIAL FOURTH-CLASS RATE
POSTAGE & FEES PAID
NASA
Permit No. G-27

NASA

POSTMASTER: If Undeliverable (Section 158 Postal Manual) Do Not Return